Stony Brook University

The effects of marine particle composition on phytoplankton coagulation efficiency and the use of Th-234 as a proxy for particulate organic carbon flux

A Dissertation Presented

by

Jennifer Szlosek Chow

to

The Graduate School

in Partial Fulfillment of the

Requirements

for the Degree of

Doctor of Philosophy

in

Marine and Atmospheric Science

Stony Brook University

August 2012

Stony Brook University

The Graduate School

Jennifer Szlosek Chow

We, the dissertation committee for the above candidate for the
Doctor of Philosophy degree, hereby recommend
acceptance of this dissertation.

J. Kirk Cochran – Dissertation Advisor
Professor, School of Marine and Atmospheric Sciences

Cindy Lee – Dissertation Advisor
Distinguished Professor, School of Marine and Atmospheric Sciences

Robert A. Armstrong - Chairperson of Defense
Associate Professor, School of Marine and Atmospheric Sciences

Anja Engel
Adjunct Professor, School of Marine and Atmospheric Sciences

Cynthia Hughes Pilskaln
Professor, School for Marine Science and Technology, University of Massachusetts Dartmouth

This dissertation is accepted by the Graduate School

Charles Taber
Interim Dean of the Graduate School

Abstract of the Dissertation

The effects of marine particle composition on phytoplankton coagulation efficiency and the use of Th-234 as a proxy for particulate organic carbon flux

by

Jennifer Szlosek Chow

Doctor of Philosophy

in

Marine and Atmospheric Science

Stony Brook University

2012

This dissertation investigates two parameters important for estimating and predicting organic matter export from the surface ocean: controls on the POC/^{234}Th of marine particles and the coagulation efficiency of algal cells. Specifically, the sources of variability in POC/^{234}Th and coagulation efficiency of *Emiliania huxleyi* are studied. The research explores two methods commonly employed– the ^{234}Th-proxy method for estimating POC flux, and Couette flow device experiments for experimentally deriving coagulation efficiency values.

Applications of ^{234}Th/^{238}U disequilibrium as a flux proxy for particulate organic carbon (POC) in the oceans commonly rely on characterizing the POC/^{234}Th in filterable particles and using this as representative of the sinking flux. To better understand the relationship between ^{234}Th and POC, marine particles were collected in the northwestern Mediterranean Sea (spring, 2003 and 2005). First, we evaluated the role of particle settling velocity and chemical composition on POC/^{234}Th of material collected by settling velocity sediment traps. This study provides evidence that marine particle source (e.g.,

phytoplankton aggregates, zooplankton fecal pellets, degraded biogenic material) has a stronger influence on the POC/^{234}Th than the particle size (vis-à-vis particle settling velocity). We found no consistent trend in POC/^{234}Th with settling velocity, contrary to the canonical view of differential scaling of POC and ^{234}Th with volume and surface area. The source material of the slow and fast settling particles result in similarly low POC/^{234}Th due to carbon degradation of material in slow settling velocity classes and carbon assimilation of material in fast settling velocity classes. Results revealed a factor of 3 drop in POC/^{234}Th from 313 to 1918 m due to a combination of POC losses (dissolution and degradation) and ^{234}Th gains (continued scavenging of ^{234}Th and disaggregation of fast settling particles with depth).

Motivated by the variability in POC export estimates of the pumps versus the traps, we investigated relationships and linkages between filterable particles and those collected in sediment traps by comparing their POC/^{234}Th ratios and compositions (organic and radiochemical). Principal components analysis showed little overlap in composition between filterable particles and sediment trap-collected material, despite similar (within a factor of ~2) POC/^{234}Th and POC flux estimates of the 1-70 μm pump fraction and sediment traps. The relative separation of particles according to freshness were: small pump fraction (1-70 μm) > large pump fraction (>70 μm) > time series and settling velocity sediment trap fractions. The small pump fraction was enriched in indicators of fresh phytoplankton and calcifying algae whereas traps contained biomarkers indicative of fecal pellets and bacterially degraded organic matter. Indicators enriched in the large pump fraction appeared to be consistent with algal material from diatoms and coccolithophores as well as fecal pellets. The pigment composition data of the filterable particles indicated that lateral advection and vertical mixing occurred as well as large short-term changes (5 d) in POC/^{234}Th (1.7-3×) at the base of the mixed later (~300 m). Coupled with significant short-term variation in water column ^{234}Th distributions, these results imply that a thorough understanding of a given oceanic region is required to validate the use of ^{234}Th as a proxy for POC flux.

To experimentally assess the controls on and rates of phytoplankton aggregation, we used Couette flow device experiments to derive coagulation efficiencies of *Emiliania huxleyi*; to our knowledge, this has not been done previously. In chemostat experiments

conducted in 2006 and 2007, *E. huxleyi* was grown at different growth rates and we conducted replicate Couette flow coagulation experiments at multiple growth rates and assessed the relationship of cell coagulation efficiency with cell growth rate and indicators of cell stickiness. Analogs for cell stickiness that were characterized include the sugar composition of high molecular weight dissolved material and the abundance of transparent exopolymer particles (TEP). Coagulation efficiencies increased from 0.2 to 1 as cell growth rates declined from ~0.6 to ~0.1 d^{-1}. We observed a significant positive correlation between growth rates of cells and total alkalinity and a negative correlation between growth rates of cells, TEP/chlorophyll *a*, concentrations of detached coccoliths, and sugars specific to coccolith formation ($p<0.01$). Experiment replication showed coagulation efficiencies of cells at similar growth rates were enhanced by the presence of TEP on cell surfaces and calcite coverage of the coccosphere. Based on our findings we propose that the method by which TEP is included within an aggregate (e.g., TEP matrix embedding cells, free TEP gluing cells together, or exopolymer coating on cells leading to cell-cell contacts) could influence aggregate strength and its likelihood to sink intact beyond the mixed layer.

This dissertation highlights the utility of organic matter composition and settling velocity data of trap and filterable particles for evaluating a representative POC/^{234}Th and assessing the accuracy of the ^{234}Th proxy method for estimating POC flux. Results also show that Couette flow coagulation experiments and algal exudate characterization help increase our mechanistic understanding of the tie between cell environment and physiology changes and phytoplankton aggregation and export dynamics.

DEDICATION

To my parents who never doubted my desire to earn a PhD,

my husband who helped me keep at it,

and my daughter who helped me envision a future with it.

TABLE OF CONTENTS

LIST OF TABLES

LIST OF FIGURES

ACKNOWLEDGEMENTS

It takes a village to do science! I'm grateful that my village has been populated with extremely talented, experienced, generous, patient, and supportive people. Amongst these people, first I would like to thank my advisors Cindy Lee and J. Kirk Cochran. I thank them for not giving up on me. I've learned nearly all I know about how science works and how a scientist works from them. I thank them for providing me with many opportunities (international cruises, meetings, and workshops). I thank them for their time, energy, and persistence. Their steadfast encouragement, guidance, and ability to help me evaluate my work, how I work, and what I'm passionate about has helped me grow into a more confident and mature person. Thank you for all you gave of yourselves. I truly appreciate it!

I'm very fortunate to have had the opportunity to work very closely with all of my committee members Rob Armstrong, Anja Engel, and Cindy Pilskaln. I thank my committee for their ideas and assistance with data analysis and writing. There have been numerous hours spent discussing and mapping out chapters in the conference room of Challenger. My advisors and committee members are exceptional at navigating the storytelling and communication side of science and I appreciate all they have taught me. Although unplanned, I must acknowledge how inspired and grateful I have been to have 3 very strong and accomplished scientists on my committee who happen to be female. In addition, I'd like to thank Anja Engel for encouraging me to pursue research in Germany. It was an enriching academic and personal experience. I thank her for hosting me in her lab and for her family being a tremendous support as I lived abroad for 1.5 years.

I've had wonderful colleagues. They made the lab and field a fun and positive place to work. I've learned so much about the true collaborative spirit of science by working within the MedFlux program. I thank my MedFlux collaborators Michael Peterson, Stewart Wakeham, Juan-Carlos Miquel, Pere Masque, Beat Gassler, Scott Fowler, David Hirschberg, Madeleine Goutx, and Christian Tamburini for their respect and their interest in my development as a scientist. Our time in the field and meeting rooms were always motivating and informative. I thank them for our discussions and their feedback on my work. Steffi Koch, Judith Piontek, Julia Wohlers, Mirko Lunau, and Corinna Borchard were

great lab mates in Germany who patiently helped the American in a new institute dealing with a new language.

My lab mates Lynn Abramson (and her husband Ariel "Eric" Abramson), Zhanfei Liu, Jianhong Xue, and Gillian Stewart have been my "academic siblings". They've been with me on my first trip to Europe, we've taken apart HPLCs together, gone to sea together, been silly and theatrical over our love of marine particles together, we've run the streets of Monaco in heels racing to catch a sampling time point before dinner together, and we've lived together–taking me in when I needed a family most. I thank them for their mentoring, for their example, their support, encouragement, and their devotion.

My friends have been a wonderful support along the way, encouraging me…even after many years have gone by and they've moved away going off into the world to pursue their careers. I am grateful for their continued support. Office mates (Aleya Kaushik, Beth Weinman, Meredith Hayes), flat mates (Felix Mark, Felix Fundel, Lena Brey, Magdalena Gutowska, Frank Melzner), institute and department friends (Joe Olson, Juliet Kinney, Zosia Baumann, Bessy Alexandratos, Maddalena Bayer, Steffi Koch, Catherine Vogel, Carolyn Hall, Teresa Mathews, Lora Clarke, Ann Zulkowsky, Caterina Panzeca) were always there with ears ready to listen, arms ready for a hug, and sneakers ready for a run!

I thank my dear close friends for their enduring patience. My visits and contact have been short and infrequent through the years yet I know they are all there rooting for me. I appreciate their understanding and positive attitudes. Their listening to me and lending experience and help where they can. I want to especially thank Nicole Estvanik Taylor, Donna Furlani, Angela Chou, and Eliza Slavet for making each moment together fun and motivational!

There are numerous support staff and faculty who have provided much of their time and assistance. I thank David Hirschberg, Nicole Händel, Tarik Toubal, Beat Gasser, Umesh Gangishetti, and Shelagh Palma for their help in the laboratory. I'd also like to thank Carol Dovi, Christine Fink, Anne McElroy, Eileen Goldsmith, Nancy Glover, Katerina Panagiotakopoulou, and Maria Riegert, for all of their administrative assistance. Many thanks also to faculty who have offered helpful discussion through the years: Mary Scranton, Bob Aller, Nick Fisher, and Steve Munch.

Support for the MedFlux program and students were provided by the National Science Foundation Chemical Oceanography Program and by the International Atomic Energy Agency in Monaco. Support for the 2006 and 2007 Emiliania huxleyi chemostat experiments and coagulation efficiency experiments came from Helmholtz Association and the German Academic Exchange Service (DAAD). I thank the crews and captains of the CCGC Amundsen Fall 2003 and the R/V Endeavor Spring 2005 and 2006 for a wonderful sea-going experience! Their assistance and hard work made our job possible and our stay comfortable and memorable. I thank my co-authors from Chapter 2 [J.K.C., J.C.M., P.M., R.A.A., S.W.F., B.G., and D.J.H.] and the publisher Elsevier Limited (Oxford) for allowing me to reuse my journal article [Szlosek et al., 2009] in my dissertation.

Lastly, I must thank my family. My grandparents, aunts, uncles, cousins, siblings, parents, family-in-law, husband, and daughter have been an essential support. My wish to be a scientist started at a young age. My parents, Joanne Benson and Edward Szlosek, and my step-parents, Jackie Szlosek and Craig Benson, have been an endless source of encouragement. Through good days and bad they were living through the PhD process with me. And as my PhD years kept ticking away they did not give up on me, but kept up that bubbly enthusiasm and support. Thank you Bekki and Michael, my sister and brother, for all your love. And thank you Taiying and Randy Chow, my parents-in-law, and Bruce, my brother-in-law for your love, support, and helpful insight on the defense and dissertation process. I am grateful for the time my mothers Joanne and Taiying spent with my family to help us take care of our infant daughter so I could get back to work on my dissertation. I am so blessed to have met my husband, Wesley Chow. He has been my partner, my coach, and my best cheerleader. Thank you for keeping me laughing. Thank you for all your love. Thank you for putting so much of your life on hold so I could pursue this goal. Thank you for not letting me give up. And thank you for Josephine, our daughter. Having both of you in my life has given this goal more meaning and my future career more direction.

CHAPTER 1

Introduction

1. Methods for Estimating Marine Particle Flux and their Importance

Phytoplankton growth fuels the passage of atmospheric carbon dioxide into particulate organic carbon (POC), of which, <1% will reach the ocean sediment where it will be sequestered from the atmosphere for hundreds of thousands of years. One method of marine particle production is the coagulation of colloids and particles by their collision and subsequent sticking (McCave, 1984; Alldredge and Silver, 1988). Colloidal material may originate from fibrillar exudates released from phytoplankton and bacteria. The coagulation-aggregation process produces a large portion of the POC that is exported from the surface ocean (Silver and Gowing, 1991). Scientists studying the ocean's CO_2 absorption are particularly concerned with quantifying the production of POC and the magnitude of material exported below the upper ~100 m of the water column, where wind driven mixing can release respired CO_2 back into the atmosphere.

Methods for estimating the magnitude of exported POC include models based on phytoplankton production such as primary and new production estimates, sediment trap collection, and using radionuclides such as ^{234}Th or ^{210}Po as proxies. Each method has issues that might affect the accuracy of the POC export estimates. Of these methods, measurements of $^{234}Th/^{238}U$ disequilibrium and the POC/^{234}Th ratio of sinking particulate matter in the upper ocean have been used in large-scale oceanographic field programs to estimate the downward flux of particulate organic carbon from the euphotic zone; this method is popular due to the ease of the methodology and study programs (Benitez-Nelson and Moore, 2006; Waples et al., 2006). Therefore, studies that improve our understanding of the limits of applying the ^{234}Th proxy method are valuable.

Developing a quantitative understanding of the processes controlling the variability in POC/^{234}Th ratios of marine particles is thus essential for validating the use of ^{234}Th to estimate POC fluxes from the surface ocean. Also important for improving our

understanding of POC export is to unveil how efficiently particles coagulate and the dependency of phytoplankton attachment on bloom conditions. This dissertation investigates two parameters important for estimating and predicting POC export from the surface ocean: POC/^{234}Th variability of marine particles and the coagulation efficiency of algal cells.

2. The POC/^{234}Th ratio and the ^{234}Th Approach for Estimating POC Flux

To improve carbon cycle models, it is necessary to estimate accurately the POC exported from the surface ocean in different oceanographic settings and during different seasons. Therefore, a time efficient and logistically practical method is valuable. An increasingly common oceanographic practice uses thorium-234, a particle-reactive radionuclide produced by dissolved ^{238}U that acts as a tracer of particle export on short time scales of days to months ($t_{1/2}$ = 24.1 d), (Coale and Bruland, 1985). ^{234}Th rapidly and readily adsorbs to particles, resulting in a disequilibrium between ^{234}Th and ^{238}U (Bruland and Coale, 1986). This scavenging process leads to a deficit of ^{234}Th that can be used to determine the flux of thorium out of the upper ocean water column. As such ^{234}Th is used as a proxy for estimating the flux of a particular chemical class (e.g., POC), by assuming that the ratio of fluxes (POC flux : ^{234}Th flux) are proportional to the ratio (POC/^{234}Th) measured on sinking particles (Buesseler et al., 1992)–this method is often referred to as the ^{234}Th approach.

Concern over the variability in the ^{234}Th-derived POC export values has led to organized efforts by the scientific community to investigate assumptions of the ^{234}Th approach and the sources of variability in the POC/^{234}Th ratio. Underlying assumptions are: 1) losses of ^{234}Th and POC from the surface occur due to vertical sinking over 1 dimension; 2) the measured POC/^{234}Th is representative of the majority of the export and is the ratio that represents particles that sank over the timescale (and area) that created the ^{234}Th deficit; and 3) ^{234}Th acts as an indiscriminant tracer of particles (adsorbing to all material regardless of its composition). Research investigating these assumptions is important for assessing the limitations of the ^{234}Th approach and suggesting best practices for accurately applying this valuable field method.

2.1. POC/^{234}Th versus Particle Size

2.1.1. Accepted Methods

Particulate material (>1 μm) collected by *in situ* pump filtration, sediment trap, or bottle collection from a depth at the base of the mixed layer is sampled for POC/^{234}Th measurements. Models predict a strong relationship between particle size and settling velocity (Alldredge and Gotschalk, 1989) and early field studies have pointed to large, rare particles providing a large contribution to the export (McCave, 1975; Fowler and Knauer, 1986). Therefore the practice of most researchers has been to use the POC/^{234}Th ratio of the large particles (>53 μm) filtered *in situ* to represent the POC export from the mixed layer (Buesseler et al., 2006).

In general, the POC/^{234}Th ratio increases with increasing particle size (Buesseler et al., 1998; Charette and Moran, 1999; Burd et al., 2000; Cochran et al., 2000, Buesseler et al., 2001; Benitez-Nelson et al., 2001; Moran et al., 2003; Speicher et al., 2006). The accepted reasoning for this trend hinges on findings that POC and ^{234}Th are each dependent on different particle size parameters–POC contained within the particle, is proportional to volume, while ^{234}Th, adsorbed onto surface sites scales with particle surface area (Buesseler et al., 2006). A few exceptions to the trend of increasing POC/^{234}Th and particle size are: 1) constant or decreasing POC/^{234}Th with increasing particle size observed for particles that originate in oligotrophic regions with small phytoplankton cells and high rates of nutrient recycling (Buesseler et al., 1995, 1998; Bacon et al., 1996; Brew et al., 2009); and 2) constant POC/^{234}Th with size observed and theoretically shown to occur due to aggregation and disaggregation of particles that are aggregates of cells or small primary particles, and where the primary particles of the aggregates set the POC/^{234}Th, regardless of size (Buesseler et al., 2006; Waite and Hill, 2006; Speicher et al., 2006; Burd et al., 2007; Brew et al., 2009). Because POC flux estimates are linearly dependent on the magnitude of the POC/^{234}Th, variability of this ratio has a direct effect on POC flux estimates. Hence, the choice of what particle size class to use in POC flux estimates is an important one.

2.1.2. Concerns with Accepted Methods

The large variability observed in pump and trap shallow water POC/^{234}Th has led many to believe that the biological source of the primary particles (e.g., cells, fecal pellets, etc) establishes the POC/^{234}Th (Buesseler et al., 2006 and references therein). Some authors have noted that using the POC/^{234}Th of intermediate and small size fractions (10-53 μm and 1-10 μm, respectively) yields an equivalent or larger POC flux estimate to that obtained using the ratio of the large particles (Moran et al., 2003; Hung et al., 2010). Additionally, studies have observed that the POC/^{234}Th of the small or intermediate size fraction is more similar to that of sediment traps (0.5–2 μmol OC dpm ^{234}Th) than is the ratio in the large size fraction (Hung et al., 2010; Hung and Gong, 2010; Lepore et al., 2009; Buesseler et al., 2006; Waite and Hill, 2006). To ascertain what size fraction might best represent the majority of the POC and ^{234}Th flux, efforts have been made to look at the fractionation of POC and ^{234}Th among various particle size classes by determining their correlation with one another (Smith et al., 2006; Speicher et al., 2006; Waite and Hill, 2006; Burd et al., 2007; Brew et al., 2009; Lepore et al., 2009). The results of these studies have found POC and ^{234}Th to correlate well for small to intermediate sized particles or equally well for all size classes (Speicher et al., 2006; Brew et al., 2009; Lepore et al., 2009).

However, evidence still points to mass sedimentation and rapid flux of particles (Lee et al., 2009; Xue et al., 2009; McDonnell and Buesseler, 2010) and the potential importance of the large or fast settling particles to the POC and ^{234}Th flux (Trull et al., 2008; and this work). New collection techniques are being employed that allow for the *in situ* separation of particles by their settling velocity, thus breaking studies from their reliance on large particles to represent sinking flux (Peterson et al., 2005; Gustafsson et al., 2006). By studying the particle settling velocity distribution as material exits the euphotic zone, relationships between POC/^{234}Th and particle dynamics and properties (e.g., source, alteration, size) can be discerned more accurately. Through such collection techniques the utility of ^{234}Th is expanded to include particle dynamics of material in the ocean interior. Settling velocity separation techniques deployed simultaneously with time series sediment traps allow ^{234}Th to be used as a tracer of particle processes in the Twilight Zone, in which the POC flux attenuates rapidly with depth due to heterotrophic and other processes. The

POC/^{234}Th potentially reveals whether processes such as disaggregation and ^{234}Th release as colloids, ^{234}Th decay or additional ^{234}Th scavenging, and particle exchange occur.

2.2. POC/^{234}Th and Collection Method

2.2.1. Accepted Methods

The ^{234}Th approach is most commonly carried out using the large particle fraction filtered by *in situ* pumps (Buesseler et al., 2006). This ratio is then applied to the water column ^{234}Th deficit estimated by measurements of ^{234}Th activity on MnO_2-impregnated cartridges deployed on pumps or measured in small volume water samples. Alternatively, the POC/^{234}Th ratio from sediment traps may be applied to the water column ^{234}Th deficit (Schmidt et al., 2002). In general, a factor of 2 agreement between the ^{234}Th-derived POC fluxes and those directly measured in sediment traps is considered good (Buesseler et al., 2006). Yet, significant lack of agreement between pump- and trap-derived POC export commonly occurs (Cochran et al., 2009). Recent efforts (e.g. this study) have focused on understanding POC/^{234}Th variability and assessing what filterable size fraction might best represent the sinking flux.

2.2.2. Concerns with Accepted Methods

Factors contributing to the lack of agreement in ^{234}Th-based vs. trap-derived POC flux estimates include physical advection, differences in material collected by bottles and pump filtration, and hydrodynamic effects on sediment trap collection efficiency. For example, studies have shown marked differences in POC measured on filtered bottle samples and that collected on *in situ* pump filters due to DOC adsorption on filters (Moran et al., 1999) or under-collection of motile zooplankton (Liu et al., 2005). Concerns over the ^{234}Th approach center on the potential temporal disconnection between the ^{234}Th deficit, representing export occurring over several weeks (see Cochran and Masqué, 2003 and references therein), and the POC/^{234}Th ratio of particles collected on a given sampling day, which represent filterable particles in the water column on that day, but perhaps not representative of particles leaving the surface ocean in the prior weeks (Buesseler et al., 2006). And as mentioned earlier, concerns over what size particle is most representative of the majority of the POC and ^{234}Th flux has prompted some workers to measure up to 5

particle size classes ranging from 1 to 100 μm in diameter (Speicher et al., 2006; Brew et al., 2009). An additional factor is the effect of advective processes on the ^{234}Th deficit. Due to the large contribution of the dissolved ^{234}Th signal to the water column Th deficit, advective processes can require application of non-steady-state models to the ^{234}Th flux (Savoye et al., 2006; Cochran et al., 2009).

The artifact most commonly ascribed to sediment trap-derived POC fluxes is under- or over-collection of the flux by the trap. The reliability of the trap POC/^{234}Th ratio is tied to the ability of the trap to collect a sample that is indicative of all the export. Depending on the geometry and aspect ratio of the trap opening, currents above ~ 12 cm s^{-1} can wash particles out of the trap mouth (Gust et al., 1996; Gardner, 2000; Fabrés et al., 2002; Martín et al., 2006). Other concerns pertain to loss of trapped POC due to collection of heterotrophs or heterotrophic activity (e.g., swimmers, bacteria) (Peterson et al., 1993; Passow et al., 2006); and abiotic dissolution (Wakeham et al., 1993; Antia, 2005). Additionally, traps not only capture particles that sink from directly above, but also those that are carried horizontally, potentially from long distances. However, awareness of these issues has led to trap designs that exclude swimmers (Peterson et al., 1993) or float neutrally buoyantly; Buesseler et al., 2000) to minimize artifacts.

2.3. POC/^{234}Th and Particle Composition

The source of the biological components of aggregates, the inclusion of inorganic matter, and biological and physical modification of aggregates all interact and contribute to the measured POC/^{234}Th. In their review, Buesseler et al. (2006) included variations in volume-to-surface area (V:SA) ratios and particle morphology, interactions between dissolved Th and ligands such as acidic polysaccharides, increased Th scavenging, and carbon degradation and assimilation, as leading factors causing POC/^{234}Th variability. Some of these influences are a direct outcome of ecosystem responses to seasonal changes such as the cell size of the dominant phytoplankton species, progression of the phytoplankton bloom (i.e., increase in Th ligands), heterotrophic consumption of phytoplankton (e.g., bacteria, protozoa, zooplankton). Others are modifying processes of the surface export that occur with depth and time. Depending on the residence time of

particles within the mixed layer, processes such as increased Th scavenging, carbon degradation and assimilation, Th ligands, and disaggregation can all play a role.

Although attention has been given to V:SA effects on the POC/^{234}Th of particles exiting the mixed layer, there are few studies that relate particle source, composition and chemistry to the POC/^{234}Th ratio variability. A few recent studies have explained the POC/^{234}Th relationship with size and POC flux in terms of the contribution made by phytoplankton and zooplankton species (Buesseler et al., 2008; Steinberg et al., 2008; Brew et al., 2009; Maiti et al., 2010) and fecal pellets Rodriguez y Baena et al. (2006). Yet, a more holistic approach to investigating the effect of biological, chemical, and physical changes on the POC/^{234}Th ratios, as reported in the present study, is crucial to investigating the comparability of the pump and trap POC flux estimates and more fully understanding the POC/^{234}Th variability.

3. Phytoplankton Aggregation

Phytoplankton blooms followed by organic matter export are explicit in the general model for the ocean biological pump (Chisholm, 2000; Falkowski et al., 2000). Organic matter export is thought to occur due to zooplankton production of fecal pellets, and to particle aggregation/sedimentation. The onset and magnitude of phytoplankton sedimentation events in the upper ocean are dependent on the stages of phytoplankton blooms as well as the phytoplankton functional groups present, such as diatoms or coccolithophores (Stemmann et al., 2002; Jin et al., 2006). Export occurs because cells collide, attach, and eventually form an aggregate that sinks. Cell or particle collisions are dependent on the density of particles in the water (Jackson, 1990; Jackson and Lochmann, 1993; Jackson, 2005) and the physical forces that bring particles together (McCave, 1984). In addition, stickiness and coagulation efficiency may vary with the physiological state of the cells. Cells undergoing nutrient stress have been shown to create more transparent exopolymer particles (TEP), and the increased concentration of TEP may lead to increased coagulation efficiency. Furthermore the actual chemical composition of algal and bacterial exudates and mucus is highly dependent on cell physiology, and environmental factors such as nutrient availability (Decho, 1990; Arnosti, 1993; Myklestad, 1995; Aluwihare & Repeta, 1999; Claquin et al., 2008).

Coagulation efficiency (the "stickiness" factor, α) is a term that represents the probability that when particles collide they will adhere to one another (O'Melia and Tiller 1993); it is a complex function of physical and chemical factors. Values for the coagulation efficiency (α) of phytoplankton can be derived experimentally (Kiørboe et al., 1990; Drapeau et al., 1994; Hansen et al., 1995; Engel, 2000; Kahl et al., 2008), and is a parameter used in aggregation models to interpret relative changes in carbon export over the duration of a bloom (Jackson and Lochmann, 1993; Kahl et al., 2008; Karakas et al., 2009). Despite modelers continuing to point out the potential influence of coagulation efficiency on aggregation processes, values for α are substituted into model runs to determine the effect on the model output with little scientific reasoning or understanding of how and why coagulation efficiency varies (Jackson 1990; Hill 1992; Riebesell and Wolf-Gladrow 1992). We are only starting to understand what physiological and environmental factors affect α.

3.1. Coagulation Studies–Methodology and Issues

The physical mechanisms that force particles together are dependent on particle size (McCave, 1984; Jackson and Lochmann, 1993). The initial stages of aggregation, or coagulation, are dominated by laminar shear bringing particles together (McCave, 1984; Jackson and Lochmann, 1993). Coagulation studies have been performed using Couette flow devices (van Duuren, 1968; Drapeau et al., 1994) or annular flumes (Kahl et al., 2008). The principle of these experiments is to impart a known shear flow on the sample, causing particle collisions, and to monitor the size spectra with time while observing exponential decay of the particle density–a direct outcome of particles successfully attaching to one another upon collision. From this, α can be estimated using Smoluchowski coagulation kinetics (Birkner and Morgan, 1968; Camp and Stein, 1943; Dam and Drapeau, 1995; Jackson, 1990; Jackson, 2005; Kiørboe et al., 1990).

The coagulation efficiency must be a number between 0 and 1, as is true for all probability factors. However, in practice the coagulation efficiency estimated from experimental data can be >1 or be < 0 due to underestimating the particle density (Engel, 2000) or preformed aggregates disaggregating. Such values are physically undefined, and therefore the experiment in some way violated the conditions upon which the calculations are predicated. Theoretical considerations for conducting experiments assume the volume

of solid particles within the suspension is conserved and the equations applied are valid for the initiation of aggregation, thus shear must dominate the physical interaction of particles (Jackson and Lochmann, 1993).

Literature documenting use of Couette flow devices demonstrates numerous experimental aberrations of this theoretical criterion. For example, some authors have documented lack of volume conservation due to losses or gains in particle numbers because, of 1) growth of the cells during the experiment (Dam and Drapeau, 1995) and 2) loss of flocs from suspension to the Couette chamber surfaces (Kiørboe et al., 1990). In addition, Coulter Counters do not detect TEP abundance or size quantitatively (Alldredge et al., 1993), and are limited to yielding the solid volume concentration of particles. Therefore, special measures are needed to account for TEP interaction with cells during coagulation (Engel, 2000).

The Smoluchowski coagulation equation is dependent on the initial suspension being monodisperse (Birkner and Morgan, 1968; Camp and Stein, 1943; Jackson, 1990; Kiørboe et al., 1990; Jackson, 2005). To comply with this requirement, monocultures are generally used and represented as a Gaussian distribution (Kiørboe et al., 1990). Hence, a correction factor needs to be applied to account for the spread in the size of the primary particles (Kiørboe et al., 1990; Dam and Drapeau, 1995). Yet, cells rarely follow a Gaussian distribution (Armstrong, 2003) and are rarely clean of cellular debris, leading to shifts in cell peak shape and location along the particle size distribution (PSD). Such variability in the cell PSD can lead to low signal : noise ratios due to the sensitivity of the coagulation calculations on the PSD range used in particle enumeration. This is especially the case for low shear levels that mimic open ocean conditions. Variations in the cell abundances at the beginning of coagulation experiments have also been found to affect α due to the sensitivity of the Smoluchowski coagulation equation (Kiørboe et al., 1990), further complicating interpretations of the value of α on changes in the cells species or environmental conditions.

To better understand environmental and physiological influences on coagulation, experimental issues such as TEP abundance, cell numbers, and size distribution should be controlled or monitored. One pressing ramification of the experimental errors associated with this technique is the difficulty of achieving reproducible results: few experiments

published have errors associated with their attachment probabilities or mention replicate experiments.

3.2. Coagulation Studies–Effect of Phytoplankton Species and Physiology

Phytoplankton aggregation is generally observed to increase as cells senesce towards the end of a bloom. It has been proposed that this is due to an increase in chemically reactive exudates on cell surfaces and an increase in TEP, which increase particle reactivity and densities (Passow and Alldredge, 1995; Engel, 2000). Additionally, authors have observed that coagulation efficiency correlates with organic-matter glue constituents such as TEP and dissolved carbohydrates (Alldredge et al., 1995; Dam and Drapeau, 1995; Kiørboe and Hansen, 1993; Engel 2000; Kahl et al., 2008). Hence, the α of a single algal species is likely to change with the growth stage and nutrient status of the cells. Furthermore, aggregation that is promoted by algal stickiness can vary between species depending on the chemical reactivity of the exudates and how they are associated with the cell. Kiørboe and Hansen (1993) conducted a study comparing the coagulation efficiency of six diatom species grown in batch cultures and found differences in the coagulation efficiency between species. They inferred that the different chemical properties of particulate mucus of an algal species led to different modes of sticking such as cell-cell and cell-TEP. Dam and Drapeau (1995), Mopper et al. (1995), and Passow and Alldredge (1995) documented cell-TEP sticking of diatoms grown in a natural assemblage of diatoms in a mesocosm and showed that surface reactive carbohydrate concentrations, such as acidic sugars and uronic acids, changed over the course of the phytoplankton bloom.

Phytoplankton species can influence particle coagulation due to differences in TEP production (Engel, 2000; Kahl et al., 2008), cell morphology (Jackson and Lochmann, 1993), surface chemistry (Mopper et al., 1995; Passow et al., 2005), size, and density (Jackson and Kiørboe, 2008). Missing from previously published coagulation studies is an important functional group of phytoplankton, the coccolithophores. Coccolithophores produce large blooms (Balch et al., 2005) and calcite tests that affect aggregate and fecal pellet settling rates (De La Rocha and Passow, 2007; Iversen and Ploug, 2010). Data and model results have suggested a dominant role for $CaCO_3$ in the export of organic matter (Klaas and Archer, 2002; Jin et al., 2006). Acidic polysaccharide exudates produced by

coccolithophores for laying down their calcite tests promote interactions with cations and trace metals (De Jong et al., 1979; Borman et al., 1982; Kok et al., 1986; Langer et al., 2009). Additionally, $CaCO_3$ has shown high affinities for trace metals such as thorium (Chase et al., 2002; Luo and Ku, 2004). Hence its deposition may be important for understanding radionuclide and trace metal scavenging in the ocean water column.

Coccoliths and intact coccolithophores have long been observed in association with mucus material at the continental slope (de Wilde et al., 1998; McCave et al., 2001) and in sediment traps (Honjo, 1982; Cadée, 1985; Riemann, 1989). Yet, relatively little is known about what controls coccolithophore aggregation and deposition (De La Rocha and Passow, 2007; Biermann and Engel, 2010). Recently, studies have documented the association of coccolithophores with TEP and the formation of coccolithophore aggregates within laboratory roller tanks and in the field (Engel et al., 2009a,b; Biermann and Engel, 2010; Harlay et al., 2011). Calcified cells flocculate and form aggregates more readily because of the presence of Ca^{2+}, which is important for promoting cationic bridge formation of mucus fibrils (Mopper et al., 1995; Leppard, 1995; Decho, 1990) and dense aggregates (Kranck, 1973; Hamm, 2002; Engel et al., 2009b).

Studies with cells undergoing environmental perturbations, such as nutrient depletion, permit investigators to qualitatively describe dependency of phytoplankton coagulation on physiological and environmental parameters. These types of studies coupled with data regarding the chemical composition of TEP precursors, such as dissolved sugars (Passow, 2002; Borchard et al., 2011), help inform our understanding of bloom dynamics and POC export, and serve as a step towards unraveling the mechanisms that control coagulation of marine particles that typify surface ocean environments (e.g., mixtures of phytoplankton species, dust, terrestrial material, cellular debris, and heterotrophic organisms).

4. Dissertation Objectives and Organization

This dissertation investigates two parameters important for estimating and predicting organic matter export from the surface ocean: controls on the POC/^{234}Th of marine particles and the coagulation efficiency of algal cells. Specifically, the sources of variability in POC/^{234}Th and coagulation efficiency of *Emiliania huxleyi* are studied. The research explores two methods commonly employed– the ^{234}Th-proxy method for estimating POC

flux, and Couette flow device experiments for experimentally deriving coagulation efficiency values. The objectives of this dissertation are to:

1. Study the variability of the POC/^{234}Th ratio due to particle size, settling velocity, composition, depth, and sample collection method.
2. Determine the coagulation efficiency for *Emiliania huxleyi*.
3. Study the affect of *E. huxleyi* cell physiology on coagulation.

Chapter 2 evaluates the role of particle settling velocity and chemical composition on POC/^{234}Th ratios of material collected by sediment trap in the northwest Mediterranean. Separation of sinking particles by settling velocity at multiple depths within the water column allows the affects of ^{234}Th decay, POC degradation, and adsorption to inorganic minerals on POC/^{234}Th to be investigated.

Chapter 3 addresses the difference in POC/^{234}Th observed between particles collected by sediment trap and *in situ* filtration in the northwest Mediterranean. Using the data collected during the 2005 MedFlux field season, the effects of numerous biogeochemical factors on POC/^{234}Th are observed and summarized. This chapter discusses the influence of particle chemical composition and source on the POC/^{234}Th first introduced in the previous chapter.

Chapter 4 experimentally derives coagulation efficiency values for *Emiliania huxleyi* at different growth rates for the first time. This chapter details best methods for utilizing Couette flow devices in coagulation studies to promote reproducible experimental results. Within this chapter, the influence of coccolith presence, TEP abundance, and dissolved carbohydrate composition on coagulation efficiency of *E. huxleyi* was evaluated.

Chapter 5 summarizes major findings of this research and suggests future work.

References

Alldredge, A.L., Silver, M.W., 1988. Characteristics, dynamics, and significance of marine snow. Progress in Oceanography 20, 41-82.

Alldredge, A.L., Gotschalk, C.C., 1989. Direct observations of the mass flocculation of diatom blooms: characteristics, settling velocities and formation of diatom aggregates. Deep-Sea Research 36, 159-171.

Alldredge, A.L., Passow, U., Logan, B.E., 1993. The abundance and significance of a class of large, transparent organic particles in the ocean. Deep-Sea Research 40, 1131-1140.

Alldredge, A.L., Gotschalk, C., Passow, U., Riebesell, U., 1995. Mass aggregation of diatom blooms: Insights from a mesocosm study. Deep-Sea Research I 42, 9-28.

Aluwihare, L.I., Repeta, D.J., 1999. A comparison of the chemical characteristics of oceanic DOM and extracellular DOM produced by marine algae. Marine Ecology Progress Series 186, 105-117.

Antia, A.N., 2005. Particle-associated dissolved elemental fluxes: revising the stochiometry of mixed layer export. Biogeosciences Discussions 2, 275-302.

Armstrong, R.A., 2003. A hybrid spectral representation of phytoplankton growth and zooplankton response: The "control rod" model of plankton interaction. Deep-Sea Research II 50, 2895-2916.

Arnosti, C., 1993. Structural characterization and bacterial degradation of marine carbohydrates. Ph.D. Thesis, Woods Hole Oceanographic Institute, Woods Hole, MA.

Bacon, M.P., Cochran, J.K., Hirschberg, D., Hammar, T.R., Fleer, A.P., 1996. Export flux of carbon at the equator during the EqPac time-series cruises estimated from ^{234}Th measurements. Deep-Sea Research II 43, 1133-1153.

Balch, W.M., Gordon, H.R., Bowler, C., Drapeau, D.T., Booth, E.S., 2005. Calcium carbonate budgets in the surface global ocean based on MODIS data. Journal of Geophysical Research 110, C07001.

Benitez-Nelson, C.R., Buesseler, K.O., Karl, D., Andrews, J., 2001. A time-series study of particular matter export in the North Pacific subtropical gyre based upon ^{234}Th: ^{238}U disequilibrium. Deep-Sea Research 48 (12), 2595-2611.

Benitez-Nelson, C.R., Moore, W.S., 2006. Future applications of ^{234}Th in aquatic ecosystems. Marine Chemistry 100 (3-4), 163-165.

Biermann, A., Engel, A., 2010. Effect of CO_2 on the properties and sinking velocity of aggregates of the coccolithophore *Emiliania huxleyi*. Biogeosciences 7 (3), 1017-

1029.

Birkner, F.B., and J.J. Morgan, 1968. Polymer flocculation kinetics of dilute colloidal suspensions. Journal of the American Water Works 60, 175-191.

Borchard, C., Engel, A., 2011. Organic matter exudation by *Emiliania huxleyi* under simulated future ocean conditions. Biogeosciences Discussions 9, 1199-1236.

Borman, A.H., de Jong, E.W., Huizinga, M., Kok, D.J., Westbroek, P., Bosch, L., 1982. The role in $CaCO_3$ crystallization of an acid Ca^{2+}-binding polysaccharide associated with coccoliths of *Emiliania huxleyi*. European Journal of Biochemistry 129, 179-183.

Brew, H.S., Moran, S.B., Lomas, M.W., Burd, A.B., 2009. Plankton community composition, organic carbon and thorium-234 particle size distributions, and particle export in the Sargasso Sea. Journal of Marine Research 67, 845-868.

Bruland, K.W., Coale, K.H., 1986. Surface Water $^{234}Th/^{238}U$ disequilibria: spatial and temporal variations of scavenging rates within the Pacific Ocean. In: Burton, J.D., Brewer, P.G., Chesselet, R. (Eds.), Dynamic Processes in the Chemistry of the Upper Ocean. Plenum Press, pp 159-172.

Buesseler, K.O., Cochran, J. K., Bacon, M. P., Livingston, H. D., Casso, S. A., Hirschberg, D., Hartman, M. C., Fleer, A. P., 1992. Determination of thorium isotopes in seawater by nondestructive and radiochemical procedures. Deep-Sea Research I 39, 1103-1114.

Buesseler, K.O., 1998. The decoupling of production and particulate export in the surface ocean. Global Biogeochemical Cycles 12 (2), 297-310.

Buesseler, K.O., 1998. The decoupling of production and particulate export in the surface ocean. Global Biogeochemical Cycles 12 (2), 297-310.

Buesseler, K.O., Ball, L., Andrews, J., Cochran, J.K., Hirschberg, D.J., Bacon, M.P., Fleer, A., Brzezinski, M., 2001. Upper ocean export of particulate organic carbon and biogenic silica in the Southern Ocean along 170°W. Deep-Sea Research II 48 (4275-4297).

Buesseler, K.O., Benitez-Nelson, C.R., Moran, S.B., Burd, A., Charette, M., Cochran, J.K., Coppola, L., Fisher, N.S., Fowler, S.W., Gardner, W.D., Guo, L.D., Gustafsson, O., Lamborg, C., Masqué, P., Miquel, J.C., Passow, U., Santschi, P.H., Savoye, N., Stewart, G., Trull, T., 2006. An assessment of particulate organic carbon to thorium-234 ratios in the ocean and their impact on the application of ^{234}Th as a POC flux proxy. Marine Chemistry 100, 213-233.

Buesseler, K.O., Trull, T.W., Steinberg, D.K., Silver, M.W., Siegel, D.A., Saitoh, S.I., Lamborg, C.H., Lam, P.J., Karl, D.M., Jiao, N.Z., Honda, M.C., Elskens, M., Dehairs, F., Brown, S.L., Boyd, P.W., Bishop, J.K.B., Bidigare, R.R., 2008. VERTIGO (VERtical Transport In the Global Ocean): as study of particle source and flux attenuation in the North Pacific.

Deep-Sea Research II 55 (14-15), 1522-1539.

Buesseler, K.O., Steinberg, D.K., Michaels, A.F., Johnson, R.J., Andrews, J.E., Valdes, J.R., Price, J.F., 2000. A comparison of the quantity and quality of material caught in a neutrally buoyant versus surface-tethered sediment trap. Deep-Sea Research I 47, 277-294.

Buesseler, K.O., Andrews, J.A., Hartman, M.C., Belastock, R., Chai,, F., 1995. Regional estimates of the export flux of particulate organic carbon derived from thorium-234 during the JGOFS EqPac program. Deep-Sea Research II 42 (2-3), 777-804.

Burd, A.B., Moran, S.B., Jackson, G.A., 2000. A coupled adsorption-aggregation model of the POC/^{234}Th ratio of marine particles. Deep-Sea Research I 47, 103-120.

Burd, A.B., Jackson, G.A., Moran, S.B., 2007. The role of the particle size spectrum in estimating POC fluxes from ^{234}Th/^{238}U disequilibrium. Deep-Sea Research I 54, 897-918.

Cadée, G.C., 1985. Macroaggregates of *Emiliania huxleyi* in sediment traps. Marine Ecology Progress Series 24, 193-196.

Camp, T.R., and Stein, P.C., 1943. Velocity gradients and internal work in fluid motion. Journal of Boston Society of Civil Engineers 30, 219-237.

Charette, M.A., Moran, S.B., Bishop, J.K.B., 1999. ^{234}Th as a tracer of particulate organic carbon export in the subarctic Northeast Pacific Ocean. Deep-Sea Research II 46 (11-12), 2833-2861.

Chase, Z., Anderson, R.F., Fleisher, M.Q., Kubik, P.W., 2002. The influence of particle composition and particle flux on scavenging of Th, Pa and Be in the ocean. Earth and Planetary Science Letters 204, 215-229.

Chisholm, S.W., 2000. Oceanography: Stirring times in the Southern Ocean. Nature 407, 685-687.

Claquin, P., Probert, I., Lefebvre, S., and Veron, B., 2008. Effects of temperature on photosynthetic parameters and TEP production in eight species of marine microalgae. Aquatic Microbial Ecology 51, 1-11.

Coale, K.H., Bruland, K.W., 1985. ^{234}Th:^{238}U disequilibria within the California Current. Limnology and Oceanography 30 (1), 22-33.

Cochran, J.K., Buesseler, K.O., Bacon, M.P., Wang, H.W., Hirschberg, D.J., Ball, L., Andrews, J., Crossin, G., Fleer, A., 2000. Short-lived thorium isotopes (^{234}Th, ^{228}Th) as indicators of POC export and particle cycling in the Ross Sea, Southern Ocean. Deep-Sea Research II 47, 3451-4390.

Cochran, J.K., Masqué, P., 2003. Short-lived U/Th radionuclides in the ocean: tracers for scavenging rates, export fluxes, and particle dynamics. In: Bourdon, B., Henderson, G.M., Lundstrom, C.C., Turner, S.P. (Eds.), Uranium-Series Geochemistry, Reviews in Mineralogy and Geochemistry, vol. 52. Mineralogy Society of America, Washington, DC, pp. 461-492.

Cochran, J.K., Miquel, J-C., Armstrong, R.A., Fowler, S.W., Masqué, P., Gasser, B., Hirschberg, D.J., Szlosek, J., Rodriguez y Baena, A.M., Verdeny, E., Stewart, G.M., 2009. Time-series measurements of ^{234}Th in water column and sediment trap samples from the northwestern Mediterranean Sea. Deep-Sea Research II 56, 1487-1501.

Dam, H.G., Drapeau, D.T., 1995. Coagulation efficiency, organic-matter glues and the dynamics of particles during a phytoplankton bloom in a mesocosm study. Deep-Sea Research II 42, 111-123.

de Jong, E.W., van Rens, L., Westbroek, P., Bosch, L., 1979. Biocalcification by the marine alga *Emiliania huxleyi* (Lohmann) Kamptner. European Journal of Biochemistry 99, 559-567.

De La Rocha, C.L., Passow, U., 2007. Factors influencing the sinking of POC and the efficiency of the biological carbon pump. Deep-Sea Research II 54, 639-658.

de Wilde, P.A.W.J., Duineveld, G.C.A., Berghuis, E.M., Lavaleye, M.S.S., Kok, A., 1998. Late-summer mass deposition of gelatinous phytodetritus along the slope of the N.W. European Continental Margin. Progress in Oceanography 42, 165-187.

Decho, A.W., 1990. Microbial exopolymer secretions in ocean environments: their role(s) in food webs and marine processes. Oceanography and Marine Biology Annual Review 28, 73-153.

Drapeau, D.T., Dam, H.G., Grenier, G., 1994. An improved flocculator design for use in particle aggregation experiments. Limnology and Oceanography 39, 723-729.

Engel, A., 2000. The role of transparent exopolymer particles (TEP) in the increase in apparent particle stickiness (α) during the decline of a diatom bloom. Journal of Plankton Research 22, 485-497.

Engel, A., Szlosek, J., Abramson, L., Liu, Z., Lee, C., 2009. Investigating the effect of ballasting by $CaCO_3$ in *Emiliania huxleyi*, I: Formation, settling velocities and physical properties of aggregates. Deep-Sea Research II 56, 1396-1407.

Engel, A., Abramson, L., Szlosek, J., Liu, Z., Stewart, G., Hirschberg, D., Lee, C., 2009. Investigating the effect of ballasting by $CaCO_3$ in *Emiliania huxleyi*, II: Decomposition of particulate organic matter. Deep-Sea Research II 56, 1408-1419.

Fabrés, J., Calafat, A., Sanchez-Vidal, A., Canals, M., Heussner, S., 2002. Composition and spatio-temporal variability of particle fluxes in the Western Alboran Gyre, Mediterranean Sea. Journal of Marine Systems 33-34, 431-456.

Falkowski, P., Scholes, R. J., Boyle, E., Canadell, J., Canfield, D., Elser, J., Gruber, N., Hi30, bbard, K., Hogberg, P., Linder, S., Mackenzie, F. T., Moore, B., Pedersen, T., Rosenthal,Y., Smetacek, V., Steffen, W., 2000. The global carbon cycle: A test of our knowledge of Earth as a system. Science 290, 291-296.

Fowler, S.W., Knauer, G.A., 1986. Role of large particles in the transport of elements and organic compounds through the oceanic water column. Progress in Oceanography 16, 147-194.

Gardner, W.D., 2000. Sediment trap technology and surface sampling in surface waters. In: Hanson, R.B., Ducklow, H.W., Field, J.G. (Eds.), The Changing Ocean Carbon Cycle, A Midterm Synthesis of the Joint Global Ocean Flux Study. Cambridge University Press, pp. 240-281.

Gust, G., Bowles, W., Giordano, S., Huettel, M., 1996. Particle accumulation in a cylindrical sediment trap under laminar and turbulent steady flow: an experimental approach. Aquatic Sciences 58, 297-326.

Gustafsson, O., Larsson, J., Andersson, P., Ingri, J., 2006. The POC/^{234}Th ratio of settling particles isolated using split flow-thin cell fractionation (SPLITT). Marine Chemistry 100 (3-4), 314-322.

Hamm, C.E., 2002. Interactive aggregation and sedimentation of diatoms and clay-sized lithogenic material. Limnology and Oceanography 47 (6), 1790-1795.

Hansen, J.L.S., Timm, U., Kiørboe, T., 1995. Adaptive significance of phytoplankton stickiness with emphasis on the diatom *Skeletonema costatum*. Marine Biology 123, 667-676.

Harlay, J., Borges, A.V., Van Der Zee, C., Delille, B., Godoi, R.H.M., Schiettecatte, L.-S., Roevros, N., Aerts, K., Lapernat, P.-E., Rebreanu, L., Groom, S., Daro, M.-H., Van Grieken, R., Chou, L., 2010. Biogeochemical study of a coccolithophore bloom in the northern Bay of Biscay (NE Atlantic Ocean) in June 2004. Progress in Oceanography 86, 317-336.

Hill, P.S., 1992. Reconciling aggregation theory with observed vertical fluxes following phytoplankton blooms. Journal of Geophysical Research 97, 2295-2308.

Honjo, S., 1982. Seasonality and interaction of biogenic and lithogenic particulate flux at the Panama Basin. Science 218, 883-884.

Hung, C.-C., Xu, C., Santschi, P.H., Zhang, S.-J., Schwehr, K.A., Quigg, A., Guo, L., Gong, G.-C.,

Pinckney, J.L., Long, R.A., Wei, C.-L., 2010. Comparative evaluation of sediment trap and ^{234}Th-derived POC fluxes from the upper oligotrophic waters of the Gulf of Mexico and the subtropical northwestern Pacific Ocean. Marine Chemistry 121, 132-144.

Hung, C.-C., Gong, G.-C., 2010. POC/^{234}Th ratios in particles collected in sediment traps in the northern South China Sea. Estuarine, Coastal and Shelf Science 88 (3), 303-310.

Iversen, M.H., Ploug, H., 2010. Ballast minerals and the sinking of carbon flux in the ocean: carbon-specific respiration rates and sinking velocity of marine snow aggregates. Biogeosciences 7, 2613-2624.

Jackson, G.A., 1990. A model of the formation of marine algal flocs by physical coagulation processes. Deep-Sea Research Part A. Oceanographic Research Papers 37 (8), 1197-1211.

Jackson, G.A., Lochmann, S., 1993. Modeling coagulation of algae in marine ecosystems. In: Buffle, J. and van Leeuwen, H.P. (Eds.), Environmental Particles, vol. 2. Lewis Publisher, Ann Arbor, pp. 387-414.

Jackson, G.A. (Ed.), 2005. Coagulation theory and models of oceanic plankton aggregation. CRC Press, Boca Raton, FL.

Jackson, G.A., Kiørboe, T., 2008. Maximum phytoplankton concentrations in the sea. Limnology and Oceanography 53 (1), 395-399.

Jin, X., Gruber, N., Dunne, J.P., Sarmiento, J.L., Armstrong, R.A., 2006. Diagnosing the contribution of phytoplankton functional groups to the production and export of particulate organic carbon, $CaCO_3$, and opal from global nutrient and alkalinity distributions. Global Biogeochemical Cycles 20, GB2015.

Kahl, L.A., Vardi, A., Schofield, O., 2008. Effects of phytoplankton physiology on export flux. Marine Ecology Progress Series 354, 3-19.

Karakas, G., Nowald, N., Schäfer-Neth, C., Iversen, M., Barkmann, W., Fischer, G., Marchesiello, P., Schlitzer, R., 2009. Impact of particle aggregation on vertical fluxes of organic matter. Progress in Oceanography 83, 331-341.

Kiørboe, T., Andersen, K.P., Dam, H.G., 1990. Coagulation efficiency and aggregate formation in marine phytoplankton. Marine Biology 107, 235-245.

Kiørboe, T., Hansen, J.L.S., 1993. Phytoplankton aggregate formation: observations of patterns and mechanisms of cell sticking and the significance of exopolymeric material. Journal of Plankton Research 15, 993-1018.

Klaas, C., Archer, D.E., 2002. Association of sinking organic matter with various types of

mineral ballast in the deep sea: Implications for the rain ratio. Global Biogeochemical Cycles 16, 1116.

Kok, D.J., Blomen, L.J.M.J., Westbroek, P., Bijvoet, O.L.M., 1986. Polysaccharide from coccoliths ($CaCO_3$ biomineral): influence on cyrstallization of calcium oxalate monohydrate. European Journal of Biochemistry 158, 167-172.

Kranck, K., Milligan, T.G., 1988. Macroflocs from diatoms: *in situ* photography of particles in Bedford Basin, Nova Scotia. Marine Ecology Progress Series 44, 183-189.

Langer, G., Nehrke, G., Thoms, S., Stoll, H., 2009. Barium partitioning in coccoliths of *Emiliania huxleyi*. Geochemica et Cosmochimica Acta 73, 2899-2906.

Lee, C., Peterson, M.L., Wakeham, S.G., Armstrong, R.A., Cochran, J.K., Miquel, J.C., Fowler, S.W., Hirschberg, D., Beck, A., Xue, J., 2009. Particulate organic matter and ballast fluxes measured using time-series and settling velocity sediment traps in the northwestern Mediterranean Sea. Deep-Sea Research II 56 (18), 1420-1436.

Lepore, K., Moran, S.B., Burd, A.B., Jackson, G.A., Smith, J.N., Kelly, R.P., Kaberi, H. Stavrakakis, S., Assimakopoulou, G., 2009. Sediment trap and *in-situ* pump size-fractionated POC/^{234}Th ratios in the Mediterranean Sea and Northwest Atlantic: Implications for POC export. Deep-Sea Research I 56, 599-613.

Leppard, G.G., 1995. The characterization of algal and microbial mucilage and their aggregates in aquatic ecosystems. Science of the Total Environment 165, 103-131.

Liu, Z., Stewart, G., Cochran, J.K., Lee, C., Armstrong, R.A., Hirschberg, D.J., Gasser, B., Miquel, J.-C., 2005. Why do POC concentrations measured using Niskin bottle collections differ from those using *in situ* pumps? Deep-Sea Research I 52, 1324-1344.

Luo, S., Ku, T.-L., 2004. On the importance of opal, carbonate, and lithogenic clays in scavenging and fractionating ^{230}Th, ^{231}Pa and ^{10}Be in the ocean. Earth and Planetary Science Letters 220, 201-211.

Maiti, K., Benitez-Nelson, C.R., Buesseler, K.O., 2010. Insights into particle formation and remineralization using the short-lived radionuclide, Thorium-234. Geophysical Research Letters 37, L15608.

Martín, J., Palanques, A., Puig, P., 2006. Composition and variability of downward particulate matter fluxes in the Palamós submarine canyon (NW Mediterranean). Journal of Marine Systems 60, 75-97.

McCave, I.N., 1975. Vertical flux of particles in the ocean. Deep-Sea Research 22, 491-502.

McCave, I.N., 1984. Size spectra and aggregation of suspended particles in the deep ocean. Deep-Sea Research 31 (4), 329-352.

McCave, I.N., Hall, I.R., Antia, A.N., Chou, L., Dehairs, F., Lampitt, R.S., Thomsen, L., van Weering, T.C.E., Wollast, R., 2001. Distribution, composition and flux of particulate material over the European margin at 47˚-50˚N. Deep-Sea Research II 48, 3107-3139.

McDonnell, A.M.P., Buesseler, K.O., 2010. Variability in the average sinking velocity of marine particles. Limnology and Oceanography 55 (5), 2085-2096.

Mopper, K., Zhou, J., Ramana, K.S., Passow, U., Dam, H.G., Drapeau, D.T., 1995. The role of surface-active carbohydrates in the flocculation of a diatom bloom in a mesocosm. Deep-Sea Research II 41, 47-73.

Moran, S.B., Charette, M.A., Pike, S.M., Wicklund, C.A., 1999. Differences in seawater particulate organic carbon concentration in samples collected using small-volume and large-volume methods: the importance of DOC adsorption to the filter blank. Marine Chemistry 67, 33-42.

Moran, S.B., Weinstein, S.E., Edmonds, H.N., Smith, J.N., Kelly, R.P., Pilson, M.E.Q., Harrison, W.G., 2003. Does $^{234}Th/^{238}U$ disequilibrium provide an accurate record of the export flux of particulate organic carbon from the upper ocean? Limnology and Oceanography 48, 1018-1029.

Myklestad, S.M., 1995. Release of extracellular products by phytoplankton with special emphasis on polysaccharides. Science of the Total Environment 165, 155-164.

O'Melia, C.R., Tiller, C.L. (Eds.), 1993. Physicochemical aggregation and deposition in aquatic environments. Lewis Publishers, Boca Raton, FL.

Passow, U., Alldredge, A.L., 1995. Aggregation of a diatom bloom in a mesocosm: The role of transparent exopolymer particles (TEP). Deep-Sea Research II 42 (1), 99-109.

Passow, U., 2002. Transparent exopolymer particles (TEP) in aquatic environments. Progress in Oceanography 55, 287-333.

Passow, U., Dunne, J., Murray, J.W., Balistrieri, L., Alldredge, A.L., 2006. Organic carbon to ^{234}Th ratios of marine organic matter. Marine Chemistry 100 (3-4), 323-336.

Peterson, M.L., Hernes, P.J., Thoreson, D.S., Hedges, J.I., Lee, C., Wakeham, S.G., 1993. Field evaluation of a valved sediment trap. Limnology and Oceanography 38, 1741-1761.

Peterson, M.L., Wakeham, S.G., Lee, C., Askea, M., Miquel, J.C., 2005. Novel techniques for collection of sinking particles in the ocean and determining their settling rates. Limnology and Oceanography Methods 3, 520-532.

Riebesell, U., Wolf-Gladrow, D.A., 1992. The relationship between physical aggregation of

phytoplankton and particle flux: a numerical model. Deep-Sea Research 39 (7/8), 1085-1102.

Riemann, F., 1989. Gelatinous phytoplankton detritus aggregates on the Atlantic deep-sea bed: Structure and mode of formation. Marine Biology 100, 533-539.

Rodriguez y Baena, A.M., Fowler, S.W., and J.C. Miquel, 2007. Particulate organic carbon: natural radionuclide ratios in zooplankton and their freshly produced fecal pellets from the NW Mediterranean (MedFlux 2005). Limnology and Oceanography 52 (3), 966-974.

Savoye, N., Benitez-Nelson, C., Burd, A.B., Cochran, J.K., Charette, M., Buesseler, K.O., Jackson, G.A., Roy-Barman, M., Schmidt, S., Elskens, M., 2006. ^{234}Th sorption and export models in the water column: A review. Marine Chemistry 100 (3-4), 234-249.

Schmidt, S., Andersen, V., Belviso, S., Marty, J.-C., 2002. Strong seasonality in particle dynamics of north-western Mediterranean surface waters as revealed by ^{234}Th/^{238}U. Deep-Sea Research I 49 (8), 1507-1518.

Silver, M.W., Gowing, M.M., 1991. The particle flux and biological components. Progress in Oceanography 26, 75-113.

Smith, J.N., Moran, S.B., Speicher, E.A., 2006. On the accuracy of upper ocean particulate organic carbon export fluxes estimated from ^{234}Th/^{238}U disequilibrium. Deep-Sea Research I 53 (5), 860-868.

Speicher, E.A., Moran, S.B., Burd, A.B., Delfanti, R., Kaberi, H., Kelly, R.P., Papucci, C., Smith, J.N., Stavrakakis, S., Torricelli, L., Zervakis, V., 2006. Particulate organic carbon export fluxes and size-fractionated POC/^{234}Th ratios in the Ligurian, Tyrrhenian and Aegean Seas. Deep-Sea Research I 53, 1810-1830.

Steinberg, D.K., Van Mooy, B.A.S., Buesseler, K.O., Boyd, P.W., Kobari, T., Karl, D.M., 2008. Bacterial vs. zooplankton control on sinking particle flux in the ocean's twilight zone. Limnology and Oceanography. 53 (4), 1327-1338.

Stemmann, L., Gorsky, G., Marty, J.-C., Picheral, M., Miquel, J.-C., 2002. Four-year study of large-particle vertical distribution (0-1000m) in the NW Mediterranean in relation to hydrology, phytoplankton, and vertical flux. Deep-Sea Research II 49 (11), 2143-2162.

Trull, T., Buesseler, K., Bray, S., Moy, C., Ebersbach, F., Lamborg, C., Pike, S., Manganini, S., 2008. *In-situ* measurement of mesopelagic particle sinking rates and the control of carbon transfer to the ocean interior during the Vertical Flux in the Global Ocean (VERTIGO) voyages in the North Pacific. Deep-Sea Research II 55 (14-15), 1684-1695.

van Duuren, F.A., 1968. Defined velocity gradient model flocculator. Journal of the Sanitary Engineering Division: Proceedings of the American Society of Civil Engineers 94, 671-682.

Waite, A.M., Hill, P.S., 2006. Flocculation and phytoplankton cell size can alter ^{234}Th-based estimates of the vertical flux of particulate organic carbon in the sea. Marine Chemistry 100 (3-4), 366-375.

Wakeham, S.G., Lee, C., 1993. Production, transport, and alteration of particulate organic matter in the marine water column. In: Engel, M.H., Macko, S.A. (Eds.), Organic geochemistry. Plenum Press, pp. 145-169.

Waples, J.T., Benitez-Nelson, C., Savoye, N., Rutgers van der Loeff, M., Baskaran, M., Gustafsson, O., 2006. An introduction to the application and future use of ^{234}Th in aquatic systems. Marine Chemistry 100 (3-4), 166-189.

Xue, J., Armstrong, R.A., 2009. An improved "benchmark" method for estimating particle settling velocities from time-series sediment trap fluxes. Deep-Sea Research II 56, 1479-1486.

CHAPTER 2

Particulate organic carbon–^{234}Th relationships in particles separated by settling velocity in the northwest Mediterranean Sea

J. Szlosek[a], J.K. Cochran[a], J.C. Miquel[b], P. Masqué[c], R.A. Armstrong[a], S.W. Fowler[a,b], B. Gasser[2], D.J. Hirschberg[a]

[a]Marine Sciences Research Center, Stony Brook University, Stony Brook, NY 11794-5000, USA

[b]Marine Environmental Laboratories, International Atomic Energy Agency, MC98000 Monaco

[c]Institut de Ciència i Tecnologia Ambientals–Departament de Física, Universitat Autònoma de Barcelona, 08193 Bellaterra, Spain

Szlosek, J., Cochran, J.K., Miquel, J.C., Masqué, P., Armstrong, R.A., Fowler, S.W., Gasser, B., Hirschberg, D.J., 2009. Particulate organic carbon-^{234}Th relationships in particles separated by settling velocity in the northwest Mediterranean Sea. Deep-Sea Research II 56, 1519-1532.

Abstract

In order to better understand the relationship between the natural radionuclide ^{234}Th and particulate organic carbon (POC), marine particles were collected in the northwestern Mediterranean Sea (spring/summer, 2003 and 2005) by sediment traps that separated them according to their *in situ* settling velocities. Particles also were collected in time-series sediment traps. Particles settling at rates of >100 m d^{-1} carried 50% and 60% of the POC and ^{234}Th fluxes, respectively, in both sampling years. The POC flux decreased with depth for all particle settling velocity intervals, with the greatest decrease (factor of ~2.3) in the slowly settling intervals (0.68–49 m d^{-1}) over trap depths of 524–1918 m, likely due to dissolution and decomposition of material. In contrast the flux of ^{234}Th associated with the slowly settling particles remained constant with depth, while ^{234}Th fluxes on the rapidly settling particles increased. Taking into account decay of ^{234}Th on the settling particles, the patterns of ^{234}Th flux with depth suggest that either both slow and fast settling particles scavenge additional ^{234}Th during their descent or there is significant exchange between the particle classes. The observed changes in POC and ^{234}Th flux produce a general decrease in POC/^{234}Th of the settling particles with depth. There is no consistent trend in POC/^{234}Th with settling velocity, such as might be expected from surface area and volume considerations. Good correlations are observed between ^{234}Th and POC, lithogenic material and $CaCO_3$ for all settling velocity intervals. Pseudo-K_ds calculated for ^{234}Th in the shallow traps (2005) are ranked as lithogenic material ≤opal <calcium carbonate <organic carbon. Organic carbon contributes ~33% to the bulk K_d, and for lithogenic material, opal and $CaCO_3$, the fraction is ~22% each. Decreases in POC/^{234}Th with depth are accompanied by increases in the ratio of ^{234}Th to lithogenic material and opal. No change in the relationship between ^{234}Th and $CaCO_3$ was evident with depth. These patterns are consistent with loss of POC through decomposition, opal through dissolution and additional scavenging of ^{234}Th onto lithogenic material as the particles sink.

1. Introduction

Thorium-234, a particle-reactive radionuclide, is a useful tracer of particle export on short time scales of days to months ($t_{1/2}$ = 24.1 d) (Coale and Bruland, 1985). The

disequilibrium between ^{234}Th and its parent, ^{238}U, results from rapid hydrolyzation of the ^{234}Th atoms and their adsorption to surface sites of particles (Bruland and Coale, 1986). This scavenging process leads to a deficit of ^{234}Th relative to its parent ^{238}U, which can be used to determine the flux of thorium out of the upper ocean water column by the following equation

$$P_{Th} = \lambda \int_{z_2}^{z_1} \left(A_U - A_{Th,tot} \right) dz \quad (1)$$

where P_{Th} is the overall flux of ^{234}Th removed from the depths z_1 to z_2 by the flux of particles. The ^{234}Th decay constant is λ (0.0288 d^{-1}), A_U is the activity of ^{238}U, and $A_{Th,tot}$ is the total activity of ^{234}Th (Buesseler et al., 1992). The export flux of carbon P_{POC}, through depth z_2 can be calculated as (Buesseler et al., 1992):

$$P_{POC} = \frac{POC}{^{234}Th_p} P_{Th} \quad (2)$$

where $POC/^{234}Th_p$ is the ratio of POC to ^{234}Th on particles settling through depth z_2. Measurements of ^{234}Th/^{238}U disequilibrium and the POC/^{234}Th ratio of sinking particulate matter in the upper ocean have been used increasingly in oceanographic field programs to estimate the downward flux of particulate organic carbon (POC) from the euphotic zone (see reviews by Cochran and Masqué, 2003; Buesseler et al., 2006). It is clear that the POC/^{234}Th ratio (hereafter referred as C/^{234}Th) of marine particles can vary significantly in space and time due to changes in biological productivity, particle export, particle size distribution, and acid polysaccharide content of sinking particles. Developing a quantitative understanding of the processes controlling the variability in C/^{234}Th ratios of marine particles is thus essential for validating the use of ^{234}Th to estimate POC fluxes from the surface ocean (Moran et al., 2003; Buesseler et al., 2006).

The MedFlux program used indented rotating sphere (IRS) sediment traps to collect particles separated by their *in situ* settling velocities. The traps were programmed such that the carousel collected particles separated into 11 settling velocity intervals ranging from ~0.7 to >980 m d^{-1} throughout the trap deployment (Peterson et al., 2005, 2009). The IRS sediment traps in settling velocity (SV) mode were deployed along with IRS sediment traps operated in a in time-series (TS) mode in 2003 and 2005 at the French JGOFS time-series site, DYnamique des Flux Atmosphérique en MEDiterrannée (DYFAMED).

Here we present C/^{234}Th data for samples collected by sediment traps operated in TS and SV sampling modes. Our goal is to assess sources of variability for the C/^{234}Th in different settling velocity intervals. Samples were collected from the bottom of the euphotic zone during two spring phytoplankton bloom periods in 2003 and 2005, respectively. In 2005, additional traps were deployed at mid- and deep-water depths to evaluate the variability in the C/^{234}Th ratio with particle settling velocity, chemical composition, and depth.

2. Methods

2.1. Sample Collection

MedFlux sampling occurred at the French JGOFS time-series site, DYFAMED (43°25'N, 7°52'E; water depth ~2300 m), located in the Ligurian Sea, northwest Mediterranean. Further information on the region is included in the Preface of this volume (Lee et al., 2009). Collection techniques included large volume *in situ* pumps, moored swimmer-exclusion (IRS) sediment traps, and a large floating sediment trap, or NetTrap, used to collect fresh, sinking particles below the euphotic zone (Peterson et al., 2009).

2.1.1. Sediment Traps

Time-series (TS) traps were deployed from 6 March to 6 May 2003 with cups collecting over 5- to 6-day time intervals and from 4 March to 1 May 2005 with 5-day time intervals. Particles with settling velocities from 0.68 to >980 m d^{-1} were separated into 11 settling velocity intervals (Table 2.1); the intervals were slightly different in 2003 and 2005. Carousel rotation times were changed in 2005 to better resolve material flux shifts in the faster settling velocities. Further details on the operation of the IRS traps in a settling velocity mode have been given in Peterson et al. (2005). A single mooring was used in each deployment period such that time-series and duplicate settling velocity traps were deployed on the same array. Of the two SV traps (SV1 and SV2) deployed at 313 m in 2005, SV1 was contaminated; consequently only data from SV2 will be discussed. The duplicate SV traps at both 524 and 1918 m in 2005 operated successfully and allowed us to evaluate reproducibility.

The intended trap deployment depths were 200 m in 2003 and 2005 as well as 400 and 1800 m in 2005. Actual trap depths were 238 m in 2003 and 313, 524, and 1918 m in 2005. Deployment depths were corrected for the mooring wire angle by using information provided by current meters mounted on each array. Mean current velocities at the shallow traps were 4.5 cm s^{-1} (238 m) and 12 cm s^{-1} (313 m) in 2003 and 2005, respectively (Cochran et al., 2009).

TS and SV trap sampling tubes were split for chemical characterization using a McLane™ WSD splitter. One split was filtered on 0.4 μm Nuclepore filters for determination of ^{234}Th and another was filtered onto Whatman GF/F filters for measurement of POC. Other splits were taken for organic composition (Wakeham et al., 2009), ballast minerals (Lee et al., 2009), and mass flux (Armstrong et al., 2009).

The length of the sediment trap deployments necessitated the use of poisons to prevent bacterial decomposition of the captured samples. Sampling tubes were poisoned with mercuric chloride by a small poison diffuser containing 0.5 g NaCl and 14 mg $HgCl_2$ as described in Peterson et al., (2005). A recent study by Liu et al. (2006) has shown that the use of $HgCl_2$ as a poison affects the total abundance of organic matter and the composition of many classes of organic compounds by abiotic oxidation and dissolution. ^{234}Th could be desorbed from particles due to the increased ionic strength of the mercuric chloride brine. However, ^{210}Po was measured in the overlying water of each sampling tube in 2003 and none was detected (Stewart et al., 2007a). We conclude on this basis that there was little release of ^{234}Th due to the trap poison.

2.2. Sample Analyses

2.2.1. ^{234}Th Activity

Non-destructive beta counting was used to measure ^{234}Th activities of the particulate fractions. Filter material was mounted for beta counting according to the methods of Buesseler et al. (1998) and Cochran et al. (2000, 2009). The beta counting efficiency (0.41 ± ~5%) was determined by evaporating an aliquot of ^{238}U (with ^{234}Th in equilibrium) onto filters mounted in the same manner as the samples. Filters were counted over 2 half-lives of ^{234}Th ($t_{1/2}$ = 24.1 days). Errors include the 1σ counting error and appropriate calibration errors.

2.2.2. Decay Correction of SV Trap ^{234}Th Data

^{234}Th activities must be corrected for decay from the time of measurement to that of collection. For the time-series traps, this correction is straightforward because the collection interval is small compared with the half-life of ^{234}Th. In the case of the settling velocity traps, the material collected for each settling velocity interval may have entered the trap uniformly throughout the deployment or at anytime during the trap deployment. For a sediment trap collecting particles over a long time interval relative to the half-life of ^{234}Th, the standard method of decay correction, assuming a constant flux of ^{234}Th during the collection interval, is to calculate the effective time during the deployment to which the activity must be corrected (Spencer et al. 1978). If t_1 is the start of the deployment and t_2 is the recovery, the effective "mid-point" of the deployment for decay correction of ^{234}Th activities is $t_1 + \Delta t$, where

$$\Delta t = -\frac{1}{\lambda}\ln\left[\frac{1-e^{-\lambda(t_2-t_1)}}{\lambda(t_2-t_1)}\right] \quad . \tag{3}$$

Sample ^{234}Th activities are generally measured some time after trap recovery, but can readily be corrected for decay from measurement to trap recovery (t_2). The appropriate factor (F) by which activities at trap recovery should be multiplied for decay correction is then

$$F = 1/e^{-\lambda(T-\Delta t)} \tag{4}$$

where $T = t_2 - t_1$. This correction was applied erroneously in Spencer et al. (1978) because they corrected radionuclide activities at the time of trap recovery by a factor of $1/e^{-\lambda\Delta t}$ rather than the formulation in Eq. 4

For the shallow traps in 2003 and 2005, we have time-series records of the ^{234}Th flux that clearly show variation throughout the SV trap deployments (Figs. 2.1, 2.2). Thus an alternate approach is to use the variation in ^{234}Th flux with time as recorded in the TS traps to calculate a correction factor (F) that can be applied to the SV trap samples. We

determine F by applying a decay-weighted averaging procedure to the TS trap record:

$$F = \frac{\sum_i \frac{dpm_i}{e^{-\lambda \Delta t_i}}}{\sum_i dpm_i} \quad (5)$$

where dpm_i is the activity in TS cup i at the time of trap recovery, λ is the decay constant for ^{234}Th and Δt_i is the time between recovery and the midpoint of TS cup i. This procedure assumes that the temporal pattern of ^{234}Th flux as recorded in the time-series trap was the same for all the settling velocity fractions. If the ^{234}Th flux is constant with time, Eq. 5 yields results identical to Eq. 4.

The two methods give decay correction factors that agree to within ~10%. The correction factors assuming constant flux into the SV trap (Eq. 4) were 2.72 and 2.44 for 2003 and 2005, respectively. The correction factors calculated taking the TS temporal variation of ^{234}Th flux into account (Eq. 5) were 2.91 and 2.73 for 2003 and 2005, respectively. Time-series traps deployed with the deep SV traps (524 m, 1918 m) in 2005 did not function, and, in correcting the deep trap ^{234}Th data for decay, we have assumed that the temporal variation in ^{234}Th flux observed in the shallow trap applied at depth as well. In fact, ^{234}Th data from a TS trap deployed at 924 m in 2005 gave a decay-correction factor (Eq. 5) of 2.52, in reasonably good agreement with that from the 313 m trap (F = 2.73). In reporting the SV trap ^{234}Th data (Table 2.1) for 2003 and 2005, we use the decay-correction factors derived from Eq. 5 applied to the shallow TS traps in each year. If information is lacking on variations in ^{234}Th flux coincident with the collection of particles in SV traps, decay-correction factors for ^{234}Th must be calculated using Eqns. 3 and 4.

We checked the validity of using Eq. 5 for decay correction by comparing the total ^{234}Th dpm captured in the SV trap to that of the TS traps at the same depths. In 2003 the time-integrated decay-corrected ^{234}Th fluxes in the SV traps were 36.7 × 10^3 dpm m^{-2} and 45.9 × 10^3 dpm m^{-2} for SV1 and SV2, respectively (Table 2.1). For SV1 and SV2 these were factors of ~0.7 and ~0.8, respectively, less than the time-integrated ^{234}Th flux measured in the TS trap (51.7 × 10^3 dpm m^{-2}). However, the SV traps also accumulated less total mass of material than did the TS trap, by factors of ~0.8 and ~0.9 for SV1 and SV2, respectively. Thus perhaps the differences in the integrated ^{234}Th activity among the TS and SV traps

may be due, in part, to variability in the fluxes entering duplicate traps at a single depth. Offsets between the TS and SV traps at 313 m also were evident in 2005; the integrated ^{234}Th and mass fluxes in the SV trap were 1.1 and 1.4 times, respectively, those of the TS trap. We conclude that these differences are principally related to the ability of traps operated in different modes at the same depth to capture comparable fluxes and particle types.

2.2.3. POC Measurements

Prior to POC analyses, inorganic carbon was removed by fuming the samples with concentrated HCl. Two replicate splits of the trap material collected in each sample tube for both the TS and SV traps were designated for POC and total carbon (TC) measurements. The trap splits were filtered onto combusted GF/F filters. POC and TC were measured on all punches using a Carlo Erba model 1602 CNS analyzer. All carbon measurements were blank-corrected and had an error of ±5%.

3. Results

3.1. ^{234}Th and OC Fluxes in Shallow Time–Series Traps–2003 and 2005

During the first two weeks of the 2003 trap deployment, the OC flux was nearly 3 times higher than the trap time-weighted average of 2.3 mmol m^{-2} d^{-1} (Fig. 2.1a; Table 2.1). The maximum OC flux coincided with a period of high sea surface chlorophyll observed by satellite (see Lee et al., 2009). OC flux then decreased, dropping an order of magnitude by DOY 90. Mass flux generally followed OC flux patterns, with maximum values of ~1000 mg m^{-2} d^{-1} (Lee et al., 2009). Correspondingly, ^{234}Th flux followed the temporal trends of OC flux (Fig. 2.1a).

Similar to 2003, ^{234}Th and OC fluxes in the shallow trap in 2005 were highest at the beginning of the trap deployment period (Fig. 2.2a). The time-weighted average OC flux was 1.3 mmol m^{-2} d^{-1}. Mass flux peaked at ~900 mg m^{-2} d^{-1}, and again the pattern in the OC flux with time mirrored that of mass flux. The range of ^{234}Th flux values over the 55-day deployment was comparable to that in 2003 (Fig. 2.2a; Table 2.1). The average ^{234}Th flux for the spring 2005 deployment was approximately equivalent to that in 2003 (~1200 dpm m^{-2} d^{-1}), whereas the average OC flux was a factor of 2 smaller.

3.2. C/^{234}Th Ratios in Time-Series Traps

C/^{234}Th ratios did not vary significantly with time in 2003 (Fig. 2.1b). Values ranged from 1.8 ± 0.2 and 3.6 ± 0.2 μmol dpm^{-1} with a time-weighted average of 2.8 ± 0.1 μmol dpm^{-1} (Table 2.1). Conversely, the C/^{234}Th ratio of the 2005 313 m TS trap demonstrated a marked change over the trap deployment. During the first half of the deployment (DOY 65–90) there was little variation in the C/^{234}Th, averaging 0.9 ± 0.01 μmol dpm^{-1}; however, after DOY 90 the C/^{234}Th steadily increased (Fig. 2.2b). Over the 55-d deployment the C/^{234}Th ratios ranged from 0.8 ± 0.02 to 4.1 ± 0.4 μmol dpm^{-1} and the time-weighted average C/^{234}Th ratio for the entire deployment was 1.1 ± 0.03 μmol dpm^{-1} (Table 2.1). The mean TS trap C/^{234}Th values in 2003 and 2005 were lower than prior trap-derived C/^{234}Th measurements made at the DYFAMED site (4.9 ± 0.2 – 7.8 ± 0.3 μmol dpm^{-1}; Schmidt et al., 2002).

3.3. Fluxes in Settling Velocity Traps

The SV trap collects material for the settling velocity intervals throughout the duration of the trap deployment. Calculation of an average flux in each settling velocity interval is not possible because of uncertainty in the constancy of the flux with time. Different settling velocity intervals were used in 2005 than in 2003 to increase the resolution of the faster settling velocity intervals where fluxes were greatest in 2003, but this made it difficult to compare directly the results from the two years. To facilitate the analysis of SV trap data from both years and different depths we use a calculated parameter referred to as the time-integrated flux density (FD; see Armstrong et al., 2009). Used in the sense of "probability density", the FD indicates the probability or frequency that part of the total trap flux fell at a rate a specified settling velocity interval. We define FD as the time-integrated flux (the amount of a chemical constituent per square meter integrated over the trap deployment period; e. g., mmol C m^{-2} or dpm ^{234}Th m^{-2}) for an individual SV sediment trap sampling tube divided by the settling velocity interval (SVI_i) for that sampling tube. The unit-less quantity of the settling velocity interval (SVI_i) is the log of the maximum settling velocity – log of the minimum settling velocity ($SVI_i = \log(SV_{max,i}) - \log(SV_{min,i})$) for each settling

velocity interval, *i*. This normalized flux, FD, allows one to compare how the total flux is distributed over the spectrum of settling velocities in different years from observing the box heights as seen in Figs. 2.3 and 2.4. Furthermore, one may examine the total trap flux between years by comparing the summed areas of all boxes, which represent the time-integrated fluxes over the period of deployment. The OC and ^{234}Th time-integrated fluxes will henceforth be referred to as the OC_i and $^{234}Th_i$ where *i* designates the settling velocity interval and the units are the total mmol C m^{-2} or total dpm ^{234}Th m^{-2} captured in that settling velocity interval over the whole trap deployment (Table 2.1).

In 2003 and 2005, ~ 50% of the OC in the shallow traps (238 m and 313 m) settled at rates ≥ 100 m d^{-1} (Figs. 2.3a,b). Similarly, a large portion of the ^{234}Th settled at rates > 100 m d^{-1} for both years. The >100 m d^{-1} portion of the settling velocity spectrum had 57% and 69% of the ^{234}Th in the 2003 SV1 and SV2 traps, respectively, and 59% of the ^{234}Th in the 2005 shallow SV trap (Figs. 2.4a,b). The greatest proportion of OC and ^{234}Th fell within the settling velocity range of 196–490 m d^{-1}. This settling velocity interval contained nearly 26% (SV1 only) and ~24% of the total OC for 2003 and 2005, respectively, and 30–40% of the ^{234}Th (Table 2.1). In 2003 and 2005, the OC FD loosely followed the mass FD trends with settling velocity (Lee et al., 2009; Armstrong et al., 2009).

3.4. Variation of C/^{234}Th with Settling Velocity in Shallow SV Traps–2003 and 2005

The C/^{234}Th ratios of the shallow SV traps of 2003 and 2005, did not demonstrate a discernable trend with settling velocity (Figs. 2.5a and b, respectively, Table 2.1). The weighted average C/^{234}Th in 2003 was 3.4 ± 0.1 for SV1 (Table 2.1). Ignoring the maximum at 98–196 m d^{-1} for 2003 SV1, the C/^{234}Th ratios of individual settling velocity intervals varied less than 30% in 2003 and in 2005. The weighted average C/^{234}Th for 2005 (1.2 ± 0.03 μmol dpm^{-1}) agreed well with the time-weighted average for the TS trap deployed on the same array (1.1 ± 0.03 μmol dpm^{-1}) and was a factor of ~3 less than the weighted average values for 2003. In 2005, there was no single settling velocity interval that demonstrated a clear peak in the C/^{234}Th ratio as was seen in 2003 (Figs. 2.5a,b). Moreover, the settling velocity intervals covering the range of 98–196 m d^{-1} generally had

lower C/^{234}Th ratios in 2005, possibly indicating compositional differences between the 2003 and 2005 fast settling particles.

3.5. Variation of OC, ^{234}Th and C/^{234}Th in SV Traps with Depth (2005)

In 2005, 60% of the time-integrated OC flux (OC_i) occurred in the fast settling velocity intervals at 313, 524, and 1918 m (Fig. 2.6a). The probability that material will settle at intermediate settling velocities drops sharply at velocities lower than 326–490 m d^{-1} and 196–326 m d^{-1} for the shallowest trap (Table 2.1). The total OC collected in each trap decreased with depth (Table 2.1).

As with OC flux density, the ^{234}Th flux densities were high at settling velocities of 196–980 m d^{-1}, and decreased within the intermediate settling velocity intervals. Conversely, there was a slight increase in the ^{234}Th FD within the slowest settling velocity intervals (Fig. 2.6b). The time-integrated ^{234}Th flux ($^{234}Th_i$) at 1918 m was higher (mean 104 × 10^3 dpm m^{-2}) than those at 313 m and 524 m (both ~80 × 10^{3}dpm m^{-2}), largely due to higher ^{234}Th FDs in the faster settling velocity intervals at 1918 m relative to the other depths (Table 2.1). The weighted average C/^{234}Th decreased with depth, with values of 1.2 ± 0.03 μmol dpm^{-1}, 0.96 ± 0.02 μmol dpm^{-1}, 0.47 ± 0.01 μmol dpm^{-1} at 313, 524, and 1918 m, respectively (Table 2.1; Fig. 2.6c). Some overlap was evident in a few SV intervals at 313 m and 524 m, while the C/^{234}Th ratios at 1918 m were generally lower than those at the shallower depths in all size classes (except the most rapidly settling; Fig. 2.6c).

4. Discussion

4.1. Controls on C/^{234}Th Variation with Settling Velocity in Shallow Traps

There is no clear trend of C/^{234}Th with settling velocity in the shallow traps in either 2003 or 2005 (Figs. 2.5a,b). The C/^{234}Th ratio might be expected to increase with increasing settling velocity, if settling velocity increases with particle dimension and if POC correlates with particle volume while ^{234}Th correlates with surface area. However, increases in C/^{234}Th with settling velocity are not evident in the data (other than increases from the 0.7–5.4 m d^{-1} to the 5.4–11 m d^{-1} interval and from the 490–980 m d^{-1} to the >980 m d^{-1} interval, indicated by the arrows in Fig. 2.6c). Instead, particle composition and type are the dominant factors in controlling C/^{234}Th in the shallow traps. Additional factors

related to changes in C and ^{234}Th as particles settle through the water column affect C/^{234}Th in the deeper SV traps (see below). Organic compositional data show that the slowly settling particles in 2003 were bacterially reworked material, while the rapidly settling material consisted of fecal pellets and fresh and aggregated diatoms (Wakeham et al., 2009). These basic differences in particle type will affect the C/^{234}Th ratio; fecal pellets will have low ratios (Rodriguez y Baena et al., 2007), while fresh phytoplankton will tend to have higher ratios. Indeed, Stewart et al. (2007b) noted a consistent variation in C/^{234}Th (as well as C/^{210}Po) with particle type in the 2003 time-series trap at 238 m, with the ratios varying in the sequence: fresh phytoplankton > degraded material > fecal pellets. In the time-series trap, these variations are displayed with time as the bloom progresses. The SV traps sort the particles into settling velocity intervals throughout the deployment, but to the extent that fresh and degraded material and fecal pellets have different settling velocities, the trends seen in the TS trap are preserved in the SV trap as the settling particles are sorted into settling velocity intervals.

Organic compositional analyses of material from the 2005 traps are not complete, but visual observations of the material suggest fewer diatoms and gelatinous zooplankton and more crustacean zooplankton relative to 2003. These differences are consistent with lower C/^{234}Th ratios in 2005 relative to 2003 (Fig. 2.5a,b).

4.2. Effect of Changes in OC with Depth on C/^{234}Th of Settling Particles

Recent publications reviewing the use of ^{234}Th as a POC export proxy have addressed a number of possible sources for C/^{234}Th variability (e.g., Cochran and Masqué, 2003; Moran et al., 2003; Buesseler et al. 2006). These include preferential loss or uptake of POC, degradation of the particles, decrease in the volume to surface area (V:SA) of sinking particles, and preferential adsorption of ^{234}Th by acidic polysaccharides (Buesseler et al., 1995, 2006; Burd et al., 2000; Quigley et al., 2002; Moran et al., 2003; Passow et al., 2006; Santschi et al., 2006). We are able to consider some of these possibilities using the 2005 SV data at 313, 524, and 1918 m. To our knowledge, these data comprise the first record in the literature of changes with depth in the chemical composition of particles separated according to settling velocity.

The time-integrated flux densities for OC (Fig. 2.6a) are similar for the shallow traps (313 m and 524 m) at fast settling velocities (98–980 m d^{-1}). Between 313 m and 524 m there is relatively little change in flux of OC with depth in the rapid settling velocity intervals (Fig. 2.6a). This may indicate that when material is settling at fast rates, significant alteration of material by degradation does not occur over depths of ~200 m. Between the 524 m and 1918 m traps, there is a 25–36% decrease in OC_i for the four settling velocity intervals in the range of 140–980 m d^{-1} (Fig. 2.6a, Table 2.1). The %OC on a mass basis decreases by a factor of ~1.6 from 524 to 1918 m for these settling velocity intervals. Indeed, the decrease of bulk OC with depth observed in this study has been documented previously in sediment traps from the DYFAMED site (Miquel et al., 1994).

OC decreases significantly within the four settling velocity intervals of 10.9–21.8 to 49–98 m d^{-1} progressively over the three trap depths (313, 524, and 1918 m; Fig. 2.6a, Table 2.1); the average change in OC_i in these settling velocity intervals from 313 m to 524 m is ~ 3 mmol C m^{-2} and from 524 to 1918 m is ~2 mmol C m^{-2}. The %OC of the 10.9–98 m d^{-1} settling velocity intervals also decreased with depth by a factor of ~1.5 for both depth intervals of 313–524 m and 524–1918 m. As stated previously, the limited number of samples (duplicates at only two depths: 524 and 1918 m) does not allow confidence intervals to be placed on the change in time-integrated OC flux with depth. However, it is likely some of the OC decrease was due to dissolution of POC as a consequence of cell death as material is exported and undergoes disaggregation and re-aggregation within the water column (Lee et al., 2009). Goutx et al. (2007) also show significant loss of C from slowly settling particles collected at the DYFAMED site in 2003.

The loss of OC from the settling particles is accompanied by a decrease in the C/^{234}Th ratio with depth (Fig. 2.6c). Processes of aggregation, disaggregation and fragmentation, dissolution and degradation of sinking particles can partly explain the decreases in %OC and C/^{234}Th (Fig. 7A). Through the mesopelagic (or "Twilight Zone") organic matter may become the limiting factor in the aggregate matrix, maintaining the role of a glue such that when the aggregate is saturated or reaches its carrying capacity (Passow, 2004; Hamm, 2003; De La Rocha and Passow, 2006), it is disrupted by the impinging force of shear erosion resulting from the particle's fall (Hill, 1998). This possible mechanism is consistent with our observations from MedFlux as well as the "ballast hypothesis" (Armstrong et al.,

2002; Klaas and Archer, 2002). A more extensive discussion of the mechanisms controlling the relationship between OC and ballast minerals is found in this issue in Lee et al. (2009) and Armstrong et al. (2009).

Mechanisms for the decrease in OC FD in slowly settling particles with depth include incorporation into particles settling at faster rates and loss to the DOC and DIC pools by dissolution or degradation (Fig. 2.7a). There also may be significant losses of POC from the fast settling particles between the 524 m and 1918 m traps caused by disaggregation of the material into smaller particles settling at lower rates. Admittedly, Fig. 2.7a is an oversimplification of the many biotic and abiotic processes involved in altering the absolute abundances of OC associated with sinking particles. However, collection of particles separated by settling velocity is a critical first step in modeling the rates of processes shown in Fig. 2.7a.

4.3. Effect of Changes in ^{234}Th with Depth on C/^{234}Th of Settling Particles

Unlike the decreases observed in OC FDs of the fast settling material (98–980 m d^{-1}) with depth, the ^{234}Th FD is highest at 1918 m (Fig. 2.6b). At the slower settling velocities (<98 m d^{-1}), there is no change in ^{234}Th flux density with depth, also in contrast to the pattern in OC (Fig. 2.6a,b). A simplified conceptual model of the processes affecting ^{234}Th in settling particles is shown in Fig. 2.7b. In addition to transformations among particle settling velocity intervals (mediated by aggregation and disaggregation; β_1 and β_{-1} in Fig. 2.7b) that affect both OC and ^{234}Th, thorium is also subject to additional scavenging and decay as particles settle.

The topic of ^{234}Th decay on particles has received recent attention in the context of its effect on the POC/^{234}Th ratios of filterable particles used to calculate the POC export from the surface (Cai et al., 2006). Cai et al. (2006) observe various trends in POC/^{234}Th with size in filterable particles that they attribute to ^{234}Th decay. Our settling velocity data allow us to assign times for transit of particles to depth and thus estimate directly the effect of decay on the ^{234}Th of the settling particles. Particles in the settling velocity intervals <49 m d^{-1} (0.7–5.44, 5.44–10.9, 10.9–21.8, and 21.8–49 m d^{-1}) demonstrate no change in ^{234}Th with depth (Fig. 2.6b) These particles would take 28–1991 days to transit the distance between the 524 and 1918 m traps and should show significant ^{234}Th decay. The fact that the ^{234}Th

activity is constant with depth suggests that other processes must add ^{234}Th to these particle classes as they settle. Such processes include additional scavenging of ^{234}Th (via adsorption), the addition of material and associated ^{234}Th from the more rapid settling velocity intervals (disaggregation), and the incorporation of high molecular weight dissolved organic material (>10 kDa) that is rich in acidic polysaccharides and associated thorium (Quigley et al., 2002, 2006; Passow et al., 2006, Santschi et al., 2006; Fig. 7A, B). Given the very large effect of decay on these slowly settling particles, the lack of change in ^{234}Th activity with depth implies that disaggregation of large, rapidly settling particles (β_1 Fig. 2.7b) or additional scavenging of ^{234}Th by the slowly settling particles (k_1 in Fig. 2.7b) are important.

In contrast, little change due to decay would be expected for the rapidly settling particles. Assuming a mean settling rate of ~600 m d^{-1} for the fast settling velocities (196–980 m d^{-1}), radioactive decay would cause reductions of less than 10% in the ^{234}Th activity between 524 and 1918 m, yet the time-integrated flux density of ^{234}Th in the rapidly settling particles increases by a factor of ~1.3 between 524 and 1918 m (Fig. 2.6b). If the change is due entirely to scavenging of ^{234}Th, the increase in the integrated flux of the rapidly settling particles with depth (~23 × 10^3 dpm m^{-2}) is equivalent to the removal of ~0.01 dpm ^{234}Th l^{-1} during the trap deployment, if the particles scavenge continuously over the ~1400 m between the traps. This is a small fraction of the total ^{234}Th present in the deep water at the DYFAMED site (~2.7 dpm l^{-1}; Cochran et al., 2009) and the scavenging would not be apparent in water column profiles of ^{234}Th.

Although advective transport of particles carrying ^{234}Th from long distances into the vicinity of deep traps is unlikely due to the prevailing currents at the DYFAMED site, it is important also to consider this as a possible mechanism for increasing ^{234}Th in material caught in deep traps. The DYFAMED site is generally regarded as being uninfluenced by coastal waters, and it has been suggested that the particle variability is predominantly driven by local climate effects and phytoplankton growth in the surface waters because a geostrophic front cuts off coastal inputs (Béthoux et al., 1998; Millot, 1999; Stemmann et al., 2002). Schröder et al. (2006) showed that infiltration of the deep eastern Mediterranean water did not occur at the DYFAMED site in 2005. Lateral transport of a

nepheloid layer would provide additional particle surfaces for ^{234}Th adsorption, but such a feature is uncommon at the DYFAMED site (Stemmann, 1998).

Despite this, the influence of lateral transport on Th profiles and fluxes at the DYFAMED site may wax and wane depending on variations in the intensity of seasonal export events (Cochran et al., this issue). Also, a large "statistical funnel" (Siegel et al., 1990) influences the deep traps, such that the effective lateral transport of particles to deep traps integrates over a larger area than that of shallow sediment traps due to the greater amount of time it would take particles to settle to 1918 m (Cochran et al., this issue).

Data from another thorium isotope are needed to fully constrain even the relatively simple model of coupled Th/particle dynamics shown in Fig. 2.7b. Cochran et al. (1993, 2000) and Murnane et al. (1996) used ^{228}Th and ^{234}Th applied to filterable particles in this fashion. Indeed, Cai et al. (2006), have proposed that the comparison of the ^{234}Th/^{228}Th ratio on large filterable particles collected by *in situ* pump relative to the ratio in the dissolved phase can be used as to gauge the amount of time for particle aggregation. Measurements of ^{228}Th on the 2005 SV and water column samples are in progress. One caveat in incorporating ^{228}Th into the model of Fig. 2.7b is that its activity in solution changes significantly with depth, following its parent ^{228}Ra (Moore, 1969). Thus to fully apply the model requires knowledge of ^{228}Th in the dissolved phase.

4.4. Effects of Composition on POC and ^{234}Th of Trapped Material

Additional compound class data will help elucidate the extent of degradation of organic matter through the water column and its resultant contribution to the decrease in C/^{234}Th with depth. A good correlation between OC and ^{234}Th in the settling velocity intervals, coupled with the change in the relationship from the shallow- and mid-water traps (313, 524 m) to the deep-water trap (1918 m) in 2005 (Fig. 2.8a) suggest that both OC and ^{234}Th are affected by interactions among the settling velocity intervals as the particles settle (Fig. 2.7a,b).

^{234}Th is also correlated to varying degrees with the major ballast mineral components of the flux (lithogenic aluminosilicates, calcium carbonate, and opal; Fig. 2.8b–d). The correlations with both lithogenic material and $CaCO_3$ are good, and there is little change in the slope of the relationship between ^{234}Th and $CaCO_3$ with depth (Fig. 2.8c). Indeed, both

total trap ^{234}Th (dpm) and $CaCO_3$ (mg) increase with depth; the percentage of the contribution of $CaCO_3$ to ballast minerals also increases with depth, largely as a result of the relative loss of opal.

In contrast to the correlation between ^{234}Th and $CaCO_3$ (Fig. 2.8c), the shallow and deep traps fall into separate groups for the correlation of lithogenic material with ^{234}Th (Fig. 2.8b). The total mg of lithogenic material settling into the deep traps is ~90% that reaching the 524 m traps. This is equivalent to an increase in the specific activity of ^{234}Th with respect to lithogenic material (dpm $g_{lithogenic}^{-1}$) and suggests that this fraction is scavenging additional ^{234}Th with depth. Indeed, the larger role played by sinking lithogenic material in scavenging Th has been emphasized by Luo and Ku (2004). The correlation of opal with ^{234}Th is not as good as correlations of lithogenic material or $CaCO_3$ with ^{234}Th, consistent with prior work that showed that opal was not a strong scavenger of Th (Chase et al., 2002; Luo and Ku, 2004). In addition, the specific activity of ^{234}Th with respect to opal (dpm g_{opal}^{-1}) increases with depth, likely due to silica dissolution (Lee et al., 2009).

The slopes of Figures 2.8a–d can be used to calculate particle-water partition coefficients (K_ds) for a pure end-member representing OC or ballast minerals such as lithogenic material, $CaCO_3$ or opal. The particle-water partitioning coefficient or psuedo-K_d is equal to the specific activity of thorium on the particle (dpm ^{234}Th g_i^{-1} where *i* represents OC or ballast mineral content) divided by the dissolved ^{234}Th activity (dpm ^{234}Th g^{-1} of water) in the water through which the particles sink. Chase et al. (2002) also referred to sediment trap-derived particle-water partitioning coefficients as 'pseudo-K_d', but unlike the derivation of Chase et al. (2002), we use measured dissolved ^{234}Th activity instead of the total ^{234}Th activity. We determine the average water column dissolved ^{234}Th activities using trapezoidal integration of water column ^{234}Th profiles obtained during the trap deployment period (Cochran et al., 2009). The dissolved ^{234}Th activity representative of 0–524 m (2.3 dpm L^{-1}) for the shallow traps was derived from two profiles of water column ^{234}Th activities (March 9 and 13, 2005) and the dissolved ^{234}Th activity representing the 0–1918 m (2.4 dpm L^{-1}) for the deep traps came from a single profile that extended to 1800 m (March 13, 2005: Cochran et al., 2009). Via this calculation, we determine a pseudo-K_d using the slopes of the correlation plots (Figs. 2.8a–d; Table 2.2).

The pseudo-K_ds in the 313 and 524 m traps are ranked in the sequence lithogenic material ≤opal <$CaCO_3$ <OC (Table 2.2). For the 1918 m trap, the ranking is lithogenic ≤$CaCO_3$ <opal < OC. One must use caution when interpreting pseudo-K_ds from deep trap data because the slope of the correlation of thorium with organic carbon and ballast minerals may change as the composition of sinking particles changes due to degradation and dissolution. For example, the increases in the deep trap pseudo-K_ds for OC and opal (Table 2.2) most likely result from the decreases in OC and silica from the sinking particles.

Our values for the end-member pseudo-K_ds are generally within the range of those reported elsewhere (Chase et al., 2002; Luo and Ku, 2004; Li, 2005). Luo and Ku (2004) and Li (2005) used sediment trap data from open ocean sites, including the equatorial Pacific and the Southern Ocean to determine pseudo-K_ds for ^{230}Th and found lithogenic material to be a strong scavenger of Th, with values on the order of 10^8 g g^{-1}. Our results suggest that the pseudo-K_d for lithogenic material is most similar to opal in the shallow traps and to $CaCO_3$ in the deep trap (Table 2.2). The pseudo-K_d for lithogenic material at the DYFAMED site is 2 orders-of-magnitude less, and that for opal approximately 10× greater than the values derived by Chase et al. (2002), Luo and Ku (2004) and Li (2005). The difference in K_ds for the lithogenic material at the DYFAMED site relative to the Equatorial Pacific and Southern Ocean may be due to the fact that pulses of lithogenic material followed intense dust deposition events in 2005 and are evident in high percentages of lithogenic material in the fast settling velocity intervals (Lee et al., 2009). Because this material settled at accelerated rates, ^{234}Th may not have had time to attain sorption equilibrium before reaching the traps. As well it may have had different surface area-to-volume characteristics than lithogenic material at open ocean sites.

Chase et al. (2002) showed carbonate was at least as important as lithogenic material for the adsorption of Th and our results support this conclusion. Chase et al. (2002) and Luo and Ku (2004) assumed that the contribution of Th sorption onto organic matter played an insignificant role in the bulk partition coefficient of Th. We observe the highest Th pseudo-K_ds for OC in the shallow and deep traps (45.4×10^6 and 86.3×10^6, respectively). This may be due to the presence of acidic-rich polysaccharides that form organic coatings on biogenic particles (Passow, 2002). Indeed, Quigley et al. (2002) found the K_d for ^{234}Th to colloidal organic matter with a high percent of acidic polysaccharides to be ~10^8. Li (2005)

pointed out the importance of including the contribution of OC to the bulk K_d of Th and found that it contributed 22 ± 6%. Following the approach of Li (2005), we calculate that OC contributes 33% to the bulk K_d of particles settling into the 313 and 524 m traps and 30% to the bulk K_d in the 1918 m trap (Table 2.2).

5. Conclusions

The use of sediment traps to collect particles separated by settling velocity permits relationships among ^{234}Th, organic carbon, and ballast minerals to be determined. Data from sediment trap deployments in the northwest Mediterranean in spring, 2003 and 2005 show no clear trend in C/^{234}Th ratios with settling velocity. Instead variation in C/^{234}Th appears to be more strongly influenced by composition of the material, type of particle, and processes that affect OC and ^{234}Th with depth such as remineralization and degradation of OC and the continuous scavenging of ^{234}Th onto sinking particles.

The preponderance of the ^{234}Th flux is associated with rapidly sinking particles. Greater than 60% of the ^{234}Th was associated with particles that settled at rates greater than 100 m d^{-1}. In 2005, SV traps were deployed at several depths, and the total ^{234}Th reaching the deep trap (1918 m) was a factor of 1.3 greater than that reaching the trap at 524 m. The largest increase in ^{234}Th was observed for the fast settling velocities (196–980 m d^{-1}). The effect of radioactive decay on ^{234}Th may be estimated because the settling velocities are known. Such estimates predict very large decreases in ^{234}Th for the slowly settling particles and negligible change for the rapidly settling material. The contrast between predictions and observations suggests either that ^{234}Th continues to be scavenged as particles settle, or there are significant interactions (aggregation, disaggregation) between the fast and slowly setting particles. In contrast to the pattern seen in ^{234}Th, organic carbon decreases by a factor of ~2 through the water column, with the greatest decrease in the slowly settling particles. These changes resulted in a ~3-fold drop in the C/^{234}Th ratio with depth.

Correlations between ^{234}Th and OC, $CaCO_3$, lithogenic material and opal show varying relationships with trap depth. Good correlations (R^2>0.8) are evident between ^{234}Th and OC, $CaCO_3$ and lithogenic material. The relationship between ^{234}Th and $CaCO_3$ is similar at all depths, largely because both the total ^{234}Th (dpm) and the total $CaCO_3$ (mg) increase

proportionally the same with depth. The ratio of ^{234}Th to lithogenic material increases in the 1918 m trap relative to those at 313 m and 524 m, possibly due to additional scavenging of ^{234}Th onto this material as it sinks. Decreases in the slope of the OC–^{234}Th relationship and the opal–^{234}Th relationship with depth are due to decomposition of the organic material and dissolution of opal, respectively. Pseudo-K_ds calculated for the shallow (313 m and 524 m) 2005 traps range from 5.5×10^6 for opal to 45.4×10^6 for organic carbon. OC provides the greatest contribution to the calculated bulk Th K_d (~33%), with lithogenic material, $CaCO_3$ and opal each contributing ~22%. Pseudo-K_ds for the deep trap material range from 5.9×10^6 for lithogenic material to 86.3×10^6 for OC, with OC comprising the largest relative contribution (~30%) to the bulk K_d, followed by $CaCO_3$, lithogenic material and opal at 20–26%.

Measuring the OC, ^{234}Th, ballast minerals, and organic composition of particles separated by settling velocity over multiple depths provides valuable information on the effects of composition and particle dynamics on variations in OC, ^{234}Th, and the C/^{234}Th ratio. With settling velocities and fluxes known, data on additional radionuclides (e.g. ^{228}Th and ^{210}Po) can provide powerful constraints on the rates of transformations and interactions among settling particles.

References

Armstrong, R.A., Lee, C., Hedges, J. I., Honjo, S., Wakeham, S., 2002. A new, mechanistic model for organic carbon fluxes in the ocean based on the quantitative association of POC with ballast minerals. Deep-Sea Research II 49, 219-236.

Armstrong, R.A., Peterson, M.L., Lee, C., Wakeham, S.G., 2009. Settling velocity spectra and the ballast ratio hypothesis. Deep-Sea Research II 56, 1470-1478.

Béthoux, J. P., Prieur, L., 1983. Hydrologie et circulation en Méditerranée Nord-Occidentale. Pétroles et Techniques 299, 25-34.

Bruland, K.W., Coale, K.H., 1986. Surface Water $^{234}Th/^{238}U$ disequilibria: spatial and temporal variations of scavenging rates within the Pacific Ocean. In: Burton, J.D., Brewer, P.G., Chesselet, R. (Eds.), Dynamic Processes in the Chemistry of the Upper Ocean. Plenum Press, pp 159-172.

Buesseler, K., Ball, L., Andrews, J., Benitez-Nelson, C., Belastock, R., Chai, F., Chao, Y., 1998. Upper ocean export of particulate organic carbon in the Arabian Sea derived from thorium-234. Deep-Sea Research I 45, 2461-2487.

Buesseler, K.O., Cochran, J. K., Bacon, M. P., Livingston, H. D., Casso, S. A., Hirschberg, D., Hartman, M. C., Fleer, A. P., 1992. Determination of thorium isotopes in seawater by nondestructive and radiochemical procedures. Deep-Sea Research I 39, 1103-1114.

Buesseler, K.O., Benitez-Nelson, C.R., Moran, S.B., Burd, A., Charette, M., Cochran, J.K., Coppola, L., Fisher, N.S., Fowler, S.W., Gardner, W.D., Guo, L.D., Gustafsson, O., Lamborg, C., Masqué, P., Miquel, J.C., Passow, U., Santschi, P.H., Savoye, N., Stewart, G., Trull, T., 2006. An assessment of particulate organic carbon to thorium-234 ratios in the ocean and their impact on the application of ^{234}Th as a POC flux proxy. Marine Chemistry 100, 213-233.

Burd, A.B., Moran, S.B., Jackson, G.A., 2000. A coupled adsorption–aggregation model of the POC/^{234}Th ratio of marine particles. Deep-Sea Research I 47, 103-120.

Cai, P., M. Dai, W. Chen, T. Tang, K. Zhou, 2006. On the importance of the decay of ^{234}Th in determining size-fractionated C/^{234}Th ratio on marine particles. Geophysical Research Letters 33, L23602.

Chase, Z., Anderson, R.F., Fleisher, M.Q., Kubik, P.W., 2002. The influence of particle composition and particle flux on scavenging of Th, Pa and Be in the ocean. Earth and Planetary Science Letters 204, 215-229.

Coale, K.H., Bruland, K.W., 1985. $^{234}Th:^{238}U$ disequilibria within the Californian current. Limnology and Oceanography 30, 22-33.

Cochran, J.K., Buesseler, K.O., Bacon, M.P., Livingston, H.D., 1993. Thorium isotopes as indicators of particle dynamics in the upper ocean: results from the JGOFS North Atlantic Bloom experiment. Deep-Sea Research I 40, 1569-1595.

Cochran, J.K., Buesseler, K.O., Bacon, M.P., Wang, H.W., Hirschberg, D.J., Ball, L., Andrews, J., Crossin, G., Fleer, A., 2000. Short-lived thorium isotopes (^{234}Th, ^{228}Th) as indicators of POC export and particle cycling in the Ross Sea, Southern Ocean. Deep-Sea Research II 47, 3451-4390.

Cochran, J.K., Masqué, P., 2003. Short-lived U/Th radionuclides in the ocean: tracers for scavenging rates, export fluxes, and particle dynamics. In: Bourdon, B., Henderson, G.M., Lundstrom, C.C., Turner, S.P. (Eds.), Uranium-Series Geochemistry, Reviews in Mineralogy and Geochemistry, vol. 52. Mineralogy Society of America, Washington, DC, pp. 461-492.

Cochran, J.K., Miquel, J-C., Armstrong, R.A., Fowler, S.W., Masqué, P., Gasser, B., Hirschberg, D.J., Szlosek, J., Rodriguez y Baena, A.M., Verdeny, E., Stewart, G.M., 2009. Time-series measurements of ^{234}Th in water column and sediment trap samples from the northwestern Mediterranean Sea. Deep-Sea Research II 56, 1487-1501.

De La Rocha, C.L., Passow, U., 2006. Accumulation of mineral ballast on organic aggregates. Global Biogeochemical Cycles 20, GB1013.

Goutx, M., Wakeham, S.G., Lee, C., Duflos, M., Guigue, C., Liu, Z., Moriceau, B., Sempéré, R., Tedetti, M., Xue, J., 2007. Composition and degradation of marine particles with different settling velocities in the northwest Mediterranean Sea. Limnology and Oceanography 52, 1645-1664.

Hamm, C.E., 2002. Interactive aggregation and sedimentation of diatoms and clay-sized lithogenic material. Limnology and Oceanography 47 (6), 1700-1795.

Hill, P.S., 1998. Controls on floc size in the sea. Oceanography, 11, 13-18.

Klaas, C., Archer, D.E., 2002. Association of sinking organic matter with various types of mineral ballast in the deep sea: Implications for the rain ratio. Global Biogeochemical Cycles 16, 1116.

Lee, C., Wakeham, S.G., 1992. Organic matter in the water column – future research challenges. Marine Chemistry 39, 95-118.

Lee, C., Armstrong, R.A., Cochran, J.K., Engel, A., Fowler, S.W., Goutx, M., Masqué, P., Miquel, J.C., Peterson, M., Tamburini, C., Wakeham, S., 2009a. MedFlux: investigations of particle flux in the Twilight Zone. Deep-Sea Research II 56 (18), 1363-1368.

Lee, C., Peterson, M.L., Wakeham, S.G., Armstrong, R.A., Cochran, J.K., Miquel, J.C., Fowler, S.W., Hirschberg, D., Beck, A., Xue, J., 2009b. Particulate organic matter and ballast

fluxes measured using time-series and settling velocity sediment traps in the northwestern Mediterranean Sea. Deep-Sea Research II 56 (18), 1420-1436.

Li, Y.-H., 2005. Controversy over the relationship between major components of sediment-trap materials and the bulk distribution coefficients of ^{230}Th, ^{231}Pa, and ^{10}Be. Earth and Planetary Science Letters 233, 1-7.

Liu, Z., Lee, C., Wakeham, S.G. 2006. Effects of mercuric chloride and protease inhibitors on degradation of particulate organic matter from the diatom *Thalassiosira pseudonana*. Organic Geochemistry 37, 1003-1018.

Luo, S., Ku, T.-L., 2004. On the importance of opal, carbonate, and lithogenic clays in scavenging and fractionating ^{230}Th, ^{231}Pa and ^{10}Be in the ocean. Earth and Planetary Science Letters 220, 201-211.

Millot, C., 1999. Circulation in the Western Mediterranean Sea. Journal of Marine Systems 20, 432-442.

Miquel, J.C., Fowler, S.W., La Rosa, J., Buat-Menard, P., 1994. Dynamics of the downward flux of particles and carbon in the open northwestern Mediterranean Sea. Deep-Sea Research I 41, 243-261.

Moore, W. S., 1969. Measurement of ^{228}Ra and ^{228}Th in seawater. Journal of Geophysical Research 74, 694-704.

Moran, S.B., Weinstein, S.E., Edmonds, H.N., Smith, J.N., Kelly, R.P., Pilson, M.E.Q., Harrison, W.G., 2003. Does ^{234}Th/^{238}U disequilibrium provide an accurate record of the export flux of particulate organic carbon from the upper ocean? Limnology and Oceanography 48, 1018-1029.

Murnane, R.J., Cochran, J. K., Buesseler, K.O., Bacon, M. P., 1996. Least-squares estimates of thorium, particle, and nutrient cycling rate constants from the JGOFS North Atlantic Bloom Experiment. Deep-Sea Research I 43, 239-258.

Passow, U., 2002. Transparent exopolymer particles (TEP) in aquatic environments. Progress in Oceanography 55, 287-333.

Passow, U., 2004. Switching perspectives: Do mineral fluxes determine particulate organic carbon fluxes or vice versa? Geochemistry, Geophysics, Geosystems 5, Q04002.

Passow, U., Dunne, J., Murray, J.W., Balistrieri, L., Alldredge, A.L., 2006. Organic carbon to ^{234}Th ratios of marine organic matter. Marine Chemistry 100 (3-4), 323-336.

Peterson, M.L., Hernes, P.J., Thoreson, D.S., Hedges, J.I., Lee, C., Wakeham, S.G., 1993. Field evaluation of a valved sediment trap. Limnology and Oceanography 38, 1741-1761.

Peterson, M.L., Wakeham, S.G., Lee, C., Askea, M., Miquel, J.C., 2005. Novel techniques for collection of sinking particles in the ocean and determining their settling rates. Limnology and Oceanography Methods 3, 520-532.

Peterson, M.L., Fabres, J., Wakeham, S.G., Lee, C., Miquel, J.C., 2009. Sampling the vertical flux in the upper water column using a large diameter free-drifting NetTrap adapted to an indented rotating sphere settling velocity sediment trap. Deep-Sea Research II 56, 1547-1557.

Quigley, M.S., Santschi, P.H., Hung, C.-C., Guo, L., Honeyman, B.D., 2002. Importance of acid polysaccharides for ^{234}Th complexation onto marine organic matter. Limnology and Oceanography 47, 367-377.

Rodriguez y Baena, A.M., Fowler, S.W., and J.C. Miquel, 2007. Particulate organic carbon: natural radionuclide ratios in zooplankton and their freshly produced fecal pellets from the NW Mediterranean (MedFlux 2005). Limnology and Oceanography 52 (3), 966-974.

Santschi, P.H., Murray, J.W., Baskaran, M., Benitez-Nelson, C.R., Guo, L.D., Hung, C.-C., Lamborg, C., Moran, S.B., Passow, U., Roy-Barman, M. 2006. Thorium speciation in seawater. Marine Chemistry 100, 250-268.

Schmidt, S., Andersen, V., Belviso, S., Marty, J.-C., 2002. Strong seasonality in particle dynamics of north-western Mediterranean surface waters as revealed by ^{234}Th/^{238}U. Deep-Sea Research I 49(8), 1507-1518.

Schröder, K., Gasparini, G.P., Tangherlini, M., Astraldi, M., 2006. Deep and intermediate water in the western Mediterranean under the influence of the Eastern Mediterranean Transient. Geophysical Research Letters 33, L21607.

Siegel, D.A., Deuser, W.G., 1997. Trajectories of sinking particles in the Sargasso Sea: modeling of statistical funnels above deep-ocean sediment traps. Deep-Sea Research I 44, 1519-1541.

Spencer, D. W., Brewer, P. G., Fleer, A., Honjo, S., Krishnaswami, S., Nozaki, Y. 1978. Chemical fluxes from a sediment trap experiment in the deep Sargasso Sea. Journal of Marine Research 36, 493-523.

Stemmann, L., 1998. Particulate matter spatio-temporal analysis using a new video system, in the north-western Mediterranean Sea. Influence of biological production, terrigenous inputs and hydro-dynamical forcings. Ph.D. Thesis, Universite d'Oceanologie Biologie, Paris, France.

Stemmann, L., Gorsky, G., Marty, J.-C., Picheral, M., Miquel, J.-C., 2002. Four-year study of large-particle vertical distribution (0-1000m) in the NW Mediterranean in relation

to hydrology, phytoplankton, and vertical flux. Deep-Sea Research II 49 (11), 2143-2162.

Stewart, G., Cochran, J.K., Xue, J., Lee, C., Wakeham, S.G., Armstrong, R.A., Masqué, P., Miquel, J.C, 2007a. Exploring the connection between ^{210}Po and organic matter in the northwester Mediterranean. Deep-Sea Research I 54, 415-427.

Stewart, G., Cochran, J.K., Miquel, J.C., Masqué, P., Szlosek, J., Rodriguez y Baena, A.M., Fowler, S.W., Gasser, B., Hirschberg, D.J., 2007b. Comparing POC export from ^{234}Th/^{238}U and ^{210}Po/^{210}Pb disequilibria with estimates from sediment traps in the northwest Mediterranean. Deep-Sea Research I 54, 1549-1570.

Wakeham, S.G., Lee, C., Peterson, M.L., Liu, Z., Szlosek, J., Putnam, I., Xue, J., 2009. Organic compound composition and fluxes in the twilight zone–time-series and settling velocity sediment traps during MedFlux. Deep-Sea Research II 56, 1437-1453.

Table 2.1. Fluxes and compositional data for settling velocity and time series sediment traps (2003 and 2005).

Year	Date	Depth (m)	Trap ID	Settling Velocity class, *i* ($m\ d^{-1}$)	Midpoint date	Mass ($g\ m^{-2}$)	OC_i ($mmol\ m^{-2}$)	% OC	$^{234}Th_i$ ($10^3\ dpm\ m^{-2}$)			$C/^{234}Th^{\dagger}$ ($\mu mol\ dpm^{-1}$)		
2003	6 March-6 May	238	SV1	0.68-1.4	NA	1.32	14.8	12.9	3.37	±	0.21	4.41	±	0.29
				1.4-2.7	"	1.37	10.7	9.5	2.90	±	0.18	3.67	±	0.23
				2.7-5.4	"	1.19	11.8	12.0	2.71	±	0.18	4.36	±	0.30
				5.4-11	"	0.93	7.4	9.5	1.66	±	0.16	4.48	±	0.45
				11-22	"	0.66	5.6	10.1	1.45	±	0.15	3.86	±	0.40
				22-49	"	0.98	7.2	8.8	1.68	±	0.09	4.28	±	0.24
				49-98	"	1.05	6.2	7.1	1.92	±	0.16	3.21	±	0.28
				98-196	"	1.43	12.3	10.3	1.97	±	0.16	6.24	±	0.51
				196-490	"	5.59	32.1	6.9	13.7	±	0.94	2.35	±	0.17
				490-980	"	1.71	12.7	8.9	4.07	±	0.25	3.13	±	0.20
				>980	"	1.07	2.9	3.2	1.33	±	0.16	2.15	±	0.26
				Total		**17.30**	**123.7**	**8.5**	**36.7**	**±**	**1.1**		NA	
				Weighted Avg								**3.37**	**±**	**0.12**
		238	SV2	0.68-1.4	NA	1.04	10.7	12.3	2.85	±	0.27	3.74	±	0.36
				1.4-2.7	"	0.92	M	M	1.89	±	0.22		M	
				2.7-5.4	"	0.63	4.3	8.2	1.42	±	0.18	3.03	±	0.39
				5.4-11	"	0.72	4.3	7.2	2.13	±	0.19	2.02	±	0.19
				11-22	"	0.68	5.2	9.2	1.64	±	0.18	3.19	±	0.35
				22-49	"	0.77	4.9	7.6	1.94	±	0.19	2.51	±	0.25
				49-98	"	1.35	M	M	2.47	±	0.22		M	
				98-196	"	2.68	16.4	7.4	5.35	±	0.80	3.07	±	0.46
				196-490	"	8.24	40.5	5.9	18.7	±	1.47	2.17	±	0.18
				490-980	"	1.92	13.3	8.3	7.56	±	0.36	1.76	±	0.09
				>980	"	0.07	M	M		BD			M	
				Total		**19.02**	**99.58**	-	**45.9**	**±**	**1.8**			
		238	TS	NA	3/8/03	4.03	20.9	6.2	11.44	±	0.97	1.82	±	0.16
				"	3/13/03	4.13	29.6	8.6	8.58	±	0.78	3.46	±	0.32
				"	3/18/03	4.55	22.1	5.8	11.40	±	0.73	1.94	±	0.13
				"	3/23/03	2.47	18.8	9.2	5.77	±	0.52	3.27	±	0.30
				"	3/28/03	1.06	5.0	5.7	2.98	±	0.33	1.68	±	0.19
				"	4/3/03	0.83	5.7	8.3	1.81	±	0.14	3.18	±	0.30
				"	4/9/03	0.72	6.0	10.0	1.90	±	0.13	3.15	±	0.26
				"	4/15/03	0.94	10.6	13.6	2.92	±	0.12	3.64	±	0.20
				"	4/21/03	0.96	9.8	12.3	3.10	±	0.11	3.17	±	0.15
				"	4/27/03	0.49	6.4	15.7	1.84	±	0.08	3.50	±	0.19
				"	5/3/03	0.92	7.7	10.1	3.01	±	0.09	2.57	±	0.10
					Total	**21.09**	**142.79**	**8.1**	**51.7**	**±**	**1.6**		NA	
					Weighted Avg							**2.76**	**±**	**0.10**

Table 2.1. *continued*

Year	Date	Depth (m)	Trap ID	Settling Velocity class, *i* ($m\ d^{-1}$)	Midpoint date	Mass ($g\ m^{-2}$)	OC_i ($mmol\ m^{-2}$)	% OC	$^{234}Th_i$ ($10^3\ dpm\ m^{-2}$)			C/$^{234}Th^{\dagger}$ ($\mu mol\ dpm^{-1}$)		
2005	4 March-28 April	313	SV2	0.68-5.4	NA	4.88	15.8	4.1	15.4	±	0.54	1.02	±	0.04
				5.4-11	"	1.15	5.3	5.5	3.34	±	0.36	1.59	±	0.18
				11-22	"	1.20	7.5	7.5	3.38	±	0.34	2.22	±	0.23
				22-49	"	1.28	5.6	5.3	3.94	±	0.35	1.42	±	0.13
				49-98	"	1.47	8.6	7.0	5.24	±	0.37	1.64	±	0.12
				98-140	"	1.64	5.8	4.3	4.60	±	0.38	1.26	±	0.11
				140-196	"	2.16	6.7	3.7	5.55	±	0.43	1.21	±	0.10
				196-326	"	4.43	12.9	3.5	12.4	±	0.61	1.04	±	0.05
				326-490	"	4.15	10.2	2.9	11.0	±	0.54	0.93	±	0.05
				490-980	"	3.42	14.2	5.0	10.7	±	0.50	1.32	±	0.07
				>980	"	0.33	3.0	11.0	1.64	±	0.19	1.82	±	0.22
				Total		**26.10**	**95.5**	**4.4**	**77.2**	**±**	**1.4**		NA	
				Weighted Avg.								**1.24**	**±**	**0.03**
		313	TS	NA	3/6/05	4.53	10.9	2.9	12.5	±	0.39	0.87	±	0.03
				"	3/11/05	4.34	10.9	3.0	11.3	±	0.32	0.97	±	0.03
				"	3/16/05	1.64	3.9	2.8	4.4	±	0.21	0.88	±	0.05
				"	3/21/05	2.10	7.2	4.1	7.4	±	0.23	0.96	±	0.04
				"	3/26/05	2.08	6.2	3.6	6.6	±	0.20	0.94	±	0.03
				"	3/31/05	4.40	10.3	2.8	12.5	±	0.23	0.82	±	0.02
				"	4/5/05	1.73	6.8	4.7	4.5	±	0.13	1.52	±	0.05
				"	4/10/05	0.41	2.7	7.8	1.2	±	0.06	2.25	±	0.13
				"	4/15/05	1.35	7.6	6.7	2.3	±	0.08	3.23	±	0.13
				"	4/20/05	0.73	5.7	9.3	1.5	±	0.06	3.85	±	0.17
				"	4/25/05	0.13	1.5	13.4	0.4	±	0.03	4.06	±	0.36
					Total	**23.45**	**73.5**	**3.8**	**64.6**	**±**	**0.7**		NA	
					Weighted Avg.							**1.14**	**±**	**0.03**
		524	SV1	0.68-5.4	NA	4.88	13.9	3.4	16.3	±	0.38	0.92	±	0.04
				5.4-11	"	1.23	4.7	4.6	4.50	±	0.20	0.88	±	0.02
				11-22	"	0.93	4.2	5.4	2.94	±	0.15	1.09	±	0.03
				22-49	"	0.88	4.2	5.7	3.04	±	0.15	0.93	±	0.03
				49-98	"	1.01	3.9	4.6	3.46	±	0.15	1.18	±	0.05
				98-140	"	0.98	3.6	4.5	3.13	±	0.15	1.16	±	0.06
				140-196	"	1.23	4.4	4.3	3.72	±	0.15	1.12	±	0.05
				196-326	"	3.04	8.5	3.4	9.17	±	0.23	1.38	±	0.07
				326-490	"	2.84	9.7	4.1	8.89	±	0.22	1.41	±	0.08
				490-980	"	7.00	15.6	2.7	17.8	±	0.29	1.04	±	0.05
				>980	"	1.86	4.6	3.0	4.96	±	0.16	0.85	±	0.03
				Total	"	**25.88**	**77.2**	**3.6**	**78.0**	**±**	**0.72**		NA	
				Weighted Avg.								**0.99**	**±**	**0.02**
			SV2	0.68-5.4	NA	5.13	14.1	3.3	16.6	±	0.33	1.48	±	0.10
				5.4-11	"	0.62	4.0	7.7	2.22	±	0.11	1.02	±	0.03
				11-22	"	1.06	3.2	3.6	3.73	±	0.16	0.83	±	0.03
				22-49	"	1.30	4.2	3.9	5.23	±	0.18	0.84	±	0.03
				49-98	"	1.89	5.1	3.2	6.90	±	0.21	1.11	±	0.05
				98-140	"	1.76	5.1	3.5	5.15	±	0.24	1.00	±	0.05
				140-196	"	2.66	7.1	3.2	6.44	±	0.24	0.73	±	0.03
				196-326	"	4.29	9.4	2.6	11.2	±	0.31	0.80	±	0.03

Table 2.1. *continued*

Year	Date	Depth (m)	Trap ID	Settling Velocity class, *i* ($m\ d^{-1}$)	Midpoint date	Mass ($g\ m^{-2}$)	OC_i ($mmol\ m^{-2}$)	% OC	$^{234}Th_i$ ($10^3\ dpm\ m^{-2}$)			C/^{234}Th† ($\mu mol\ dpm^{-1}$)		
				326-490	"	3.94	9.2	2.8	11.1	±	0.30	0.85	±	0.04
				490-980	"	5.50	14.4	3.1	14.1	±	0.36	1.79	±	0.09
				>980	"	0.75	4.1	6.6	2.78	±	0.17	0.85	±	0.02
				Total		**28.89**	**79.8**	**3.3**	**85.5**	**±**	**0.82**		NA	
				Weighted Avg.								**0.93**	**±**	**0.02**
		924 m	TS	NA	3/6/05	2.02	6.73	4.0	8.5	±	0.30	0.79	±	0.03
				"	3/11/05	1.93	4.82	3.0	6.2	±	0.24	0.77	±	0.03
				"	3/16/05	2.14	5.02	2.8	8.4	±	0.22	0.60	±	0.02
				"	3/21/05	1.89	5.03	3.2	8.1	±	0.21	0.62	±	0.02
				"	3/26/05	2.56	6.38	3.0	9.9	±	0.20	0.65	±	0.02
				"	3/31/05	3.10	3.28	1.3	10.2	±	0.20	0.32	±	0.01
				"	4/5/05	2.53	5.61	2.7	7.9	±	0.17	0.71	±	0.02
				"	4/10/05	0.47	3.34	8.5	2.2	±	0.09	1.54	±	0.07
				"	4/15/05	0.37	2.63	8.6	1.9	±	0.08	1.42	±	0.07
				"	4/20/05	0.20	2.16	13.3	2.5	±	0.13	0.88	±	0.05
				"	4/25/05	0.47	3.19	8.2	1.6	±	0.06	1.95	±	0.08
					Total	**17.67**	**48.2**	**3.3**	**67.2**	**±**	**0.62**		NA	
					Weighted Avg.							**0.72**	**±**	**0.02**
		1918	SV1	0.68-5.4	NA	2.73	5.0	2.2	11.5	±	0.26	1.13	±	0.06
				5.4-11	"	0.66	2.0	3.7	2.64	±	0.13	0.46	±	0.01
				11-22	"	0.52	1.5	3.5	2.27	±	0.12	0.43	±	0.01
				22-49	"	0.65	1.6	3.0	3.16	±	0.13	0.40	±	0.01
				49-98	"	0.99	2.4	2.9	4.78	±	0.15	0.49	±	0.02
				98-140	"	1.18	3.9	4.0	5.65	±	0.17	0.69	±	0.03
				140-196	"	1.76	4.0	2.7	8.18	±	0.21	0.50	±	0.02
				196-326	"	3.48	6.1	2.1	15.4	±	0.30	0.51	±	0.02
				326-490	"	4.79	8.4	2.1	19.8	±	0.34	0.66	±	0.04
				490-980	"	6.31	11.3	2.2	24.7	±	0.37	0.75	±	0.04
				>980	"	1.01	4.0	4.7	3.50	±	0.16	0.44	±	0.01
				Total		**24.09**	**50.3**	**2.5**	**101.6**	**±**	**0.76**		NA	
				Weighted Avg.								**0.50**	**±**	**0.01**
			SV2	0.68-5.4	NA	3.09	6.9	2.7	17.2	±	0.32	1.38	±	0.15
				5.4-11	"	1.05	3.1	3.6	5.59	±	0.19	0.45	±	0.01
				11-22	"	0.59	1.8	3.6	3.12	±	0.14	0.45	±	0.01
				22-49	"	0.79	2.3	3.5	3.71	±	0.16	0.40	±	0.01
				49-98	"	1.32	3.9	3.5	6.99	±	0.19	0.35	±	0.01
				98-140	"	1.93	2.7	1.7	9.08	±	0.21	0.30	±	0.01
				140-196	"	2.50	4.1	2.0	11.8	±	0.25	0.56	±	0.02
				196-326	"	4.47	7.3	1.9	18.1	±	0.29	0.61	±	0.03
				326-490	"	3.43	5.6	2.0	12.3	±	0.27	0.58	±	0.03
				490-980	"	4.80	7.8	2.0	17.4	±	0.32	0.56	±	0.02
				>980	"	0.15	1.0	8.0	0.73	±	0.08	0.40	±	0.01
				Total		**24.13**	**46.5**	**2.3**	**106.0**	**±**	**0.77**		NA	
				Weighted Avg.								**0.44**	±	**0.01**

NA, not applicable; M, missing sample; BD, below detection.

Table 2.2. Pseudo-K_ds and trap component weight % for OC and ballast minerals for 2005 SV sediment traps.

Depth (m)	OC	Lithogenic	$CaCO_3$	Opal	Bulk K_d
313 and 524					
K_d (10^6 g g^{-1})	45.4	4.9	7.3	5.5	7.9
wt%	3.76	25.0	15.8	21.2	
% contribution to bulk K_d	33	23	22	22	
1918					
K_d (10^6 g g^{-1})	86.3	5.9	6.9	10.4	10.0
wt%	2.41	27.2	25.3	13.4	
% contribution to bulk K_d	30	24	26	20	

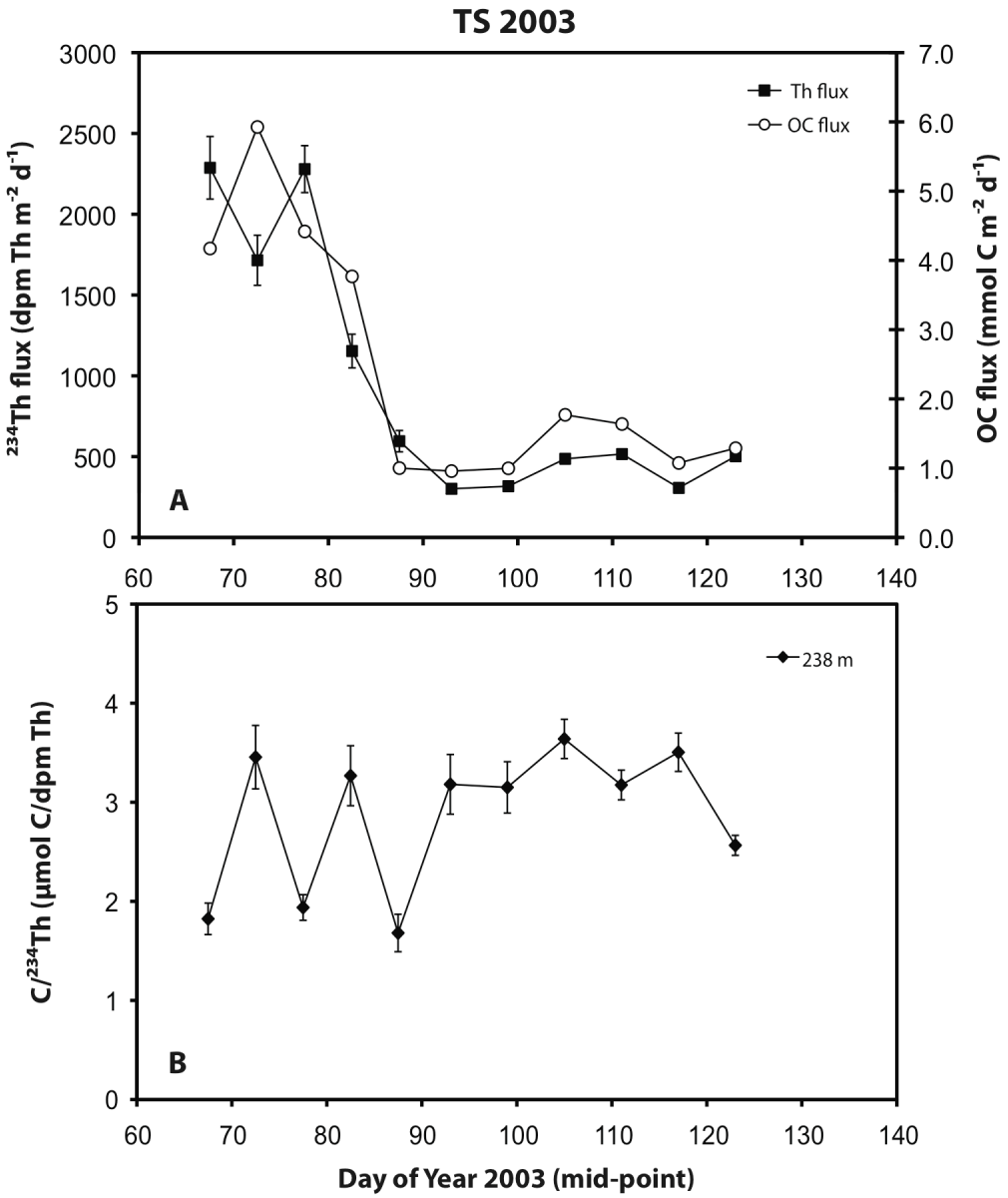

Fig. 2.1. 2003 time-series sediment trap data (238 m): (a) ^{234}Th and OC fluxes and (b) C/^{234}Th ratio (µmol C dpm Th^{-1}) ratios.

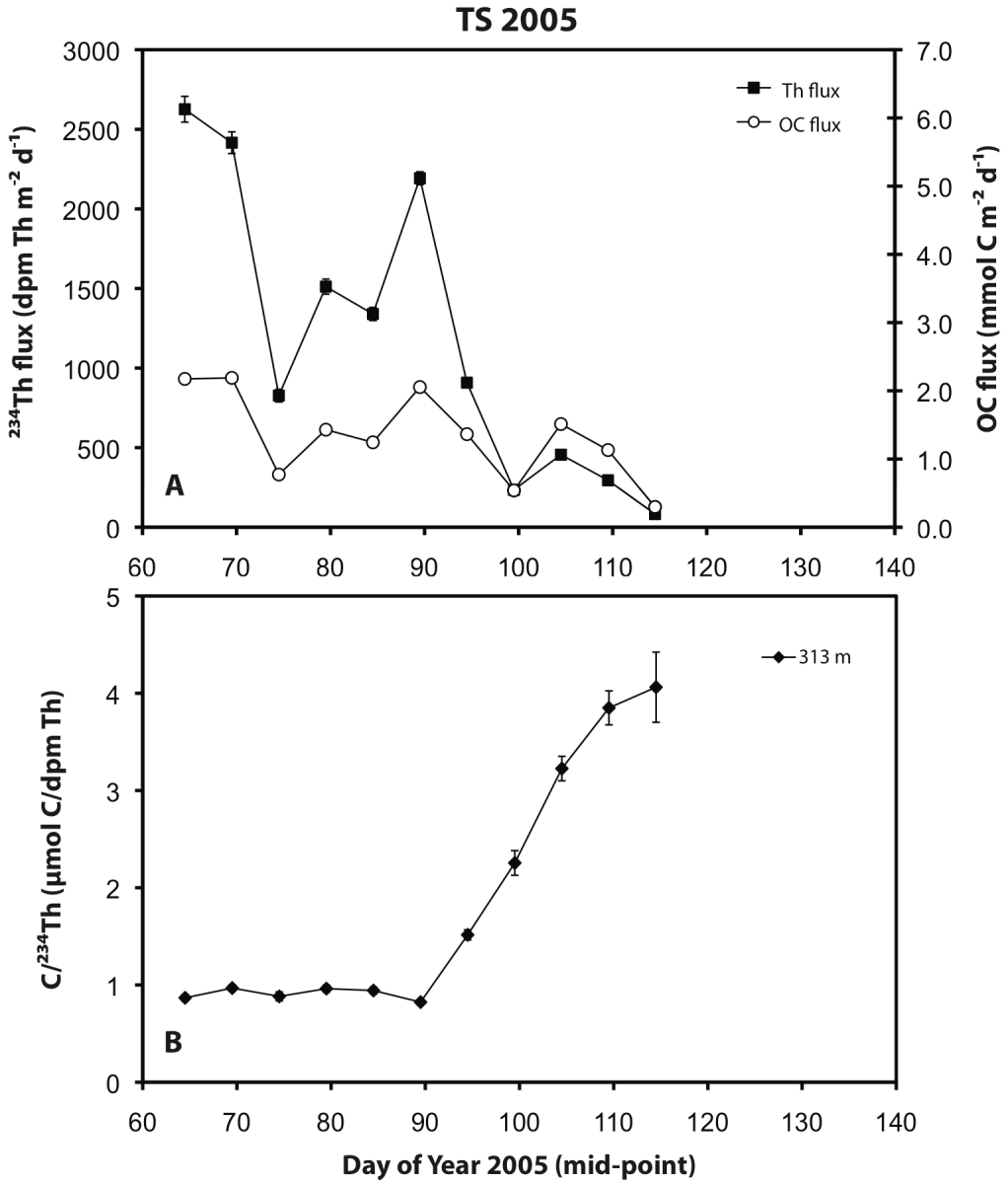

Fig. 2.2. 2005 time-series sediment trap data (313 m): (a) ^{234}Th and OC fluxes and (b) C/^{234}Th ratio (µmol C dpm Th^{-1}) ratios.

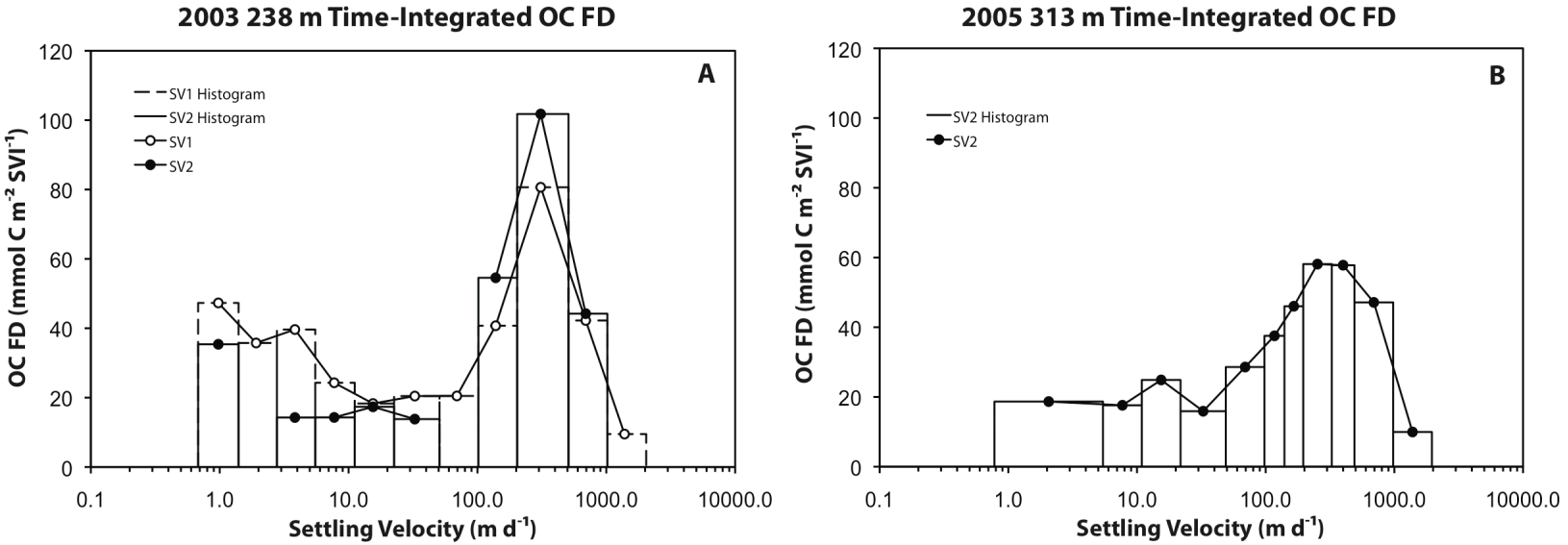

Fig. 2.3. (a) and (b) histograms of flux density (FD—see text) for 2003 (238 m) and 2005 (313 m) in which the area of the rectangles represent the time-integrated fluxes (OC: mmol m^{-2}) and the heights of the box and mid-point plotted represent the time-integrated flux densities of OC (OC: mmol m^{-2} SVI^{-1}). See text and Armstrong et al. (2009) for explanation of the calculation of time-integrated flux densities.

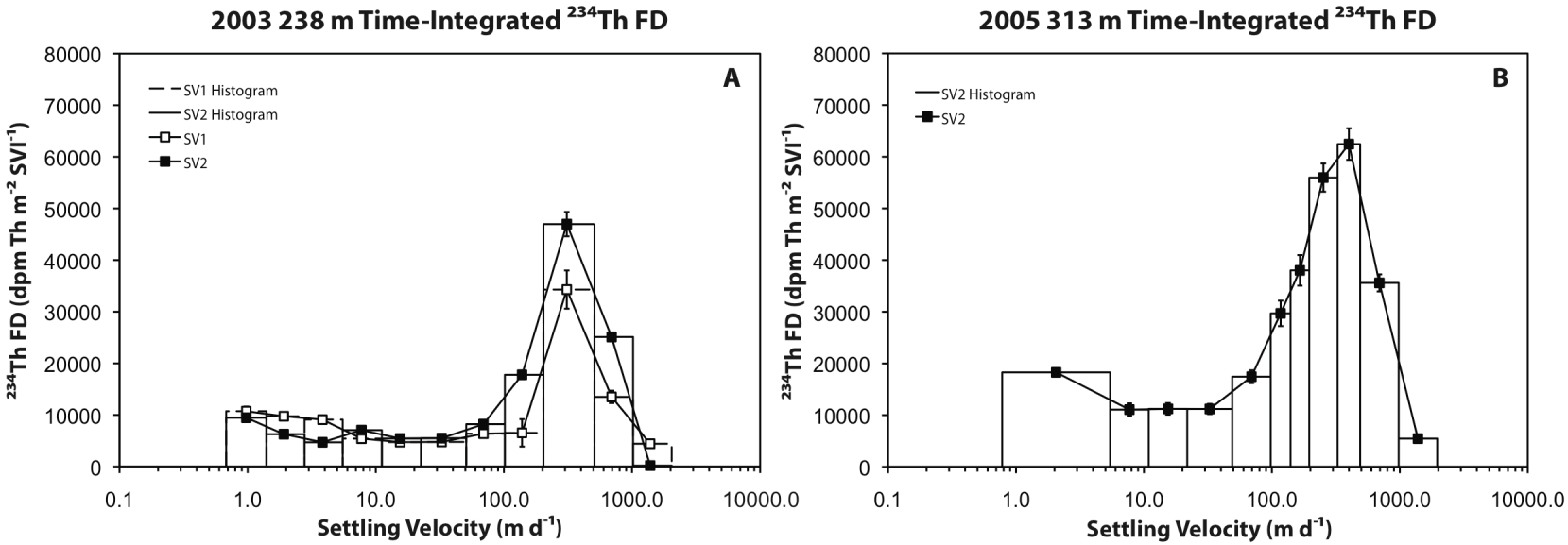

Fig. 2.4. (a) and (b) histograms of flux density (FD—see text) for 2003 (238 m) and 2005 (313 m) in which the area of the rectangles represent the time-integrated fluxes (^{234}Th: dpm m^{-2}) and the heights of the box and mid-point plotted represent the time integrated flux densities of ^{234}Th (^{234}Th: dpm m^{-2} SVI^{-1}). See text and Armstrong et al. (2009) for explanation of the calculation of time-integrated flux densities.

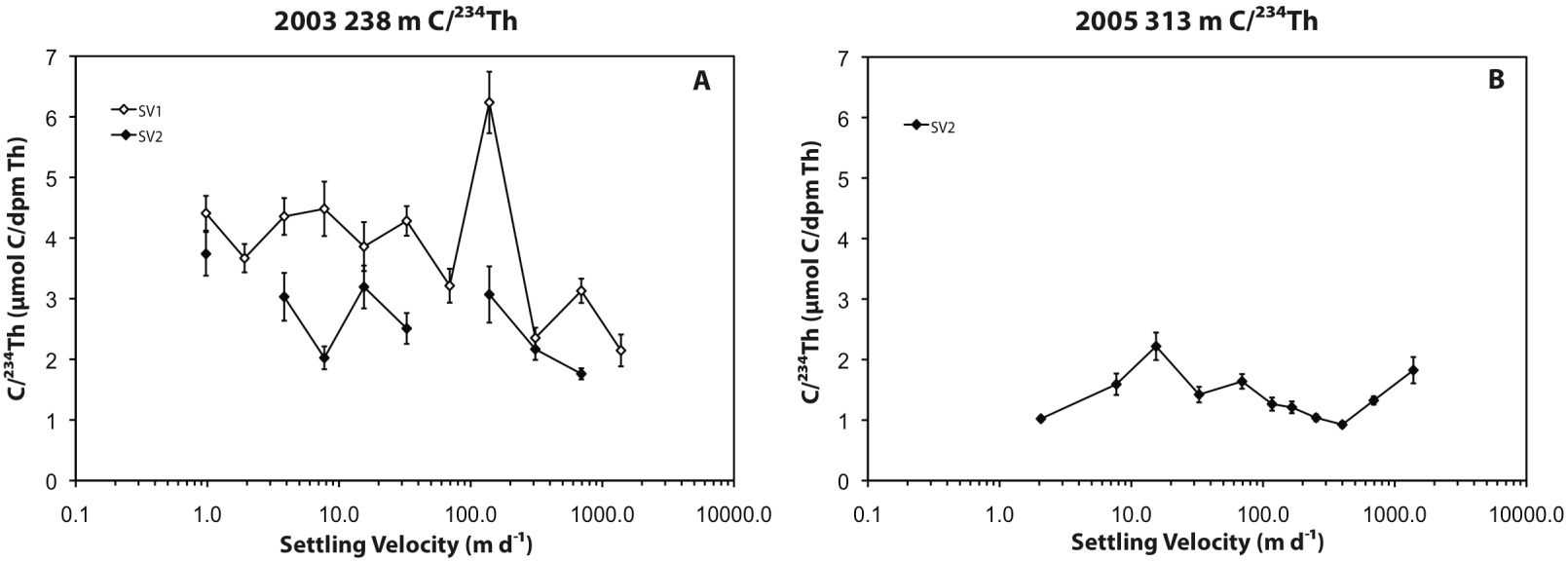

Fig. 2.5. (a) and (b) C/^{234}Th ratio values of SV trap samples for 2003 (238 m) and 2005 (313 m).

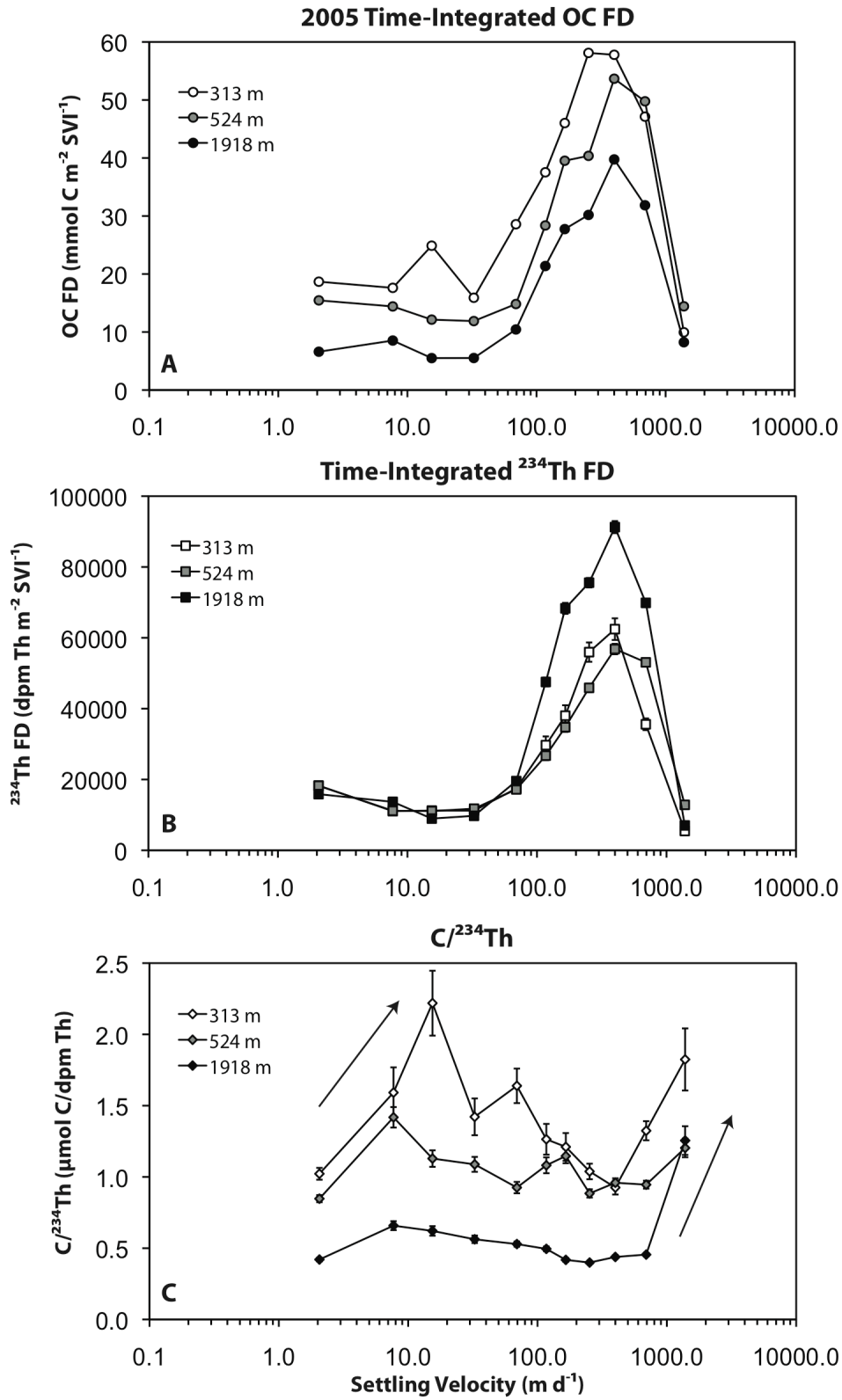
2005 Time-Integrated OC FD
OC FD (mmol C m-2 SVI-1)
313 m
524 m
1918 m
A
Time-Integrated 234Th FD
234Th FD (dpm Th m-2 SVI-1)
B
C/234Th
C/234Th (µmol C/dpm Th)
C
Settling Velocity (m d-1)

Fig. 2.6. Settling velocity plots of OC, ^{234}Th time-integrated flux densities and C/^{234}Th ratio values for 2005: 313 m SV2, average of SV1 and SV2 at 524 m, and the average of SV1 and SV2 at 1918 m. (a) Time-integrated flux densities (FD) OC with depth, (b) time–integrated FD of ^{234}Th with depth, and (c) the C/^{234}Th ratio with depth. Error bars represent the standard deviation of the duplicate traps. Arrows represent settling velocity intervals where there is an increase in C/^{234}Th with settling velocity.

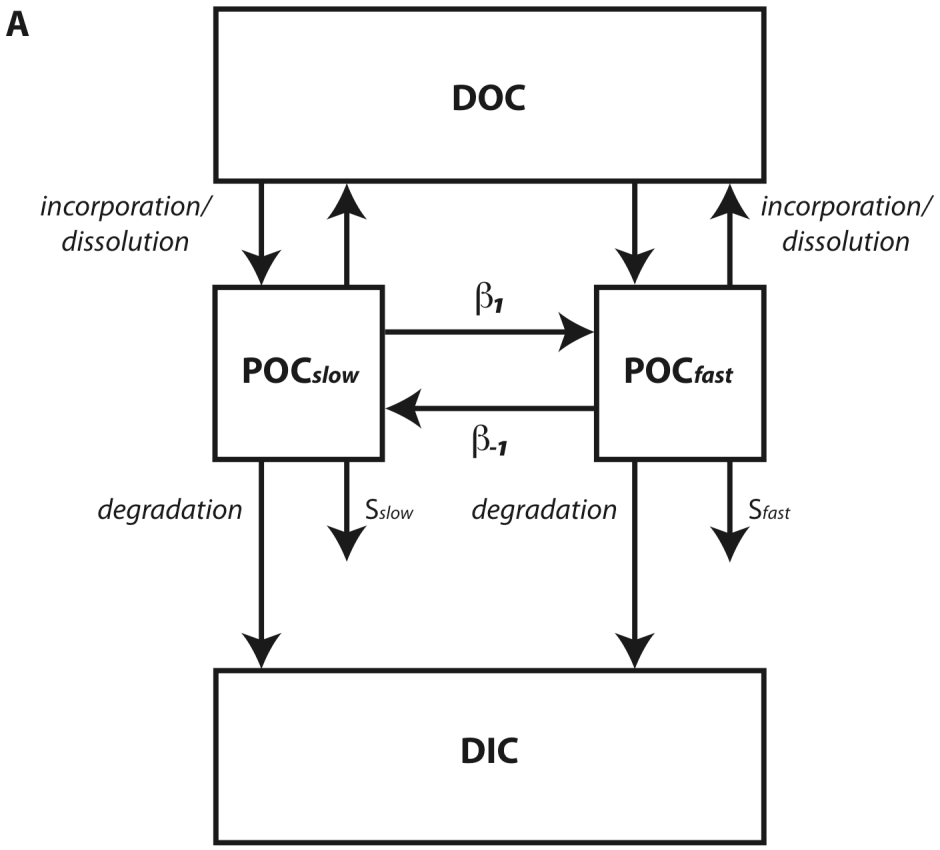
A
DOC
incorporation/
dissolution
incorporation/
dissolution
β1
POCslow
POCfast
β-1
degradation
Sslow
degradation
Sfast
DIC

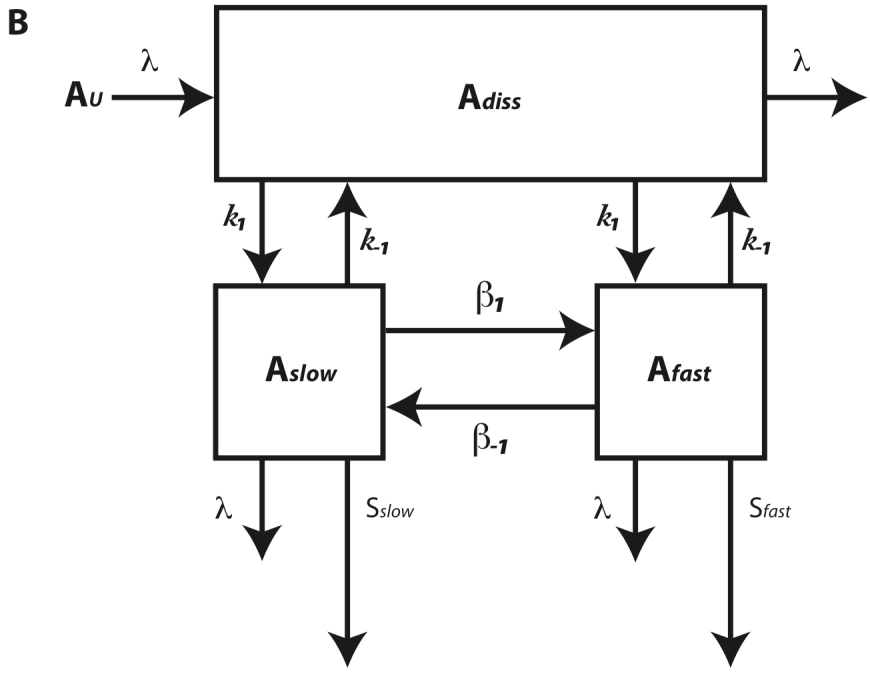
B
λ
AU
Adiss
λ
k1
k-1
k1
k-1
β1
Aslow
Afast
β-1
λ
Sslow
λ
Sfast

Fig. 2.7. (a) Schematic diagram of the transfers among DOC, POC, and DIC pools. Biotic and abiotic losses of POC are represented in a simplified way by dissolution and degradation of POC. The settling of material from one depth horizon to another results in a loss of POC from each settling velocity grouping and is represented by S_{slow} and S_{fast}. Exchange between the slow to fast settling pools is indicated by the rate constant β_1 representing processes such as aggregation and incorporation POC. Transfer in the opposite direction from fast to slow settling particles might include processes of disaggregation and degradation and is represented by the rate constant β_{-1}. (b) Schematic diagram of the exchange of ^{234}Th between dissolved and particulate pools. ^{234}Th activities of the dissolved (A_{diss}), slow settling particles (A_{slow}), and fast settling particles (A_{fast}) are represented by boxes. The activity of the dissolved parent, ^{238}U, is denoted by A_{U} and the radioactive decay from each phase is represented by λ. S_{slow} and S_{fast} represent the loss of particulate thorium by vertical settling. The first-order rate constants of adsorption of dissolved ^{234}Th onto slow and fast settling particles are k_1 and k_2, respectively. First-order rate constants for desorption from the slow and fast settling pools are k_{-1} and k_{-2}, respectively. Particle exchange is indicated by rate constants β_1 for transfer of ^{234}Th from slow to fast settling particles and β_{-1} for transfer from fast to slow settling particles.

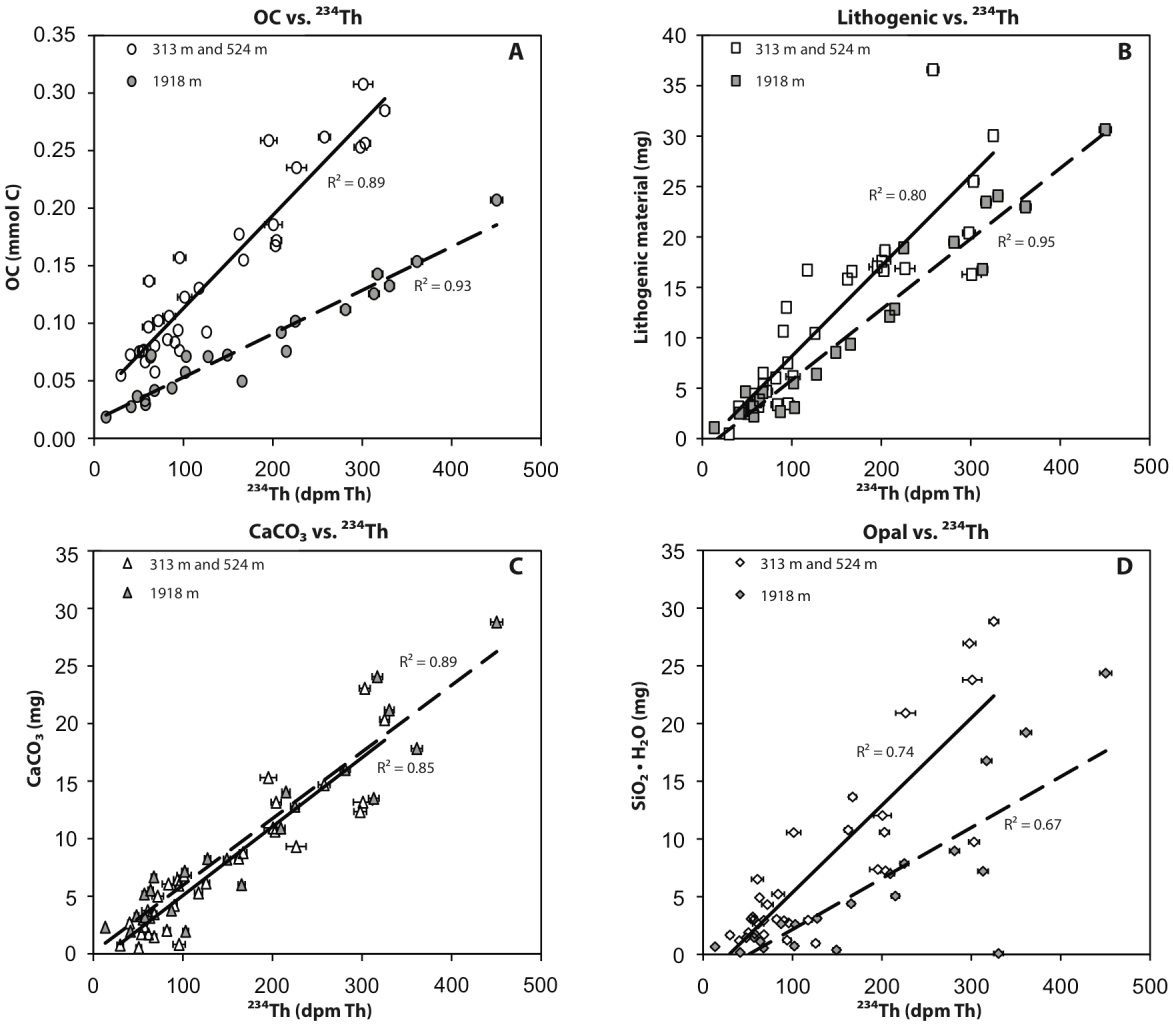
OC vs. 234Th
313 m and 524 m
1918 m
A
R2 = 0.89
R2 = 0.93
OC (mmol C)
234Th (dpm Th)
Lithogenic vs. 234Th
B
R2 = 0.80
R2 = 0.95
Lithogenic material (mg)
CaCO3 vs. 234Th
C
R2 = 0.89
R2 = 0.85
CaCO3 (mg)
Opal vs. 234Th
D
R2 = 0.74
R2 = 0.67
SiO2 • H2O (mg)

Fig. 2.8. Correlations of ^{234}Th with particulate organic carbon and ballast minerals components for shallow SV traps (313 and 524 m) and deep SV traps (1918 m) of 2005. (a) OC vs. ^{234}Th; (b) lithogenic particles vs. ^{234}Th; (C) $CaCO_3$ vs. ^{234}Th, (D) opal as $SiO2 \bullet H2O$ vs. ^{234}Th. Error bars represent one standard deviation. Best-fit lines for the shallow (313 and 524 m, solid line) and deep (1918 m, dashed line) trap data are shown with their correlation coefficients, R^2.

CHAPTER 3

Comparison of particulate organic carbon, organic compounds, and ^{234}Th in particles sampled by *in situ* filtration and sediment traps in the northwest Mediterranean Sea

Abstract

Applications of ^{234}Th/^{238}U disequilibrium as a flux proxy for particulate organic carbon (POC) in the oceans commonly rely on characterizing the POC/^{234}Th ratio in filterable particles and using this as representative of the sinking flux. To better understand the relationships and linkages between filterable particles and those collected in sediment traps, we have compared the POC/^{234}Th ratios and compositions (organic and radiochemical) of particles filtered by *in situ* pumps into two size classes (1-70 μm and >70 μm) with material collected in sediment traps operated in time-series and settling velocity modes. Principal components analysis of the compositional data revealed the pump- and sediment trap-collected material to have nearly no overlap. Sediment trap-collected material had strong chemical evidence of fecal pellets driving the flux to depth, with little compositional variance with settling velocity. In contrast, pump-collected particulate matter in the large fraction (LP; >70 μm) contained fresh diatoms and fecal pellets and in the small fraction (SP; 1-70 μm) exhibited a signal of fresh, algal-derived material (coccoliths) down to depths of >600 m, beyond the mixed layer depth. The POC/^{234}Th ratios of the particles varied in the order LP >> SP ≥ sediment trap. Application of ^{234}Th as a proxy for POC flux produced POC fluxes that bracketed the trap fluxes, but ranged over an order of magnitude depending on whether the POC/^{234}Th of the large or small particles was used in the calculation. Significant short-term variation in the POC/^{234}Th of the filterable particles and in the ^{234}Th deficit in the water column contributed to the range in calculated POC fluxes. The lack of compositional linkages between the particle pools and the possibility of significant short-term variation in water column ^{234}Th distributions implies that a thorough understanding of a given oceanic region is required to validate the use of ^{234}Th as a proxy for POC flux.

1. Introduction

The "biological organic carbon pump" refers to particulate organic carbon (POC) generation and export out of the surface mixed layer of the ocean. It provides for a biologically mediated means of removal of atmospheric carbon dioxide into the deep ocean, although only ~1% of the POC flux traverses the water column and is deposited in ocean sediments (Wakeham and Lee, 1993). Knowing the quantity of organic carbon flux that leaves the mixed layer and traverses the dark midwaters, or Twilight Zone, is necessary for studies that investigate mechanistic controls on the magnitude of POC that reaches the seafloor (Armstrong et al., 2001; Buesseler et al., 2007a; Lee et al., 2009a; Burd et al., 2010). Numerous authors have summarized the evolution and evaluation of methods used to quantify POC flux from the surface ocean (Emerson et al., 1997; Gardner, 1997, 2000; Buesseler et al., 2006, 2007b). Collection of sinking particles in particle interceptors (sediment traps) and measurement of POC collected for a given period of time is one way to determine POC flux. Additionally, a conservative financial-, logistical-, and time-efficient means of assessing POC flux is using the U-series radionuclide ^{234}Th as a proxy, a method that entails the determination of the disequilibrium between ^{234}Th and its parent ^{238}U in the water column to ascertain the ^{234}Th flux and multiplying this by the POC/^{234}Th on sinking particles. Commonly filterable particles in a large size class (e.g. >53 um) are taken as representative of sinking particles. The relatively short half-life of ^{234}Th (24.1 d) permits it to be used as a tracer of flux on a timescale of months–comparable to the time scale of the evolution of a phytoplankton bloom (Coale and Bruland, 1987, 1985; Buesseler et al., 1992).

Both sediment traps and the ^{234}Th proxy have their limitations when applied to evaluating particle and POC fluxes. The possibility of biases associated with hydrodynamic effects have been raised for traps, while the ^{234}Th proxy may be subject to non-steady state effects (Cochran et al., 2009) and a temporal disconnection between the integration time of the water column ^{234}Th deficit and the filterable particle pool sampled by pumps (Cochran and Masque, 2003; Cochran et al., 2009). In particular, the question of how well the POC/^{234}Th ratio in filterable particles corresponds to that in the sinking flux has been addressed with increasing frequency for over a decade (Buesseler, 1998; Burd et al., 2000, 2007; Coppola et al., 2002; Moran et al., 2003; Buesseler et al., 2006 and references therein;

Smith et al., 2006; Buesseler and Boyd, 2009; Hung and Gong, 2010). Comparisons between *in situ* pump and sediment trap-derived POC/^{234}Th ratios and POC export fluxes have been reviewed in Buesseler et al. (2006) and recently addressed in Hung and Gong (2010) and Hung et al. (2010).

Reccurring topics include challenges to the prevailing notion that large, rare particles (>500 μm, McCave 1975) are the dominant source of flux to midwaters (Fowler and Knauer, 1986; Altabet et al., 1991) and questions over the practice of using the pump-collected large particulate fraction (>53, >63, or >70 μm) POC/^{234}Th for POC flux estimates (Bacon et al., 1996; Moran et al. 2003; Hung and Gong 2010). Recent field programs have shown that small-to-intermediate sized particulate fractions (1-10 μm and 10-53 μm) are less variable than the largest particulate fraction (Buesseler et al., 2009; Hung and Gong, 2010) and these small-to-intermediate sized fractions carry the greatest portion of total particulate POC and ^{234}Th (Waite and Hill, 2006; Lepore et al., 2009; Hung and Gong, 2010; Hung et al., 2010).

Alternatively, characterizing settling particles by settling velocity is a powerful approach to understanding controls on POC flux (Gardner, 1997; Armstrong et al., 2009). Particle settling velocity directly relates to remineralization and degradation length scales and is thus linked to the efficiency of the biological organic carbon pump in transporting carbon through the Twilight Zone to the seafloor. Marine flocs, aggregates, and fecal pellets are often fragile and hence determining their settling velocity *in situ* is optimal for realizing accurate measurements. One such method employed in the field uses indented rotating sphere carousel (IRSC) sediment traps that collect particles on a sphere–programmed to rotate daily, dropping material into the lower column of the trap whilst the sample carousel rotates a new sampling tube into position on a fixed schedule; as such, particles are separated by settling velocity according to the rotation schedule of the carousel (Peterson et al., 2005; Lee et al., 2009b).

The magnitude of the particulate OC/^{234}Th ratio results from a combination of chemical, physical, and biological processes (Buesseler et al., 2006). Sinking particles, newly produced at ocean surface, have a POC/^{234}Th that is dependent on the abundance of POC (i.e., food web dynamics), inorganic minerals, and acidic polysaccharides present (Quigley et al., 2002; Luo and Ku, 2004; Buesseler et al., 2006). In their review of the impact of

measured POC/^{234}Th on Th-derived POC flux estimates, Buesseler et al. (2006) illustrated the ways in which particle size and biogeochemical processes would cause POC/^{234}Th ratios to increase (e.g., increased acidic polysaccharides and large volume to surface area ratio of particles), decrease (e.g., increased ^{234}Th bound on particles through small volume to surface area of particles, carbon assimilation and degradation), and remain constant (e.g., aggregation and disaggregation).

In a previous contribution (Szlosek et al., 2009), we presented measurements of POC, ^{234}Th and POC/^{234}Th in particles separated *in situ* according to settling velocity and discussed relationships among these parameters. Here we compare the composition of filterable particulate fractions collected with *in situ* pumps with sediment trap material in an attempt to relate the filterable material to the sinking material. This approach allows us to address the questions: 1) How comparable are these particle collection techniques? and 2) Which filterable fraction best represents the dominant fraction of the settling particle flux?

2. Methods

2.1. Sample Collection

2.1.1. Sediment Traps

Sampling was carried out in 2005 as part of the MedFlux program at the French JGOFS time-series DYFAMED site (43˚25'N 7˚52'E; water depth 2300 m) in the Mediterranean Sea, ~52 km from the Nice. Sediment trap moorings with IRSC sediment traps (Peterson et al., 1993) were deployed at depths of 313, 524, and 1918 m in 2005 from 4 March to 28 April. The IRSC traps were used to exclude macrozooplankton and other swimmers from the trap cups (Peterson et al., 1993). Two modes of particle collection were employed: time-series (TS) and settling velocity (SV) modes. Peterson et al. (2005) provided a description of the operation of the IRSC sediment trap in the settling velocity mode. Briefly the indented sphere was programmed to collect particles and rotate once per day, dropping the particles into the lower portion of the trap. The carousel rotated once per day, with the cups open for varying lengths of time. The particles collected in each cup then represented the different settling velocity classes.

Simultaneously, traps were deployed at the same depth operated in a time-series mode that collected the flux over 5 day periods for the 55 day deployment. Samples were taken for mass, OC, ^{234}Th activity, and organic biomarkers such as chloropigments and fucoxanthin, lipids, and amino acids. Lee et al. (2009b) and Wakeham et al. (2009) describe details regarding the sample splitting and organic chemical analyses. Deployment dates and depths as well as settling velocity classes sampled are given in the Appendix (Table 3.A1).

2.1.2. In Situ Pumps

Filterable particles were sampled *in situ* by filtering a large volume of water (100-1000 l; ~ 4-8 l min^{-1} flow rate) with battery-powered Challenger pumps (Livingston and Cochran, 1987; Buesseler et al., 1992). The pumps were equipped with pre-filters segregating particulate material into size classes of 1-70 μm, and > 70 μm. The pre-filter stack arrangement was either a 142 or 293 mm diameter Teflon mesh (cut-off diameter 70 μm) followed by a quartz microfiber filter (Whatman QM-A; nominal cut-off 1 μm).

Following the QM-A filter were two manganese oxide-impregnated wound fiber filter cartridges (Hytrex, nominal pore size 1 μm) in series for the adsorption of dissolved ^{234}Th, defined in this study as <1 μm. Final dissolved activities took into account the efficiency of the ^{234}Th scavenged onto the cartridges following the procedure described in Livingston and Cochran (1987). Although Cai et al. (2006) have proposed that MnO_2 cartridges under collect dissolved Th, prior work (summarized in Hung et al., 2008) and comparison of total Th in small volume water samples and obtained with MnO_2 cartridges used in pumps at the DYFAMED site (Cochran et al., 2009) showed good agreement between the methods. The dissolved ^{234}Th data were presented in Cochran et al. (2009). Additional small volume samples for total ^{234}Th activities (i.e., particulate + dissolved) were taken by CTD to bracket the *in situ* pump casts (Cochran et al., 2009).

2.1.3. CTD Casts

CTD casts were made either shortly before or after *in situ* pump deployment in order to characterize the hydrography of the water column at the time of the pump deployment.

2.2. Sample Analyses

2.2.1. ^{234}Th Analyses

The ^{234}Th activities of the particulate pump fractions (>1 μm) and sediment trap samples were determined by non-destructive beta counting using Risø low background beta counters (Buesseler et al., 1998, 2001; Cochran et al., 2000). Material captured on the Teflon mesh was rinsed onto 25 mm QM-A filters using filtered seawater, after which the filters were dried at 65˚C. The 1μm pre-combusted QM-A filters were dried at 65˚C and subsampled with 21-mm punches. Particulate samples were mounted in plastic sample cups and covered with plastic film and aluminum foil. The 1-70 μm samples were mounted as a stack of 21-mm punches. Sediment trap splits were re-filtered onto 25 mm Nuclepore filters with a 0.4 μm nominal pore size and dried. Further details regarding the particulate fraction subsampling and standardization of the geometry of the sample cups for beta activity detection are provided in Cochran et al. (2009).

Samples were counted over several half-lives of ^{234}Th and for a duration sufficient to reduce counting errors to <5%. Counts taken after 5 half-lives had passed were used to estimate the filter blank and contributions from long-lived beta emitters. Counting was performed at Stony Brook University School of Marine and Atmospheric Sciences (SoMAS) as well as IAEA-Marine Environmental Laboratories (MEL). The ^{234}Th activities from the pump samples and TS traps were corrected for decay to the time of collection. Samples from the SV traps were corrected for decay by utilizing the time series flux information from TS sediment traps deployed at each trap depth, as described in Szlosek et al. (2009).

Dissolved (<1 μm) ^{234}Th activities from the pump cartridges were determined by detecting the 63.3 keV gamma emission using an intrinsic germanium gamma detector. The manganese cartridges were dried and ashed in a muffle furnace (450˚C). The ash was placed in containers whose geometries had been standardized for the gamma detectors at SoMAS and MEL. Further details regarding the standardization are provided in Cochran et al. (2009). ^{234}Th in the small volume (2 l) unfiltered water samples was co-precipitated with MnO_2 and the precipitate was mounted for nondestructive beta counting, as described in Cochran et al. (2009).

2.2.2. Chemical Analyses

Particulate samples from pump fractions and sediment trap splits were used for total carbon (TC) and organic carbon (OC) analyses measured using a Carlo Erba model 1602 CNS analyzer. Splits of the sediment trap material were filtered onto GF/F 25 mm filters and dried. Duplicate 7-mm punches were taken from these filters and fumed with air saturated with HCl to eliminate $CaCO_3$ before POC measurement (Hedges and Stern 1984). The error for each carbon analysis was ± 5% (or 2%).

Measurements of organic compounds commonly used as biomarkers of particle source or transformation were made on sediment trap material splits and pump particle fractions. Details regarding extraction and analysis of pigments–comprising chloropigments and fucoxanthin–are given in Wakeham et al. (2009). Additionally, Wakeham et al. (2009) documented the methods for measuring total hydrolysable amino acids, and Abramson et al. (2010) discussed organic composition analysis of the pump-filtered particulate fractions.

2.2.3. Statistical Analyses

Abramson et al. (2010) performed principal component analysis (PCA) of the 2005 pump and TS sediment trap compositional data. Here we reexamine the PCA of the 2005 trap and pump data by including POC concentration (μmol l^{-1} or mg g^{-1}) and ^{234}Th concentration (dpm l^{-1} or dpm g^{-1}) data. We also include the SV compositional data in our PCA analyses. The relationships between samples are inferred by the patterns formed by their sample site scores on a 2D plane consisting of one axis defined by principal component 1 (PC 1) and a second axis defined by principal component 2 (PC 2). Compositional variables (e.g., individual amino acid abundances) plot out positively or negatively with increasing absolute magnitude that is scalable to the influence the variable has on processes that explain the first and second orders of variation in samples. In environmental biogeochemical studies the sample site scores often spread out according to their source and degree of degradation along PC1 and PC2 (Gõni et al., 2000; Sheridan et al., 2002; Engel et al., 2009; Abramson et al., 2010).

3. Results

3.1. POC/^{234}Th Ratios of Pump and Trap–Collected Particles

The ratios of particulate organic carbon to ^{234}Th, referred hereafter as C/Th ratios, were determined in material collected by IRSC sediment traps in TS and SV modes (Table 3.1). In addition, ratios were measured for material filtered *in situ* into 1-70 μm and > 70 μm fractions. We refer to these filtered fractions as small particles (SP) for the 1-70 μm fraction and large particles (LP) for the > 70 μm fractions (Table 3.1). As discussed in Szlosek et al. (2009), the mass-weighted average C/Th for the TS and SV sediment trap samples are comparable. The C/Th values in the SP fraction are within a factor of 2 of those from the trap whereas the LP pump fraction C/Th are up to 10-20 times greater than the trap ratios for the shallow and deep depths, respectively. The disparity in C/Th between particle collection techniques is evident in Fig. 3.1a, b.

The response of the C/Th ratio to time-dependent inputs, such as dust and Chl-*a* abundance, varied with particle collection method. The TS sediment trap C/Th values followed the same pattern as the trap OC%. For the first 25 days of the 55 day trap deployment the 313 m C/Th changed relatively little (mean 0.9 ± 0.01 μmol dpm^{-1}) and subsequently increased to a maximum of 4.1 ± 0.4 μmol dpm^{-1}. An increase in TS trap C/Th occurred as surface Chl-*a* levels rose and atmospheric dust events occurred (Fig. 3.1a,b). In contrast, LP and SP C/Th ratios were higher than those of the TS sediment trap material sampled at the same time (Table 3.1). High C/Th in filterable particles correlated with high fluorescence Chl-*a* seen in CTD casts taken within hours of the *in situ* pump casts (Appendix Fig. 3.A1, Cochran et al., 2009). Upper water column CTD fluorescence Chl-*a* values are nearly twice as large as satellite surface Chl-*a* data at the time of the pump casts (~1 μg l^{-1} on DOY 68 and 73; Lee et al., 2009b). We also observed relatively high LP and SP C/Th in samples taken 6 days after trap recovery (DOY 120) despite the rapid decrease in satellite-detected Chl-*a* occurring after trap recovery (Fig. 3.1a, b).

The shallow (313 m) IRSC sediment traps in settling velocity mode had average C/Th ratios of 1.2 ± 0.03 μmol dpm^{-1} (see Appendix Table 3.A2) with little (~30%) variation across the range of settling velocities. As noted by Szlosek et al. (2009), if one assumes that large particles have greater settling velocities, there was no correlation in C/Th with the volume: surface area of the SV fractions, (Table 3.A2).

The C/Th ratios for *in situ* pump samples taken throughout the water column are given in Table 3.2. In March, the C/Th ratios ranged from 1.6-20 μmol dpm^{-1} and 0.6-6 μmol dpm^{-1} for the LP and SP fractions, respectively, with mean values (0-300 m) of 5.3 ± 0.08 μmol dpm^{-1} for the LP fraction and 3.2 ± 0.2 μmol dpm^{-1} for the SP fraction. In April the water column C/Th ratios varied from 8-47 μmol dpm^{-1} and 2-16 μmol dpm^{-1} for the LP and SP pump fractions, respectively. Mean values in the upper water column (0-300 m) were over 2 times greater than in March: 16 ± 9 μmol dpm^{-1} for the LP fraction and 8.8 ± 2.2 μmol dpm^{-1} for the SP fraction. Greater errors in the C/Th estimates for the >70 μm fraction in 2005 arose from uncertainty in the LP ^{234}Th activities that were generally ≤0.002 dpm l^{-1}.

The C/Th of the filterable particles changed with depth at the DYFAMED site, as shown also in studies elsewhere (Cochran et al., 2000; Buesseler et al., 2006; Cai et al., 2006). In mid-March the SP and LP fraction C/Th were comparable below 100 m and both fractions showed a maximum in the photic zone (Table 3.2). In late April, the values of the >70 μm fraction were high (>10 μmol C dpm $^{234}Th^{-1}$) throughout the water column and did not show any clear trend with depth. Satellite sea-surface chlorophyll data indicated high chlorophyll at the surface during this time period (see Stewart et al., 2007). As sea-surface chlorophyll levels intensified, the C/Th of the >70 μm and 1-70 μm were closer in magnitude and the peak values of C/Th shifted down through the water column as time progressed.

3.2. Principal Component Analysis

We performed PCAs using the complete 2005 sediment trap and *in situ* pump data (Fig. 3.2a) and using trap data and the *in situ* pump data from depths 300 m and greater (Fig. 3.2b). The latter was done because a large proportion of pump samples (63%) were from within the upper waters (0-300 m) and, with a deep chlorophyll maximum at ~25 m, we found that the sample site scores were skewed in a way that exaggerated the differences between SP, LP and trap samples when including these 0-300 m pump samples. The PCA using all the data explained 40.4% of the variability, with PC1 and PC2 representing 22.5% and 17.9% of the variability, respectively (Fig. 3.2a). For samples from 300 m and deeper, the first two principal components accounted for ~43% of the total sample variability, with

PC1 representing 23.6% and PC 2 representing 19.0% of the variability (Fig. 3.2b). SP and LP samples plotted closer together in the ≥ 300 m PCA than when the 0-300 m samples were included (Fig 3.2a,b).

For both PCAs, PC1 seemed to indicate the degree of biogenic source and possibly extent of degradation. Many of the details of the two PCAs were the same except that the orientation of sample site scores and variable loadings were reversed. Regions of the PCA can be designated as representing specific compositional types or biogenic source based on the clustering of variable loadings for biomarkers that are representative of diatoms, fecal pellets, etc. The PCA that included data from the upper 300 m (Fig. 3.2a) and was thus skewed toward that depth region shows separation mainly along the PC1 axis.

On the negative portion of PC1, compositional types include fresh phytoplankton characterized by Chl-*a*, glutamic acid (GLU), and aspartic acid (ASP) and most likely dominated by calcium carbonate-bearing plankton such as coccolithophores (King, 1974; Weiner and Erez, 1984). Also negative on PC1, but not far from the origin, is fucoxanthin ("fuco"), a pigment indicative of the presence of diatoms. Other biomarkers of diatoms-the amino acids glycine (GLY), serine (SER), and threonine (THR)–plot on the positive side of PC1 (Swift and Wheeler, 1991; Ingalls et al., 2003). Both diatoms and prymnesiophyceae (coccolithophores) are phytoplankton groups dominant in early spring blooms of the NW Mediterranean (Gutiérrez-Rodríguez et al., 2010). Markers of bacterially reworked material (e.g., the microbial product of chlorophyll alteration, pheophytin ("phytin"), and the degradation product of ASP and GLU, ß-alanine (BALA)) plot negatively on PC1, but close to the origin, possibly indicating bacterial degradation as the dominant alteration process affecting aggregates containing coccolithophores.

Conversely, on the positive portion of PC1, there are variable loadings that represent zooplankton-produced alteration products of chlorophyll, namely pheophorbide ("phide") and pyropheophorbide ("pyrophide") that we interpret as indicative of fecal pellets (Currie, 1962; Mantoura and Llewellyn, 1983; Welschmeyer and Lorenzen, 1985). Of note, ^{234}Th plots near these loadings, suggesting that the presence of fecal pellets could have yielded a relative enrichment of ^{234}Th as has been reported elsewhere (Stewart and Fisher, 2003; Rodriguez y Baena, et al., 2007).

For the PCA that excluded the filterable particle data from less than 300 m (Fig. 3.2b),

the pump and sediment trap sample site scores weakly suggest the PC2 axis separates samples according to depth with shallow material plotting more positively. However, it is more difficult to distinguish the separation of samples along PC2 because the positive portion of PC2 is less descriptive. The variable loadings there include biomarkers present in much of marine and terrestrial organic matter: arginine (ARG), valine (VAL), tyrosine (TYR), and phenylalanine (PHE). However, moving down PC2 the biomarkers shift from those representing fresh algal material (POC, Chl-*a*, GLU, fuco, and THR) to zooplankton and bacteria-produced chlorophyll degradation products (phide, pyrophide, phytin, γ-aminobutyric acid-GABA, and BALA).

When comparing the organic biomarker composition of TS and SV sediment trap samples with pump samples we see a clear separation between the SP, LP, and sediment trap material (Fig. 3.2a). The SP samples plot furthermost on the negative portion of the PC1 axis and sediment trap material plots on the positive portion of PC1. The LP samples lie between, and overlap, these two end-members. Not surprisingly, the SV and TS samples plot on top of each other. To investigate if there are compositional differences in the fast versus slowly settling particles, samples of different settling velocity classes are plotted in different colors on the PCA figures (3.2a, b). We include all particles that settle at rates ≤ 40 m d^{-1} as the slow settling class and particles settling at rates >49 to 979 m d^{-1} as the fast settling class. We observe a slight shift of the SV settling velocity classes, with faster settling particles being closer to the origin and the slowly settling particles being more positive along PC1 for trap depths of 313 and 524 m.

3.3. Water Column ^{234}Th Deficits and Fluxes

The water column ^{234}Th deficits calculated from the disequilibrium with its parent, ^{238}U, have been reported in Cochran et al. (2009). Deficits are determined from both pump and small volume samples (Table 3.5; Cochran et al., 2009). Water column ^{234}Th profiles based on the data from pump casts are shown in Appendix Fig. 3.A1. In 2005, ^{234}Th deficits did not penetrate as deeply as previous years (2003; Stewart et al., 2007) and were limited to the upper water column due to density stratification and the timing of the sampling during the early stages of the bloom. Particulate ^{234}Th activities (>1 μm) within the water column peak at the depths of the deep chlorophyll maximum (DCM, Cochran et al., 2009). In

addition, density horizons observed below the DCM show marked ^{234}Th deficits coincident with fluorescence maxima (Cochran et al., 2009).

The ^{234}Th deficits yielded a range of (steady state) ^{234}Th fluxes from 630-2200 dpm m^{-2} d^{-1} in March, 2005. The ^{234}Th fluxes calculated from the water column deficits are a factor of 1.2-1.8 greater than trap ^{234}Th fluxes. Hence, by the end of April there was a slight surplus of ^{234}Th in the water column, yielding a "negative" flux (Cochran et al., 2009)

Thorium-234 data for the 2005 time series and sediment trap samples were discussed in detail in Szlosek et al. (2009). The two traps moored together at 313 m one in each mode, TS and SV mode, showed relatively good agreement, with overall ^{234}Th fluxes of ~1200 and ~1400 dpm m^{-2} d^{-1}, respectively. The individual 5-day ^{234}Th fluxes during the TS trap deployment ranged from 70–2500 dpm m^{-2} d^{-1}.

3.4. Trap POC Fluxes

The time series sediment trap data reveal that OC fluxes were highest at the beginning of the deployment in 2005, ~2 mmol C m^{-2} d^{-1} and decreased to 0.3 mmol C m^{-2} d^{-1} by late April with a weighted mean of ~ 1.3 mmol C m^{-2} d^{-1} (Lee et al., 2009b; Szlosek et al., 2009). Moreover, 50% of the total OC flux collected in the shallow traps fell at rates of ≥100 m d^{-1} (Szlosek et al. 2009). As expected, the settling velocity class containing the largest abundance of OC was 196–490 m d^{-1} (Szlosek et al., 2009).

4. Discussion

4.1. Comparison of Biogeochemical Influences on Pump and Trap C/Th

Studies that observe similar C/Th ratios for pump and trap samples often conclude that pump-derived C/Th can be used together with water column ^{234}Th deficits to reliably predict the settling POC flux (Buesseler et al., 2006). Recently, Hung and Gong (2010) propose a more accurate POC flux estimate is obtained when using trap-derived C/Th ratios with water column 234Th deficits. Despite these comparisons, compositional data for pump and trap material is rarely obtained to confirm that the filterable particles are representative of the sinking material. Biological, chemical, and physical processes act on particles as they settle, and thus, compositional data enable an assessment of the dominant processes affecting the C/Th ratio. Table 3.3 summarizes the C/Th values and

compositional types of each fraction sampled in 2005. The compositional types listed in Table 3.3 are derived from our interpretations of the cluster of variable loadings from the PCAs (Fig. 3.2a, b). These data allow us to (1) test the implied assumption that similar C/Th may indicate similarity between pump and trap caught material and (2) investigate the effects of biogeochemical processes on the C/Th ratio, as proposed by Buesseler et al. (2006).

The chemical composition data reveal significant differences between the filterable SP fraction and the TS and SV sediment trap material despite the fact that the C/Th ratios are within a factor of 2– agreement that is considered to be good by most workers (e.g. Buesseler et al., 2006; Fig. 3.2a, b, Table 3.1, 3.2, 3.A2). The composition of the SP fraction is consistent with fresh algal material containing diatoms and coccolithophores in contrast to the sediment trap material that plots near pigments indicative of fecal pellets (zooplankton-altered chlorophyll degradation products, labelled as phide and pyrophide) in the PCA (Fig. 3.2a). The similar C/Th ratios of traps and the SP fraction sampled by pumps most likely arise from two distinct combinations of biogeochemical processes. First, the low C/Th of the SP fraction may be a result of its dimensional quality of having a low volume to surface area ratio (*V*:SA) such that there are proportionally more surface sites onto which ^{234}Th can adsorb (Cochran et al., 2000; Buesseler et al., 2006). In contrast, the low C/Th of the sediment trap material may reflect the high abundance of fecal pellets captured in the traps, with preferential assimilation of carbon by zooplankton and retention of Th within the pellet (Coale, 1990).

As noted by Szlosek et al. (2009), there is no trend in C/Th with settling velocity– contradicting expectations of a scaling of C/Th with size (i.e., settling velocity; Alldredge and Gotschalk, 1989). Speicher et al. (2006) document a similar finding in which C/Th showed no relationship with particle size (1, 10, 20, 53, 70, 100 μm) in the northwest Mediterranean. One mechanism by which C/Th can be maintained over variable particle sizes or settling velocities is through particle aggregation or disaggregation (Burd et al., 2000; Buesseler et al., 2006; Waite and Hill, 2006; Burd et al., 2007). If the biological source of the primary particles (e.g., cells, fecal pellets, etc) establishes the C/Th (Buesseler et al., 2006 and references therein) in the upper water column, the C/Th of the settling particles can be maintained despite aggregation or fragmentation (growing or shrinking of

aggregate size) if the primary particles remain coherent. Thus, *V*:SA is no longer a modulating factor for the C/Th. Two aggregation/disaggregation scenarios that would yield similar C/Th ratios and chemical composition among SV classes are 1) fast settling particles disaggregate to form slowly settling ones at depth or 2) a continuum of particles (slow to fast, small to large) undergoes rapid exchange of material by aggregation and disaggregation processes throughout the water column, gradually homogenizing their chemical composition with depth. In fact, these ideas were first expressed by Lee et al. (2009) in their review of the MedFlux composition data.

The PCA does not conclusively rule out either of the two aggregation/disaggregation scenarios described above because the slow and fast settling velocity classes are chemically similar to one another (Fig. 3.2a, b) at all depths (313, 524, 1918 m). However at 313 m, site scores of slow and fast settling velocity classes plot over a large range of PC2 values whereas at 524 and 1918 m the range of PC2 values covered by the slow and fast settling velocity classes are similar–more condensed, and located more negatively on PC2 suggesting greater alteration of fresh algal material with depth (as indicated by the biomarkers pyrophide, phytin, BALA, phide, GABA). In addition to the overall consolidation of sample site scores for 524 and 1918 m, the spread of the site scores for slow and fast SV classes are relatively equal for these depths. This is in contrast with the 313 m SV sediment trap sample site scores, in which there is a greater spread in the slow SV class site scores with the site score of a single slow SV class (0.68–5.4 m d^{-1}) having negative PC2 values. Fast SV classes of the 313 m trap, on the other hand, remained near the origin of PC2, in proximity to the foci of fresh algal composition indicators fuco and MET (Fig. 3.2b). This downshift in the spread of site scores along PC2 for 313 m compared to 524 and 1918 m is consistent with particle exchange that homogenizes chemical composition occurring by the time particles settle to the depths of these two deeper traps. Supporting this, Marty et al. (2009) document lipid class and organic matter data in 2004 at the DYFAMED site that suggest rapid and extensive exchange of the dissolved, suspended and sinking pools of material by 200 m.

Despite our observations made from the PCA data, compositional variability between slow and fast settling velocity classes is low and no sediment trap site scores cross over to the negative side of PC1 where fresh algal indicators of diatoms and coccolithophores are

present, for example. Accordingly, the second scenario cannot be ruled out: similar chemical compositions of slow and fast settling particles may suggest that rapidly settling material could have disaggregated into particles of slower settling velocities prior to trap interception.

The activities of ^{234}Th on the slow and fast settling particles provide clues to possible interactions among the SV classes. Szlosek et al. (2009) observed that the ^{234}Th flux increased with depth in the rapidly settling particles but remained essentially constant in the slow SV classes despite settling rates that would have permitted significant ^{234}Th decay in these particles. They suggested that ^{234}Th could be supplied to the slowly settling particles either by disaggregation at depth of rapidly sinking aggregates (with minimal ^{234}Th decay during sinking) or by additional scavenging of ^{234}Th onto the slowly settling particles, sufficient to offset Th decay. Either mechanism would attenuate any decrease in ^{234}Th among the SV classes and cause the C/Th ratio to remain the same or to decrease during settling. Indeed the SV sediment trap data display decreases in C/Th with increasing depth (Szlosek et al., 2009). Mass weighted C/Th at 313 m and 524 m were within 24% of each other (1.27 ± 0.03 μmol dpm $^{-1}$ and 0.967 ± 0.02 μmol dpm^{-1}, respectively). At 1918 m, ratios dropped to nearly half those at 524 m (0.47 ± 0.01) (Szlosek et al., 2009). However, there are additional, offsetting influences such as carbon assimilation, degradation, and abiotic dissolution (Coale, 1990; Bacon et al., 1996; Rutgers van der Loeff et al., 2002; Liu et al., 2009) that affect C on the settling particles and the particulate C/Th ratio. Thus we examine the chemical composition data to attempt to resolve the factors causing the decrease in C/Th from 313 m to 1918.

The PCA results show a marked difference in the 1918 m data in comparison with the data of the shallower SV sediment traps: the orientation of the slow and fast settling particle class site scores are reversed (Fig. 3.2b) compared with those at 313 and 524 m. Site scores of the fast SV class plot solely around phide (the zooplankton-derived degradation product) and indicators of diatoms and bacterially degraded algal material (GLY, SER, and GABA), implying the presence of fecal pellets containing diatom material and possibly bacterially reworked diatom aggregates. Thus, changes to both carbon (assimilation and degradation) and ^{234}Th (disaggregation of rapidly settling surface

particles and ^{234}Th adsorption at depth) combine to cause decreases in C/Th of trap material with depth.

4.2. Temporal and Spatial Variability of Filterable Particles

A major issue in using the ^{234}Th as a particle flux proxy is the difference in the time frame and location represented by the ^{234}Th deficit (dominated by the dissolved ^{234}Th; Cochran et al., 2009) versus that of the POC and ^{234}Th measured on filterable particles. In this section, we focus on how the C/Th and chemical composition of the SP and LP pump fractions helps us understand the timing of particle production and its horizontal and vertical transport in the water column.

The C/Th in the LP fraction is commonly used to derive POC flux estimates based on the premise that the larger fraction best represents the sinking particles (e.g. Bishop et al., 1977, 1978 and others thereafter). To investigate how robust this assumption is, we used compositional data to ascertain whether LP samples below the chlorophyll maximum (>25 m) correlated with their counterpart at the chlorophyll maximum (25 m) (e.g., whether March LP samples below 25 m are correlated with March LP sample at 25 m; Table 3.4). Overall there was little change in the chemical composition of the LP material below the chlorophyll maximum. Correlation coefficients for 25 m pump samples with those taken at depths from 50–1800 m ranged from 0.66–0.95 with an average of 0.8 ± 0.1 (Table 3.4). Exceptions to this trend were 100 and 150 m samples on March 13-14, as discussed below. This comparison suggests that the LP fraction generated in the euphotic zone does indeed sink. Furthermore, there is evidence that LP material sank rapidly, on the order of a few days- the compound ratios of phytin : Chl-*a* and ("phide + pyrophide") : Chl-*a* at 600 and 1800 m are fresher (i.e. lower) than at the chlorophyll maximum (Table 3.2). Additionally, the C/Th ratios at 1800 m are higher than those observed at 600 m signifying little degradation or assimilation of POC occurred between the time of particle production at the surface and collection at depth.

In contrast, the ^{234}Th deficit represents export occurring over a radioactive mean-life (35 days; Cochran and Masqué, 2003; Cochran et al., 2009) and it is reasonable to question whether the LP fraction collected in a pump cast is representative of the flux that resulted in the ^{234}Th deficit. Over the 2 sampling times, 5 days apart, in March, the LP fraction C/Th

exhibits a factor of 1.7 to 3 change at depths of 150-350 m–a depth range that might be used to integrate the export of flux from the surface. Given this large variability in the C/Th within a short time span (March 9-14), it is likely the LP C/Th ratio would vary equally as much over the time span represented by the ^{234}Th deficit–several weeks prior to the March sampling days.

Additionally, advection may transport water and particles laterally or vertically and imprint their signatures on the water column sampled. Markedly, our compositional data of the LP fraction revealed a depth interval in which the source of the particles was significantly different from that in the rest of the water column. As noted above, the correlation coefficients for the LP fraction from March 9 at 100 and 150 m with that at 25 m were low (r^2 = 0.06 and 0.05, respectively). This low correlation may be due to the high fucoxanthin content in these March 9 samples, unlike those taken on other sampling dates in March. The difference in composition of the 100 and 150 m samples is not as apparent in the C/Th ratio, which is within a factor of 0.7–1.6 with those at the same depths on the March 13-14 sampling dates. However, the fuco: Chl-*a* ratio of the March 9 samples is 5-7 times greater than all other March LP pump fraction samples, indicative of diatoms. (Table 3.2). The placement of their site scores on the negative portion of PC1 in the PCA analysis supports the hypothesis that these samples contain fresh diatom material instead of fecal pellets containing diatom fragments (Fig. 3.2b, Table 3.2). Thus, filterable material collected at 100 m within a time span of ~5 days at the DYFAMED site can show variation in C/Th that may be caused by lateral advection of new production produced off-site. Indeed, Flexas et al. (2002) and Roy-Barman et al. (2002) have suggested that lateral advection can occur at DYFAMED.

Generally, SP C/Th ratios reported in the literature are lower than LP (e.g. Buesseler et al., 2006), as was observed in the present study. When comparing the SP fraction to the LP fraction, the expectation is for it to be less dense and sink more slowly due to its size (Alldredge and Gotschalk, 1989). Its composition would either reflect this by being more highly degraded (Wakeham and Lee, 1993), which in addition to its lower *V*:SA would yield lower C/Th ratios (Buesseler et al., 2006). Alternatively, the SP fraction may have disaggregated from the LP fraction resulting in a similar chemical composition and C/Th ratio (Burd et al., 2007; Burd and Jackson, 2009). Waite and Hill (2006) proposed that

during *in situ* pump filtration, cross-filter shear stresses in close proximity to the prefilter may cause large, delicate floc-like aggregates, high in OC, to disaggregate. However, our PCA shows distinct separation between the LP and SP fractions, such that large particle break-up at during filtration by *in situ* pumps does not seem to be occurring (Fig. 3.2a).

Indeed, our composition data suggest that the LP and SP fractions are derived from different pools of algal aggregates. Explanation for the observed separation on the PCA of particles sampled by *in situ* pumps was presented by Abramson et al. (2010), who found that the SP fraction (1-70 μm) had a statistically significant enrichment of aspartic and glutamic acids, reflecting calcifying organisms as its source. Conversely, the LP fraction (>70 μm) had greater abundances of organic compounds that are markers of diatoms (GLY; SER; THR; fuco), in addition to the presence of aspartic and glutamic acids. Both the cluster of LP site scores plotting close to the sediment trap samples and compound ratios in the LP samples suggest the presence of zooplankton alteration products (Fig. 3.2a,b, Table 3.2; Abramson et al., 2010). Therefore, the LP fraction appears to consist of algal material from diatoms and coccolithophores as well as fecal pellets.

A surprising outcome of the chemical composition analysis on the pump SP fractions is that in March 2005, a high chlorophyll signal persists to 1800 m (Abramson et al., 2010). This material was not observed in the LP fraction or in the sediment traps. As seen from the PCA (Fig. 3.2a), the SP samples collected during MedFlux 2005 separate from the LP fraction, which is more similar to the material collected by the sediment traps (Fig. 3.2a). As well, the C/Th ratio in the SP fraction sampled in March varies little with depth (2.8 ± 1.2 μmol dpm^{-1}; Table 3.2). Both lines of evidence suggest that there was minimal bacterial or zooplankton reworking of the SP fraction. For example, Abramson et al. (2010) pointed out the phytin : Chl-*a* was <1 in March. Conversely, phytin : Chl-*a* were >1 for most LP and sediment trap samples in March and April and for the SP fraction in April (Table 3.2). These results are contrary to the prevailing notion that the organic matter in the SP fraction below the euphotic zone must be highly degraded (Wakeham and Lee, 1993). According to Stokes' Law and field-determined decay constants for Chl-*a*, the chlorophyll in SP fraction particles should degrade rapidly during settling, over a depth scale of 2.5-17 m below the euphotic zone (Abramson et al., 2010).

Abramson et al. (2010) suggested that the deep chlorophyll signal of the SP fraction could be the result of rapidly sinking aggregates that fragmented, resulting in a background of fresh algal material or that this fraction could could have been transported from the surface by physical advection. It is possible that physical advection of small particles contributed to the lack of variability C/Th with depth in March. In fact, there was an anomalously high winter mixing period that lasted from January through spring of 2005 (Font et al., 2007; Miquel et al., 2011). Such mixing could have allowed particles to be distributed throughout the water column, facilitating the injection of fresh algal material deep into the water column. Therefore, it appears that in episodic high-energy environments the dissolved and small particulate pools of ^{234}Th are greatly affected by physical advection and can change on rapid timescales.

4.3. Comparison of ^{234}Th– and Trap–Derived POC Fluxes

In previous sections, we have seen that the pump-collected particles and trap material at the DYFAMED site in spring, 2005 are compositionally distinct. In particular, the SP fraction comprises fresh phytoplankton material (with a relatively high surface area and low C/Th ratio), while the LP fraction includes both fresh diatoms and zooplankton-altered material (i.e fecal pellets). Fecal pellets dominate the sediment trap material, which has relatively low C/Th ratios affected by physical interactions among the fast and slowly settling particles and modifications to both the C (decreases) and ^{234}Th (increases) of the particles during settling that combine to produce lower C/Th ratios (Szlosek et al., 2009).

A common approach in applying the ^{234}Th-POC flux proxy is to use the C/Th ratio of the large filterable particles as the best approximation to that in the settling material:

$$J_{POC} = (POC/^{234}Th)_{LP} * J_{Th} \quad (1)$$

Table 3.5 summarizes the results of this approach applied to the pump casts in March-April, 2005. The C/Th ratios of the LP fraction (3-5 μmol dpm^{-1}) are several times greater than those of material caught in the traps (~1 μmol dpm^{-1}). The POC fluxes calculated using Eq. 1 are ~4 times greater than those in the trap for the March 9 pump cast, but are comparable for the March 13 cast, largely due to the factor of 4 decrease in the water column ^{234}Th deficit between March 9 and March 13 (Table 3.5). The SP C/Th ratios are

generally more similar to the trap values, and the POC fluxes generated using them are within a factor of 2 of the trap values (Table 3.5). For the April 29–30 pump cast, the LP C/Th ratios are ~3 times those of the trapped material while the SP C/Th ratios are within a factor of 2 (Table 3.5). However, the water column ^{234}Th deficit is essentially zero within the uncertainty at that time, making it not possible to calculate a meaningful POC flux from the ^{234}Th proxy.

Relatively better agreement between trap POC fluxes and those determined with the ^{234}Th proxy using the small particle C/Th ratios has been noted by other workers (Moran et al., 2003; Hung and Gong, 2007; Savoye et al., 2008; Lepore et al., 2009; Hung and Gong, 2010). In the present case, we calculate POC fluxes from two water column ^{234}Th profiles taken 4 days apart that range from 4 times less to 4 times greater than the integrated trap POC flux over the same time period, depending on the choice of C/Th in filterable particles to represent the sinking flux (Table 3.5). Indeed, one may be "lucky" and hit the trap flux precisely, as is the case using the LP C/Th and water column ^{234}Th deficit on March 13 (Table 3.5).

A variety of factors must contribute to the lack of agreement in ^{234}Th- vs trap-derived POC flux estimates. Cochran et al. (2009) discussed in detail the non-steady-state nature of the water column ^{234}Th deficit (highlighted in Table 3.5), which is dominated by the "dissolved" ^{234}Th. Advection can act differentially on particles and dissolved solutes–notably, the spatial integration for the latter is much greater than for the former. Even in the case of particles, advective influences may act differently depending on particle class. The sediment trap material sampled at DYFAMED in 2005 is dominated by rapidly settling fecal pellets, whereas the filterable material, especially the small particle fraction, is likely subject to greater advective influences. This is apparent in the presence of fresh phytoplankton in the SP fraction throughout the water column in March, 2005, as noted above.

Sediment trap material as well may be subject to collection biases, for example, that might have arisen from the exceptional mixing at DYFAMED occurring from winter through early spring, 2005 (See the Appendix for additional detail on the hydrography at the DYFAMED site in 2005). Current meters at 250 and 425 m measured currents of 12.37 ± 6.5 cm s^{-1} (range 0.5–27.1 cm s^{-1}) and 14.17 ± 7.0 cm s^{-1} (range 0.7–28.9 cm s^{-1}) (Lee et al.,

2009b). In their review of the 1988–2005 flux record at DYFAMED, Miquel et al. (2011) noted that spring, 2005 had a maximum current of 34 cm s^{-1} and 41.6% of the current measurements made were above 12 cm s^{-1}—the limit for acceptable collection efficiency according to trap performance studies (Fabrés et al., 2002; Martín et al., 2006). Furthermore, Miquel et al. (2011) argued that the flux estimates for 2005 must be used with caution because of the likelihood of under-collection by sediment traps. As well, chemical composition data show that the traps in spring, 2005 under-collected the SP fraction. Abramson et al. (2010) estimated that the SP fraction typically represented only 1-10% of the trap material, despite the fact that the SP material was effectively transported to depth in the water column. Could the high current velocities have caused the fresh rapidly settling algal aggregates that are present in the deep SP fraction to have been missed by the sediment traps?

In fact, past trap studies at DYFAMED seem to confirm this trend even without the intensity in winter mixing observed in 2005. In spring of 2003 (MedFlux) and summer season in 2004 (DYNAPROC 2), IRS and drifting sediment traps, respectively, collected bacterial and zooplankton reworked material and noted the absence of fresh phytoplankton material in all settling velocity classes (Marty et al., 2009; Wakeham et al., 2009). In contrast, Alonso-González et al. (2010) found that the slow SV classes (1-10 m d^{-1}) of an IRSC SV trap deployed at 260 m in the Atlantic south of the Canary Islands in June–December 2005 contained the fresh algal biomarker, chlorophyll-*a*. The currents were lower during that study (average 7 m s^{-1}), but the persistence of the fresh algal signal at depth in the water column could not be determined as there were no sediment traps deployed in the deep water column (Alonso-González et al., 2010).

It is also plausible that the relatively short filtration times (~2 h), fast settling rates of fecal pellets, and diel migratory patterns of some zooplankton (Welschmeyer, 1982; Lorenzen and Welschmeyer, 1983; Welschmeyer and Lorenzen, 1984) may have prevented the filterable particles from accurately representing the contribution of fecal pellets to the exported flux. Thus, C/Th of the SP and LP pump fractions might be elevated with respect to the bulk of flux due to the absence of fecal pellets. This is especially true for the SP fraction that had (phide + pyrophide): Chl-*a* ratios <<1. However, we note the (phide + pyrophide) : Chl-*a* compound ratios of the upper 300 m LP fraction are similar to those for

the trap at 313 m (6.4 ± 6.1 and 8.1 ± 8.2 , respectively; Table 3.2), suggesting that the former most likely contained fecal pellets. Indeed, the LP fraction site scores may plot close to those of the SV trap for this reason (Fig. 3.2a,b). Rodriguez y Baena et al. (2007) reported C/Th for freshly collected fecal pellets from zooplankton at DYFAMED as 2.6, 10, and 13.4 μmol C dpm^{-1} Th for salps, euphausiids, and copepods, respectively. These relatively high values suggest that the effect of carbon assimilation on C/Th may not be as dramatic as suggested by Buesseler et al. (2006). Hence, the high and variable C/Th of the LP fraction in March and April (Table 3.2) may have resulted from the presence of euphausiid and copepod fecal pellets. It is possible that *in situ* filtration missed rapidly settling fecal pellets such as from salps (1000–3600 m d^{-1}; Bruland and Silver, 1981; Morris et al., 1988) as well as degraded fecal pellets (Yoon et al., 1996) and those ballasted by lithogenic material (Fowler et al., 1987; Buat-Ménard et al., 1989; Miquel et al., 2011). Collecting such material in the traps would have resulted in relatively lower C/Th ratios in trap material.

5. Summary and Conclusions

Selecting a POC/^{234}Th ratio to use in conjunction with water column ^{234}Th deficits is critical to its application of ^{234}Th as a proxy for POC flux in the oceans. In this study, we have used organic chemical and radionuclide data for particles collected by *in situ* filtration in two size classes, SP (1-70 μm) and LP (> 70 μm), as well as those collected by sediment traps (in both time-series and settling-velocity modes) to examine linkages among the particles. The C/Th ratios of the SP fraction and sediment trap material are similar to each other (0.5–2) and to values observed in previous studies (Buesseler et al., 2006; Waite and Hill 2006; Lepore et al. 2009; Hung and Gong 2010; Hung et al. 2010), yet principal components analysis (PCA) shows little overlap in chemical composition between these two particulate pools. The SP fraction contains fresh algal biomarkers of coccolithophores and diatoms and its C/Th is low relative to the LP fraction, likely due to the effect of low *V*:SA. Moreover, the SP fraction exhibited a detectable Chl-*a* signal to depths of 1800 m in March, 2005 due to the rapid sinking of fresh algal aggregates and physical advection of surface material to the deep water column by anomalously strong winter-early spring mixing (2005) in the NW Mediterranean. However, no fresh algal material was detected in any of the trap fractions, and high currents at the mouth of the trap may have led to under-

collection of the fresh, small particles. Most trap samples contained biomarkers indicative of fecal pellet and bacterially degraded material; carbon assimilation and degradation likely led to the relatively low C/Th ratios in the trapped material. The lack of dependency of the C/Th and composition data with settling velocity (Lee et al., 2009b; Szlosek et al., 2009) suggested there was either extensive exchange of slow and fast settling particles prior to trap collection or fast settling aggregates fragmented prior to trap interception. In comparison, the pump LP fraction C/Th was high (range of 3–11 μmol dpm^{-1} at 300 m) and variable (decreasing by a factor of ~2 in 5 d) and contained biomarkers of both fresh algal material and fecal pellets. The C/Th ratios in the LP fraction are comparable to those determined on fresh fecal pellets from zooplankton at the DYFAMED site (Rodriguez y Baena et al., 2007).

There is a high correlation between the composition of the LP fraction in mid- and deep waters with that at the chlorophyll maximum at ~25 m, suggesting that the LP-type material was indeed sinking. Thus, both large and small particles filtered *in situ* as well as material collected in traps represent components of the sinking flux, yet these particle pools are compositionally distinct. With respect to application of the ^{234}Th proxy for POC flux, the C/Th in neither filterable fraction accurately represents that in trapped material. In particular, the large short-term changes in both the C/Th of filterable particles and the water column ^{234}Th deficit make it difficult to apply the proxy with any confidence at the DYFAMED site. A similar conclusion was reached by Stewart et al. (2007), who observed offsets between Th- and Po-derived POC fluxes and sediment trap POC fluxes in samples collected in the 2003 MedFlux expedition. In aggregate, our results suggest that facile application of the ^{234}Th proxy for POC flux is unwise and that considerable effort must be expended to constrain its validity in any given oceanic region.

References

Abramson, L., Lee, C., Liu, Z.F., Wakeham, S.G., Szlosek, J., 2010. Exchange between suspended and sinking particles in the northwest Mediterranean as inferred from the organic composition of *in situ* pump and sediment trap samples. Limnology and Oceanography 55 (2), 725-739.

Alldredge, A.L., Gotschalk, C.C., 1989. Direct observations of the mass flocculation of diatom blooms: characteristics, settling velocities and formation of diatom aggregates. Deep-Sea Research 36, 159-171.

Alonso-González, I.J., Arístegui, J., Lee, C., Sanchez-Vidal, A., Calafat, A., Fabrés, J., Sangrá, P., Masqué, P., Hernández-Guerra, A., Benítez-Barrios, V., 2010. Role of slowly settling particles in the ocean carbon cycle. Geophysical Research Letters 37, L13608.

Altabet, M.A., Deuser, W.G., Honjo, S., Stienen, C., 1991. Seasonal and depth-related changes in the source of sinking particles in the North Atlantic. Nature 354 (6349), 136-139.

Armstrong, R.A., Lee, C., Hedges, J. I., Honjo, S., Wakeham, S., 2002. A new, mechanistic model for organic carbon fluxes in the ocean based on the quantitative association of POC with ballast minerals. Deep-Sea Research II 49, 219-236.

Armstrong, R.A., Peterson, M.L., Lee, C., Wakeham, S.G., 2009. Settling velocity spectra and the ballast ratio hypothesis. Deep-Sea Research II 56, 1470-1478.

Bacon, M.P., Cochran, J.K., Hirschberg, D., Hammar, T.R., Fleer, A.P., 1996. Export flux of carbon at the equator during the EqPac time-series cruises estimated from ^{234}Th measurements. Deep-Sea Research II 43, 1133-1153.

Bishop, J.K., Edmond, J.M., Ketten, D.R., Bacon, M.B., Silker, W.B., 1977. The chemistry, biology and vertical flux of particulate matter from the upper 400 m of the equatorial Atlantic Ocean. Deep-Sea Research I 24, 511-548.

Bishop, J.K.B., Ketten, D.R., Edmond, J.M., 1978. The chemistry, biology, and vertical flux of particulate matter from the upper 400 m of the Cape Basin in the southeast Atlantic Ocean. Deep-Sea Research 25, 1121-1161.

Bruland, K.W., Silver, M.W., 1981. Sinking rates of fecal pellets from gelatinous zooplankton (Salps, Pteropods, Doliolids). Marine Biology 63, 295-300.

Buat-Ménard, P., Davies, J., Remoudaki, E., Miquel, J.-C., Bergametti, G., Lambert, C.E., Ezat, U., Quetal, C., La Rosa, J., Fowler, S.W., 1989. Non steady-state biological removal of atmospheric particles from Mediterranean surface waters. Nature 340 (6229), 131-134.

Buesseler, K.O., Cochran, J. K., Bacon, M. P., Livingston, H. D., Casso, S. A., Hirschberg, D., Hartman, M. C., Fleer, A. P., 1992. Determination of thorium isotopes in seawater by nondestructive and radiochemical procedures. Deep-Sea Research I 39, 1103-1114.

Buesseler, K.O., 1998. The decoupling of production and particulate export in the surface ocean. Global Biogeochemical Cycles 12 (2), 297-310.

Buesseler, K.O., Ball, L., Andrews, J., Cochran, J.K., Hirschberg, D.J., Bacon, M.P., Fleer, A., Brzezinski, M., 2001. Upper ocean export of particulate organic carbon and biogenic silica in the Southern Ocean along 170°W. Deep-Sea Research II 48 (4275-4297).

Buesseler, K.O., Andrews, J.E., Pike, S., Charette, M.A., Goldson, L.E., Brzezinski, M.A., Lance, V.P., 2005. Particle export during the Southern Ocean Iron Experiment (SOFeX). Limnology and Oceanography 50, 311-327.

Buesseler, K.O., Benitez-Nelson, C.R., Moran, S.B., Burd, A., Charette, M., Cochran, J.K., Coppola, L., Fisher, N.S., Fowler, S.W., Gardner, W.D., Guo, L.D., Gustafsson, O., Lamborg, C., Masqué, P., Miquel, J.C., Passow, U., Santschi, P.H., Savoye, N., Stewart, G., Trull, T., 2006. An assessment of particulate organic carbon to thorium-234 ratios in the ocean and their impact on the application of ^{234}Th as a POC flux proxy. Marine Chemistry 100, 213-233.

Buesseler, K.O., Lamborg, C.H., Boyd, P.W., Lam, P.J., Trull, T.W., Bidigare, R.R., Bishop, J.K.B., Casciotti, K.L., Dehairs, F., Elskens, M., Honda, M., Karl, D.M., Siegel, D.A., Silver, M.W., Steinberg, D.K., Valdes, J., Mooy, B.V., Wilson, S., 2007a. Revisiting carbon flux through the ocean's twilight zone. Science 316, 567-570.

Buesseler, K.O., Antia, A.N., Chen, M., Fowler, S.W., Gardner, W.D., Gustafsson, O., Harada, K., Michaels, A.F., Rutgers van der Loeff, M., Sarin, M., Steinberg, D.K., Trull, T., 2007b. An assessment of the use of sediment traps for estimating upper ocean particle fluxes. Journal Marine Research 65, 345-416.

Buessler, K.O., Boyd, .P.W., 2009. Shedding light on processes that control particle export and flux attenuation in the twilight zone of the open ocean. Limnology and Oceanography 54 (4), 1210-1232.

Burd, A.B., Moran, S.B., Jackson, G.A., 2000. A coupled adsorption-aggregation model of the POC/^{234}Th ratio of marine particles. Deep-Sea Research I 47, 103-120.

Burd, A.B., Jackson, G.A., 2009. Particle aggregation. Annual Reviews of Marine Science 1, 65-90.

Burd, A.B., Hansell, D.A., Steinberg, D.K., Anderson, T.R., Aristegui, J., Baltar, F., Beaupre, S.R., Buesseler, K.O., DeHairs, F., Jackson, G.A., Kadko, D.C., Koppelmann, R., Lampitt, R.S., Nagata, T., Reinthaler, T., Robinson, C., Robison, B.H., Tamburini, C., Tanaka, T., 2010. Assessing the apparent imbalance between geochemical and biochemical indicators

of meso- and bathypelagic biological activity: What the @$#! is wrong with present calculations of carbon budgets? Deep-Sea Research II 57 (16), 1557-1571.

Burd, A.B., Jackson, G.A., Moran, S.B., 2007. The role of the particle size spectrum in estimating POC fluxes from $^{234}Th/^{238}U$ disequilibrium. Deep-Sea Research I 54, 897-918.

Cai, P., M. Dai, W. Chen, T. Tang, K. Zhou, 2006. On the importance of the decay of ^{234}Th in determining size-fractionated C/^{234}Th ratio on marine particles. Geophysical Research Letters 33, L23602.

Charette, M.A., Moran, S.B., Bishop, J.K.B., 1999. ^{234}Th as a tracer of particulate organic carbon export in the subarctic Northeast Pacific Ocean. Deep-Sea Research II 46 (11-12), 2833-2861.

Clegg, S.L., Whitfield, M., 1990. A generalised model for the scavenging of trace metals in the open ocean, I, particle cycling. Deep-Sea Research I 37, 809-832.

Coale, K.H., Bruland, K.W., 1985. ^{234}Th:^{238}U disequilibria within the California Current. Limnology and Oceanography 30 (1), 22-33.

Coale, K.H., Bruland, K.W., 1987. Oceanic stratified euphotic zone as elucidated by ^{234}Th:^{238}U disequilibria. Limnology and Oceanography 32 (1), 189-200.

Coale, K.H., 1990. Labyrinth of doom: a device to minimize the "swimmer" component in sediment trap collections. Limnology and Oceanography 35 (6), 1376-1381.

Cochran, J.K., Buesseler, K.O., Bacon, M.P., Wang, H.W., Hirschberg, D.J., Ball, L., Andrews, J., Crossin, G., Fleer, A., 2000. Short-lived thorium isotopes (^{234}Th, ^{228}Th) as indicators of POC export and particle cycling in the Ross Sea, Southern Ocean. Deep-Sea Research II 47, 3451-4390.

Cochran, J.K., Masqué, P., 2003. Short-lived U/Th radionuclides in the ocean: tracers for scavenging rates, export fluxes, and particle dynamics. In: Bourdon, B., Henderson, G.M., Lundstrom, C.C., Turner, S.P. (Eds.), Uranium-Series Geochemistry, Reviews in Mineralogy and Geochemistry, vol. 52. Mineralogy Society of America, Washington, DC, pp. 461-492.

Cochran, J.K., Miquel, J-C., Armstrong, R.A., Fowler, S.W., Masqué, P., Gasser, B., Hirschberg, D.J., Szlosek, J., Rodriguez y Baena, A.M., Verdeny, E., Stewart, G.M., 2009. Time-series measurements of ^{234}Th in water column and sediment trap samples from the northwestern Mediterranean Sea. Deep-Sea Research II 56, 1487-1501.

Coppola, L., Roy-Barman, M., Wassmann, P., Mulsow, S., Jeandel, C., 2002. Calibration of sediment traps and particulate organic carbon export using ^{234}Th in the Barents Sea. Marine Chemistry 80, 11-26.

Currie, R., 1962. Pigments in zooplankton faeces. Nature 193, 956-957.

Emerson, S., Quay, P., Karl, D., Winn, C., Tupas, L., Landry, M., 1997. Experimental determination of the organic carbon flux from open-ocean surface waters. Nature 389 (6654), 951-954.

Engel, A., Abramson, L., Szlosek, J., Liu, Z., Stewart, G., Hirschberg, D., Lee, C., 2009. Investigating the effect of ballasting by $CaCO_3$ in *Emiliania huxleyi*, II: Decomposition of particulate organic matter. Deep-Sea Research II 56, 1408-1419.

Fabrés, J., Calafat, A., Sanchez-Vidal, A., Canals, M., Heussner, S., 2002. Composition and spatio-temporal variability of particle fluxes in the Western Alboran Gyre, Mediterranean Sea. Journal of Marine Systems 33-34, 431-456.

Flexas, M.M., Durrieu de Madron, X., Garcia, M.A., Canals, M., Arnau, P., 2002. Flow variability in the Gulf of Lions during the MATER HFF experiment (March-May 1997). Journal of Marine Systems 33-34, 197-214.

Font, J., Puig, P., Salat, J., Palanques, A., Emelianov, M., 2007. Sequence of hydrographic changes in NW Mediterranean deep water due to the exceptional winter of 2005. Scientia Marina 71 (2), 339-346.

Fowler, S.W., Knauer, G.A., 1986. Role of large particles in the transport of elements and organic compounds through the oceanic water column. Progress in Oceanography 16, 147-194.

Fowler, S.W., Buat-Ménard, P., Yokoyama, Y., Ballestra, S., Holm, E., van Nguyen, H., 1987. Rapid removal of Chernobyl fallout from Mediterranean surface waters by biological activity. Nature 329, 56-58.

Gardner, W.D., 1980. Sediment trap dynamics and calibration: a laboratory evaluation. Journal of Marine Research 38, 17-39.

Gardner, W.D., 1980. Field assessment of sediment traps. Journal Marine Research 38, 41-52.

Gardner, W.D., 1985. The effect of tilt on sediment trap efficiency. Deep-Sea Research 32 (3), 349-361.

Gardner, W.D., 1997. The flux of particles to the deep sea: Methods, measurements, and mechanisms. Oceanography 10 (3), 116-121.

Gardner, W.D., 2000. Sediment trap technology and surface sampling in surface waters. In: Hanson, R.B., Ducklow, H.W., Field, J.G. (Eds.), The Changing Ocean Carbon Cycle, A Midterm Synthesis of the Joint Global Ocean Flux Study. Cambridge University Press,

pp. 240-281.

Gõni, M.A., Yunker, M.B., Macdonald, R.W., Eglinton, T.I., 2000. Distributions and sources of organic biomarkers in arctic sediments from the Mackenzie River and Beaufort Shelf. Marine Chemistry 71 (23-51).

Gutiérrez-Rodriguez, A., Latasa, M., Estrada, M., Vidal, M., Marrase, C., 2010. Carbon fluxes through major phytoplankton groups during the spring bloom and post-bloom in the Northwestern Mediterranean Sea. Deep-Sea Research I: Oceanographic Research Papers 57 (4), 486-500.

Hedges, J.I., Stern, J.H., 1984. Carbon and nitrogen determinations of carbonate-containing solids. Limnology and Oceanography 29, 657-663.

Hung, C.-C., Gong, G.-C., 2007. Export flux of POC in the main stream of the Kuroshio. Geophysical Research Letters 34, L18606.

Hung, C.-C., Moran, S.B., Cochran, J.K., J.K., Guo, L., Santschi, P.H., 2008. Comment on "How accurate are ^{234}Th measurements in seawater based on the MnO_2-impregnated cartridge technique?" by Pinghe Cai et al. . Geochemistry Geophysics Geosystems 9, Q02009.

Hung, C.-C., Xu, C., Santschi, P.H., Zhang, S.-J., Schwehr, K.A., Quigg, A., Guo, L., Gong, G.-C., Pinckney, J.L., Long, R.A., Wei, C.-L., 2010. Comparative evaluation of sediment trap and ^{234}Th-derived POC fluxes from the upper oligotrophic waters of the Gulf of Mexico and the subtropical northwestern Pacific Ocean. Marine Chemistry 121, 132-144.

Hung, C.-C., Gong, G.-C., 2010. POC/^{234}Th ratios in particles collected in sediment traps in the northern South China Sea. Estuarine, Coastal and Shelf Science 88 (3), 303-310.

Ingalls, A.E., Lee, C., Wakeham, S.G., Hedges, J.I., 2003. The role of biominerals in the sinking flux and preservation of amino acids in the Southern Ocean along 170˚W. Deep-Sea Research II 50, 709-734.

King, J., K., 1974. Preserved amino acids from silicified protein in fossil radiolaria. Nature 252, 690-692.

Lee, C., Armstrong, R.A., Cochran, J.K., Engel, A., Fowler, S.W., Goutx, M., Masqué, P., Miquel, J.C., Peterson, M., Tamburini, C., Wakeham, S., 2009a. MedFlux: investigations of particle flux in the Twilight Zone. Deep-Sea Research II 56 (18), 1363-1368.

Lee, C., Peterson, M.L., Wakeham, S.G., Armstrong, R.A., Cochran, J.K., Miquel, J.C., Fowler, S.W., Hirschberg, D., Beck, A., Xue, J., 2009b. Particulate organic matter and ballast fluxes measured using time-series and settling velocity sediment traps in the northwestern Mediterranean Sea. Deep-Sea Research II 56 (18), 1420-1436.

Lepore, K., Moran, S.B., Burd, A.B., Jackson, G.A., Smith, J.N., Kelly, R.P., Kaberi, H. Stavrakakis, S., Assimakopoulou, G., 2009. Sediment trap and in-situ pump size-fractionated POC/^{234}Th ratios in the Mediterranean Sea and Northwest Atlantic: Implications for POC export. Deep-Sea Research I 56, 599-613.

Liu, Z., Mao, J., Peterson, M.L., Lee, C., Wakeham, S.G., Hatcher, P.G., 2009. Characterization of sinking particles from the northwest Mediterranean Sea using advanced solid-state NMR. Geochimica et Cosmochimica Acta 73, 1014-1026.

Livingston, H.D., Cochran, J.K., 1987. Determination of transuranic and thorium isotopes in ocean water: In solution and in filterable particles. Journal of Radioanalytical and Nuclear Chemistry 115 (2), 299-308.

Lorenzen, C.J., Welschmeyer, N.A., 1983. The *in situ* sinking rates of herbivore fecal pellets. J. Plankton Res. 5, 929-933.

Luo, S., Ku, T.-L., 2004. On the importance of opal, carbonate, and lithogenic clays in scavenging and fractionating ^{230}Th, ^{231}Pa and ^{10}Be in the ocean. Earth and Planetary Science Letters 220, 201-211.

Mantoura, R.F.C., Llewellyn, C.A., 1983. Trace enrichment of marine algal pigments for use with HPLC-diode array spectroscopy. Journal of High-Resolution Gas Chromotography and Chromotography Communications 7, 632-635.

Martín, J., Palanques, A., Puig, P., 2006. Composition and variability of downward particulate matter fluxes in the Palamós submarine canyon (NW Mediterranean). Journal of Marine Systems 60, 75-97.

Marty, J.C., Goutx, M., Guigue, C., Leblond, N., Raimbault, P., 2009. Short-term changes in particulate fluxes measured by drifting sediment traps during end summer oligotrophic regime in the NW Mediterranean Sea. Biogeosciences 6 (5), 887-899.

McCave, I.N., 1975. Vertical flux of particles in the ocean. Deep-Sea Research 22, 491-502.

Miquel, J.-C., Martín, J., Gasser, B., Rodriguez y Baena, A., Toubal, T., Fowler, S.W., 2011. Dynamics of particle flux and carbon export in the northwestern Mediterranean Sea: A two decade time-series study at the DYFAMED site. Progress in Oceanography 91, 461-481.

Moran, S.B., Weinstein, S.E., Edmonds, H.N., Smith, J.N., Kelly, R.P., Pilson, M.E.Q., Harrison, W.G., 2003. Does ^{234}Th/^{238}U disequilibrium provide an accurate record of the export flux of particulate organic carbon from the upper ocean? Limnology and Oceanography 48, 1018-1029.

Morris, R.J., Bone, Q., Head, R., Braconnot, J.C., Nival, P., 1988. Role of salps in the flux of

organic matter to the bottom of the Ligurian Sea. Marine Biology 97 (2), 237-241.

Peterson, M.L., Hernes, P.J., Thoreson, D.S., Hedges, J.I., Lee, C., Wakeham, S.G., 1993. Field evaluation of a valved sediment trap. Limnology and Oceanography 38, 1741-1761.

Peterson, M.L., Wakeham, S.G., Lee, C., Askea, M., Miquel, J.C., 2005. Novel techniques for collection of sinking particles in the ocean and determining their settling rates. Limnology and Oceanography Methods 3, 520-532.

Quigley, M.S., Santschi, P.H., Hung, C.-C., Guo, L., Honeyman, B.D., 2002. Importance of polysaccharides for ^{234}Th complexation to marine organic matter. Limnology and Oceanography 47, 367-377.

Rodriguez y Baena, A.M., Fowler, S.W., and J.C. Miquel, 2007. Particulate organic carbon: natural radionuclide ratios in zooplankton and their freshly produced fecal pellets from the NW Mediterranean (MedFlux 2005). Limnology and Oceanography 52 (3), 966-974.

Roy-Barman, M., Coppola, L., Souhaut, M., 2002. Thorium isotopes in the western Mediterranean Sea: an insight into the marine particle dynamics. Earth and Planetary Science Letters 196, 161-174.

Rutgers van der Loeff, M.M., Buesseler, K.O., Bathmann, U., Hense, I., Andrews, J., 2002. Comparison of carbon and opal export rates between summer and spring bloom periods in the region of Antarctic Polar Front, SE Atlantic. Deep-Sea Research II 49 (18), 3849-3870.

Savoye, N., Benitez-Nelson, C., Burd, A.B., Cochran, J.K., Charette, M., Buesseler, K.O., Jackson, G.A., Roy-Barman, M., Schmidt, S., Elskens, M., 2006. ^{234}Th sorption and export models in the water column: A review. Marine Chemistry 100 (3-4), 234-249.

Savoye, N., Trull, T.W., Jacquet, S.H.M., Navez, J., Deharis, F., 2008. ^{234}Th-based export fluxes during a natural iron fertilization experiment in the Southern Ocean (KEOPS). Deep-Sea Research II 55, 841-855.

Sheridan, C.C., Lee, C., Wakeham, S.G., Bishop, J.K.B., 2002. Suspended particle organic composition and cycling in surface and midwaters of the equatorial Pacific Ocean. Deep-Sea Research I 49 (11), 1983-2008.

Smith, J.N., Moran, S.B., Speicher, E.A., 2006. On the accuracy of upper ocean particulate organic carbon export fluxes estimated from ^{234}Th/^{238}U disequilibrium. Deep-Sea Research I 53 (5), 860-868.

Speicher, E.A., Moran, S.B., Burd, A.B., Delfanti, R., Kaberi, H., Kelly, R.P., Papucci, C., Smith, J.N., Stavrakakis, S., Torricelli, L., Zervakis, V., 2006. Particulate organic carbon export fluxes and size-fractionated POC/^{234}Th ratios in the Liguarian, Tyrrhenian

and Aegean Seas. Deep-Sea Research I 53, 1810-1830.

Stewart, G., Cochran, J.K., Miquel, J.C., Masque, P., Szlosek, J., Rodriguez y Baena, A.M., Fowler, S.W., Gasser, B., Hirschberg, D.J., 2007. Comparing POC export from $^{234}Th/^{238}U$ and $^{210}Po/^{210}Pb$ disequilibria with estimates from sediment traps in the northwest Mediterranean. Deep-Sea Research I 54, 1549-1570.

Stewart, G.M., Fisher, N.S., 2003. Bioaccumulation of polonium-210 in marine copepods. Limnology and Oceanography 48, 2011-2019.

Suess, E., 1980. Particulate organic carbon flux in the oceans–surface productivity and oxygen utilization. Nature 288, 260-263.

Swift, D.M., Wheeler, P., 1991. Evidence of an organic matrix from diatom biosilica. Journal of Phycology 28, 202-209.

Szlosek, J., Cochran, J.K., Miquel, J.C., Masqué, P., Armstrong, R.A., Fowler, S.W., Gasser, B., Hirschberg, D.J., 2009. Particulate organic carbon–^{234}Th relationships in particles separated by settling velocity in the northwest Mediterranean Sea. Deep-Sea Research II 56, 1519-1532.

Waite, A.M., Hill, P.S., 2006. Flocculation and phytoplankton cell size can alter ^{234}Th-based estimates of the vertical flux of particulate organic carbon in the sea. Marine Chemistry 100 (3-4), 366-375.

Wakeham, S.G., Lee, C., 1993. Production, transport, and alteration of particulate organic matter in the marine water column. In: Engel, M.H., Macko, S.A. (Eds.), Organic geochemistry. Plenum Press, pp. 145-169.

Wakeham, S.G., Lee, C., Peterson, M.L., Liu, Z., Szlosek, J., Putnam, I., Xue, J., 2009. Organic compound composition and fluxes in the twilight zone–time-series and settling velocity sediment traps during MedFlux. Deep-Sea Research II 56, 1437-1453.

Weiner, S., Erez, J., 1984. Organic matrix of the shell of the foraminifer, Heterostegina depressa. Journal of Foraminiferal Research 14, 206-212.

Welschmeyer, N.A., 1982. The dynamics of phytoplankton pigments: Implications for zooplankton grazing and phytoplankton growth. Ph.D. Thesis, University of Washington, Seattle, Washington, 176 p.

Welschmeyer, N.A., Lorenzen, C.J., 1984. Carbon-14 labeling in phytoplankton carbon and chlorophyll *a* carbon: Determination of specific growth rates. Limnology and Oceanography 29, 135-145.

Welschmeyer, N.A., Lorenzen, C.J., 1985. Chlorophyll budgets: Zooplankton grazing and phytoplankton growth in a temperate fjord and the Central Pacific Gyres. Limnology

and Oceanography 30, 1-21.

Yoon, W.D., Marty, J.-C., Sylvain, D., Nival, P., 1996. Degradation of faecal pellets in *Pegea confoederata* (*Salpidae, Thaliacea*) and its implication in the vertical flux of organic matter. Journal of Experimental Marine Biology and Ecology 203, 147-177.

Table 3.1. Pump and trap POC/^{234}Th

				POC/^{234}Th (μmol dpm^{-1})								
				Trap weighted averages			*In situ* Pump					
							>70 μm			1-70 μm		
Year	Sample ID	Depth (m)	Date									
2005	SV2	313	4 March-28 April	1.2	±	0.03		NA			NA	
	TS	"	"	1.1	±	0.03		"			"	
	pump	300	9 March		NA		5.0	±	0.3	2.04	±	0.10
	pump	"	14 March		"		3.0	±	0.2	0.67	±	0.04
	pump	"	30 April		"		11.4	±	5.3	2.53	±	0.63
	SV1	524	4 March-28 April	0.99	±	0.02		NA			NA	
	SV2	"	"	0.93	±	0.02		"			"	
	pump	600	9 March		NA		12.9	±	4.1	3.9	±	0.9
	pump	500	14 March		"		6.1	±	0.7	2.8	±	0.4
	pump	"	30 April		"		22	±	14	1.9	±	0.5
	TS	924	4 March-28 April	0.72		0.02		NA			NA	
	pump	800	9 March		NA		15.5	±	4.3	1.4	±	0.1
	pump	900	14 March		"		6.7	±	1.1	2.9	±	0.7
	SV1	1918	"	0.50	±	0.011		NA			NA	
	SV2	"	"	0.44	±	0.009		"			"	
	pump	1800	9 March		NA		4.7	±	0.8	1.9	±	0.4

NA- Not applicable

Table 3.1. POC/^{234}Th ratios for pump filtered fractions and sediment trap mass weighted averages.

Table 3.2. POC/^{234}Th and pigment compound ratios

	> 70 µm				1-70 µm			
Depth (m)	POC/^{234}Th	fuco : Chl-*a*	phytin : Chl-*a*	(phide + pyro) : Chl-*a*	POC/^{234}Th	fuco : Chl-*a*	phytin : Chl-*a*	(phide + pyro) : Chl-*a*
March 9 pumps, March 4-9 Traps:								
2	4.8 ± 0.5	0.0	7.7	9.4	3.4 ± 0.3	0.03	0.05	0.08
25	7.4 ± 0.6	4.1	20.1	19.8	4.1 ± 0.3	0.03	0.04	0.06
60	7.3 ± 0.7	0.0	25.4	12.9	3.3 ± 0.2	0.03	0.03	0.09
100	2.9 ± 0.3	28.2	0.6	1.3	2.9 ± 0.2	0.03	0.06	0.10
150	2.8 ± 0.2	20.4	0.3	1.1	2.8 ± 0.2	0.03	0.07	0.07
200	3.3 ± 0.2	NA	NA	NA	3.0 ± 0.2	0.02	0.05	0.08
300	5.0 ± 0.3	"	"	"	2.0 ± 0.1	0.02	0.08	0.13
TS 313		0.00	0.87	3.40				
350	2.5 ± 0.1	NA	NA	NA	2.8 ± 0.1	0.02	0.04	0.07
400	1.8 ± 0.1	"	"	"	3.8 ± 0.2	0.03	0.05	0.06
600	12.9 ± 4.1	0.0	2.9	0.8	3.9 ± 0.9	2.27	0.14	0.17
800	15.5 ± 4.3	NA	NA	NA	1.4 ± 0.1	1.64	0.03	0.21
TS 924		0.31	0.78	3.57				
1200	19.0 ± 8.1	NA	NA	NA	2.7 ± 0.5	0.10	0.18	0.48
1500	4.9 ± 0.8	"	"	"	2.1 ± 0.4	0.09	0.31	0.62
1800	4.7 ± 0.8	0.0	1.5	2.5	1.9 ± 0.4	0.52	0.08	0.23
March 13-14 pumps, March 9-14 Traps:								
5	19.9 ± 6.5	1.0	1.1	1.9	5.9 ± 0.6	0.03	0.03	0.01
25	8.2 ± 0.9	5.0	27.5	9.8	3.6 ± 0.3	0.02	0.02	0.01
50	3.8 ± 0.4	4.8	3.3	5.5	4.3 ± 0.5	0.03	0.04	0.03
75	4.3 ± 0.4	0.0	3.0	5.6	3.9 ± 0.4	0.03	0.04	0.01
100	3.9 ± 0.2	NA	NA	NA	3.4 ± 0.2	0.03	0.04	0.05
150	1.8 ± 0.1	"	"	"	1.4 ± 0.1	0.03	0.04	0.10
200	1.6 ± 0.1	"	"	"	3.1 ± 0.2	0.02	0.06	0.08
300	3.0 ± 0.2	"	"	"	0.7 ± 0.0	0.02	0.08	0.12
TS 313		0.34	0.94	2.81				
350	2.5 ± 0.1	NA	NA	NA	0.6 ± 0.0	0.02	0.09	0.10
400	1.7 ± 0.1	"	"	"	1.2 ± 0.1	0.03	0.10	0.10
500	6.1 ± 0.7	"	"	"	2.8 ± 0.4	0.03	0.08	0.14
600	7.2 ± 1.0	"	"	"	1.9 ± 0.3	0.17	0.07	0.22
800	3.7 ± 0.4	0.0	2.5	1.1	2.5 ± 0.4	0.36	0.04	0.15
900	6.7 ± 1.1	NA	NA	NA	2.9 ± 0.7	0.18	0.05	0.16
TS 924		0.32	0.79	3.71				

continued

Table 3.2. *continued*

Depth (m)	> 70 µm POC/^{234}Th	fuco : Chl-*a*	phytin : Chl-*a*	(phide + pyro) : Chl-*a*	1-70 µm POC/^{234}Th	fuco : Chl-*a*	phytin : Chl-*a*	(phide + pyro) : Chl-*a*
April 29-30 pumps, April 23-28 Traps:								
0	46.85 ± 60.13	NA	NA	NA	14.66 ± 2.10	1.40	0.91	0.07
25	14.10 ± 3.51	11.9	0.2	3.1	14.02 ± 1.63	1.74	0.85	0.20
35	14.59 ± 2.73	10.0	0.6	9.7	14.17 ± 1.69	2.04	0.79	0.43
50	11.66 ± 1.77	29.7	0.5	9.3	8.11 ± 1.18	2.31	0.74	0.68
75	11.01 ± 1.63	21.3	23.3	21.0	16.38 ± 9.26	4.01	3.86	1.47
100	15.52 ± 3.64	37.0	0.5	12.8	4.27 ± 0.88	0.00	1.59	0.96
125	9.96 ± 2.50	12.0	1.1	5.1	6.01 ± 1.64	0.00	1.36	0.23
150	13.92 ± 6.34	22.3	1.8	5.4	5.50 ± 1.92	0.00	0.56	0.49
200	11.02 ± 2.70	11.3	0.8	2.9	2.13 ± 0.58	0.00	1.46	1.05
300	11.35 ± 5.27	0.0	2.5	4.9	2.53 ± 0.63	0.00	0.50	0.87
TS 313		0.00	0.42	3.56				
500	22.14 ± 13.79	0.0	2.1	6.9	1.95 ± 0.52	0.00	0.37	0.80
750	7.94 ± 2.51	0.0	1.5	17.1	2.98 ± 1.07	0.00	1.07	1.92
TS 924		0.00	1.33	4.25				

NA - Not Available

Table 3.2. POC/^{234}Th and pigment compound ratios of pump fractions. POC/^{234}Th and pigment compound ratios of TS similar depths and time frames are provided for reference. Pigment compound ratios indicate source and extent of alteration of chlorophyll-*a*. They include fucoxanthin : chlorophyll-*a* (fuco, diatom derived pigment), pheophytin : chlorophyll-*a* (phytin, bacterial degradation product of chlorophyll), pheophorbide and pyropheophorbide : chlorophyll-*a* (phide + pyro, zooplankton alteration products of chlorophyll).

Table 3.3. Comparison of pump and trap POC/^{234}Th and composition types

	In situ Pump				Time Series		Settling Velocity			
	Small Particles		Large Particles				*slow*		*fast*	
Depth (m)	C/Th	composition	C/Th	composition	C/Th	composition	C/Th	composition	C/Th	composition
300 - 350	0.6 - 2.8	fresh algal material	2.5 - 11.4	bacterially reworked phytoplankton, fresh coccolithophores	1.1	fecal pellets	1.33	marine and terrestrial organic matter	1.04	marine and terrestrial organic matter
500 - 600	1.9 - 3.9	fresh algal material	6.1 - 22.1	bacterially reworked phytoplankton, fresh diatoms	NA		1.10	marine and terrestrial organic matter	1.05	fecal pellets
800 - 900	1.4 - 2.9	fresh algal material	3.7 - 15.5	bacterially reworked phytoplankton	0.72	fecal pellets	NA		NA	
1800 - 1900	1.9	fresh algal material	4.7	bacterially reworked phytoplankton	NA		0.91	fecal pellets	0.56	fecal pellets

NA – Not Applicable

Table 3.3. Depth profile of pump and trap POC/^{234}Th ranges and compositional types. Composiitonal types are based on the PCA where clustering of variable loadings for biomarkers are used to infer biogenic source or alteration. For example, fresh algal material are characterized by the presence of Chl-*a* that can be differentiated between the functional groups of coccolithophores (GLU, glutamic acid; ASP, aspartic acid) and diatoms (fuco, fucoxanthin; GLY, glycine; SER, serine; THR, threonine). Bacterially reworked material is indicated by presence of pheophytin (phytin), β-alanine (BALA), and γ-aminobutyric acid (GABA). Fecal pellets are inferred from the presence of zooplankton-produced alteration products of chlorophyll (phide, pheophorbide; pyrophide, pyropheophorbide). Non-specific tracers of marine and terrestrial organic matter include arginine (ARG), valine (VAL), tyrosine (TYR), and phenylalanine (PHE).

Table 3.4. LP fraction correlation coefficients

Date	Depth (m)	R^2
Reference samples		
3/9/05	25	-
3/13/05	"	-
3/9/05	60	0.95
"	100	0.06
"	150	0.05
"	600	0.86
"	800	bd
"	1200	bd
"	1500	bd
"	1800	0.73
3/13-14/05	50	0.66
"	75	0.78
"	800	0.84
"	900	bd

bd - below detection.

Table 3.4. Correlation coefficients derived from comparison of amino acid and pigment data of March LP fraction samples from > 25 m with that of the LP fraction at 25 m in March.

Table 3.5. Comparison of ^{234}Th-derived and sediment trap C/Th and POC fluxes at 300 m

	Water Column Sampling							Sediment Traps		
Date	Sampling technique	^{234}Th deficit (10^4 dpm/m^2)	^{234}Th flux (dpm m^{-2} d^{-1})	C/Th (>70 µm) (µmol/dpm)	C/Th (1-70 µm) (µmol/dpm)	POC Flux (>70 µm) (mmol C m^{-2} d^{-1})	POC Flux (1-70 µm) (mmol C m^{-2} d^{-1})	Trap Date	Trap C/Th (µmol/dpm)	POC Flux (Trap) (mmol C m^{-2} d^{-1})
3/2/05	Small Volume	2.4 ± 2.9	690 ± 834	–	–	–	–	–	–	–
3/8-9/05	Small Volume	9.3 ± 1.4	2670 ± 402	–	–	–	–	3/4-3/9/05	0.87 ± 0.03	2.18
3/9/05	*In situ* Pump	7.5 ± 1.2	2160 ± 350	5.0 ± 0.3	2.04 ± 0.10	10.8	4.3	3/9-14/05	0.97 ± 0.03	2.30
3/11/05	Small Volume	14.1 ± 1.7	4050 ± 490	–	–	–	–	"	"	"
3/13/05	*In situ* Pump	2.2 ± 1.3	630 ± 370	3.0 ± 0.2	0.67 ± 0.04	1.9	0.4	"	"	"
3/14/05	Small Volume	4.6 ± 1.4	1320 ± 400	–	–	–	–	"	"	"
4/29-30/05	*In situ* Pump	-4.1 ± 17	-1180 ± 4890	11.4 ± 5.3	2.53 ± 0.63	NC	NC	4/23-28/05	4.06 ± 0.36	0.30

NC - not calculated

Table 3.5. Summary of pump and trap-derived POC flux estimates March to April, 2005. Water column ^{234}Th deficits and fluxes are determined from both pump and small volume samples. C/Th ratios for each filterable particle class and TS sediment trap samples are reported. Pump-derived POC flux estimates for each particle class are given.

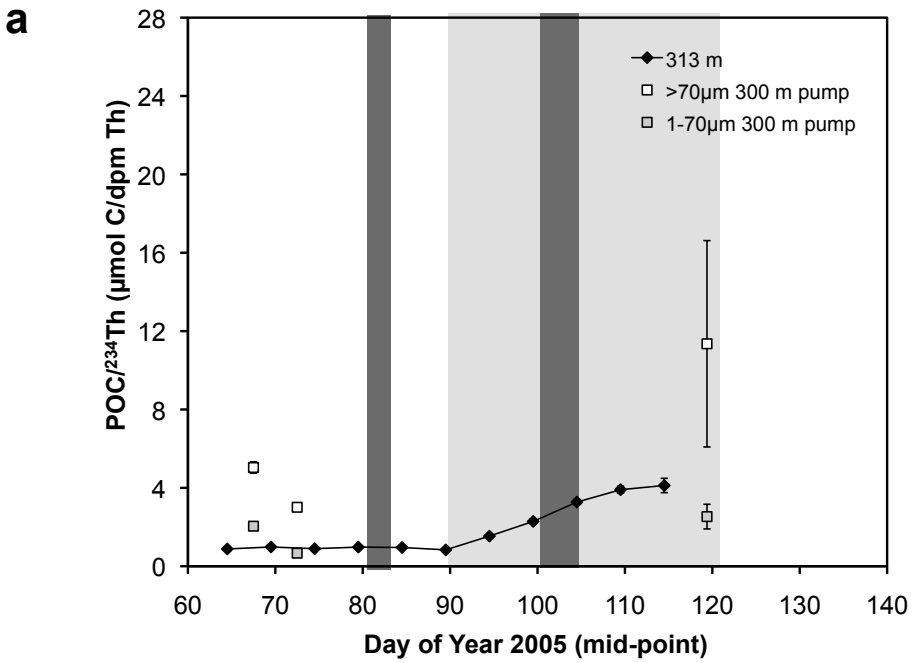
a
313 m
>70µm 300 m pump
1-70µm 300 m pump
POC/234Th (µmol C/dpm Th)
Day of Year 2005 (mid-point)
0
4
8
12
16
20
24
28
60
70
80
90
100
110
120
130
140

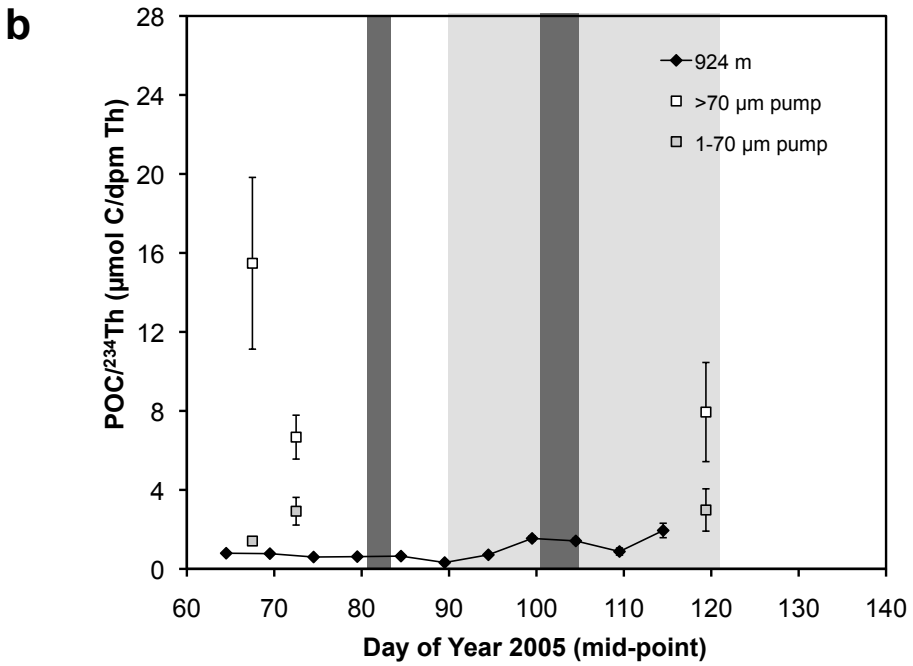
b
924 m
>70 µm pump
1-70 µm pump
POC/234Th (µmol C/dpm Th)
Day of Year 2005 (mid-point)
0
4
8
12
16
20
24
28
60
70
80
90
100
110
120
130
140

Fig. 3.1. Time Series sediment trap and *in situ* pump POC/^{234}Th ratios for DYFAMED, spring 2005, at (a) 313 m and (b) 924 m. Pump POC/^{234}Th are from 300 m in (a) and 800 and 900 m in (b). Dust events highlighted in dark grey. Satellite chlorophyll peak highlighted in light grey.

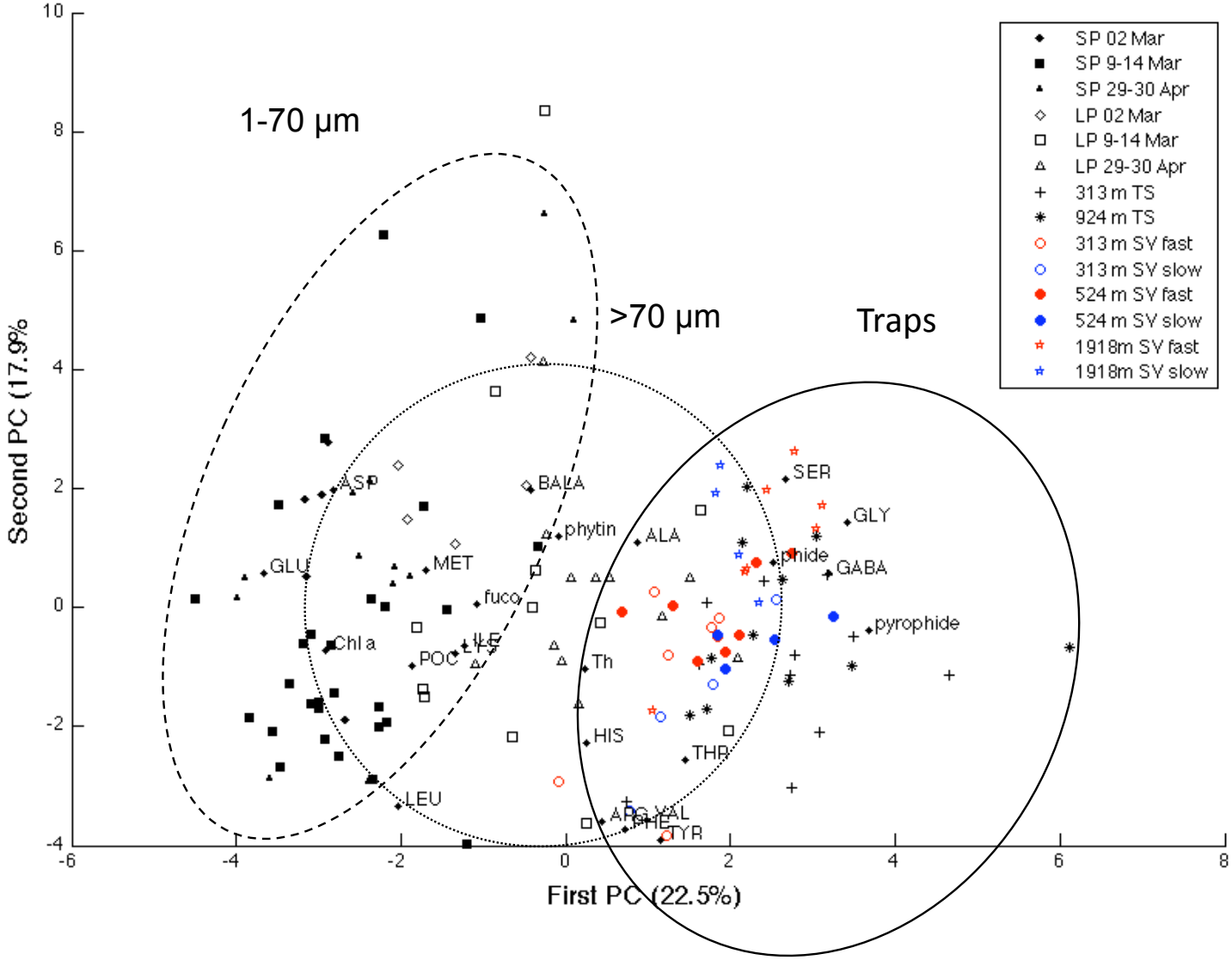
1-70 µm
>70 µm
Traps
SP 02 Mar
SP 9-14 Mar
SP 29-30 Apr
LP 02 Mar
LP 9-14 Mar
LP 29-30 Apr
313 m TS
924 m TS
313 m SV fast
313 m SV slow
524 m SV fast
524 m SV slow
1918m SV fast
1918m SV slow
Second PC (17.9%)
First PC (22.5%)
ASP
BALA
phytin
ALA
SER
GLY
GLU
MET
fuco
phide
GABA
pyrophide
Chl a
POC
ILE
LYS
Th
HIS
THR
LEU
VAL
TYR

Figure. 3.2a. Principal components analysis of all the pump and sediment trap (SV and TS modes) amino acid, pigment, POC, and ^{234}Th data. Variable loadings are scaled up (10×) and plotted on PC1 and PC2 axes with sample site scores.

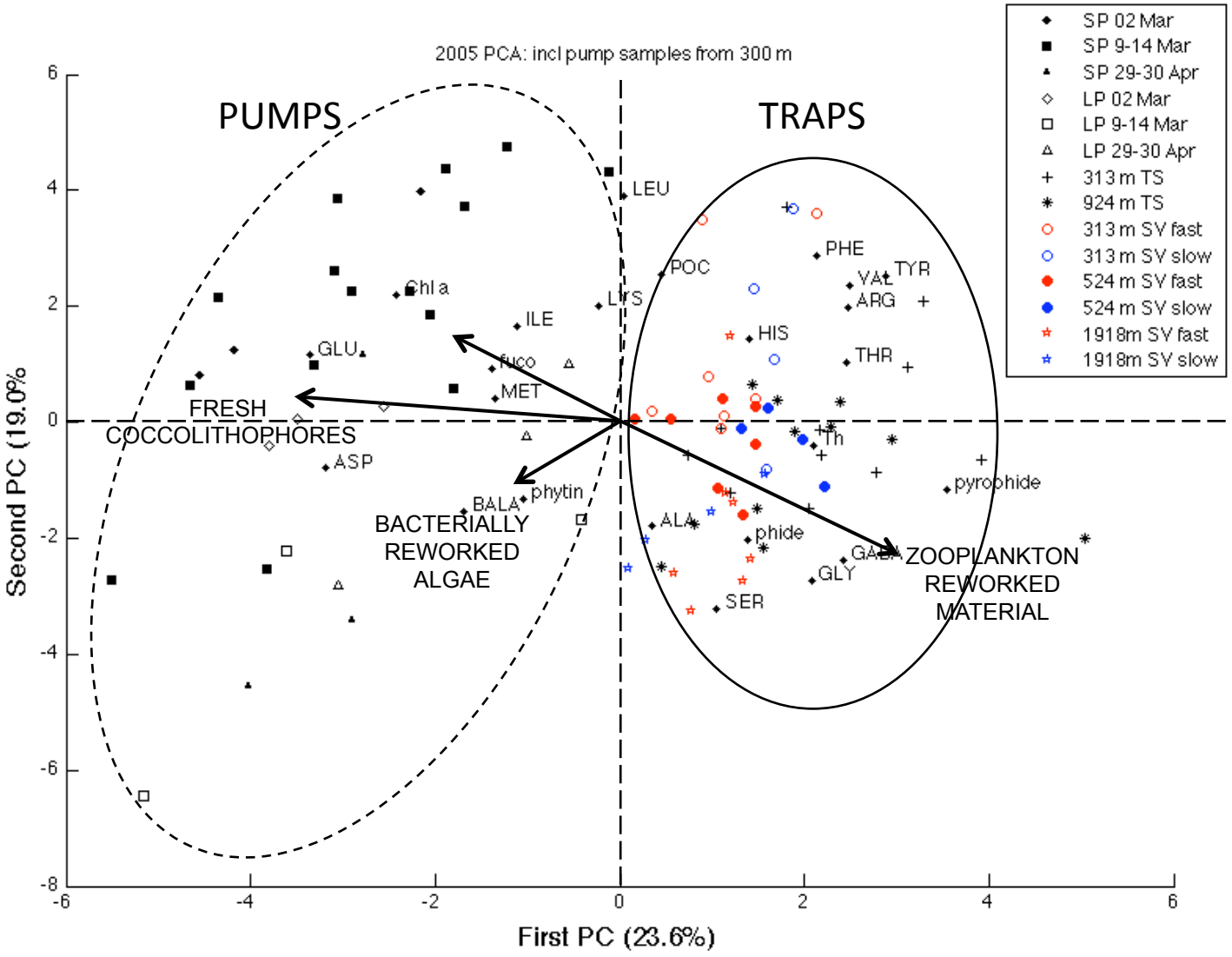
2005 PCA: incl pump samples from 300 m
PUMPS
TRAPS
SP 02 Mar
SP 9-14 Mar
SP 29-30 Apr
LP 02 Mar
LP 9-14 Mar
LP 29-30 Apr
313 m TS
924 m TS
313 m SV fast
313 m SV slow
524 m SV fast
524 m SV slow
1918m SV fast
1918m SV slow
LEU
POC
PHE
TYR
VAL
ARG
LYS
Chl a
ILE
HIS
GLU
fuco
THR
MET
Th
FRESH
COCCOLITHOPHORES
ASP
pyrophide
phytin
BALA
ALA
phide
GABA
GLY
SER
BACTERIALLY
REWORKED
ALGAE
ZOOPLANKTON
REWORKED
MATERIAL
Second PC (19.0%)
First PC (23.6%)
6
4
2
0
-2
-4
-6
-8
-6
-4
-2
0
2
4
6

Figure. 3.2b. Principal components analysis of pump and sediment trap (SV and TS modes) amino acid, pigment, POC, and ^{234}Th data from samples at or below 300 m. Variable loadings are scaled up (10×) and plotted on PC1 and PC2 axes with sample site scores.

CHAPTER 4

The role of calcification and transparent exopolymer particles on the coagulation efficiency of *Emiliania huxleyi* cells

Abstract

Experimental estimates of coagulation efficiency of *Emiliania huxleyi* cells were made using Couette flow devices in 2006 and 2007. *E. huxleyi* was grown as part of a chemostat study to understand biogeochemical processes of the cells at different growth rates. Novel statistical techniques are introduced for the reduction of variability in coagulation efficiency estimates from replicate coagulation experiments. *E. huxleyi* coagulation efficiency increases from 0.20 to 1 as cell growth rates decline and nutrients become more limited. To better understand the mechanisms that drive coccolithophore coagulation we measured the abundance and size spectra of transparent exopolymer particles (TEP), sugar composition of the total and colloidal organic matter pools, and estimated the detached coccolith abundance of the cultures. We observed a correlation between growth rate of cells and TEP : Chl-*a*, total alkalinity, and concentrations of detached coccoliths and sugars specific to coccolith formation ($p<0.01$). Although cell growth rates and environmental conditions were similar between years we observed ~30% higher coagulation efficiencies for cells at low growth rates (0.03–0.12 d^{-1}) in 2007 when there was a higher percentage of fully calcified cells. The important role of coccolith presence on aggregation was supported by the significant correlation of aggregate number with coccolith sugar and detached coccolith abundances. Furthermore, we found that TEP coated cells were more likely to form aggregates when interacting with other cells than with free, amorphous TEP.

1. Introduction

Although most (> 90%) organic matter produced in the surface ocean is remineralized within the epipelagic zone (Eppley and Peterson, 1979; Martin et al., 1987), phytoplankton-derived aggregates are a major source of transporting organic matter to the deep sea

(Honjo, 1982; Fowler and Knauer, 1986). The onset and magnitude of phytoplankton sedimentation events in the upper ocean are dependent on the stages of phytoplankton blooms as well as the phytoplankton functional groups present (Stemmann et al., 2002; Jin et al., 2006). Coccolithophores are an important group of phytoplankton that produce large blooms (Balch et al., 2005) and produce calcite tests that affect aggregate and fecal pellet settling rates (De La Rocha and Passow, 2007; Iversen and Ploug, 2010). In the past decade increasing attention has been given to the role of mineral ballast on the efficiency of carbon export (Armstrong et al., 2001; Klaas and Archer, 2002; Jin et al., 2006; Passow and De La Rocha, 2006). Data and model results have indicated the dominant role of $CaCO_3$ for exporting organic matter (Klaas and Archer, 2002; Jin et al., 2006), yet relatively little is known about what controls coccolithophore aggregation (De La Rocha and Passow, 2007; Biermann and Engel, 2010).

Coagulation studies have been performed using Couette flow devices (van Duuren, 1968; Drapeau et al., 1994) or annular flumes (Kahl et al., 2008) to impart a constant laminar shear, which allows observation of the propensity of phytoplankton cells to attach to one another. Such studies with cells undergoing environmental perturbations, such as nutrient depletion, permit investigators to qualitatively describe dependency of phytoplankton aggregate formation on physiological and environmental parameters. The ratio of total cell collisions to those that result in cells attaching to one another is referred to as the attachment probability, α, in the fields of physics, colloid chemistry, and engineering. Within marine studies this term has also been referred to as coagulation efficiency (Kiørboe et al., 1990), stickiness (Alldredge and Silver, 1988; Jackson, 1990; Kiørboe et al., 1990; Engel, 2000), stickiness efficiency (Kahl et al., 2008), sticking coefficient (Logan et al., 1995), sticking factor (Celenza, 1999), coalescence efficiency (McCave, 1984), collision efficiency factor (Gibbs, 1983), and particle stability factor (Weilenmann et al., 1989). Values for the coagulation efficiency of phytoplankton can be derived experimentally (Kiørboe et al., 1990; Drapeau et al., 1994; Hansen et al., 1995; Engel, 2000; Kahl et al., 2008); this value has been used in aggregation models to interpret relative changes in carbon export over the duration of a bloom (Jackson and Lochmann, 1993; Kahl et al., 2008; Karakas et al., 2009).

The rates at which particles aggregate and sink depend on the size and concentration of the colliding particles. Jackson and Kiørboe (2008) used this dependence to describe the maximum concentration of an algal bloom; they suggested that coagulation rate increases with particle concentration squared and that particle loss due to aggregation will eventually equal the algal growth rate and thus be an upper limit on cell concentration. For a bloom, the maximum algal concentration is as a function of cell growth rate, turbulent shear rate, particle coagulation efficiency, and algal diameter. In a study of diatoms, Kahl et al. (2008) found that the stickiness coefficient, α, was dependent on the physiological state of the cells, and that this could have a significant effect on the critical concentration of algal cells, and in turn the subsequent export flux.

One of the physiological factors that appeared to promote phytoplankton aggregation is the production of TEP by phytoplankton cells as they deplete nutrients (Logan et al., 1995; Passow and Alldredge, 1995a; Engel, 2000; Passow, 2002). In fact, Passow et al. (1995) found the ratio of TEP : cells was a crucial factor in determining when aggregation and sedimentation of a diatom-dominated mesocosm bloom occurred. Coccoliths and intact coccolithophores have long been observed in association with mucus material at the continental slope (de Wilde et al., 1998; McCave et al., 2001) and in sediment traps (Honjo, 1982; Cadée, 1985; Riemann, 1989). Recently, studies have documented the association of coccolithophores with TEP and the formation of coccolithophore aggregates within laboratory roller tanks (Engel et al., 2009a,b; Biermann and Engel, 2010). However, the conditions leading to the initial formation of the aggregates have not been reported.

The amount of mineral ballast, TEP size spectra, chemical composition of dissolved organic matter (DOM) exudates from coccolithophores, and the abundance of free coccoliths are all contributing factors to coccolithophore aggregation (De La Rocha and Passow, 2007; Engel et al., 2009a,b; Biermann and Engel, 2010). Surface-active polysaccharides such as acidic sugars and those containing uronic acids and sulfate-half ester groups have been shown to correlate with coagulation efficiency and TEP (Mopper et al., 1995; Passow and Alldredge, 1995a). Of particular relevance to the coagulation of *E. huxleyi* is the production of coccolith polysaccharides known to be important for deposition of coccoliths to the coccosphere (de Jong et al., 1976, 1979). In fact, Engel et al. (2009a)

proposed that these TEP precursors might catalyze aggregate formation of calcifying coccolith cells at a rate faster than that observed for non-calcifying strains. Thus, a motivation of our study was to investigate the affect exopolymer particle chemical composition and abundance had on the coagulation efficiency and rate of aggregate formation.

In addition to the abundance of TEP playing a role in coagulation efficiency of cells (Logan et al., 1995), an important factor on aggregation may be the configuration of TEP within an aggregate–i.e., cells colliding with cells, or cells colliding with TEP (Kiørboe and Hansen, 1993; Logan et al., 1995). The distinction of how cells become incorporated within aggregates may influence the strength of the aggregate; aggregates are often observed to be delicate and can disaggregate due to shear stress as they sink (Alldredge and Silver, 1988; Hill, 1998). $CaCO_3$-ballasted aggregates have been shown to be small, dense, and robust (De La Rocha and Passow, 2007; Engel et al., 2009b; Biermann and Engel, 2010; Iversen and Ploug, 2010), and thus less likely to disaggregate. Here we report on coagulation studies performed with *Emiliania huxleyi*, a cosmopolitan coccolithophore species, and the relationship of coagulation to cell growth rate, TEP, and calcite ballast. We investigated the processes that influence coagulation efficiency for *E. huxleyi*, describing the coagulation efficiency of *E. huxleyi* using Couette flow devices as cells undergo nutrient depletion. We aimed to garner a more complete understanding of the processes that yield coccolithophore aggregates by characterizing TEP, the sugar composition of the colloidal pool, and the abundance of coccoliths.

2. Methods

2.1. Phytoplankton Cultures

E. huxleyi, strains TQ26 (Codenet culture collection) and PML B92/11 (Plymouth culture collection of marine algae), were used in coagulation experiments in 2006 and 2007, respectively. Cells were grown in continuous culture as part of a larger coccolithophore biogeochemistry study (for details, see Borchard et al., 2011). Coccolithophore cell inoculates were >60% calcifying in 2006, and >99% calcifying in 2007, as determined by microscopic observation (Koch, Borchard pers. comm). Additionally, 2007 PIC/POC ratios of cells at the initial dilution rate (0.43±0.39, 0.3 d^{-1}, day 10) were 2× that of 2006 (0.21,

0.25 d^{-1}, day 26). Chemostat cell abundances were maintained at ~10^5 cells ml^{-1}. The 8.5-l chemostat vessels were operated at 3 sequential dilution rates of 0.25, 0.10, and 0.05 d^{-1} in 2006, and 2 sequential dilution rates of 0.30 and 0.10 d^{-1} in duplicate in 2007, a constant temperature of 15˚C, a light: dark cycle of 16: 8 h, and constant aeration and stirring (20–100 rotations min^{-1}). Photon flux densities were 180 µmol photons m^{-2} s^{-1} in 2006 and 300 µmol photons m^{-2} s^{-1} in 2007. The growth medium was enriched 0.2-µm filtered North Sea water sterilized using UV-light for 24 h. Trace metals and vitamins were added according to f/2 medium (Guillard and Ryther, 1962), and nutrient were 50 µmol l^{-1} NO_3 and 3 µmol l^{-1} PO_4 in 2006 and 30 µmol l^{-1} NO_3 and 1 µmol l^{-1} PO_4 in 2007. During chemostat experiments cells experienced P-limitation in both years. Yet, in 2007 P-limitation was more severe and P cell quotas fell below a critical value at the lower growth rate (Borchard et al., 2011). Specific growth rates were determined using total cell biovolume that was loss-corrected using the dilution rate of the chemostat (Koch, 2007; Table 4.1). Cells reached steady state prior to experiment days, except for day 10 and 22 in 2007. Culture material used for coagulation efficiency experiments was collected from the overflow of the chemostats. Growth rates do not match the targeted dilution rate and those reported in Table 4.1 are the mean of daily growth rates for the days over which chemostat overflow was collected for material used to conduct replicate coagulation efficiency experiments.

2.2. Chemical Analyses

Borchard et al. (2011) and Borchard and Engel (2012) describe detailed methods for nutrients (phosphate, ammonia, nitrate, and nitrite), chlorophyll-*a*, total particulate carbon (TPC), particulate organic and inorganic carbon (POC and PIC), and total alkalinity. Combined carbohydrate (CCHO) samples were also collected for neutral and amino sugar and sugar acid analysis by high-performance anion-exchange chromatography with pulse amperometric detection (HPAEC-PAD) according to methods outlined in Engel and Händel (2011). Samples were desalted by membrane desalination (1 kDa MWCO, Spetra Por) at 0˚C for 6 h. The chromatographic system consisted of a Dionex 3000 Ion Chromatography System with a PAD and an AS50 autosampler. These methods permit the detection of the neutral sugars (fucose (Fuc), rhamnose (Rha), arabinose (Ara), galactose (Gal), glucose (Glc), mannose (Man), and xylose (Xyl)), amino sugars (galactosamine (GalN) and

glucosamine (GlcN), and sugar acids (galacturonic acid (Gal-URA) and glucuronic acid (Glc-URA)). Some sugars were quantified together due to co-elution: Ara+GalN, Man+Xyl, and Gal-URA+Glc-URA. The detection limit for sugars was 10 nM (Engel and Händel, 2011). In 2006, neutral sugars were analyzed on samples that were filtered using 0.45 µm syringe filters (GHP membrane, Acrodisk, Pall Corporation) prior to desalinazation (1 kDa cut off). This high molecular weight dissolved fraction is <0.45 µm and >1 kDa. We refer to this fraction as <0.45 µm-HMW-dCCHO. In 2007, samples were unfiltered, 0.45 µm syringe-filtered, and 1000 kDa ultrafiltered via centrifugation (1000 kDa MWCO, Macrosep™, Pall Corporation) for neutral, amino, and acidic sugar composition prior to membrane dialysis. We refer to the size fractions as total combined carbohydrates (tCCHO), <0.45 µm-HMW-dCCHO, and <1000 kDa-HMW-dCCHO, respectively. Combined carbohydrate samples were stored at -20˚C prior to desalination, acid hydrolysis, and neutralization, and analysis (Engel and Händel, 2011; Borchard and Engel, 2012).

2.3. Transparent Exopolymer Particle Analysis

Within 3 months of sample collection, TEP abundance was determined on triplicate samples before and after coagulation using the Alcian blue colorimetric technique detailed in Passow and Alldredge (1995b). Absorbance of TEP samples was calibrated to the absorbance of known quantities of xanthan gum (Passow and Alldredge, 1995b). The detection limit of TEP abundance was ~50 µg XG eq l^{-1}. All colorimetric TEP samples were corrected for the presence of Alcian blue stainable material on cell surfaces according to methods of Engel et al., 2004. In 2006, samples representing material before coagulation were from the chemostat overflow, the same pool of material used to fill the Couette flow devices. In 2007, samples representing material before coagulation came from the chemostat on the day of sampling. In both years, samples representing the suspension after coagulation were taken from material gently emptied from the annular space within the Couette chambers at the conclusion of the experiment.

In 2007, TEP area and volume in the samples taken before and after coagulation were also enumerated by microscopy as described in Engel (2009). In brief, duplicate slides were prepared according to Passow and Alldredge (1994) and Logan et al. (1994) within 2 hours of sampling. Each filter mounted for microscopy was photographed with a Zeiss

AxioCam MC5 at 200× magnification on a Zeiss AxioSkop plus 2 compound microscope. AxioCam software was used to record 30-35 fields of view at 4000×999 pixels for each filter. Each pixel represented 0.33 μm × 0.33 μm. Images were split into separate colors, showing 256 channels of gray. The red image yields the highest contrast. Its grayscale threshold was adjusted manually to get the best coverage of all Alcian blue stained particles and to avoid the inclusion of the background. TEP that was larger than 0.2 μm^2 was included and all particles on the edge of the photograph were removed from calculations. Parameters estimated semi-automatically using NIH software ImageJ 1.42h include area, perimeter, fit ellipse (major and minor axes) and circularity.

2.4. Coagulation Measurements

2.4.1. Coagulation Theory

Coagulation efficiency studies have employed Smoluchowski kinetics assuming the experiment suspension is monodisperse, conserves volume, and that hydrodynamic effects between particles can be ignored, i.e. the rectilinear model of coagulation (Camp and Stein, 1943; Birkner and Morgan, 1968; Kiørboe et al., 1990; Dam and Drapeau, 1995). When considering a suspension of particles that are all the same size (monodisperse), such as monocultures, coagulation does not occur via differential settling because the settling velocity of all particles is equal. In this case, coagulation can be achieved and coagulation efficiency estimated using a horizontal Couette flow device (Drapeau et al., 1994). A Couette flow device consists of a fixed inner cylinder and an outer rotating cylinder that creates a two-dimensional flow that promotes coagulation (Donnelly, 1991). The mean shear rate, $\overline{G}$, of the laminar flow depends on the angular velocity and the inner and outer radii (van Duuren, 1968). Cell size spectra were monitored over time to observe the decrease in total particle concentration as cells formed larger particles.

The particle coagulation is the probability that when two particles collide they attach. Birkner and Morgan (1968) expressed the initial stages of coagulation as a first order rate equation when the suspension is monodisperse and volume conserving. Using this approximation the aggregation model presented in Jackson (1990) becomes:

$$\begin{aligned}\frac{dC}{dt} &= -\alpha\overline{\beta}_{11}\overline{C}_{1,t\to 0}\cdot C_1 = -\alpha\left(\frac{4}{3}\overline{G}(2\cdot\overline{d}_1/2)^3\right)\overline{C}_{1,initial}\cdot C_1 \\ &= -\frac{8\alpha\overline{G}}{\pi}\left(\frac{1}{6}\pi\overline{d}_1{}^3\cdot\overline{C}_{1,initial}\right)\cdot C_1 = -\frac{8\alpha\overline{G}}{\pi}\overline{V}_{1,initial}\cdot C_1\end{aligned} \quad (1)$$

where , *C* is the volume concentration of particles, α the efficiency factor or coagulation efficiency, β is a rate constant or operator called the coagulation kernel, and *d* is the particle diameter. The term, $\overline{\beta}_{11}\overline{C}_{1,t\to 0}$, is the coagulation rate and is assumed to accurately describe the dominant particle-particle interactions throughout the coagulation experiment.

Below we describe measurement methods used to collect the necessary particle concentration, size spectra, and volume data, and then the detailed development of mathematical methods for calculating coagulation efficiency based on this data.

2.4.2. Coagulation Experiments

Coagulation experiments were conducted using two Couette flow devices in parallel. We refer to individual Couette flow devices as A, B, C, and D. The four Couette flow devices were made following the design of Drapeau et al. (1994). The coagulation incubations were carried out at the same time each day (3 h after the light cycle started) in semi-darkness at 15˚C for 4 h. The same sample from the chemostat overflow was used to fill the Couette chamber of each Couette flow device. All chemostat overflow samples were collected on one day for each dilution rate in 2006, but in 2007, there were two experiment days for each dilution rate. In order to collect ~3 l of material, the length of time the overflow was collected was dependent on the chemostat dilution rate and occurred over the 2–3 days prior to the experiment day.

The Couette flow device was filled (~1.2 l) and rotated at a speed that created a mean shear rate, $\overline{G}$, of 0.86 s^{-1}. This shear rate is in range of that typical for the ocean surface (10^{-2} to 10 s^{-1}) (Grant et al., 1962; Soloviev et al., 1988). Subsamples of ~ 20 ml were taken at some or all of the following time points: t = 1, 15, 30, 60, 90, 120, 150, 180, and 240 minutes, and kept cold and dark for up to 30 min prior to particle size enumeration using an electronic particle size counter (Coulter Multisizer III, Beckman Coulter). The Coulter Counter was outfitted with a 100 μm aperture to measure the particle concentration of

discrete bins logarithmically sectioned within the range of 2 to 60 μm equivalent spherical diameter (ESD). Triplicate measurements were performed on 500-1000 μl subsamples at each time point and averaged. If necessary, the sample was diluted with 0.2 μm (Minisart 2000, Sartorius) pre-filtered seawater to keep the coincidence of particles at the aperture < 5%. Cell growth was monitored in a parallel 1 l bottled sample over the course of the coagulation experiment; no detectable growth was observed over the 240 min coagulation incubations.

Coulter Counter results were used to determine the total number concentration of particles (# ml^{-1}), *C*, at each time point. Equation 1 tracks the temporal variance in the total number of particles. Although the derivation of Eq. 1 is contingent on collisions between monomers dominating the coagulation process, large particles sweep a larger volume of space as they move. Hence, the influence of larger particles interacting with other particles must be considered (Elimelech et al., 1995). Therefore the term chosen for the solid volume fraction of particles, $\overline{V}_{1,initial}$, from Eq. 1 includes the volumes of all particles with an ESD that ranged from the size of cells up to 60 μm, the large end of Coulter Counter detection range.

Operationally we define *C* as the sum of the particles enumerated for discrete bins of the size spectra by the Coulter Counter. In practice, however, *C* represents the sum of particles for a portion of the full size spectra and we acknowledged this by recasting it as $\sum C$ with operationally defined upper and lower bounds on the summation. Eq. 1 becomes

$$d\sum_{i=1}^{\infty} C_i/C_1 = -\frac{8\alpha\overline{G}}{\pi}\sum_{i=1}^{\infty}\overline{V}_{1,initial}dt \quad . \tag{2}$$

The bounds on $\sum C$ are $i = 1$ and ∞ where *i* corresponds to bins representing particle diameters. For this study, the bounds on $\sum C$ are the cut-off value, x_{cut}, and 60 μm. Integrating Eq. 2 yields

$$\log_e \sum_{i=1}^{\infty} C_{i,t}/t = -\alpha\frac{8\overline{G}}{\pi}\phi \tag{3}$$

where $\sum_{i=1}^{\infty}\overline{V}_{1,initial}$ of Eq. 2 is renamed Φ. The Coulter Counter reports the solid volume fraction, or particle volume fraction, of all particles in units of μm^3 ml^{-1}. In all equations this quantity must be unit-less and is transformed to ppm. The term on the left side of Eq. 3 is estimated as the linear slope of $\sum_{i=1}^{\infty} C_{i,t}$ plotted on a $\log_e$ scale versus the time(s) of the

respective experiment time point. Hereafter the left hand side of Eq. 3 is referred to as $slope$. The simple expression of coagulation efficiency then becomes

$$\alpha = -\frac{slope \cdot \pi}{8\overline{G}\phi} \quad . \tag{4}$$

This equation has the constant 8 in the denominator rather than 7.824, as in other coagulation efficiency studies (Kiørboe et al., 1990; Dam and Drapeau, 1995; Engel, 2000; Vieira et al., 2008). This results from using the rectilinear coagulation kernel for shear (Pruppacher and Klett, 1980; Elimelech et al., 1995; see Appendix for explanation) that reduces to $8 \cdot \overline{G} \cdot \frac{1}{6}\overline{d}_1^3$ or $8 \cdot \overline{G} \cdot 0.167\overline{d}_1^3$ (Kriest and Evans, 1999) instead of $8 \cdot \overline{G} \cdot 0.163\overline{d}_1^3$ as reported in Kiørboe et al. (1990).

2.4.3. Calculation of Volume Concentration of Particles

Use of coagulation theory requires particle volume to be conserved over the course of a coagulation experiment. Taking advantage of this theory Φ used in Eqs. 3 and 4 equals the initial particle volume fraction, which in this experiment represents the solid volume fraction of the subsample from the Couette flow device at the beginning of the coagulation incubation. The material enumerated by the Coulter Counter is referred to as Coulter Counter detectable particles (CCP). As done for $\sum C$ in Eq. 3, we estimated Φ by summing the CCP volume per milliliter ($\mu m^3\ ml^{-1}$) for particles in the largest Coulter Counter bin (60 μm) down to those having a diameter equal to the smallest monomer, or cell. This lower limit on particle size is designated by the size spectra cut-off value, or x_{cut}. The total volume of solid particles per milliliter ($\mu m^3\ ml^{-1}$) was then converted to ppm by making the volume conversion between units of cubic micrometers and milliliters then multiplying by 10^6 (Table 4.2).

One effect of TEP is to increase water particle concentration leading to higher collision rates and potentially higher coagulation efficiencies (Kiørboe et al., 1994; Jackson, 1995). The electronic particle detection does not detect TEP directly because of its gel-like composition rendering it the same density of water. Because TEP is not accounted for explicitly in Φ a may be enhanced and >1 (Engel, 2000). Microscope samples can be used to derive a Φ that includes all Alcian blue stained material and thus account for TEP presence

(micro-Φ). However, micro-Φ will include TEP material coating solid particles such as cells. Because the Coulter Counter particle enumeration already accounts for all solid particles including Alcian blue stained cells it is necessary to subtract out Alcian stained blue cells from the micro-Φ; this was accomplished as follows. First, the equivalent spherical volume (ESV) of all particles, micro-Φ (ppm), was calculated using the area measurements (Engel, 2009). Second, the microscope "cell" volume concentration (i.e., Alcian blue stained cells), cell-Φ (ppm), was determined as ESV with particles that satisfy the criterion of a circularity value approximating a sphere (≥ 0.7) and feret diameter between 3 and 7 μm. Circularity is calculated by relating the area and perimeter of a particle ranking its symmetry (0 to 1, where 1 is a circle) with respect to that characteristic of a circle ($perimeter^2 = 4\pi \times area$). Lastly, the microscope cell-Φ was subtracted from micro-Φ. The remainder is the TEP-Φ for the experiment. TEP-Φ includes amorphous TEP and TEP aggregates (Table 4.2). As explained in Engel (2000), new estimates of the coagulation efficiency value, α', were made taking into account the TEP-Φ by adding it to the Coulter Counter Φ in Eq. 4 (Table 4.3).

2.4.4. Mathematical Methods for Calculating Coagulation Efficiency

Here we detail calculation steps and criteria used to estimate α values and illustrate rubrics that can be used to address some common issues that arise when using Coulter Counter data from Couette flow device coagulation incubations.

First, we use an α model proposed by Kiørboe et al. (1990) to account for the slight variation in cell size of the monodisperse suspension, i.e. the normal distribution of the monomers described by mean and variation, μ_{mono} and σ^2_{mono}, respectively. The equation taken from Kiørboe et al. (1990) and used in numerous other studies (Drapeau et al., 1994; Dam and Drapeau, 1995; Vieira et al., 2008) is

$$\alpha_{var}(x_{cut}) = -\frac{slope(x_{cut}) \cdot \pi}{8\overline{G}\phi} \cdot \exp(1.5S^2/\overline{d}_1{}^2) \tag{5}$$

where α_{var} and $slope$ are dependent on the x_{cut}, S^2 is equal to variance in the size distribution of the cells, or σ^2_{mono}, and $\overline{d}_1$ is the mean diameter of the monomers, or μ_{mono}. It should be noted, Kiørboe et al. (1990) derived the exponential term in Eq. 5 by assuming the cell size distribution was described equally well by a normal distribution or lognormal distribution.

Second, we established a methodology for estimating the lower and upper bound on the

monomer diameters. Contrary to assumptions made in Eq. 5, the monomer (cell) peak does not follow a Gaussian function. Coulter Counter particle size distributions (PSD) were fit to a Gauss peak curve as part of the exploratory data analysis of this work. We observed the Coulter Counter PSDs were narrower than the Gaussian model peaks and the right shoulder of the cell peaks were slightly broader than the Gaussian counterpart (Appendix, Fig. 4.A1). Moreover the equivalent spherical diameter where the monomer peak started and ended was not consistent experiment to experiment. Thus, it was necessary to derive a mathematically consistent method for setting the bounds on the monomer size range. To do this we used a local method sensitivity analysis where the simple derivative of the output, α, was evaluated for a given input value, x_i iteratively for x = 2.5 μm to 4.5 μm, comprised of 45 bins, where 2.5 and 4.5 μm represent the lower bound on the cell diameter. We determine a numerical value for the first derivative, α'(x), with the central differences method: $\alpha'(x) \approx [\alpha(x+\Delta x) - \alpha(x-\Delta x)]/2\Delta x$. The best estimate for x_{cut} that is applied to our calculations of coagulation efficiency is referred to as x^*_{cut}. We define x^*_{cut} as the smallest diameter of a monomer (cell), and is the diameter where the first derivative of α was at a minimum (Appendix, Fig. 4.A2). We defined the largest diameter of a monomer (cell) as the Coulter Counter bin located to the right of the monomer peak where the integrated number concentration of cells–integrated from x_{cut} to largest cell diameter–are equivalent for the Gaussian model for the monomer curve and Coulter Counter PSD. In general, the largest cell diameter is approximately 7 μm for all experiments.

Third, we accounted for the larger $slope$ values that occurred on the right side of the monomer peak ($x > \overline{d}_1$). Recall $\sum C$, Φ, and $\overline{d}_1$ are all dependent on the cut-off value, x_{cut}. Using the Coulter Counter bins we stepped forward the cut-off as a value equal to or larger than the diameter where the monomer peak occurs ($x_{cut} > \mu_{mono}$). We found coagulation efficiencies to be highly dependent on x_{cut}. When x_{cut} used was between μ_{mono} and 7 μm, the α varied over a factor of 10. Therefore the selection of a cut-off value can vastly affect the reported α values. Furthermore, if x_{cut} is not controlled for, then the comparison of α values generated from replicate experiments or different cell media would mostly likely be affected (Appendix, Fig. 4.A2). To account for the larger $slope$ values, we report α as an mean of all individual α(x) from x^*_{cut} to ~7 μm. The mean α for the monomer peak is then referred to as $\alpha_{complete}$:

$$\alpha_{complete} = \left[\left(\frac{\sum \alpha(x_{cut,m})}{N}\right) \pm \sigma_\alpha\right] \cdot \exp(1.5S^2/\bar{d}_1{}^2) \quad (6)$$

where *N* is the number of Coulter Counter bins between x^*_{cut} and the end of the monomer peak, ~7 μm.

Finally, we determined an α value that reflects the enhancement of particle volume fraction, Φ, attributable to TEP–referred to as α'. We recalculate $\alpha_{complete}$ as α' after the methods of Engel (2000) using Φ_{TEP} as defined earlier:

$$\alpha'_{complete} = \alpha_{complete} \cdot \frac{\phi}{\phi + \phi_{TEP}} . \quad (7)$$

2.5. Estimates of Detached Coccoliths

The suspension sampled from the overflow of the chemostat contains free coccoliths, which can detach from the cell either before or after they are carried into the collection vessel with the overflow. Determination of the lower bound on cell diameters (x^*_{cut}) requires enumerating the abundance and size range of detached coccoliths. Coccolith detachment was estimated from 3 methods: Coulter Counter PSD, image analysis of microscope samples, and calculations based on Fritz and Balch (1996) (Appendix, Table 4.A1). The latter two methods most likely underestimate the detached coccoliths, therefore values estimated from Coulter Counter data are reported (Table 4.4). However, values from all methods are similar when normalized to values from experiment day 14 (see Appendix for more description and comparison of methods). *Emiliania huxleyi* coccoliths have been reported as having diameters of 2.5 to 3.0 μm (van der Wal et al., 1983). Fritz (1999) found *E. huxleyi* coccolith total length and total width to be 2.99 ± 0.29 μm and 2.40 ± 0.26 μm for growth rate of 0.37 d^{-1} and 3.10 ± 0.30 μm and 2.50 ± 0.25 μm for growth rate of 0.20 d^{-1}, which are similar to growth rates used in 2007. Using the Coulter Counter, we enumerated the coccoliths within the PSD by assuming that all particles with an equivalent spherical diameter less than the cut-off value, x^*_{cut}, are coccoliths.

To compare the effect of the detached coccoliths on the coccosphere diameter we estimated the number of layers of coccoliths on cells using a power law function from Fritz and Balch (1996). In, 2007 we assumed that non-calcifying cells had a diameter of 2.7 μm and each additional layer of coccoliths added 0.798 μm (Balch et al., 1993) to the

preexisting diameter. We calculated the surface area of coccospheres using the mean cell diameter (d_1 from Eq. 6, Table 4.4) from the Coulter Counter PSD. The surface area per coccolith was taken from Fritz and Balch (1996) and used to estimate the cumulative number of coccoliths necessary for each layer. Fritz and Balch (1996) estimated the change in coccosphere diameter for every added/lost plate as

$$\frac{\Delta d}{coccolith} = 0.195 \times n^{-0.465}, \quad (8)$$

where Δd is the change in cell diameter for every coccolith detached and n is the number of attached coccoliths or cumulative number of coccoliths per cell. The shift in coccosphere diameter between growth rates is divided by the Δd/coccolith value for the respective n, yielding an estimate of detached coccoliths per experimental growth rate. We also calculated the ratio of detached to attached coccoliths per cell per growth rate (Table 4.4).

2.6. Statistical Analyses

A correlation matrix was used to evaluate the relationships between variables measured for the 2007 coagulation experiment samples. The significance of correlation coefficients was determined by student t-test (double tail) at $p<0.05$ and $p<0.01$ significance. In addition, principal components analysis (PCA) was carried out using MATLAB to elucidate data trends in multi-dimensional space. Prior to PCA, sample data was demeaned and standardized. PCA represents each sample with a sample site score and each variable with a different scale, a variable loading. The full PCA determines a set of sample site scores and associated variable loadings for every component (number of components is equal to the number of variables measured). We limit our PC comparisons to the first and second principle components (PC1 and PC2), which represent ~80% of the total variability in the samples. Compositional variables (e.g., total alkalinity, TEP: Chl-*a*) plot positively or negatively with increasing absolute magnitude that is scalable to the influence the variable had on processes that explain the first and second orders of variation in samples. In environmental biogeochemical studies the sample site scores often spread out according to their source and degree of degradation along PC1 and PC2 (Gõni et al. 2000; Sheridan et al. 2002; Engel et al. 2009b; Abramson et al. 2010; Xue et al., 2011).

3. Results

3.1. Chemostat Biogeochemistry

Biogeochemical results of the 2006 and 2007 chemostat studies are discussed in more detail in Koch (2007) and Borchard et al. (2011), respectively. In 2006 and 2007, cell PIC and POC quotas were primarily affected by growth rate. The amount of calcite per cell increased under N- and P-depletion in 2006, and under P-depletion in 2007 (Koch, 2007; Borchard et al., 2011). Phosphate was not detectable at any time (Table 4.1). There was a decline in nitrate and nitrite in 2006 as growth rate decreased; however, in 2007 on sampling day 22 ammonium and nitrite increased to concentrations near that on sampling day 10, after which the ammonium and nitrite levels decreased to a minimum (Table 4.1). In 2006, steady state of total cell biovolume was achieved prior to all experiment days. For 2007, cell biovolume reached steady state before sampling day 14 (Borchard et al., 2011). We observed very low growth rates of cells on day 22 and the 2 days prior over which time the overflow was collected. In 2007, the volume concentration of Coulter Counter detectable particles (CCP) decreased at the low dilution rate whereas 2006 CCP showed less of a difference with growth rate (Table 4.2).

For similar growth rates, the total alkalinity (TA) of 2006 experiments are ~250-700 μmol kg^{-1} seawater (SW) greater than 2007 values (Table 4.1). The difference in 2006 and 2007 TA was most likely due to the degree of calcification of the cells in the chemostat inoculate since initial TA values were similar between years (2460 μmol kg^{-1} SW and 2440 μmol kg^{-1} SW for 2006 and 2007, respectively) (Koch, 2007; Borchard et al., 2011). As previously described, the batch culture used to seed the chemostats in 2006 was approximately 60% calcifying whereas the initial culture used in 2007 was >99% calcifying. Further discussion of *E. huxleyi* calcification in 2006 and 2007 chemostat experiments are provided in Koch (2007) and Borchard et al. (2011), respectively. In 2006, PIC/POC increased as the dilution rate and growth rate decreased; however, in 2007, it dropped. Notably, initial PIC/POC was higher in 2007 and dropped by a factor of ~3 between duplicate sampling days 10 and 14 (Table 4.1) most likely due to initial build up of coccolithophore biomass that occurred prior to day 12 (Borchard et al., 2011). After sampling on day 14 the remainder of PIC/POC remained relatively unchanged (Table 4.1).

In 2006, PIC/POC increased when transitioning from high to low growth rates. In the same way, we observed differences in the coccolith detachment rate between years as cells transitioned from high to low growth rates (see Results below).

Table 4.A2 reports the CCHO composition (% mol) and CCHO totals as concentrations (μmol l^{-1}) for each size fraction (tCCHO, <0.45 μm-HMW-dCCHO, and <1000 kDa-HMW-dCCHO) and sample source (chemostat and coagulation experiment replicates). In 2006, only the <0.45 μm-HMW-dCCHO fraction was sampled and CCHO totals increased as the cell growth decreased. In 2007, CCHO totals of each size fraction varied with growth rate; yet, on average the concentration of CCHO totals increased for cells at lower growth rates (Table 4.A2).

The 2006 CCHO totals (<0.45 μm-HMW fraction) were greater than CCHO totals for both the HMW dissolved fractions in 2007 (<0.45 μm-HMW and <1000 kDa-HMW) (Table 4.A2). Of the sugars separated in this study all but glucosamine and galactosamine are generally found in coccolithophores (Fichtinger-Schepman et al., 1979) and referred to as coccolithophore associated polysaccharides (CAP). The greater abundance of non-calcifying coccolithophores in 2006 might have led to this difference. de Jong et al. (1979) found non-calcifying coccolithophores to release more CAP into the cell medium than calcifying coccolithophores. In 2006, the apparent changes in composition with decreasing cell growth rate are a decrease in glucose and an increase in rhamnose, galactose, and arabinose (Table 4.A2). In 2007, the HMW dissolved sugar composition switched between dominance of glucose vs. uronic acids on the first vs. second experiment day of each dilution rate; this difference in adjacent experiment days existed despite their having similar growth rates (Table 4.A2).

In 2007, sugar samples from the chemostat and each coagulation experiment were indistinguishable from one another for nearly each sample set (i.e., given experiment day and size fraction). Q mode analysis–used to characterize relationship between samples–revealed correlation coefficients of 0.69 to 0.99 (average 0.90) with the exception of <1000 kDa-HMW-dCCHO samples on experiment day 14 (R^2 of chemostat and coagulation replicates one and two were 0.25 and 0.16). The lack of significant difference in sample source suggests samples from the over flow were not significantly different from those sampled from the chemostat on the experiment day. Additionally, this finding signifies that

the coagulation of the material did not cause an appreciable difference in sugar composition. Mass balance of sugars was not always achieved among the two HMW dissolved pools: half of the <0.45 μm-HMW-dCCHO samples had smaller abundances than the <1000 kDa-HMW-dCCHO abundances, contrary to expectation given the <0.45 μm theoretically should include macromolecules >1000 kDa. Uncentrifuged material unaccounted for in the Macrosep™ tubes would explain enhanced concentrations of the <1000 kDa-HMW-dCCHO. For this reason, we focus on the trends in <1000 kDa-HMW-dCCHO composition between experiment days and not absolute concentrations. PCA of the 2007 data revealed CCHO samples could be differentiated by dilution rate (PC1, 61.4% variation explained) and abundance of Rha versus Ara+GalN, Man+Xyl, and GlcN (PC2, 18.7% variation explained)(Fig. 4.1).

3.2. TEP

3.2.1. Colorimetric TEP Concentrations

TEP_{color} concentrations are expressed in xanthan gum equivalents per liter (μg XG eq l^{-1}) and per cell (μg XG eq $cell^{-1}$) and range from ~130 to 1160 μg XG eq l^{-1} (or ~0.3 to 2.2 pg XG eq $cell^{-1}$) in 2006 (Table 4.2). In 2007, TEP_{color} abundances were similar and ranged from 0 to ~830 μg XG eq l^{-1} (or 0 to ~3.2 pg XG eq $cell^{-1}$) (Table 4.2). In both years, TEP_{color} abundance increased as the growth rate decreased (Table 4.2). Although dilution rates were nearly equivalent, day 25 TEP concentrations were higher than on day 22. It is possible that TEP production could have changed over short time scales such as the 3 days over which the overflow material was collected. On a per cell basis 2007, day 22 TEP_{color} was ~25% lower for flocculated material than for material sampled prior to coagulation incubations. The same trend occurred for 2006, day 40 TEP_{color} samples. Pre-coagulation samples were taken from the chemostat on the sampling day (2007) or from the chemostat overflow (2006). Differences in TEP abundance before and after coagulation experiments for both years may be due to settling of flocs (either preformed or formed during incubation) onto the inner cylinder of the Couette chamber. Another possible explanation for 2007 samples is that material captured within the overflow vessel experienced conditions slightly different than cells that remained in the stirred chemostats. Temperature was dependent on ambient air of the cold room. Temperatures in the cold

room were not as well controlled as that of the water jacket surrounding the chemostats. We observed the coagulation experiment TEP_{color} was negligible and hence lower than chemostat TEP_{color} values (negative cell corrected TEP_{color} values imply less than 100% of cell surfaces were coated with TEP-like material at that time). On day 40 in 2006 and day 22 in 2007 the difference between chemostat and coagulation experiment TEP_{color} was significant to 1 SE (Table 4.2). However, on experiment day 25 TEP_{color} of the chemostat and coagulation experiment were not statistically different.

3.2.2. Microscopic TEP Volume Concentration and Area

Total volume concentration of TEP (as ppm) was determined assuming particles had spherical geometry (Engel, 2009). As seen for TEP_{color}, the TEP_{micro} also increases with decreasing growth rate (Table 4.2). In 2007, the lower growth rate samples had a 5x increase in the volume concentration of TEP and a 7x increase in the volume concentration of flocs, i.e., particles larger than cells (Table 4.2). The volume concentration of Alcian blue stained coccoliths increased by nearly a factor of ~3 between days 14 and 25 (Table 4.2). Like TEP_{color} concentrations, TEP_{micro} areas showed an increase between duplicate days 22 and day 25. Additionally, the volume concentration of Alcian blue stained cells increased on the second experiment day of each dilution rate, similar to the pattern observed for uronic acids mentioned above (Fig. 4.1, Table 4.A2). Most 2006 TEP_{micro} samples were photographed after being stored for one year; hence, the resolution of most images do not yield consistent results for size fractions, such as Alcian blue stained coccoliths and particles larger than cells, and they were not sampled for TEP_{micro} fractions.

3.2.3. TEP Size Spectra

The TEP volume concentration of size classes (1 μm bins for diameters 0-35 μm, first bin represents 0.4–1 μm) determined by image analysis was plotted versus sampling day (Fig. 4.2). The abundance of cell-sized TEP increased on the second experiment day for each dilution rate. Additionally, for experiments conducted with cells of relatively low growth rates (duplicate days 22 and 25) we observed an increase in the number of particles larger than cells, indicating there was more coagulation at low growth rates.

3.3. Particle Coagulation Efficiency

Particle coagulation efficiencies (α) for the 2006 and 2007 experiments are given for α_{var} using a cut-off (x_{cut}) of 2 μm (α(x=2μm)) and a Gaussian fit curve-derived cut off, x^*_{cut} (See Appendix for methods used to determine x^*_{cut}), using Eq. 5 (Table 4.3). We also determined the term $\alpha_{complete}$ by averaging the $slope$ over the whole monomer peak, and adjusted $\alpha_{complete}$ to give α', which accounts for the contribution of TEP to the total particle concentration (Table 4.3). There was no clear trend between α_{var} and growth rate. Additionally, replicates of α_{var} were highly variable in comparison to $\alpha_{complete}$ and α'. Appendix Figure 4.A3 depicts the difference in α_{var} and $\alpha_{complete}$. For $\alpha_{complete}$ and α', there was an increase in coagulation efficiency as exponential growth rate decreased. This trend has been reported for other phytoplankton species (Engel, 2000).

Coagulation efficiencies for 2006 ranged from 0.23 to 1.35 ($\alpha_{complete}$) and 0.20 to 1.01 (α') (Table 4.3). In 2007, $\alpha_{complete}$ (0.36 to 1.19) and α' (0.32 to 1.15) values were within range of those in 2006, although values were higher for similar exponential growth rates (Table 4.3). Engel (2000) shows that accounting for enhancement of collisions due to the TEP particle abundance (here termed α') reduces the coagulation efficiency to less than or close to 1, the theoretical upper limit for the attachment rate/collision rate (Alldredge and McGillivary, 1991). Henceforward, we will use α' as the coagulation efficiency in our data analysis and discussion. When comparing α' with exponential growth rate in both 2006 and 2007(Fig. 4.3), there appears to be a 2-phased relationship where α' initially increases with growth rate and consistent across replicate coagulation experiments, but then increases significantly at low growth rates and replicate results are highly variable.

3.4. Coccolith Detachment with Growth Rate

In 2007 experiments, the number of detached coccoliths in the chemostat overflow prior to aggregation ranged from 1 to 17 coccoliths per cell, increasing with decreasing growth rate (see Appendix, Table 4.A1). The relative number of detached coccoliths per cell was ~1-2 (Table 4.4). The loss of coccoliths from coccospheres caused an observable reduction in the mean diameter of the cells (Table 4.4). The observed shift in cell diameter was greatest between days 14 and 22. Because of the relatively large decrease in the diameter

of cells between day 14 and duplicate days 22 and 25, it is plausible that there was a greater concentration of coccoliths in the overflow prior to day 22.

3.5. Coccolith Detachment with Shear

Motivated by the necessity to have a consistent method for deriving x^*_{cut} and $\alpha_{complete}$, we quantified the flux of material from the right to left side of the cell peak while particles underwent laminar shear flow (i.e., during the coagulation experiments). We focused on 3 fractions of the Coulter Counter PSD: $<x^*_{cut}$ (coccoliths), small cells (x^*_{cut} <diameter <μ_{mono}), and large cells (μ_{mono} <diameter <~7 μm). These size ranges showed the greatest amount of variability during the 4 hour coagulation experiments. In 2007, we observed that coccolith-like particles (diameter < x^*_{cut}) comprised 1–13% of the total volume of solid particles assuming spherical morphology (see Appendix, Fig. 4.A4). This quantity increased during the coagulation experiments by factors of 1.2 ± 0.09, 1.4 ± 0.03, 1.9 ± 0.18, 3.1 ± 0.26 for days 10, 14, 22, and 25, respectively. In addition, image analysis showed that the quantity of Alcian blue stained particles that were smaller than cells (i.e., coccoliths) increased by approximately (1-7) coccoliths cell^{-1} by the end of the coagulation experiments (Appendix, Table 4.A1). These data indicated coccoliths were lost from the cells while within the Couette flow device. In 2006, however, the contribution of coccoliths to the total volume changed by only a factor of 1.2 ± 0.1, on average. The initial (pre-coagulation) volume contribution of this particle class was lower than in 2007, and comprised 1–7% of the total particle volume.

In conjunction with the increase of coccolith-like particles (diameter $<x^*_{cut}$) there was a drop in cells with diameters larger than the mean (μ_{mono} <diameter <~7 μm; see Appendix, Fig. 4.A4). Consequently, the volume of cells with diameters smaller than μ_{mono} most likely increased as the result of large cells shedding coccoliths shifting to the small cell portion of the PSD (x^*_{cut} < diameter < μ_{mono}). As confirmation of a shift in cell diameter, we saw the magnitude of the 2007 α_{var} and $slope$ increased with cell size for each experiment due to higher loss rate of large cells relative to small cells (x^*_{cut} <diameter <~7 μm). In 2006, the increase in the magnitudes of α_{var} and $slope$ were less dramatic and were 1/8 that in 2007.

3.6. Statistical Analyses Results

3.6.1. PCA Results

PC1 site scores show clear differences between the two high and two low growth rates (Fig. 4.4a). Site scores for duplicate days 22 and 25 are not significantly different from each other. Their negative site scores correspond to variable loadings (Fig. 4.4b) known to be associated with aggregation. These include: all coccolith sugar fractions (CAP), total and <1000 kDa-HMW-dCHHO of the acidic sugars (URA), total CCHO, Alcian blue stained cells, coccoliths : cell, α, and circular and non-circular aggregates. Variable loadings that correspond to high growth rate experiments (days 10 and 14) are growth rate, TA, and to a lesser degree <0.45 μm-HMW-dCCHO fraction of URA.

The underlying difference between the aggregation properties of samples from duplicate days 22 and day 25 is clear from PC2 (Fig. 4.4c). It illustrates changes between the duplicate experiment days at each growth rate shown by PC2 site scores alternating between negative and positive. Likely causes for the differences between duplicate days 22 and 25 are best seen in the variable loadings (Fig. 4.4d). Day 25 is represented by positive loadings for parameters that include: Alcian blue stained cells, circular aggregates, total sugars; to a lesser extent total CAP, TEP : Chl-*a*, α; and nearly negligible, growth rate. Yet, day 22 is represented by negative loadings. These include the parameters: <1000 kDa-HMW-dURA, <0.45 μm-HMW-dURA, tURA, 0.45 μm-HMW-dCAP, non-circular aggregates, coccoliths : cell, and nearly negligible <1000 kDa-HMW-dCAP and total alkalinity (Fig. 4.4d).

3.6.2. Correlated Coefficients

The same suite of variables used for PCA analyses were also used to create a correlated coefficient matrix (Table 4.A3). We observed no strong correlation between α' and any one of the 13 variables chosen, indicating all play some role in affecting the outcome of α'. Because our study focused on the effects of physiological changes in *E. huxleyi* on its coagulation efficiency, we determined which variables changed most with growth rate. We found that growth rate correlated positively with TA, and negatively with detached coccolith : cell and TEP : Chl-*a* (p<0.01). Growth rate was also negatively correlated with

<1000 kDa-HMW-dCAP and tCAP (p<0.05). Next, we investigated whether TEP was significantly related to any one particular sugar composition category. We found TEP : Chl-*a* to be significantly correlated with <1000 kDa-HMW-dCAP (p<0.01) and total sugars (p<0.05). There was no strong correlation between TEP : Chl-*a* and acidic sugars.

4. Discussion

4.1. Coagulation Efficiency as a Function of Growth Rate

Our study showed that coagulation efficiency of *E. huxleyi* increased as the cell growth rate decreased. This pattern of an inverse relationship between coagulation efficiency and growth rate has previously been shown for diatoms from batch, mesocosm, and field cultures (Vieira et al., 2008; Kahl et al., 2008; and Engel, 2000; respectively). Table 4.A4 summarizes the coagulation efficiency from these diatom studies. In general, this study and previous studies found coagulation efficiencies of ~0 to <0.2 when cells were nutrient replete and in exponential phase, ~0.25 as cells reached stationary phase, and then a more variable value close to 1 as the cells reached senescence. Although there is considerable range in the absolute α values given in each of these studies, measurements using Couette flow device or laminar shear experiments allow for the detection of physiologically driven differences in the initiation of phytoplankton aggregation. At growth rates >0.1 d^{-1}, coagulation efficiencies of 2007 were ~75 % higher than those of 2006 (Table 4.3), while variability between replicates was ~6.3 %. Both years showed an increase in coagulation efficiency at 0.71 ± 0.32, as growth rates decreased to ~0.1 d^{-1} and lower (excluding 2007, day 25 Couette flow device D; Table 4.3).

In addition to growth rate, cell physiology and environment affect cell aggregation (e.g., Myklestad, 1995; Obernosterer & Herndl, 1995; Penna et al., 1999; Staats et al., 2000). In senescent cells, factors such as TEP abundance, cell mucus covering, and chemical composition of mucus are time and environment dependent (Decho, 1990; Myklestad, 1995; Aluwihare and Repeta, 1999; Passow, 2002). Thus, at relatively high growth rates the difference between 2006 and 2007 coagulation efficiencies may be due to biogeochemical and physical properties of the cells. The variability in apparent coagulation efficiencies between replicates and different experiment days at low growth rates are more likely due

to variability in the chemical make up, abundance, and distribution of mucus material. Of these factors, we will further explore the effects of calcification and TEP concentration.

4.2. Coagulation Efficiency as a Function of Cell Calcification

The proportion of calcifying to non-calcifying cells in culture inoculates played a role in aggregate formation. In 2006, non-calcifying cells contributed ~28% to the total cell peak particle volume at higher growth rates and~22% at lower growth rates. Since calcified cells flocculate and form aggregates more readily than non-calcified cells (see discussion below), the relatively low coagulation efficiencies observed in 2006 may be due to the lower extent of calcification. Coulter Counter data in 2006 support this: two size fractions of particles were found (2.9 μm and 4.5-5.7 μm). This combination might be explained by the presence of a mixture of single non-calcifying cells and aggregated calcifying cells. Assuming this hypothesis is correct, reducing the total Φ by 40%–to represent the 60% of cells that are calcifying–increases the coagulation efficiency to ~0.36.

Calcified cells flocculate and form aggregates more readily because of the presence of Ca^{2+}, which is important for promoting cationic bridge formation of mucus fibrils (Decho, 1990; Leppard, 1995; Mopper et al., 1995). Crystal morphology of *E. huxleyi* during normal biomineralization is regulated by CAP, pH, and solution chemistry (de Jong et al., 1979; Kok et al., 1986; Henriksen and Stipp. 2009). Of the CAP monomers detected, mannose and the uronic acids are most prevalent within the CAP structure and relevant to its promotion of cationic bridge formation. The CAP backbone consists of mannose (Kok et al., 1986) and each CAP contains ~60 uronic acid groups that differentially bind Ca^{2+} when compared other cations (de Jong et al., 1976; Borman et al., 1982). In 2007, mannose + xylose and the uronic acids, galacturonic and glucuronic acid, on average make up 40 ± 28% and 34 ± 25% of the <0.45 μm-HMW- and <1000 kDa-HMW dCCHO pools, respectively. Yet in 2006, mannose + xylose and the uronic acids constitute less of the dissolved sugar composition, 16 ± 2% (Table 4.A2). Unlike the % mannose and uronic acids, TEP abundances were similar in 2006 and 2007 (Table 4.2). Likewise, Engel et al. (2009a) observed similar total TEP abundances for calcifying and non-calcifying cultures prior to aggregation on roller tables. However, after aggregation TEP abundances in aggregates of calcifying coccolithophores were significantly higher than in aggregates of non-calcifying

coccolithophores (Engel et al., 2009a). In our study, it is possible that the higher % calcification and % mannose (+xylose) and uronic acids of 2007 material led to the formation of gel fibrils and particles that yielded more sticking events per particle collision and, hence, higher α'. We found coccoliths : cell to be highly correlated to <1000 kDa-HMW CAP (R^2 = 0.88, p<0.1) possibly signifying the release of colloidal CAP with coccoliths from cell surfaces that would promote aggregation. Engel et al. (2009a) observed calcifying cells of *E. huxleyi* aggregated more rapidly in roller tanks than non-calcifying cells. Macroscopic aggregates were observed within a few hours in calcifying cultures that were exponentially growing, but only after >24-h in non-calcifying cultures (Engel et al., 2009a). Indeed, supporting the findings of Engel et al. (2009a), we estimated α values for cells that were fully calcified and still in exponential phase (2007, growth rate 0.6 d^{-1}, day 10) that were relatively large compared to other coagulation experiments (Table 4.A4).

4.3. Coagulation Efficiency as a Function of Nutrient Availability

Nutrient availability to *E. huxleyi* affects coagulation efficiency in part through its influence on calcification rates and the ratio of detached/attached coccoliths (Linschooten et al., 1991; Balch et al., 1993; Fernández et al., 1993; Fritz, 1999). Calcification rates and coccolith abundances influence physical characteristics of coccolithophore aggregates such as size, shape, excess density, and porosity (Engel et al., 2009b; Iversen and Ploug, 2010). Cells experienced P-limitation in both 2006 and 2007 (Koch, 2007; Borchard et al., 2011; Table 4.1); however in 2007, cells at the 0.1 d^{-1} dilution rate had enhanced P-limitation where P cell quotas fell below a critical value (Borchard et al., 2011). Previous work has shown that coccoliths can tolerate phosphate limitation to a large extent (Paasche, 1998; Riegman et al., 2000; Borchard et al., 2011). Phosphate limitation may enhance cellular POC production (Riegman et al., 2000), but a decrease in cellular POC production (including TEP) may be observed when the minimum cell quota for P is reached–case in point: cells in 2007 (Borchard et al., 2011). As a result of the dissimilarity in the extent of P-limitation of cells in 2006 and 2007, we observed differences in cell diameters (cell POC-quota), density (abundance of coccoliths), and TEP production.

In 2006, the steady increase in PIC/POC , the consequent decrease in total alkalinity, and the initial increase in cell diameter, suggest cell calcification continued as the growth rate

declined. An increase of cell calcium that is concomitant with cell P-limitation has been observed before (Paasche, 1998; Riegmann et al., 2000). Müller et al. (2008) hypothesized that unlike light- and N-limited cells, P-limited cells could obtain the light energy necessary for calcification by the elongation of their time spent in G1 phase of the cell cycle. They found a rapid increase in cell calcite for exponential and late stationary phase cells, thus supporting our finding that the P-limited cells of 2006 gave rise to enhanced cell calcification rates. We calculated low detached/attached coccolith ratios that coincide with increases in cell diameter reflecting coccolith accretion onto cell surfaces. Notably, there was a significant difference in the cell diameters of 2006 day 34 and 2007 day 22; in 2006 on day 34, cell diameter was large due to increased coccolith coverage that led to higher cell densities. On experiment day 40 (growth rate of 0.05 ± 0.03), nitrogen decreased slightly (~12%) from day 34 and the coccolith balance shifted from coccolith accretion toward coccolith detachment. Studies have reported high abundance of detached coccoliths at the stationary phase when cell growth rate declines and blooms come to an end (Balch et al., 1993; Paasche, 2002)–this phenomenon corresponds to satellite detection of blooms (Balch et al., 1993; Holligan et al., 1983, 1993). As a result, the cell diameter (and density) decreases as observed for day 40. Between days 34 and 40, we also observed the TEP Φ : Cell Φ nearly doubled and coagulation efficiency increased by over a factor of 2 (Table 4.2).

In 2007, we propose P-limitation led to a greater amount of detached coccoliths relative to those accreted onto the cell surface in 2006. P-limitation, in part, initially led to enhanced calcification and enlarging of the cell diameter by greater POC-quotas within the cell (Riegman et al., 2000; Borchard et al., 2011). The medium supply was not sufficient for sustained buildup of PIC, as observed at the beginning of the chemostat experiment (Borchard et al., 2011; Table 4.1). A transition occurred when cells reach the lower dilution rate of 0.1 d^{-1}: TA and cell diameter decreased and detached/attached coccoliths increased. This is due to continued calcification that occurs when medium flow through and biomass build up is reduced (Borchard et al., 2011). One exception to the cell diameter and detached/attached coccolith ratio trend was day 25, when Coulter Counter data revealed an increase in cell diameter and lowered magnitude of detached coccoliths per cell (Table 4.4). Prior to day 25 the DIN content of the medium increased to nearly equal that measured at the beginning of the chemostat growth experiment (Table 4.1, day 10 and 22).

Hence, between experiment days 22 and 25 the cells within the chemostat may have begun to respond to the increase in DIN by increasing their growth rate (Table 4.1). The cells used for coagulation efficiency experiments on day 25 were collected from the chemostat overflow from day 23–25. We hypothesize the changes in the PSD occurred because of an increase in coccolith coverage due to lowered detachment rate of coccoliths. Supporting evidence is a drop in the estimated detached/attached coccolith ratio and stable PIC/POC from day 22 to 25. The variation between the detached/attached ratio on days 22 and 25 is likely to be a major factor in the variability observed in the coagulation efficiency of these two experiment days (mean of 0.74 ± 0.1 on day 22 and 1.15 on day 25).

Our study showed *E. huxleyi* regulated their calcification and coccolith accretion and detachment rates dependent on the cell physiology, which instigated changes in the coagulation efficiency. Fritz and Balch (1996) suggest *E. huxleyi* demonstrate a careful balance between coccolith attachment and detachment to affect their settling velocity. According to their estimates of coccolith coverage and cell density, plated cells would be able to experience the changing nutrient availability of the mixed layer by settling through 100 m over 75 days, absent of the disruption of currents or turbulence. Whereas non-calcified cells would reside within the euphotic zone for up to 1 year allowing for them to potentially seed the water column for the next spring bloom (Fritz and Balch, 1996). Cells with reduced layers of coccoliths and smaller coccospheres, often seen in the lag and stationary phase cells of batch cultures (such as the 2006 inoculum), are most comparable to cells observed at end of bloom within its center (Fritz and Balch, 1996). The ratio of detached/attached coccoliths increases as you move from the bloom periphery towards the center (Fernández et al., 1993) where detached coccoliths accumulate and are visible by satellite (Holligan et al. 1983, Balch et al., 1996). Actively growing cells at early growth stages are found concentrated along the bloom edge where detached coccoliths would be diluted laterally and show little accumulation (Fritz and Balch, 1996). Our findings suggest the conditions necessary for *E. huxleyi* aggregation and sedimentation, first, require older portions of the bloom population to be either partly calcified or to have a large abundance of Ca^{2+} sourced by detached coccoliths; and, second, TEP coverage of cells and TEP size and abundance to be extensive enough to carry the calcified cells such that they form large

aggregates that could sink without their integrity being compromised due to the disruption of shear eroding the sinking face of the aggregate.

4.4. Coagulation Efficiency as a Function of TEP Concentration

For *E. huxleyi*, our findings suggest cell-cell binding results in a higher yield of attachments for a given number of collisions compared to cell-TEP binding. We hypothesize a) the exopolymer coating on the cells were more chemically reactive (sticky) than gel particles and b) upon collision, exopolymer coating on cells promote formation of flocculant bridges, binding cells together to form robust flocs. The cell attachment mechanism that dominates the early stages of aggregation (e.g., cell-cell binding or cell-TEP binding) plays a crucial role in determining the density of aggregates, settling velocity, and floc strength. Thus, insights on the relationship between bloom conditions and specific cell attachment mechanism would abet our understanding of sedimentation events. Our study suggests aggregation is not TEP-limited and rather coagulation is related to the presence of $CaCO_3$ and Alcian blue stainable material on the cell surface. If these additional parameters are not accessed, then the export of carbon due to coccolithophore blooms may go underestimated.

PCA results Fig. 4.4d for 2007 days 22 and 25 show the form of TEP inclusion within aggregates (Alcian blue stained cells, circular vs. non-circular aggregates) was significantly different ($p<0.01$). Yet, the difference in cell and TEP particle concentrations was not ($p>0.32$). It is important to note the material identified as TEP using the standard methods (Passow and Alldredge, 1994; Passow and Alldredge, 1995b) is more inclusive than its nomenclature, "transparent exopolymer particles", suggests. Indeed, measured TEP can be in the form of particles, “free” TEP, such as amorphous particles with at least one dimension of >0.4 μm. It might also consist of “enclosed” TEP, such as aggregates containing cells glued together by TEP or aggregates with a matrix dominated by TEP with other particles embedded within (Passow and Alldredge, 1995a). Additionally, TEP measurements include exopolymer fibrils, nanometers in dimension, forming web-like microscopic features that coat filter surfaces (Kepkay, 2000; Verdugo et al., 2004; De Bodt et al., 2010). Also included are polysaccharide (PS) mucus coatings on cells that are stained by Alcian blue; such material is stained by Alcian blue, but not independent particles as

defined by TEP (Passow and Alldrege, 1994; Passow and Alldredge, 1995b; Passow, 2002). TEP measurements do not distinguish between CAP coated coccolithophores and true independent particles of TEP. We classify CAP coated coccolithophores stained by Alcian blue as Alcian blue cells ("AB cells"; Engel et al., 2004). AB cells were identified using the circularity tool of ImageJ as described in the Methods. TEP accumulation on *E. huxleyi* cell surfaces has been observed before (Engel et al., 2004; Harlay et al., 2010).

The variation observed in AB stained cells on day 22 and 25 may have resulted from fewer cells being incorporated into aggregates on day 25. It is possible that the separation of variable loadings on PC2 may be due to greater number of non-circular aggregates falling out of suspension towards the inner cylinder on day 25, though model predicted loss rates would be low (Drapeau et al., 1994). We observed a light coating of *E. huxleyi* material on the inner cylinder for both day 22 and day 25. We could not discern if the PC2 results were representing a skewed sampling of the floc material because it was not possible to collect this material from the Couette chambers quantitatively at the conclusion of the coagulation incubations without disturbing the particle size spectra greatly.

Despite the possible sources of experimentally induced changes that could skew our understanding of TEP association on days 22 and 25, the PCA findings suggest that a greater abundance of AB stained cells existed on day 25, creating more circular aggregates. In comparison to day 22, the increase in AB stained cells on day 25 could have resulted in relative depression of HMW-dCAP from the sample medium. The accumulation of CAP exudates on the coccosphere may have been facilitated by the slowed detachment rate of coccoliths observed for days 23-25. Theory and studies suggest the chemical sticky nature of TEP or CAP enhance coagulation. Indeed, the $slope$ and the coagulation efficiency results are higher on day 25 confirming that there was a greater loss of monomers during the coagulation experiment (Table 4.3).

4.5. Implications for TEP Association on Aggregate Settling and Strength

The canonical view of TEP involvement in phytoplankton aggregation is that late in the bloom when cells are reaching senescence TEP is abundant and cell aggregation begins (Alldredge et al. 1993; Kiørboe and Hansen, 1993; Passow et al., 1994). Results from select studies conflict with this prevailing model of TEP-facilitated aggregation. For example,

there can be aggregation before cell senescence occurs (Hill, 1992; Kiørboe et al., 1994; Dam and Drapeau, 1995; Passow and Alldredge, 1995a) or, conversely, there can be little sedimentation despite high concentrations of TEP and cells (Pitcher et al., 1991; Kiørboe et al., 1998). Therefore, having chemically sticky TEP occurring late in the bloom when nutrients are depleted (Smetacek and Pollehne, 1986; Hoagland et al., 1993; Passow, 2002) is not a necessity or always sufficient for flocculation to occur (Passow and Alldredge, 1995a). Surface colloid and coagulation/flocculation theory suggest that weak flocs will result from coagulation with little involvement of a coagulation aid (e.g., organic polymers) much like flocs formed by charge patch flocculation, such as at the turbidity maximum of an estuary (Edzwald et al., 1974; Somasundaran, 2006). Therefore, the capacity for the floc to resist disaggregation as it settles through the surface ocean might be highly dependent on the form of TEP involvement (free and enclosed TEP, or AB cells) with cells that developed during the initial stages of aggregation. Mass sedimentation of phytoplankton is most likely to occur once the theoretical critical concentration (Jackson and Kiørboe, 1998) of cells has occurred and the magnitude of export is enhanced by initial low coagulation efficiencies allowing for a buildup of biomass in the euphotic zone (Jackson and Lochmann, 1993). Therefore shifts in TEP abundance, TEP association with cells, and TEP chemical composition during a bloom has not only a controlling effect on the robustness of aggregates, but on the magnitude of export as well.

We propose a model for the role of TEP on coagulation that encompasses the above scenarios from past studies as well as data from this study by addressing concepts from flocculation theory (Somasundaran, 2006) and carrying capacity organic matter (Passow 2004; Passow and De La Rocha, 2006). This model, represented in Fig. 4.5, relates the organic matter glue abundance and arrangement to floc, or aggregate, formation mechanisms and robustness. As such Fig. 4.5 represents a theoretical model of how TEP arrangement within an aggregate can affect the sinking velocity and fate of the aggregate as drag forces act on its sinking surface. For a given abundance of TEP, cell density, size, and morphology the association of TEP is varied from dominating the aggregate material to being limited to the cell surface (Fig. 4.5 a-c). Cells entrained in large amorphous clumps of TEP (entrained TEP) can either have negligible sinking rates or be neutral or positively buoyant (Fig. 4.5). Examples of such aggregates have been discussed in Kiørboe et al.

(1998), Azetsu-Scott and Passow (2004), and Azetsu-Scott and Niven (2005). These follow most closely the type of flocculation referred to as network flocculation (Somasundaran, 2006; Fig. 4.5a).

The commonly proposed configuration of TEP in phytoplankton aggregates is free TEP binding together phytoplankton cells (Fig. 4.5b). Many phytoplankton aggregates depicted in previous studies show these types of associations between TEP with cells and other particle debris (Krank and Milligan, 1988; Azam and Long, 2001; Passow, 2002). These aggregates have been described as delicate (Alldredge and Gotschalk, 1989; Alldredge et al., 1990) and require in situ sampling by SCUBA divers. Such aggregates often originate from diatom blooms and relate most closely to charge patch flocculation, which is similar in strength to salt-induced flocculation. The strength of these aggregates lies between that of aggregates created by charge neutralization and bridging flocculation (Somasundaran, 2006 and references therein). As these aggregates settle, shear acts on the downward facing side of the aggregates resulting in deformation, erosion and possible breakup initiated at the bottom aggregate surface (Hill, 1998).

Fig. 4.5c shows another configuration of TEP within a phytoplankton aggregate where cells are coated with TEP forming tightly packed aggregates. In this instance, the surface coating of TEP acts as a bridging flocculant that function like springs between particles reaching beyond the repulsive barrier linking two or more particles together. Depending on the chemical composition of the bridging flocculant, when flexible these polymers move to accommodate pressures due to shear (e.g., up to 10^{-3} s^{-1} at surface when binding particles of 10 μm radius), thus, allowing for the particles to rearrange their configuration leaving the aggregate intact (Somasundaran, 2006 and references therein). Examples of bridging flocculation would include heavily ballasted aggregates typically small and spherical in shape (Hamm, 2002; Passow and De La Rocha, 2006; Engel et al., 2009a; Biermann and Engel, 2010; Iversen and Ploug, 2010). The later have been shown to achieve greater settling velocity rates in rotating tanks (Engel et al., 2009a, Biermann and Engel, 2010; Iversen and Ploug, 2010). Thus, cell-cell binding might yield small aggregates and rapid sedimentation of cells without aggregate break up and resuspension at the density gradient of the mixed layer.

5. Conclusions

Coccolithophores have been shown to be an important species for carbon export (Honjo, 1982; Cadée, 1985; Riemann, 1989; de Wilde et al., 1998). This is the first study to show the coagulation efficiency of a coccolithophore, *Emiliania huxleyi*. We found coagulation efficiency to increase as cell growth rates decreased (i.e., as a bloom progresses). The coagulation efficiencies were in range to those reported in previous studies for diatoms at similar growth stages, despite different laminar shear flow levels used to cause cell collisions.

We found coagulation efficiencies of replicate Couette coagulation experiments to be reproducible when a systematic method was used to assess the cut-off between material smaller than cells and everything larger. Additionally, there was variation in the rate at which cells were lost to the formation of aggregates that was dependent on what the numerical value assigned as the monomer diameter. Thus, reproducibility of the Couette coagulation experiments increased when the change in particle abundance with time, or $slope$, was averaged for the whole monomer peak.

The study revealed Couette coagulation at < 1 s^{-1} caused coccoliths to be sheared from the cell surface. Natural and shear induced loss of coccoliths only occurred for the 2007 experiments using a culture where >99% of the cells were calcifying. The interaction of detached coccoliths in the coagulation of cells was negligible–coccolith abundances were shown to increase during the coagulation experiment instead of decrease. Our findings show that coagulation efficiency for cells at similar growth rates were enhanced by the presence of $CaCO_3$, which we hypothesize is due to Ca^{2+}–a divalent cation shown to be important for promoting chemical associations between CAP polymers as well as organic polymers, in general (de Jong et al., 1979, 1976; Verdugo and Santschi, 2010).

Coagulation efficiency was found to be variable at low growth rates as seen in Kahl et al. (2008) and we propose this was an effect of the type of interaction TEP had with cells, either as free TEP or AB cells. The later yielded higher coagulation efficiencies and we argue using examples from flocculation theory such aggregates would resist disaggregation from shear better than aggregates formed by free TEP gluing cells together and settle at rates faster than cells entrained within large matrices of TEP. Hence, including data on the form of TEP and its association with cells and aggregates along transects of

coccolithophore blooms (from the center to edge or old to new) would increase our ability to predict when and if there will be mass sedimentation of the bloom material.

References

Abramson, L., Lee, C., Liu, Z., Wakeham. S., Szlosek, J., 2010. Exchange between suspended and sinking particles in the northwest Mediterranean as inferred from the organic composition of in situ pump and sediment trap samples. Limnology and Oceanography 55 (2), 725-739.

Alldredge, A.L., Silver, M.W., 1988. Characteristics, dynamics, and significance of marine snow. Progress in Oceanography 20, 41-82.

Alldredge, A.L., Gotschalk, C.C., 1989. Direct observations of the mass flocculation of diatom blooms: characteristics, settling velocities and formation of diatom aggregates. Deep-Sea Research 36, 159-171.

Alldredge, A.L., Granata, T.C., Gotschalk, C.C., Dickey, T.D., 1990. The physical strength of marine snow and its implications for particle disaggregation in the ocean. Limnology and Oceanography 35 (7), 1415-1428.

Alldredge, A.L., McGillivary, P., 1991. The attachment probabilities of marine snow and their implications for particle coagulation in the ocean. Deep-Sea Research 38 (4), 431-443.

Alldredge, A.L., Passow, U., Logan, B.E., 1993. The abundance and significance of a class of large, transparent organic particles in the ocean. Deep-Sea Research 40, 1131-1140.

Aluwihare, L.I., Repeta, D.J., 1999. A comparison of the chemical characteristics of oceanic DOM and extracellular DOM produced by marine algae. Marine Ecology Progress Series 186, 105-117.

Armstrong, R.A., Lee, C., Hedges, J. I., Honjo, S., Wakeham, S., 2002. A new, mechanistic model for organic carbon fluxes in the ocean based on the quantitative association of POC with ballast minerals. Deep-Sea Research II 49, 219-236.

Azam, F., Long, R.A., 2001. Sea snow microcosms. Nature 414, 495-497.

Azetsu-Scott, K., Passow, U., 2004. Ascending marine particles: significance of transparent exopolymer particles (TEP) in the upper ocean. Limnology and Oceanography 49 (3), 741-748.

Azetsu-Scott, K., Nivent, S.E.H., 2005. The role of transparent exopolymer particles (TEP) in the transport of Th-234 in coastal water during a spring bloom. Continental Shelf Research 25 (9), 1133-1141.

Balch, W.M., K.A. Kilpatrick, P.M. Holligan, and T. Cucci, 1993. Coccolith production and detachment by *Emiliania huxleyi*. Journal of Phycology 29 (5), 566-575.

Balch, W.M., Kilpatrick, K., Holligan, P.M., Harbour, D., Fernández, E., 1996. The 1991 coccolithophore bloom in the central north Atlantic. II. Relating optics to coccolith concentration. Limnology and Oceanography 41, 1684-1696.

Balch, W.M., Gordon, H.R., Bowler, C., Drapeau, D.T., Booth, E.S., 2005. Calcium carbonate budgets in the surface global ocean based on MODIS data. Journal of Geophysical Research 110, C07001.

Biermann, A., Engel, A., 2010. Effect of CO_2 on the properties and sinking velocity of aggregates of the coccolithophore *Emiliania huxleyi*. Biogeosciences 7 (3), 1017-1029.

Birkner, F.B., and J.J. Morgan, 1968. Polymer flocculation kinetics of dilute colloidal suspensions. Journal of the American Water Works 60, 175-191.

Borchard, C., Borges, A.V., Händel, N., Engel, A., 2011. Biogeochemical response of *Emiliania huxleyi* (PML B92/11) to elevated CO_2 and temperature under phosphorous limitation: a chemostat study. Journal of Experimental Marine Biology and Ecology 410, 61-71.

Borchard, C., Engel, A., 2012. Organic matter exudation by *Emiliania huxleyi* under simulated future ocean conditions. Biogeosciences Discussions 9, 1199-1236.

Borman, A.H., de Jong, E.W., Huizinga, M., Kok, D.J., Westbroek, P., Bosch, L., 1982. The Role in $CaCO_3$ Crystallization of an Acid Ca^{2+}-Binding Polysaccharide Associated with Coccoliths of *Emiliania huxleyi*. European Journal of Biochemistry 129, 179-183.

Cadée, G.C., 1985. Macroaggregates of *Emiliania huxleyi* in sediment traps. Marine Ecology Progress Series 24, 193-196.

Camp, T.R., and Stein, P.C., 1943. Velocity gradients and internal work in fluid motion. Journal of Boston Society of Civil Engineers 30, 219-237.

Dam, H.G., Drapeau, D.T., 1995. Coagulation efficiency, organic-matter glues and the dynamics of particles during a phytoplankton bloom in a mesocosm study. Deep-Sea Research II 42, 111-123.

De Bodt, C., Van Oostende, N., Harlay, J., Sabbe, K., Chou, L., 2010. Individual and interacting effects of pCO_2 and temperature on *Emiliania huxleyi* calcification: study of the calcite production, the coccolith morphology and the coccosphere size. Biogeosciences 7, 1401-1412.

de Jong, E.W., Bosch, L., Westbroek, P., 1976. Isolation and characterization of Ca^{2+}-binding polysaccharide associated with coccoliths of *Emiliania huxleyi* (Lohmann) Kamptner. European Journal of Biochemistry 70, 611-621.

de Jong, E.W., van Rens, L., Westbroek, P., Bosch, L., 1979. Biocalcification by the marine alga *Emiliania huxleyi* (Lohmann) Kamptner. European Journal of Biochemistry 99, 559-567.

De La Rocha, C.L., Passow, U., 2007. Factors influencing the sinking of POC and the efficiency of the biological carbon pump. Deep-Sea Research II 54, 639-658.

de Wilde, P.A.W.J., Duineveld, G.C.A., Berghuis, E.M., Lavaleye, M.S.S., Kok, A., 1998. Late-summer mass deposition of gelatinous phytodetritus along the slope of the N.W. European Continental Margin. Progress in Oceanography 42, 165-187.

Decho, A.W., 1990. Microbial exopolymer secretions in ocean environments: Their role(s) in food webs and marine processes. Oceanography and Marine Biology Annual Review 28, 73-153.

Donnelly, R.J., 1991. Taylor-Couette flow: The early days. Physics Today 44 (11), 32-39.

Drapeau, D.T., Dam, H.G., Grenier, G., 1994. An improved flocculator design for use in particle aggregation experiments. Limnology and Oceanography 39, 723-729.

Edzwald, J.K., Upchurch, J.B., O'Melia, C.R., 1974. Coagulation in estuaries. Environmental Science and Technology 8, 58-63.

Elimelech, M., Gregory, J., Jia, X., and Williams, R. (Eds.), 1995. Particle deposition and aggregation: measurement, modelling, and simulation. Elsevier, Oxford, pp. 441.

Engel, A., 2000. The role of transparent exopolymer particles (TEP) in the increase in apparent particle stickiness (α) during the decline of a diatom bloom. Journal of Plankton Research 22, 485-497.

Engel, A., Delille, B., Jacquet, S., Riebesell, U., Rochelle-Newall, E., Terbrüggen, A., Zondervan, I., 2004. Transparent exopolymer particles and dissolved organic carbon production by *Emiliania huxleyi* exposed to different CO_2 concentrations: a mesocosm experiment. Aquatic Microbial Ecology 34, 93-104.

Engel, A., Szlosek, J., Abramson, L., Liu, Z., Lee, C., 2009. Investigating the effect of ballasting by $CaCO_3$ in *Emiliania huxleyi*, I: Formation, settling velocities and physical properties of aggregates. Deep-Sea Research II 56, 1396-1407.

Engel, A., Abramson, L., Szlosek, J., Liu, Z., Stewart, G., Hirschberg, D., Lee, C., 2009. Investigating the effect of ballasting by $CaCO_3$ in *Emiliania huxleyi*, II: Decomposition of particulate organic matter. Deep-Sea Research II 56, 1408-1419.

Engel, A., 2009. Determination of Marine Gel Particles. In: Wurl, O. (Ed.), Practical Guidelines for the Analysis of Seawater. CRC Press, Boca Raton, FL, pp. 125-142.

Eppley, R.W., Peterson, B.J., 1979. Particulate organic matter flux and planktonic new production in the deep ocean. Nature 282, 677-680.

Fernández, E., Boyd, P., Holligan, P.M., Harbour, D.S., 1993. Production of organic and inorganic carbon within a large-scale coccolithophore bloom in the northeast Atlantic Ocean. Marine Ecology Progress Series 97, 271-285.

Fichtinger-Schepman, A.M.J., Kamerling, J.P., Vliegenthart, J.F.G., de Jong, E.W., Bosch, L., Westbroek, P., 1979. Composition of a methylated, acidic polysaccharide associated with coccoliths of *Emiliania huxleyi* (Lohmann) Kamptner. Carbohydrate Research 69, 181-189.

Fowler, S.W., Knauer, G.A., 1986. Role of large particles in the transport of elements and organic compounds through the oceanic water column. Progress in Oceanography 16, 147-194.

Fritz, J.J., Balch, W.M., 1996. A light-limited continuous culture study of *Emiliania huxleyi*: determination of coccolith detachment and its relevance to cell sinking. Journal of Experimental Marine Biology and Ecology 207, 127-147.

Fritz, J.J., 1999. Carbon fixation and coccolith detachment in the coccolithophore *Emiliania huxleyi* in nitrate-limited cyclostats. Marine Biology 133, 509-518.

Gibbs, R.J., 1982. Floc stability during Coulter counter analysis. Journal of Sedimentary Petrology 52, 657-660.

Godoi, R.H.M., Aerts, K., Harlay, J., Kaegi, R., Ro, C.-U., Chou, L., Van Grieken, R., 2009. Organic surface coating on coccolithophores - *Emiliania huxleyi*: its determination and implication in the marine carbon cycle. Microchemical Journal 91 (2), 266-271.

Goñi, M.A., Yunker, M.B., Macdonald, R.W., Eglinton, T.I., 2000. Distribution and sources of organic biomarkers in arctic sediments from the Mackenzie River and Beaufort Shelf. Marine Chemistry 71, 23-51.

Grant, H.L., Stewart, R.W., Moilliet, A., 1962. Turbulence spectra from a tidal channel. Journal of Fluid Mechanics 2, 241-268.

Guillard, R.R.L., Ryther, J.H., 1962. Studies of marine planktonic diatoms. Canadian Journal of Microbiololgy 8, 229-239.

Hamm, C.E., 2002. Interactive aggregation and sedimentation of diatoms and clay-sized lithogenic material. Limnology and Oceanography 47 (6), 1790-1795.

Hansen, J.L.S., Timm, U., Kiørboe, T., 1995. Adaptive significance of phytoplankton stickiness with emphasis on the diatom *Skeletonema costatum*. Marine Biology 123,

667-676.

Harlay, J., Borges, A.V., Van Der Zee, C., Delille, B., Godoi, R.H.M., Schiettecatte, L.-S., Roevros, N., Aerts, K., Lapernat, P.-E., Rebreanu, L., Groom, S., Daro, M.-H., Van Grieken, R., Chou, L., 2010. Biogeochemical study of a coccolithophore bloom in the northern Bay of Biscay (NE Atlantic Ocean) in June 2004. Progress in Oceanography 86, 317-336.

Henriksen, K., Stipp, S.L.S., 2009. Controlling biomineralzation: the effect of solution composition on coccolith polysaccharide functionality. Crystal Growth and Design 9, 2088-2097.

Hill, P.S., 1992. Reconciling aggregation theory with observed vertical fluxes following phytoplankton blooms. Journal of Geophysical Research 97, 2295-2308.

Hill, P.S., 1998. Controls on floc size in the sea. Oceanography 11 (2), 13-18.

Hoagland, K., Rosowski, J., Gretz, M., Roemaer, S., 1993. Diatom extracellular polymeric substances: function, fine structure, chemistry, and physiology. Journal of Phycology 29, 537-566.

Holligan, P.M., Viollier, M., Harbour, D.S., Camus, P., Champagne-Philippe, M., 1983. Satellite and ship studies of coccolithophore production along a continental shelf edge. Nature 304, 339-342.

Holligan, P.M., Fernández, E., Aiken, J., Balch, W.M., Boyd, P., Burkill, P.H., Finch, M., Groom, S.B., Malin, G., Muller, K., Purdie, D.A., Robinson, C., Trees, C.C., Turner, S.M., van der Wal, P., 1993. A biogeochemical study of the coccolithophore, *Emiliania huxleyi*, in the North Atlantic. Global Biogeochemical Cycles 7 (4), 879-900.

Honjo, S., 1982. Seasonality and interaction of biogenic and lithogenic particulate flux at the Panama Basin. Science 218, 883-884.

Iversen, M.H., Ploug, H., 2010. Ballast minerals and the sinking of carbon flux in the ocean: carbon-specific respiration rates and sinking velocity of marine snow aggregates. Biogeosciences 7, 2613-2624.

Jackson, G.A., 1990. A model of the formation of marine algal flocs by physical coagulation processes. Deep Sea Research A. 37 (8), 1197-1211.

Jackson, G.A., Lochmann, S., 1993. Modeling coagulation of algae in marine ecosystems. In: Buffle, J. van Leeuwen H.P. (Eds.), Environmental Particles. Lewis Publisher, Ann Arbor, pp. 387-414.

Jackson, G.A., 1995. TEP and coagulation during a mesocosm experiment. Deep-Sea Research II 42, 215-222.

Jackson, G.A., Kiørboe, T., 2008. Maximum phytoplankton concentrations in the sea. Limnology and Oceanography 53 (1), 395-399.

Jin, X., Gruber, N., Dunne, J.P., Sarmiento, J.L., Armstrong, R.A., 2006. Diagnosing the contribution of phytoplankton functional groups to the production and export of particulate organic carbon, $CaCO_3$, and opal from global nutrient and alkalinity distributions. Global Biogeochemical Cycles 20, GB2015.

Kahl, L.A., Vardi, A., Schofield, O., 2008. Effects of phytoplankton physiology on export flux. Marine Ecology Progress Series 354, 3-19.

Kepkay, P.E., 2000. Colloids and the ocean carbon cycle. In: Wangersky, P. (Ed.), The Handbook of Environmental Chemistry. SpringerVerlag, Berlin/Heidelberg, Heidelberg, pp. 35-56.

Kiørboe, T., Andersen, K.P., Dam, H.G., 1990. Coagulation efficiency and aggregate formation in marine phytoplankton. Marine Biology 107, 235-245.

Kiørboe, T., Hansen, J.L.S., 1993. Phytoplankton aggregate formation: observations of patterns and mechanisms of cell sticking and the significance of exopolymeric material. Journal of Plankton Research 15, 993-1018.

Kiørboe, T., Lundsgaard, C., Olsen, M., Hansen, J.L.S., 1994. Aggregation and sedimentation process during a spring phytoplankton bloom: a field experiment to test coagulation theory. Journal of Marine Research 52, 197-323.

Kiørboe, T., Tiselius, P., Mitchell-Innes, B., Hansen, J.L.S., Visser, A.W., Mari, X., 1998. Intensive aggregate formation with low vertical flux during an upwelling-induced diatom bloom. Limnology and Oceanography 43 (1), 104-116.

Klaas, C., Archer, D.E., 2002. Association of sinking organic matter with various types of mineral ballast in the deep sea: Implications for the rain ratio. Global Biogeochemical Cycles 16, 1116.

Koch, S., 2007. Growth and calcification of the coccolithophore *Emiliania huxleyi* under different CO_2 concentrations, Institut für Chemie und Biologie des Meeres der Carl von Ossietzky Universität, Oldenburg, Germany.

Kok, D.J., Blomen, L.J.M.J., Westbroek, P., Bijvoet, O.L.M., 1986. Polysaccharide from coccoliths ($CaCO_3$ biomineral): influence on cyrstallization of calcium oxalate monohydrate. European Journal of Biochemistry 158, 167-172.

Kranck, K., Milligan, T.G., 1988. Macroflocs from diatoms: in situ photography of particles in Bedford Basin, Nova Scotia. Marine Ecology Progress Series 44, 183-189.

Kriest, I., Evans, G.T., 1999. Representing phytoplankton aggregates in biogeochemical

models. Deep-Sea Research II 46, 1841-1859.

Leppard, G.G., 1995. The characterization of algal and microbial mucilage and their aggregates in aquatic ecosystems. Science of the Total Environment 165, 103-131.

Linschooten, C., van Bleijswijk, J.D.L., van Emberg, P.R., de Vrind, J.P.M., Kempers, E.S., Westbroek, P., de Vrind-de Jong, E.W., 1991. Role of the light-dark cycle and medium composition on the production of coccoliths by *Emiliania huxleyi* (Haptophyceae). Journal of Phycology 27, 82-86.

Logan, B.E., Grossart, H.-P., Simon, M., 1994. Direct observation of phytoplankton, TEP, and aggregates on polycarbonate filters using brightfield microscopy. Journal of Plankton Research 16 (12), 1811-1815.

Logan, B.E., Passow, U., Alldredge, A.L., Grossart, H.-P., Simon, M., 1995. Rapid formation and sedimentation of large aggregates is predictable from coagulation rates (half-lives) of transparent exopolymer particles (TEP). Deep-Sea Research II 42, 203-214.

Martin, J.H., Knauer, G.A., Karl, D.M., Broenkow, W.W., 1987. VERTEX: Carbon cycling in the northeast Pacific. Deep-Sea Research 34, 267-285.

McCave, I.N., 1984. Size spectra and aggregation of suspended particles in the deep ocean. Deep-Sea Research 31 (4), 329-352.

McCave, I.N., Hall, I.R., Antia, A.N., Chou, L., Dehairs, F., Lampitt, R.S., Thomsen, L., van Weering, T.C.E., Wollast, R., 2001. Distribution, composition and flux of particulate material over the European margin at 47˚-50˚N. Deep-Sea Research II 48, 3107-3139.

Mopper, K., Zhou, J., Ramana, K.S., Passow, U., Dam, H.G., Drapeau, D.T., 1995. The role of surface-active carbohydrates in the flocculation of a diatom bloom in a mesocosm. Deep-Sea Research II 41, 47-73.

Müller, M.N., Antia, A.N., LaRoche, J., 2008. Influence of cell cycle phase on calcification in the coccolithophore *Emiliania huxleyi*. Limnology and Oceanography 53 (2), 506-512.

Myklestad, S.M., 1995. Release of extracellular products by phytoplankton with special emphasis on polysaccharides. Science of the Total Environment 165, 155-164.

Obernosterer, I., Herndl, G.J., 1995. Phytoplankton extracellular release and bacterial growth: dependence on the inorganic N:P ratio. Marine Ecology Progress Series 116, 247-257.

Paasche, E., 1998. Roles of nitrogen and phosphorus in coccolith formation in *Emiliania huxleyi* (Prymnesiophyceae). European Journal of Phycology 33, 33-42.

Paasche, E., 2002. A review of the coccolithophorid *Emiliania huxleyi* (Prymnesiophyceae), with particular reference to growth, coccolith formation, and calcification–photosynthesis interactions. Phycologia 40, 503-529.

Panagiotopoulos, C., Sempéré, R., Lafont, R., Kerhervé, P., 2001. Sub-ambient temperature effects on separation of monosaccharides by HPAEC-PAD. Application to marine chemistry. Journal of Chromatography A 920, 13-22.

Passow, U., Alldredge, A.L., 1994. Distribution, size and bacterial colonization of transparent exopolymer particles (TEP) in the ocean. Marine Ecology Progress Series 113, 185-198.

Passow, U., Alldredge, A.L., 1994. Distribution, size and bacterial colonization of transparent exopolymner particles (TEP) in the ocean. Marine Ecology Progress Series 133, 185-198.

Passow, U., Alldredge, A.L., 1995a. Aggregation of a diatom bloom in a mesocosm: The role of transparent exopolymer particles (TEP). Deep-Sea Research II 42 (1), 99-109.

Passow, U., Alldredge, A.L., 1995b. A dye-binding assay for the spectrophotometric measurement of transparent exopolymer particles (TEP). Limnology and Oceanography 40, 1326-1335.

Passow, U., 2002. Transparent exopolymer particles (TEP) in aquatic environments. Progress in Oceanography 55, 287-333.

Passow, U., 2004. Switching perspectives: do mineral fluxes determine particulate organic carbon fluxes or vice versa? Geochemistry Geophysics Geosystems 5, Q04002.

Passow, U., De La Rocha, C.L., 2006. Accumulation of mineral ballast on organic aggregates. Global Biogeochemical Cycles 20, GB1013.

Penna, A., Berluti, S., Magnani, M., 1999. Influence of nutrient ratios on the *in vitro* extracellular polysaccharide production by marine diatoms from the Adriatic Sea. Journal of Plankton Research 21, 1681-1690.

Pitcher, G.C., Walker, D.R., Mitchell-Innes, B.A., Moloney, C.L., 1991. Short-term variability during an Anchor station study in the southern Benguela upwelling system: phytoplankton dynamics. Progress in Oceanography 28, 39-64.

Pruppacher, H.R., Klett, J.D. (Eds.), 1980. Microphysics of Clouds and Preciptation. D. Riedel Publishing Co., Boston, pp. 734.

Riegman, R., Stolte, W., Noordeloos, A.A.M., Slezak, D., 2000. Nutrient uptake and alkaline phosphatase (ec 3:1:3:1) activity of *Emiliania huxleyi* (PRYMNESIOPHYCEAE) during

growth under N and P limitation in continuous cultures. Journal of Phycology 36, 87-96.

Riemann, F., 1989. Gelatinous phytoplankton detritus aggregates on the Atlantic deep-sea bed: Structure and mode of formation. Marine Biology 100, 533-539.

Sheridan, C.C., Lee, C., Wakeham, S.G., Bishop, J.K.B., 2002. Suspended particle organic composition and cycling in surface and midwaters of the equatorial Pacific Ocean. Deep-Sea Research I 49, 1983-2008.

Smetacek, V., Pollehne, F., 1986. Nutrient cycling in pelagic systems: a reappraisal of the conceptual framework. Ophelia 26, 401-428.

Soloviev, A.V., Vershinsky, N.V., Bezverchnii, V.A., 1988. Small scale turbulence measurements in the thin surface layer of the ocean. Deep-Sea Research 35, 1859-1874.

Somasundaran, P., 2006. Encyclopedia of Surface and Colloid Science. vol. 6, CRC: Taylor & Francis Group, New York, pp. 6675.

Staats, N., Stal, L.J., Mur, L.R. , 2000. Exopolysaccharide production by the epipelic diatom *Cylindrotheca closterium*: effects of nutrient conditions. Journal of Experimental Marine Biology and Ecology 249, 13-27.

Stemmann, L., Gorsky, G., Marty, J.-C., Picheral, M., Miquel, J.-C., 2002. Four-year study of large-particle vertical distribution (0-1000m) in the NW Mediterranean in relation to hydrology, phytoplankton, and vertical flux. Deep-Sea Research II 49 (11), 2143-2162.

van der Wal, P., de Jong, E.W., Westbroek, P., de Bruijn, W.C., Mulder-Stapel, A.A., 1983. Ultrastructural polysaccharide localization in calcifying and naked cells of the coccolithophorid *Emiliania huxleyi*. Protoplasma 118, 157-168.

van Duuren, F.A., 1968. Defined velocity gradient model flocculator. Journal of the Sanitary Engineering Division: Proceedings of the American Society of Civil Engineers 94, 671-682.

Verdugo, P., Alldredge, A.L., Azam, F., Kirchman, D.L., Passow, U., Santschi, P.H., 2004. The oceanic gel phase: a bridge in the DOM-POM continuum. Marine Chemistry 92, 67-85.

Verdugo, P., Santschi, P.H., 2010. Polymer dynamics of DOC networks and gel formation in seawater. Deep-Sea Research II 57, 1486-1493.

Vieira, A.A.H., Ortolano, P. I. C., Giroldo, D., Oliveira, M. J. D., Bittar, T. B., Lombardi, A. T., Sartori, A. L., Paulsen, B. S., 2008. Role of hydrophobic extracellular polysaccharide

of *Aulacoseira granulata* (Bacillariophyceae) on aggregate formation in a turbulent and hypereutrophic reservoir. Limnology and Oceanography 53, 1887-1899.

Weilenmann, U., O'Melia, C.R., Stumm, W., 1989. Particle transport in lakes: models and measurements. Limnology and Oceanography 34, 1-18.

Xue, J., Lee, C., Wakeham, S.G., Armstrong, R.A., 2011. Using principal components analysis (PCA) with cluster analysis to study the organic geochemistry of sinking particles in the ocean. Organic Geochemistry 42 (4), 356-367.

Table 4.1. Biogeochemical properties of chemostat experiment day

Experiment Year	Growth Rate (d^{-1})	Experiment Day	Total N ($\mu mol\ l^{-1}$)	Total P ($\mu mol\ l^{-1}$)	Chlorophyll-*a* ($\mu mol\ l^{-1}$)	PIC/POC ($\mu M/\mu M$)	Total Alkalinity at 31.5 PSU ($\mu mol\ kg^{-1}$)	Cells $\times 10^5$ ($\#\ ml^{-1}$)
2006	0.25 ± 0.02	26	0.84 ± 0.20	0.00	n.s.	0.21	2128 ± 83	4.59
	0.05 ± 0.10	34	0.75 ± 0.01	0.00	n.s.	0.53	1592 ± 74	2.90
	0.05 ± 0.03	40	0.67 ± 0.02	0.00	n.s.	0.63	1296 ± 122	2.63
2007	0.63 ± 0.03	10	0.74	0.00	0.022 ± 0.000	0.43 ± 0.39	1815	2.04
	0.35 ± 0.00	14	0.52	0.00	0.015 ± 0.001	0.15 ± 0.04	1424	2.86
	0.03 ± 0.00	22	0.70	0.00	0.010 ± 0.001	0.17 ± 0.11	1045	2.88
	0.12 ± 0.08	25	0.31	0.00	0.011 ± 0.000	0.16 ± 0.20	1095	3.12

n.s.- not sampled

Table 4.1. Biogeochemical properties of chemostat on experiment days including total N (nitrate, nitrite, and ammonia), total P (phosphate), chlorophyll-*a*, PIC/POC, total alkalinity, and cell number per milliliter. Chlorophyll-*a* data was not determined in 2006. Data from Koch (2007) and Borchard et al. (2011).

Table 4.2. Results for 2006 and 2007 TEP_{color}, TEP_{micro}, Coulter Counter particles (CCP) and TEP particle volume fractions (Φ)

Sample ID	Cell Corrected TEP			TEP_{micro} fractions			
	TEP_{color} (μg XG eq l^{-1})	TEP_{color} per cell (pg XG eq $cell^{-1}$)	TEP_{micro} Φ† (ppm)	CCP Φ (ppm)	Total Vol. Conc. TEP_{micro} (ppm)	Vol. Conc. of coccoliths (ppm)	Vol. Conc. of AB stained cells (ppm)	Vol. Conc. of aggregates (ppm)
2006								
day 26, 0.25 ± 0.02								
chemostat	130 ± 580	0.29	n.s.	22.9	n.s.	n.s.	n.s.	n.s.
A final	175 ± 397	0.45	3.3	22.8	"	"	"	"
B final	925 ± 513	2.23	"	24.1	"	"	"	"
C final	250 ± 380	0.63	"	21.8	"	"	"	"
day 34, 0.05 ± 0.10								
chemostat	856 ± 373	2.14	n.s.	23.8	n.s.	n.s.	n.s.	n.s.
A final	792 ± 602	1.97	4.1	23.0	"	"	"	"
C final	820 ± 530	2.08	"	22.9	"	"	"	"
day 40, 0.05 ± 0.03								
chemostat	1161 ± 500	2.79	n.s.	19.8	n.s.	n.s.	n.s.	n.s.
A final	295 ± 259	0.80	5.9	18.6	"	"	"	"
C final	290 ± 847	0.76	6.4	18.5	"	"	"	"
2007								
day 10, 0.63 ± 0.03								
chemostat	b.d.	b.d.	n.s.	26.2	n.s.	n.s.	n.s.	n.s.
C final	"	"	0.19 ± 0.08	25.4	0.22 ± 0.08	0.002 ± 0.0001	0.03 ± 0.00	0.15 ± 0.08
D final	"	"	0.28 ± 0.00	29.8	0.32 ± 0.01	0.002 ± 0.0005	0.03 ± 0.01	0.23 ± 0.01
day 14, 0.35 ± 0.00								
chemostat	126 ± 115	0.44	n.s.	62.0	n.s.	n.s.	n.s.	n.s.
C final	b.d.	b.d.	0.20 ± 0.01	28.0	0.31 ± 0.03	0.01 ± 0.001	0.10 ± 0.04	0.12 ± 0.02
D final	"	"	0.17 ± 0.00	28.1	0.26 ± 0.05	0.01 ± 0.001	0.07 ± 0.05	0.11 ± 0.00
day 22, 0.03 ± 0.00								
chemostat	556 ± 197	1.93	n.s.	39.2	n.s.	n.s.	n.s.	n.s.
C final	181 ± 167	0.63	0.73 ± 0.14	21.4	0.78 ± 0.16	0.01 ± 0.005	0.03 ± 0.01	0.64 0.12
D final	76 ± 172	0.25	1.00 ± 0.49	21.7	1.04 ± 0.52	0.01 ± 0.003	0.02 ± 0.02	0.91 0.43

continued

Table 4.2., *2007 continued*

Sample ID	Cell Corrected TEP			TEP_{micro} fractions			
	TEP_{color} (µg XG eq l^{-1})	TEP_{color} per cell (pg XG eq $cell^{-1}$)	TEP_{micro}-Φ† (ppm)	CCP Φ (ppm)	Total Vol. Conc. TEP_{micro} (ppm)	Vol. Conc. of coccoliths (ppm)	Vol. Conc. of AB stained cells (ppm)	Vol. Conc. of aggregates (ppm)
day 25, 0.12 ± 0.08								
chemostat	717 ± 324	2.30	n.s.	24.8	n.s.	n.s.	n.s.	n.s.
C final	825 ± 182	3.17	0.75 ± 0.05	19.8	0.91 ± 0.07	0.04 ± 0.005	0.07 ± 0.01	0.51 ± 0.04
D final	751 ± 239	2.92	2.43 ± 0.75	19.8	2.53 ± 0.71	0.02 ± 0.009	0.03 ± 0.02	2.24 ± 0.79

n.s. – not sampled

b.d. – below detection; negative corrected TEP and TEP per cell values indicate <100% of cells were coated with Alcian blue, no excess TEP was detected

†2006 TEP Φ values are over estimates (~10×) due to calculating volumes assuming ellipsoid geometry instead of spherical geometry.

Table 4.2. Results for 2006 and 2007 transparent exopolymer particles (TEP) measurements of samples taken for colorimetric (TEP_{color}) and microscope (TEP_{micro}) techniques and Coulter Counter particles (CCP) particle volume fraction (Φ). Standard deviation of measurements in parentheses. TEP_{color}, TEP_{color} per cell, and TEP volume fraction (TEP-Φ) were corrected for Alcian blue (AB) adsorption to cell surface (see Methods). TEP-Φ values from 2006 assumed particles had ellipsoid geometry instead of standard method of assuming spherical geometry (after Engel, 2009). TEP-Φ values from 2007 assume spherical geometry of particles (methods after Engel, 2009). TEP-Φ uses microscope samples and excludes coccoliths (<3 µm) and cells (AB stained cells). Image analysis of TEP_{micro} samples used to determine particle volume concentrations of Alcian blue stained material of different sizes: coccoliths (diameter <3 µm), cells (diameter 3–7 µm), aggregates (diameter >7 µm), and total sample.

Table 4.3. Coagulation efficiency (α) values

Experiment Year	Growth Rate (d^{-1})	Experiment Day	Couette flow device ID	$\alpha(x=2\ \mu m)$ Kiørboe et al., 1990	$\alpha(x^*_{cut})$ Kiørboe et al., 1990	$\alpha_{complete}$ Kiørboe et al., 1990	α' Engel 2000
2006	0.25 ± 0.02	26	A	0.23	0.23	0.23	0.20
			B	0.19	0.19	0.30	0.26
			C	0.28	0.28	0.28	0.24
	0.05 ± 0.10	34	A	0.11	0.17	0.36	0.31
			C	0.13	0.18	0.36	0.30
	0.05 ± 0.03	40	A	0.36	0.58	0.98	0.75
			C	0.54	0.97	1.35	1.01
2007	0.63 ± 0.03	10	C	0.13	0.14	0.42	0.41
			D	0.17	0.17	0.40	0.40
	0.35 ± 0.00	14	C	0.11	0.24	0.59	0.58
			D	0.18	0.36	0.55	0.55
	0.03 ± 0.00	22	C	-0.45	0.24	0.84	0.81
			D	-0.65	0.24	0.70	0.67
	0.12 ± 0.08	25	C	-0.81	0.08	1.19	1.15
			D	-0.99	0.09	0.36	0.32

Table 4.3. Coagulation efficiency (α) values calculated after methods of Kiørboe et al. (1990) and Engel (2000). α_{var} determined using Eq. 5 with cut-off values of 2 μm and x^*_{cut}. $\alpha_{complete}$ is an average of α over the monomer peak calculated using Eq. 6. α' values take into account TEP-Φ.

Table 4.4. 2007 Cell diameters and detached coccolith estimates

Growth Rate (d^{-1})	Experiment day	Couette flow device ID	Coulter Counter estimated cell Ø (µm)	Relative No. of detached coccoliths per cell†	detached / attached coccoliths§
0.63 ± 0.03	10	C	5.49	NA	NA
		D	5.49	NA	NA
0.35 ± 0.00	14	C	5.28	1.0	0.17
		D	5.21	1.0	0.23
0.03 ± 0.00	22	C	5.00	2.3	0.49
		D	5.14	2.4	0.28
0.12 ± 0.08	25	C	5.21	0.8	0.23
		D	5.28	1.0	0.17

NA – Not Applicable

Table 4.4. Cell diameter (Ø) estimate is the diameter of the Coulter Counter cell peak at time point when aggregation starts; relative number of detached coccoliths per cell, and number of coccolith layers per cell and detached/attached ratio of coccoliths calculated using methods of Fritz et al. (1996). Cells from experiment day 10 assumed to show little to no loss of coccoliths prior to coagulation experiment. †Detached coccoliths normalized to the number lost on experiment day 14 (mean, 7.2 coccoliths per cell). §Details of calculations found in Appendix (Appendix Table 4.A1).

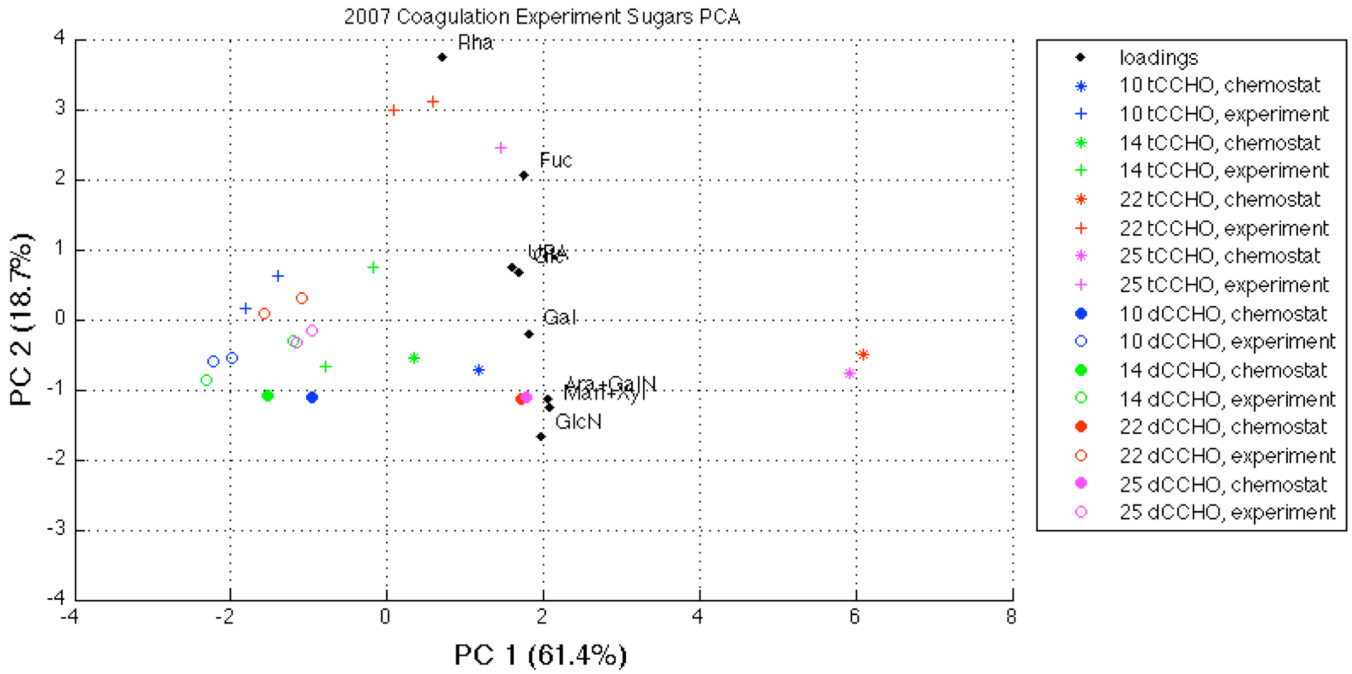

Figure 4.1. Principal components analysis on the 2007 sugar composition data. Variable loadings is scaled up 5x and plotted with sample site scores on the PC1 and PC2 axes. Experiment days are distinguished by color (blue, day 10; green, day 14; red, day 22; magenta, day 25). Sample and size fractions are distinguished by symbol (*, chemostat tCCHO; +, coagulation experiment tCCHO; filled circle, chemostat <0.45 μm-HMW-dCCHO; open circle, coagulation experiment <0.45 μm-HMW-dCCHO).

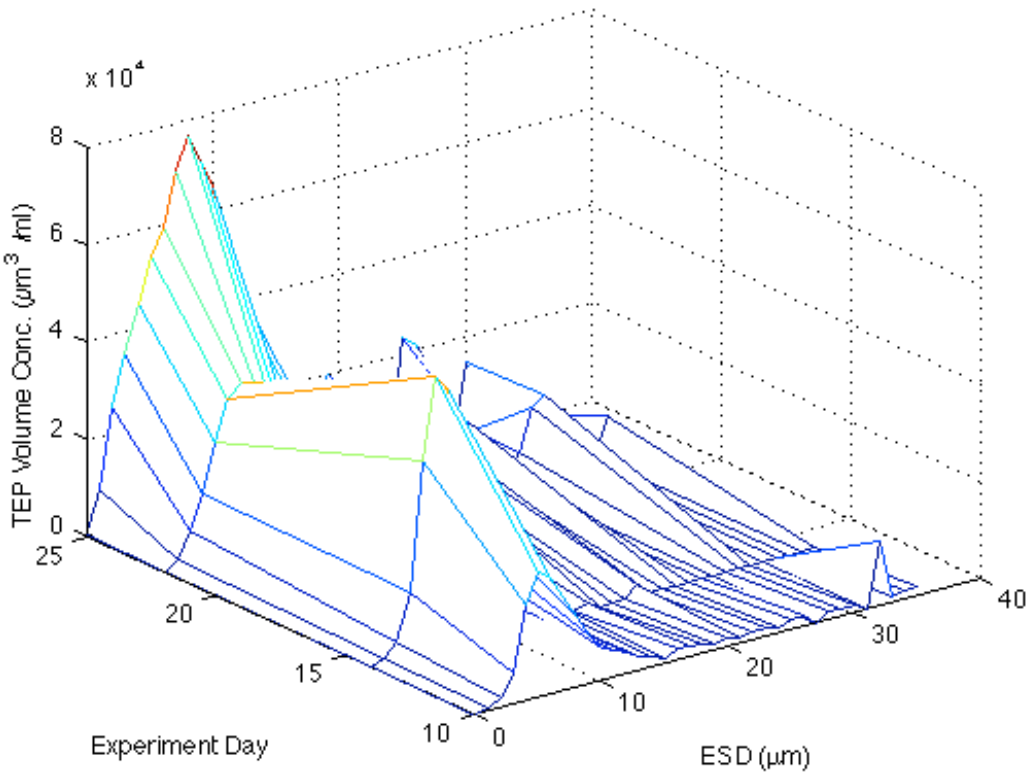

Figure 4.2. Variation in experiment day of 2007 TEP_{micro} volume concentration ($\mu m^3\ ml^{-1} \times 10^4$) for each size class as equivalent spherical diameter (ESD) in 1 µm increments. TEP volume concentration was determined assuming spherical geometry according to Engel, 2009.

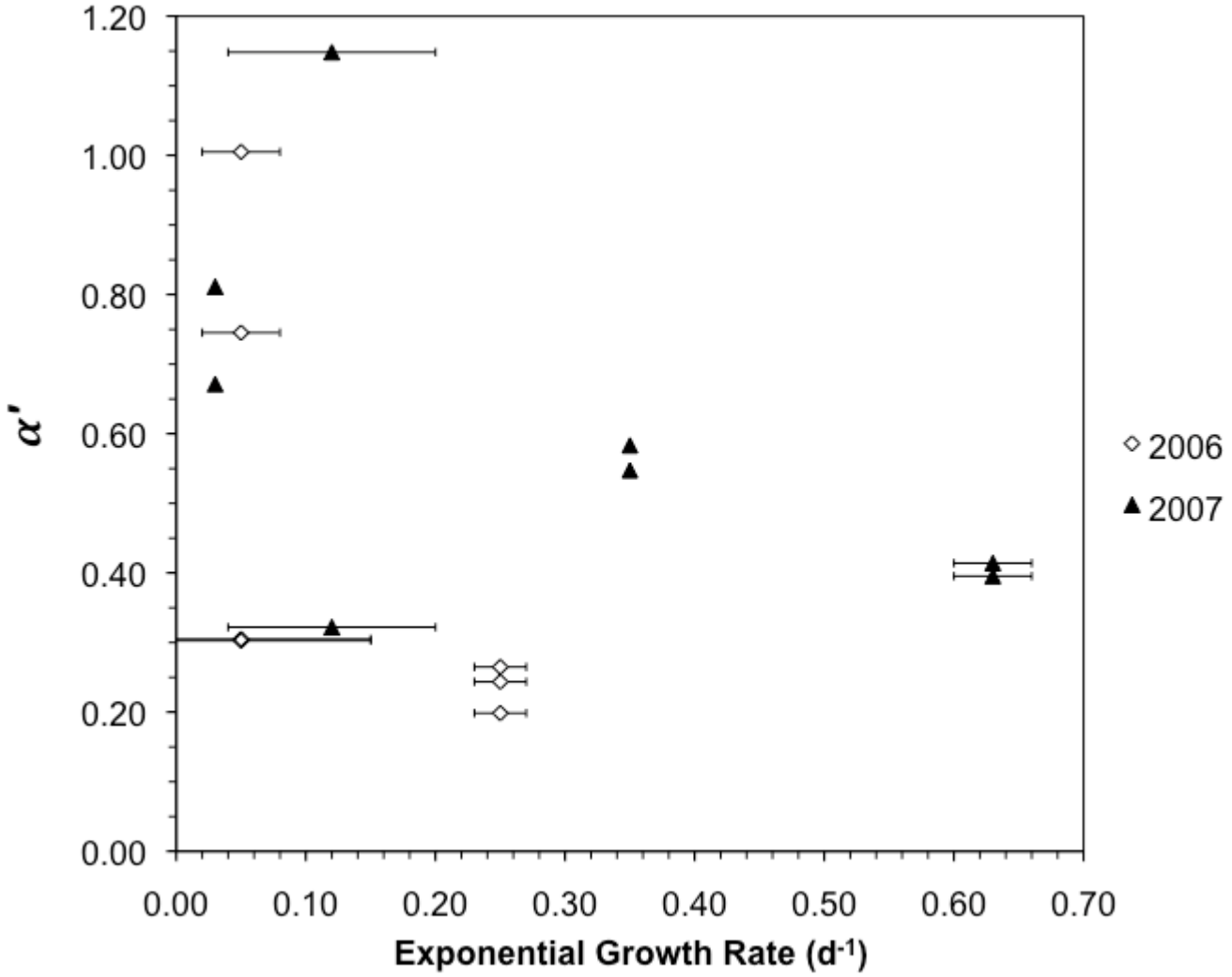
1.20
1.00
0.80
0.60
0.40
0.20
0.00
α'
0.00
0.10
0.20
0.30
0.40
0.50
0.60
0.70
Exponential Growth Rate (d-1)
2006
2007

Figure 4.3. α vs. Growth Rate for 2006 and 2007 *E. huxleyi* chemostat coagulation experiments. Coagulation efficiency represented as TEP corrected α complete, α' (Eq. 7). Open diamonds represent 2006 samples. Closed triangles represent 2007 samples. Error bars indicate standard deviation of the exponential growth rates. In comparison with the coagulation experiment performed on Couette flow device C on 2007, day 25 the experiment performed on Couette flow device D had a low *slope* (~3× lower) and low R^2 (0.78 versus 0.90) fit to the *slope*. Excluding this sample, α for both years appears have a 2-phased trend where it increases with growth rate up to a point (~0.1 d^{-1}) and then increases dramatically and replicate coagulation experiments are more variable.

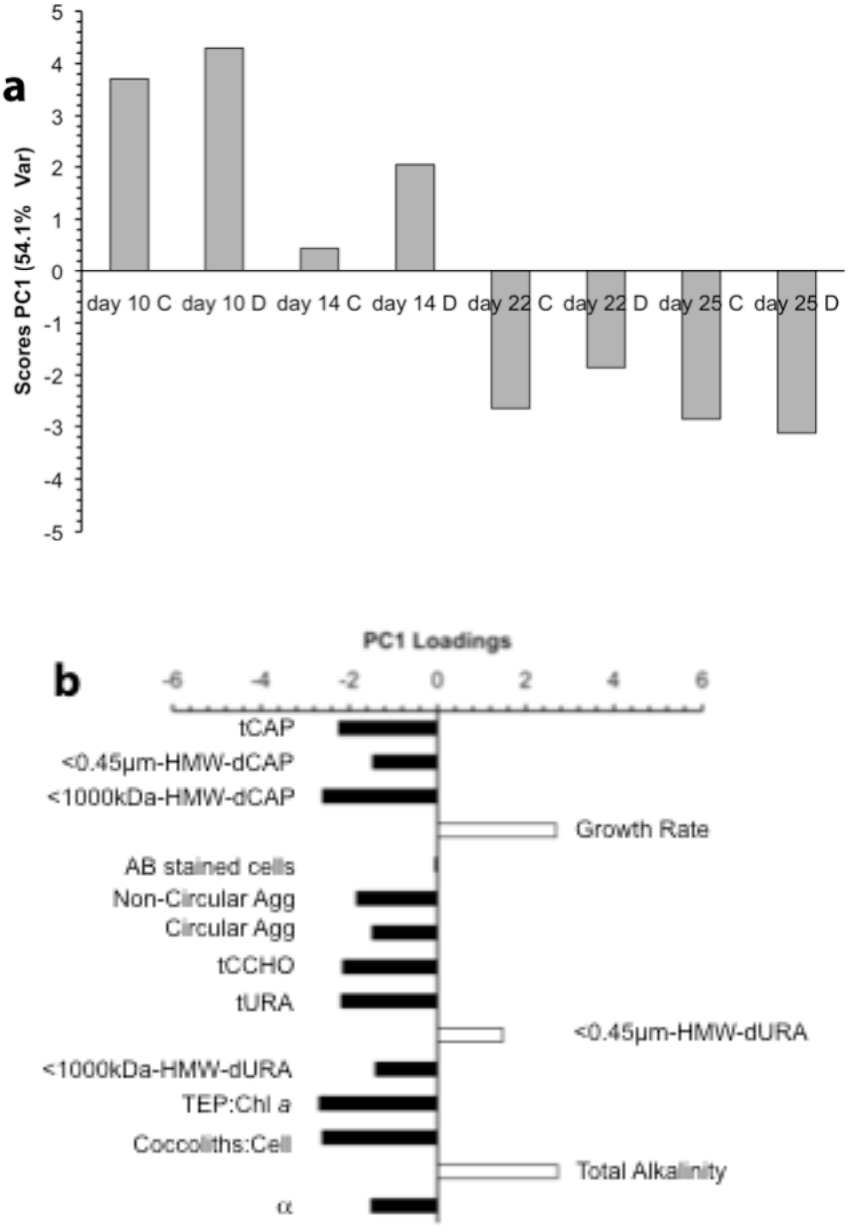
a
Scores PC1 (54.1% Var)
5
4
3
2
1
0
-1
-2
-3
-4
-5
day 10 C
day 10 D
day 14 C
day 14 D
day 22 C
day 22 D
day 25 C
day 25 D
b
PC1 Loadings
-6
-4
-2
0
2
4
6
tCAP
<0.45µm-HMW-dCAP
<1000kDa-HMW-dCAP
Growth Rate
AB stained cells
Non-Circular Agg
Circular Agg
tCCHO
tURA
<0.45µm-HMW-dURA
<1000kDa-HMW-dURA
TEP:Chl a
Coccoliths:Cell
Total Alkalinity
α

Figure 4.4a–b. 2007 principal components analysis of parameters related to aggregation: (a) PC1 site scores and (b) PC1 variable loadings. Parameters include: total coccolith acidic polylsaccharides (tCAP); <0.45 μm high molecular weight dissolved coccolith acidic polysaccharides (<0.45 μm-HMW-dCAP); <1000 kDa high molecular weight dissolved coccolith acidic polysaccharides (<1000 kDa-HMW-dCAP); growth rate; Alcian blue (AB) stained cells; non-circular aggregates; circular aggregates; total combined carbohydrates (tCCHO); total uronic acids (tURA); <0.45 μm high molecular weight dissolved uronic acids (<0.45 μm-HMW-dURA); <1000 kDa high molecular weight dissolved uronic acids (<1000 kDa-HMW-dURA); TEP to chlorophyll-*a* ratio (TEP:Chl-*a*); detached coccoliths per cell (Coccoliths:Cell); total alkalinity; and α.

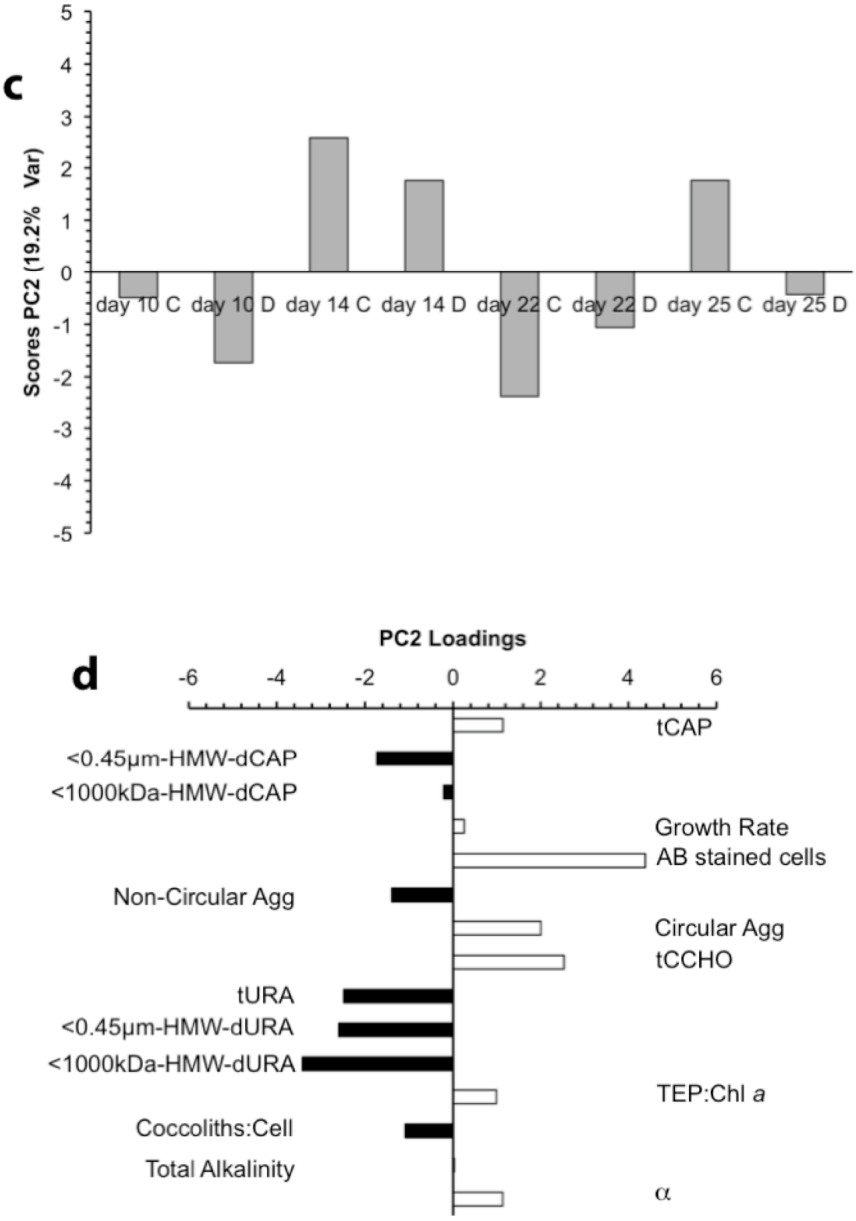
c
Scores PC2 (19.2% Var)
5
4
3
2
1
0
-1
-2
-3
-4
-5
day 10 C
day 10 D
day 14 C
day 14 D
day 22 C
day 22 D
day 25 C
day 25 D
d
PC2 Loadings
-6
-4
-2
0
2
4
6
tCAP
<0.45µm-HMW-dCAP
<1000kDa-HMW-dCAP
Growth Rate
AB stained cells
Non-Circular Agg
Circular Agg
tCCHO
tURA
<0.45µm-HMW-dURA
<1000kDa-HMW-dURA
TEP:Chl a
Coccoliths:Cell
Total Alkalinity
α

Figure 4.4c–d. 2007 principal components analysis of parameters related to aggregation: (c) PC2 site scores;and (d) PC2 variable loadings. Parameters include: total coccolith acidic polylsaccharides (tCAP); <0.45 μm high molecular weight dissolved coccolith acidic polysaccharides (<0.45 μm-HMW-dCAP); <1000 kDa high molecular weight dissolved coccolith acidic polysaccharides (<1000 kDa-HMW-dCAP); growth rate; Alcian blue (AB) stained cells; non-circular aggregates; circular aggregates; total combined carbohydrates (tCCHO); total uronic acids (tURA); <0.45 μm high molecular weight dissolved uronic acids (<0.45 μm-HMW-dURA); <1000 kDa high molecular weight dissolved uronic acids (<1000 kDa-HMW-dURA); TEP to chlorophyll-*a* ratio (TEP:Chl-*a*); detached coccoliths per cell (Coccoliths:Cell); total alkalinity; and α.

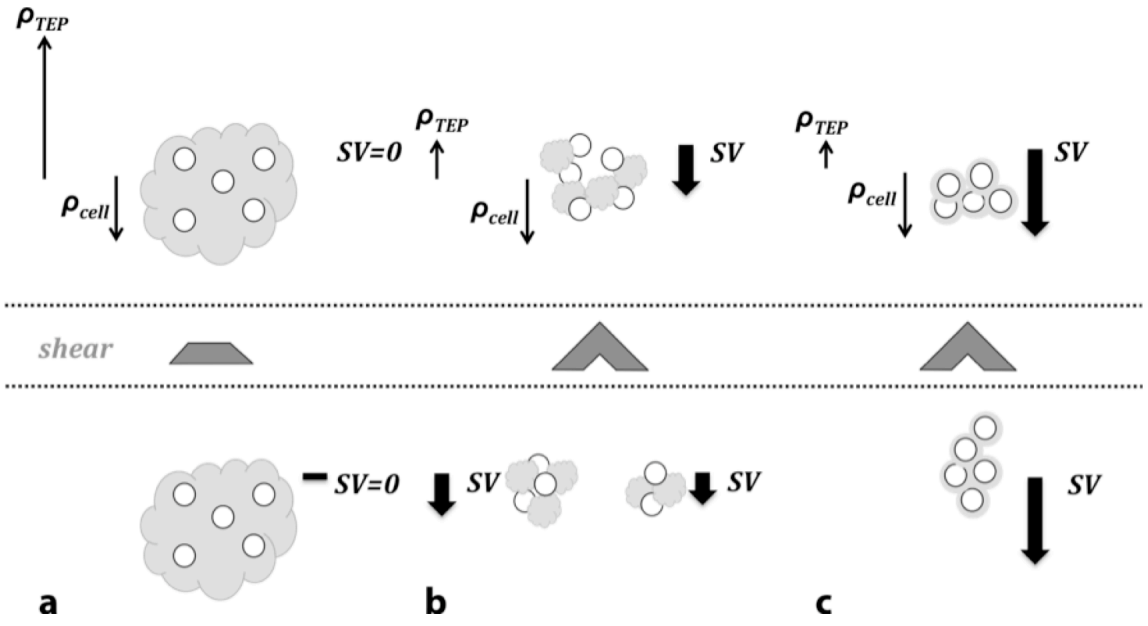

Figure 4.5. Theoretical schematic showing TEP interaction with cells in flocs and resultant effect on settling velocity for (a) largely consisting of TEP; (b) "enclosed" TEP and cells; and (c) AB cells. The result of excess density of aggregates (ρ) with respect to water density indicated with upwards (buoyant) or downwards (sinking) arrows. Magnitude of shear indicated by size of the filled in carrot symbol. The effect of the shear acting on the aggregate is illustrated at the bottom of each figure. Resultant effect of shear on settling velocity (SV) of aggregate indicated with filled in arrows.

CHAPTER 5
Conclusions

1. Summary and Implications of Major Findings

This dissertation investigates two parameters important for estimating and predicting organic matter export from the surface ocean: controls on the POC/^{234}Th of marine particles and the coagulation efficiency of algal cells. Specifically, the sources of variability in POC/^{234}Th and coagulation efficiency of *Emiliania huxleyi* are studied. The research explores two methods commonly employed– the ^{234}Th-proxy method for estimating POC flux, and Couette flow device experiments for experimentally deriving coagulation efficiency values.

Chapter 2 investigates the sources of variability in the POC/^{234}Th ratio of sinking particles collected by sediment traps in the northwest Mediterranean Sea. The use of sediment traps operating in time series and settling velocity modes provided unique context for the observed POC/^{234}Th ratios allowing associations to be made between POC/^{234}Th magnitude and marine particle source, biogeochemical processes, and particle dynamics. Assuming a linear relationship between particle settling velocity and size (Alldredge and Gotschalk, 1989), this study provides evidence that marine particle source (e.g., phytoplankton aggregates, zooplankton fecal pellets, degraded biogenic material) has a stronger influence on the POC/^{234}Th than the particle size, where POC/^{234}Th ratio scales with particle volume/surface area ratio (Buesseler et al., 2006). POC/^{234}Th ratios of particles separated into 11 settling velocity classes ranging from 0.7 to >980 m d^{-1} were within 30% of one another in spring of 2003 and 2005. Recent studies have documented nearly constant POC/^{234}Th for filtered particles of different particle sizes (Buesseler et al., 2006; Waite and Hill, 2006; Speicher et al., 2006; Brew et al., 2009). As reasoning, these studies cite models that show size invariant POC/^{234}Th of phytoplankton aggregates as they move up the particle size spectrum (Burd et al., 2007). The results of this dissertation suggest an alternative explanation for the lack of variability in POC/^{234}Th with particle

settling velocity (i.e., size) observed in this study: the different sources of material in slower and faster settling particles result in similarly low POC/^{234}Th due to more rapid carbon degradation of material in slower settling velocity classes and more rapid carbon assimilation of material in faster settling velocity classes. We observed that material from slower settling particle classes (<98 m d^{-1}) contained proportionally more indicators of bacterially reworked material than the faster settling velocity classes and both contained biomarkers indicative of zooplankton fecal pellets (Wakeham et al., 2009 and this study). Additionally, the results of this dissertation suggest that with depth, disaggregation of rapidly settling particles occurs and subsequently supplies material to the slower settling particle pool, thus diminishing variability in POC/^{234}Th with settling velocity.

In 2005, settling velocity traps were deployed at several depths. The mean POC/^{234}Th decreased over a factor of ~3 between 313 and 1918 m due to a factor of ~2 decrease in mean POC and a ~1.3 increase in mean ^{234}Th. A surprising outcome of the settling velocity data with depth was to learn that ^{234}Th of settling velocity classes <49 m d^{-1} remained constant from 313 to 1918 m and increased in the faster settling particles (98-980 m d^{-1}) between 524 to 1918 m. Unlike the conclusions of Cai et al. (2006), the decay of ^{234}Th was not detectable despite the 28–1991 days needed for particles settling at rates <49 m d^{-1} to transit the distance between 524 and 1918 m. Either 1) the decay was perfectly balanced by additional scavenging of ^{234}Th onto the slowly settling particle classes or 2) a portion of the fast settling particles disaggregated, injecting ^{234}Th into slowly settling particle class material at depth. Continued scavenging of ^{234}Th by the faster settling particles may also have occurred. We observed an increase in ^{234}Th with depth for the 5 settling velocity classes ranging from 98 to 980 m d^{-1}. Although DYFAMED has been considered an open ocean site (Andersen and Prieur, 2000) an increase in lithogenics, opal (Lee et al., 2009) and bulk mass (Martín et al., 2009) have been observed in deep water. Bulk mass of fast settling particles within the deep trap were slightly lower than at 524 m; however, an increase in the pseudo-K_ds of lithogenic material and opal for the deep trap may indicate the possibility of adsorption of ^{234}Th onto resuspended sediments. This could account for a small portion of the increase in ^{234}Th at 1918 m.

Chapter 3 results show large changes in the POC/^{234}Th of filterable particles over short timescales at DYFAMED in spring of 2005. Additionally, this study provides evidence that

pumps and traps do not collect the same material despite similar magnitudes in POC/^{234}Th. Other studies have also observed large variability in the large particle fraction (>53, >70 μm) POC/^{234}Th ratio when compared to bulk trap-collected POC/^{234}Th ratios (Hung and Gong, 2010 and references therein). Yet, the POC/^{234}Th of the large pump fraction has traditionally been applied to the ^{234}Th deficit to estimate POC flux (Bacon et al., 1996; Buesseler et al., 2006). In part, this variability in pump-derived POC/^{234}Th ratios and POC fluxes has prompted numerous ^{234}Th flux programs over the past 13 years to measure the POC/^{234}Th of three or more size fractions (Moran et al., 2003; Smith et al., 2006; Speicher et al., 2006; Waite and Hill, 2006; Burd et al., 2007; Brew et al., 2009; Lepore et al., 2009). And recently a group of studies have recommended using the POC/^{234}Th of small to intermediate sized (e.g., 1-10 μm, 10-53 μm) filterable particles (Hung et al., 2010; Hung and Gong, 2010; Hung et al., 2012). In addition to the high variability of the large particle fraction POC/^{234}Th, this recommendation is motivated by the observed similarity in the POC/^{234}Th of the small to intermediate sized pump fractions and that of sediment traps (Hung et al., 2010; Hung and Gong, 2010; Lepore et al., 2009; Buesseler et al., 2006; Waite and Hill, 2006). Indeed, we observed good agreement (within a factor of 2, Buesseler et al., 2006) of the 1-70 μm small particle (SP) fraction and trap ratios. However, the results of this chapter refute the assumption that correlation between POC/^{234}Th of the SP fraction and trap represents a correlation in the material collected by each method. The SP fraction contained fresh algal biomarkers of coccolithophores and diatoms, whereas traps contained biomarkers indicative of fecal pellets and bacterially degraded organic matter. Abramson et al. (2010) reached the same conclusion using PCA analysis of organic matter composition from the of the pump fractions and TS sediment trap material collected during 2003 and 2005 MedFlux spring field seasons.

The pigment composition of the filterable particles indicated lateral advection and vertical mixing occurred as well as large short-term changes (5 d) in POC/^{234}Th (1.7–3×) and ^{234}Th deficits (2–7×) at 300 m. The compound ratio of the diatom pigment fucoxanthin to Chl *a* was 5× higher at 100 and 150 m in March than all other pump fraction samples. This may indicate lateral advection of diatom material to the site. A striking finding that was also reported in Abramson et al. (2010) was the presence of Chl *a* in the SP fraction deep below the euphotic zone (600–1800 m) in March indicating either disaggregation of

rapidly settling fresh algal material or physical advection of small particles. An anomalously strong winter-early spring mixing event occurred in the northwest Mediterranean in 2005 (Marty and Chiavérini, 2010; Miquel et al., 2011) that may have transported the fresh algal material to deep waters. Selecting a POC/^{234}Th that is representative of the majority of sinking material that created the measured water column ^{234}Th deficit may not be possible at all oceanic sites. Savoye et al. (2006) advised using a non-steady-state ^{234}Th flux model to account for water advection and mixing. Even further complicating efforts to measure a representative POC/^{234}Th are the short-term changes in biological community structure (e.g., phytoplankton and zooplankton) that can occur within the several week timeframe (Benincá et al., 2008) that the ^{234}Th deficit is recording particle flux (Cochran and Masqué, 2003). In conjunction with Cochran et al. (2009) and Stewart et al. (2007), the results of this dissertation indicate the ^{234}Th proxy method cannot be applied with any confidence at the DYFAMED site. Our results suggest that facile application of the ^{234}Th proxy for POC flux is unwise and that considerable effort must be expended to constrain its validity in any given oceanic region.

In Chapter 4, we used Couette flow devices to experimentally derive coagulation efficiencies (α) of *Emiliania huxleyi* for the first time. In chemostat experiments conducted in 2006 and 2007, *E. huxleyi* were grown at different growth rates and we assessed the relationship of cell coagulation efficiency with cell growth rate and indicators of cell stickiness. Analogs for cell stickiness that were characterized include the sugar composition of high molecular weight dissolved material and the abundance of transparent exopolymer particles (TEP). This study provides evidence that cells have higher α values at lower growth rates. Our results indicate that conditions of high TEP abundance and cell calcite coverage yield higher coagulation efficiencies of *E. huxleyi*. Based on our findings we propose that the method by which TEP is included within an aggregate (e.g., TEP matrix embedding cells, free TEP gluing cells together, or exopolymer coating on cells leading to cell-cell contacts) could influence aggregate strength and its likelihood to sink intact beyond the mixed layer.

For relatively high growth rates (>0.1 d^{-1}) we estimated reproducible α values (variability, ±9%) that were in range of those reported in previous studies for diatoms at

similar growth stages (α, 0-0.25). Yet, at low growth rates replicate coagulation experiments yielded high α values that were variable (±24%). Kahl et al. (2008) also noted greater variability of α for senescent diatom cells. Overall, 2007 coagulation efficiency values were higher than those estimated at similar growth rates in 2006 most likely due to a higher percentage of calcified cells in 2007 (>99% calcified in 2007 and ~60% calcified in 2006). Principal components analysis of parameters important to coagulation in 2007 showed PC1 to represent 54.1% of the variability in samples and was dominated by the difference in cell growth rates, TEP : Chl *a*, and number of detached coccoliths per cell. PC2 (19.2% variability explained) is consistent with differences in characteristics of the cell medium on the first and second experiment day at each dilution rate; these differences could have contributed to higher α values on the second experiment day. The second experiment day exhibited higher amounts of Alcian blue stained cells (AB cells), circular aggregates, and total carbohydrates. This suggests a build up of exopolymeric material, and *E. huxleyi* cell surfaces led to more successful rates of cell attachment upon collision.

This dissertation demonstrates that the type of interaction TEP has with cells may affect coagulation efficiency, perhaps playing a role in the variability of α at low growth rates. AB-stained exopolymeric material on *E. huxleyi* cell surfaces increases particle surface area and contact sites (Alldredge and McGillivary, 1991) and acts as a bridging flocculant between cells whose sticking would be enhanced when there is full coverage of Ca^{2+}-bearing calcite shells on coccospheres. Coccolith associated polysaccharides are known to preferentially bind Ca^{2+} over other divalent cations (de Jong et al., 1976; Borman et al., 1982) allowing for polymer bridges to form (Decho, 1990; Leppard, 1995; Mopper et al., 1995). Organic polymers acting as bridging flocculants have the capacity to deform like springs while continuing to bind particles to each other (Somasundaran, 2006). The robustness confirmed on these cell-cell type aggregates might allow for successful passage through the mixed layer and more efficient sedimentation of algal bloom material. Indeed, in situ observations of sinking aggregates in mid-waters (below the mixed layer, 100-500 m) were found to have decreasing spherical shape (more ellipsoid) with increasing diameters and increasing settling velocities (Pilskaln et al., 1998) possibly indicating the role of flexible

exopolymer coatings on cell surfaces allowing for shear induced modification of aggregate morphology without particle fragmentation (Fig. 4.5c).

In contrast, fragile flocs often consisting of diatoms and other organic debris typifies cell-TEP type sticking (Fig. 4.5b) and would be sheared apart when sinking at similar rates due to nonuniformity in aggregate composition yielding up sites within the TEP-cell bond that cannot withstand surface shear stresses (Alldredge et al., 1990; Hill, 1998). Snapping polymers within diatom aggregates have been observed when aggregates were exposed to energy dissipation rates similar to that measured in the upper mixed layer and thermocline waters under low wind conditions (10^{-2} cm^2 s^{-3}; Alldredge et al., 1990). Export of aggregates dominated by a matrix of TEP with cells or particles embedded (Fig. 4.5a) would not be expected as these aggregates have been observed in the lab and field to be neutrally or positively buoyant (Atezsu-Scott and Passow, 2004; Azetsu-Scott and Niven, 2005; Mari, 2008; Wurl and Holmes, 2008). Hence, this dissertation suggests that including data on the form of TEP and its association with cells and aggregates along transects of coccolithophore blooms (from the center to edge or old to new) would increase our ability to predict when and if there will be mass sedimentation of the bloom material.

2. Recommendations and Directions for Future Research

Characterization of the organic chemical composition of filterable fractions and sediment trap material proved to be an important discriminating factor in the comparison of particle collection techniques (Abramson et al., 2010). The novel application of chemical composition data to POC/^{234}Th variability studies was essential for evaluating a representative POC/^{234}Th for the ^{234}Th approach. The analysis of organic composition is necessary to determine the particle biogenic source and biogeochemical processes, which this dissertation showed to be a controlling factor on POC/^{234}Th. The findings of this dissertation demonstrate the need for future ^{234}Th flux programs to validate quantitative comparisons of POC/^{234}Th between pump-filtered size fractions and bulk material derived from trap or filtered bottle material. Abramson et al. (2010) showed that organic geochemical analysis of pump fractions following the detection of ^{234}Th and subsampling for POC is feasible. Other potential methods for assessing the comparability of the pump fractions with sinking material are microscopic comparisons of pump and trap material

(e.g., scanning electron microscope imaging; Hung et al., 2012) and flow cytometry of material at the base of the photic zone or plankton and zooplankton tows to reveal epipelagic community structure.

Results of this dissertation point out compelling issues for the application of the ^{234}Th proxy method for POC flux. Our findings stress the necessity to make extensive efforts to evaluate the field site conditions to determine if the ^{234}Th approach would yield accurate estimates of POC export. Further recommendations follow directly from current publications of best practices for the ^{234}Th flux (Buesseler et al., 2006; Rutgers van der Loeff et al., 2006) and sediment trap (Gardner, 1997; Gardner, 2000; Buesseler et al., 2007) field programs. Non-steady state models of ^{234}Th flux should be applied to water column data, which requires repeatedly occupying field sites within 1–4 weeks (Savoye et al., 2006). Deploying sediment traps at depths adjacent to pump casts will allow for comparisons to be made between pump and trap material. Efforts should be made to follow recommendations issued for prevention of trap inefficiencies and degradation of collected material (Buesseler et al., 2007; Hung et al., 2012). Additionally, the oceanic site should be characterized by all data available, for example: CTD casts for hydrography, satellite sea surface temperature and chlorophyll, and current meters and Acoustic Doppler Current Profilers above traps and within euphotic zone to assess horizontal and vertical mixing and infer trap performance.

The DYFAMED site in the northwestern Mediterranean Sea was shown to be a suboptimal location for the ^{234}Th approach. In addition to the methods recommended here, the feasibility of acquiring accurate estimates of the POC flux is contingent upon the characteristics of the selected ocean region. Sites where traditional application of the large particle POC/^{234}Th to the water column ^{234}Th deficit may not be feasible include: areas of coastal upwelling and terrestrial inputs; equatorial upwelling systems; eddy systems (e.g., Hawaii Ocean Time-series Study site, Sargasso Sea, Canary Current); locations having dynamic fronts (e.g., Patagonian Shelf); regions known to have acidic acid polysaccharides that preferentially bind ^{234}Th (e.g., Gulf of Mexico, Baltic Sea); and regions known for having a dynamic succession of phytoplankton and zooplankton community structure rendering the large fraction POC/^{234}Th highly variable (e.g., Mediterranean Sea). Some sample sites might be more accommodating for the ^{234}Th approach than others. The

traditional use of the large pump fraction POC/^{234}Th might be limited to areas where primary production is dominated by diatom blooms (large cells) in an open ocean setting and the export can be generally described as one dimensional and vertical (e.g., high latitudes-North Atlantic). Areas where the application of the POC/^{234}Th from the small to intermediate pump fractions might best be applied to the ^{234}Th water column deficit are oligotrophic regions where flux is dominated by small cells (Richards and Jackson, 2007; Hung et al., 2012) and coccolithophore blooms where relatively low energy conditions promote a coccolithophore bloom following a diatom bloom (North Atlantic-south of Iceland, Southwest Pacific-south of New Zealand and the Tasman Sea). Using the POC/^{234}Th from sinking particles sampled by sediment trap might work equally well where small to intermediate pump fractions are employed. In addition the trap POC/^{234}Th might best represent the POC/^{234}Th ratio of flux where fecal pellets dominate the export (e.g., DYFAMED, Abramson et al., 2010).

The findings of this research highlight the importance of cell calcification, and TEP abundance and quality (e.g., coccolith associated polysaccharides), on the coagulation efficiency of *Emiliania huxleyi*. It would be interesting to test if these findings extend to *in situ* observations of *Emiliania huxleyi* blooms. Sampling along a transect of an *E. huxleyi* bloom, extending from the bloom center (low growth rate of cells, high detached coccolith: attached coccolith ratio) to edge (cells in exponential stage of growth, lower cell densities) would allow for the effects of coccolith detachment and coccolith coverage as well as cell growth rate and exudate abundances and composition to be studied. Samples collected along the transect could be used for Couette flow coagulation experiments performed on board. These coagulation efficiencies could be related to TEP abundance, size spectra, and coverage on cells, CCHO composition (including CAP) of the HMW dissolved pool, and calcification of the cells. Additionally, revisiting the same bloom days later might allow characterization of how lateral advection might cause changes in the density changes in particles along the transect. Measurements along this transect might show how cell and TEP density changes affect collision frequency and coagulation efficiency of cells. Furthermore if there are clear trends in coagulation efficiency along the transect, researchers might be motivated to mathematically relate coagulation efficiency to ocean color. Armed with data from such a field program, one might be able to use ocean color to

predict zones where cell coagulation, aggregation, and export are highly probable, then validate these predictions with short-term sediment trap deployments. High temporal resolution of coccolithophore bloom dynamics would be useful for such work. A possible candidate would be the hyper-spectral satellite sensors on the Sentinel-5-Precursor planned to launch in 2014 that would provide global coverage within 2 days yielding resolution of weeks instead of monthly averages (Sadeghi et al., 2012).

References

Abramson, L., Lee, C., Liu, Z.F., Wakeham, S.G., Szlosek, J., 2010. Exchange between suspended and sinking particles in the northwest Mediterranean as inferred from the organic composition of *in situ* pump and sediment trap samples. Limnology and Oceanography 55 (2), 725-739.

Alldredge, A.L., Gotschalk, C.C., 1989. Direct observations of the mass flocculation of diatom blooms: characteristics, settling velocities and formation of diatom aggregates. Deep-Sea Research 36, 159-171.

Alldredge, A.L., Granata, T.C., Gotschalk, C.C., Dickey, T.D., 1990. The physical strength of marine snow and its implications for particle disaggregation in the ocean. Limnology and Oceanography 35 (7), 1415-1428.

Alldredge, A.L., McGillivary, P., 1991. The attachment probabilities of marine snow and their implications for particle coagulation in the ocean. Deep-Sea Research 38 (4), 431-443.

Andersen, V., Prieur, L., 2000. One-month study in the open northwestern Mediterranan Sea (DYNAPROC experiment, May 1995): overview of the hydrobiogeochemical structures and effects of wind events. Deep-Sea Research II 47, 397-422.

Azetsu-Scott, K., Passow, U., 2004. Ascending marine particles: Significance of transparent exopolymer particles (TEP) in the upper ocean. Limnology and Oceanography 49 (3), 741-748.

Azetsu-Scott, K., Niven, S.E.H., 2005. The role of transparent exopolymer particles (TEP) in the transport of Th-234 in coastal water during a spring bloom. Continental Shelf Research 25 (9), 1133-1141.

Bacon, M.P., Cochran, J.K., Hirschberg, D.J., Hammar, T.R., Fleer, A.P., 1996. Export flux of carbon at the equator during the EqPac time-series cruises estimated from ^{234}Th measurements. Deep-Sea Research II 43, 1133-1153.

Benincá, E., Huisman, J., Heerkloss, R., Jöhnk, K.D., Branco, P., Van Nes, E.H., Scheffer, M., Ellner, S.P., 2008. Chaos in a long-term experiment with a plankton community. Nature 451, 822-825.

Borman, A.H., de Jong, E.W., Huizinga, M., Kok, D.J., Westbroek, P., Bosch, L., 1982. The role in $CaCO_3$ crystallization of an acid Ca^{2+}–binding polysaccharide associated with coccoliths of *Emiliania huxleyi*. European Journal of Biochemistry 129, 179-183.

Brew, H.S., Moran, S.B., Lomas, M.W., Burd, A.B., 2009. Plankton community composition, organic carbon and thorium-234 particle size distributions, and particle export in the Sargasso Sea. Journal of Marine Research 67, 845-868.

Buesseler, K.O., Benitez-Nelson, C.R., Moran, S.B., Burd, A., Charette, M., Cochran, J.K., Coppola, L., Fisher, N.S., Fowler, S.W., Gardner, W.D., Guo, L.D., Gustafsson, O., Lamborg, C., Masqué, P., Miquel, J.C., Passow, U., Santschi, P.H., Savoye, N., Stewart, G., Trull, T., 2006. An assessment of particulate organic carbon to thorium-234 ratios in the ocean and their impact on the application of ^{234}Th as a POC flux proxy. Marine Chemistry 100, 213-233.

Buesseler, K.O., Antia, A.N., Chen, M., Fowler, S.W., Gardner, W.D., Gustafsson, O., Harada, K., Michaels, A.F., Rutgers van der Loeff, M., Sarin, M., Steinberg, D.K., Trull, T., 2007. An assessment of the use of sediment traps for estimating upper ocean particle fluxes. Journal of Marine Research 65 (3), 345-416.

Burd, A.B., Jackson, G.A., Moran, S.B., 2007. The role of the particle size spectrum in estimating POC fluxes from ^{234}Th/^{238}U disequilibrium. Deep-Sea Research I 54, 897-918.

Cai, P., Dai, M., Chen, W., Tang, T., Zhou, K., 2006. On the importance of the decay of ^{234}Th in determining size-fractionated C/^{234}Th ratio on marine particles. Geophysical Research Letters 33, L23602.

Cochran, J.K., Masqué, P., 2003. Short-lived U/Th radionuclides in the ocean: tracers for scavenging rates, export fluxes, and particle dynamics. In: Bourdon, B., Henderson, G.M., Lundstrom, C.C., Turner, S.P. (Eds.), Uranium-Series Geochemistry, Reviews in Mineralogy and Geochemistry, vol. 52. Mineralogy Society of America, Washington, DC, pp. 461-492.

Cochran, J.K., Miquel, J-C., Armstrong, R.A., Fowler, S.W., Masqué, P., Gasser, B., Hirschberg, D.J., Szlosek, J., Rodriguez y Baena, A.M., Verdeny, E., Stewart, G.M., 2009. Time-series measurements of ^{234}Th in water column and sediment trap samples from the northwestern Mediterranean Sea. Deep-Sea Research II 56, 1487-1501.

de Jong, E.W., Bosch, L., Westbroek, P., 1976. Isolation and characterization of Ca^{2+}–binding polysaccharide associated with coccoliths of *Emiliania huxleyi* (Lohmann) Kamptner. European Journal of Biochemistry 70, 611-621.

Decho, A.W., 1990. Microbial exopolymer secretions in ocean environments: Their role(s) in food webs and marine processes. Oceanography and Marine Biology Annual Review 28, 73-153.

Gardner, W.D., 1997. The flux of particles to the deep sea: Methods, measurements, and mechanisms. Oceanography 10 (3), 116-121.

Gardner, W.D., 2000. Sediment trap technology and surface sampling in surface waters. In: Hanson, R.B., Ducklow, H.W., Field, J.G. (Eds.), The Changing Ocean Carbon Cycle: A Midterm Synthesis of the Joint Global Ocean Flux Study. Cambridge University Press. pp. 240-281.

Hill, P.S., 1998. Controls on floc size in the sea. Oceanography 11 (2), 13-18.

Hung, C.-C., Xu, C., Santschi, P.H., Zhang, S.-J., Schwehr, K.A., Quigg, A., Guo, L., Gong, G.-C., Pinckney, J.L., Long, R.A., Wei, C.-L., 2010. Comparative evaluation of sediment trap and ^{234}Th-derived POC fluxes from the upper oligotrophic waters of the Gulf of Mexico and the subtropical northwestern Pacific Ocean. Marine Chemistry 121, 132-144.

Hung, C.-C., Gong, G.-C., Santschi, P.H., 2012. ^{234}Th in different size classes of sediment trap collected particles from the Northwestern Pacific Ocean. Geochimica et Cosmochimica Acta 91, 60-74.

Hung, C.-C., Gong, G.-C., 2010. POC/^{234}Th ratios in particles collected in sediment traps in the northern South China Sea. Estuarine, Coastal and Shelf Science 88 (3), 303-310.

Kahl, L.A., Vardi, A., Schofield, O., 2008. Effects of phytoplankton physiology on export flux. Marine Ecology Progress Series 354, 3-19.

Lee, C., Peterson, M.L., Wakeham, S.G., Armstrong, R.A., Cochran, J.K., Miquel, J.C., Fowler, S.W., Hirschberg, D., Beck, A., Xue, J., 2009. Particulate organic matter and ballast fluxes measured using time-series and settling velocity sediment traps in the northwestern Mediterranean Sea. Deep-Sea Research II 56 (18), 1420-1436.

Lepore, K., Moran, S.B., Burd, A.B., Jackson, G.A., Smith, J.N., Kelly, R.P., Kaberi, H. Stavrakakis, S., Assimakopoulou, G., 2009. Sediment trap and *in-situ* pump size-fractionated POC/^{234}Th ratios in the Mediterranean Sea and Northwest Atlantic: Implications for POC export. Deep-Sea Research I 56, 599-613.

Leppard, G.G., 1995. The characterization of algal and microbial mucilage and their aggregates in aquatic ecosystems. Science of the Total Environment 165, 103-131.

Mari, X., 2008. Does ocean acidification induce an upward flux of marine aggregates? Biogeosciences 5, 1023-1031.

Martín, J., Sanchez-Cabeza, J.A., Eriksson, M., Lévy, I., Miquel, J.C., 2009. Recent accumulation of trace metals in sediments at the DYFAMED site (Northwestern Mediterranean Sea). Marine Pollution Bulletin 59, 146-153.

Marty, J.-C., Chiavérini, J., 2010. Hydrological changes in the Ligurian Sea (NW Mediterranean, DYFAMED site) during 1995-2007 and biogeochemical consequences. Biogeosciences Discuss 7, 1377-1406.

Miquel, J.-C., Martín, J., Gasser, B., Rodriguez y Baena, A., Toubal, T., Fowler, S.W., 2011. Dynamics of particle flux and carbon export in the northwestern Mediterranean Sea: A two decade time-series study at the DYFAMED site. Progress in Oceanography 91,

461-481.

Mopper, K., Zhou, J., Ramana, K.S., Passow, U., Dam, H.G., Drapeau, D.T., 1995. The role of surface-active carbohydrates in the flocculation of a diatom bloom in a mesocosm. Deep-Sea Research II 41, 47-73.

Moran, S.B., Weinstein, S.E., Edmonds, H.N., Smith, J.N., Kelly, R.P., Pilson, M.E.Q., Harrison, W.G., 2003. Does $^{234}Th/^{238}U$ disequilibrium provide an accurate record of the export flux of particulate organic carbon from the upper ocean? Limnology and Oceanography 48, 1018-1029.

Müller, M.N., Antia, A.N., LaRoche, J., 2008. Influence of cell cycle phase on calcification in the coccolithophore *Emiliania huxleyi*. Limnology and Oceanography 53 (2), 506-512.

Pilskaln, C.H., Lehmann, C., Paduan, J.B., Silver, M.W., 1998. Spatial and temporal dynamics in marine aggregate abundance, sinking rate and flux: Monterey Bay, central California. Deep-Sea Research II 45, 1803-1837.

Rutgers van der Loeff, M., Sarin, M.M., Baskaran, M., Benitez-Nelson, C., Buesseler, K.O., Charette, M., Dai, M., Gustafsson, O., Masqué, P., Morris, P.J., Orlandini, K., Rodriguez y Baena, A., Savoye, N., Schmidt, S., Turnewitsch, R., Vöge, I., Waples, J.T., 2006. A review of present techniques and methodological advances in analyzing ^{234}Th in aquatic systems. Marine Chemistry 100, 190-212.

Sadeghi, A., Dinter, T., Vountas, M., Taylor, B., Altenburg-Soppa, M., Bracher, A., 2012. Remote sensing of coccolithophore blooms in selected oceanic regions using the PhytoDOAS method applied to hyper-spectral satellite data. Biogeosciences 9, 2127-2143.

Savoye, N., Benitez-Nelson, C., Burd, A.B., Cochran, J.K., Charette, M., Buesseler, K.O., Jackson, G.A., Roy-Barman, M., Schmidt, S., Elskens, M., 2006. ^{234}Th sorption and export models in the water column: a review. Marine Chemistry 100, 234-249.

Smith, J.N., Moran, S.B., Speicher, E.A., 2006. On the accuracy of upper ocean particulate organic carbon export fluxes estimated from $^{234}Th/^{238}U$ disequilibrium. Deep-Sea Research I 53 (5), 860-868.

Somasundaran, P., 2006. Encyclopedia of Surface and Colloid Science. vol. 6, CRC: Taylor & Francis Group, New York, pp. 6675.

Speicher, E.A., Moran, S.B., Burd, A.B., Delfanti, R., Kaberi, H., Kelly, R.P., Papucci, C., Smith, J.N., Stavrakakis, S., Torricelli, L., Zervakis, V., 2006. Particulate organic carbon export fluxes and size-fractionated $POC/^{234}Th$ ratios in the Liguarian, Tyrrhenian and Aegean Seas. Deep-Sea Research I 53, 1810-1830.

Stewart, G., Cochran, J.K., Miquel, J.C., Masqué, P., Szlosek, J., Rodriguez y Baena, A.M., Fowler, S.W., Gasser, B., Hirschberg, D.J., 2007. Comparing POC export from $^{234}Th/^{238}U$ and $^{210}Po/^{210}Pb$ disequilibria with estimates from sediment traps in the northwest Mediterranean. Deep-Sea Research I 54, 1549-1570.

Szlosek, J., Cochran, J.K., Miquel, J.C., Masqué, P., Armstrong, R.A., Fowler, S.W., Gasser, B., Hirschberg, D.J., 2009. Particulate organic carbon–^{234}Th relationships in particles separated by settling velocity in the northwest Mediterranean Sea. Deep-Sea Research II 56, 1519-1532.

Waite, A.M., Hill, P.S., 2006. Flocculation and phytoplankton cell size can alter ^{234}Th-based estimates of the vertical flux of particulate organic carbon in the sea. Marine Chemistry 100 (3-4), 366-375.

Wakeham, S.G., Lee, C., Peterson, M.L., Liu, Z., Szlosek, J., Putnam, I., Xue, J., 2009. Organic compound composition and fluxes in the Twilight Zone–time series and settling velocity sediment traps during MedFlux. Deep-Sea Research II 56, 1437-1453.

Wurl, O., Holmes, M., 2008. The gelatinous nature of sea-surface microlayer. Marine Chemistry 110, 89-97.

REFERENCES

Abramson, L., Lee, C., Liu, Z.F., Wakeham, S.G., Szlosek, J., 2010. Exchange between suspended and sinking particles in the northwest Mediterranean as inferred from the organic composition of *in situ* pump and sediment trap samples. Limnology and Oceanography 55 (2), 725-739.

Alldredge, A.L., Silver, M.W., 1988. Characteristics, dynamics, and significance of marine snow. Progress in Oceanography 20, 41-82.

Alldredge, A.L., Gotschalk, C.C., 1989. Direct observations of the mass flocculation of diatom blooms: characteristics, settling velocities and formation of diatom aggregates. Deep-Sea Research 36, 159-171.

Alldredge, A.L., Granata, T.C., Gotschalk, C.C., Dickey, T.D., 1990. The physical strength of marine snow and its implications for particle disaggregation in the ocean. Limnology and Oceanography 35 (7), 1415-1428.

Alldredge, A.L., McGillivary, P., 1991. The attachment probabilities of marine snow and their implications for particle coagulation in the ocean. Deep-Sea Research 38 (4), 431-443.

Alldredge, A.L., Passow, U., Logan, B.E., 1993. The abundance and significance of a class of large, transparent organic particles in the ocean. Deep-Sea Research 40, 1131-1140.

Alldredge, A.L., Gotschalk, C., Passow, U., Riebesell, U., 1995. Mass aggregation of diatom blooms: Insights from a mesocosm study. Deep-Sea Research I 42, 9-28.

Aluwihare, L.I., Repeta, D.J., 1999. A comparison of the chemical characteristics of oceanic DOM and extracellular DOM produced by marine algae. Marine Ecology Progress Series 186, 105-117.

Alonso-González, I.J., Arístegui, J., Lee, C., Sanchez-Vidal, A., Calafat, A., Fabrés, J., Sangrá, P., Masqué, P., Hernández-Guerra, A., Benítez-Barrios, V., 2010. Role of slowly settling particles in the ocean carbon cycle. Geophysical Research Letters 37, L13608.

Altabet, M.A., Deuser, W.G., Honjo, S., Stienen, C., 1991. Seasonal and depth-related changes in the source of sinking particles in the North Atlantic. Nature 354 (6349), 136-139.

Aluwihare, L.I., Repeta, D.J., 1999. A comparison of the chemical characteristics of oceanic DOM and extracellular DOM produced by marine algae. Marine Ecology Progress

Series 186, 105-117.

Andersen, V., Prieur, L., 2000. One-month study in the open northwestern Mediterranan Sea (DYNAPROC experiment, May 1995): overview of the hydrobiogeochemical structures and effects of wind events. Deep-Sea Research II 47, 397-422.

Antia, A.N., 2005. Particle-associated dissolved elemental fluxes: revising the stochiometry of mixed layer export. Biogeosciences Discussions 2, 275-302.

Armstrong, R.A., Lee, C., Hedges, J. I., Honjo, S., Wakeham, S., 2002. A new, mechanistic model for organic carbon fluxes in the ocean based on the quantitative association of POC with ballast minerals. Deep-Sea Research II 49, 219-236.

Armstrong, R.A., 2003. A hybrid spectral representation of phytoplankton growth and zooplankton response: The "control rod" model of plankton interaction. Deep-Sea Research II 50, 2895-2916.

Armstrong, R.A., Peterson, M.L., Lee, C., Wakeham, S.G., 2009. Settling velocity spectra and the ballast ratio hypothesis. Deep-Sea Research II 56, 1470-1478.

Arnosti, C., 1993. Structural characterization and bacterial degradation of marine carbohydrates. Ph.D. Thesis, Woods Hole Oceanographic Institute, Woods Hole, MA.

Azam, F., Long, R.A., 2001. Sea snow microcosms. Nature 414, 495-497.

Azetsu-Scott, K., Passow, U., 2004. Ascending marine particles: significance of transparent exopolymer particles (TEP) in the upper ocean. Limnology and Oceanography 49 (3), 741-748.

Azetsu-Scott, K., Nivent, S.E.H., 2005. The role of transparent exopolymer particles (TEP) in the transport of Th-234 in coastal water during a spring bloom. Continental Shelf Research 25 (9), 1133-1141.

Bacon, M.P., Cochran, J.K., Hirschberg, D.J., Hammar, T.R., Fleer, A.P., 1996. Export flux of carbon at the equator during the EqPac time-series cruises estimated from ^{234}Th measurements. Deep-Sea Research II 43, 1133-1153.

Balch, W.M., K.A. Kilpatrick, P.M. Holligan, and T. Cucci, 1993. Coccolith production and detachment by *Emiliania huxleyi*. Journal of Phycology 29 (5), 566-575.

Balch, W.M., Kilpatrick, K., Holligan, P.M., Harbour, D., Fernández, E., 1996. The 1991 coccolithophore bloom in the central north Atlantic. II. Relating optics to coccolith concentration. Limnology and Oceanography 41, 1684-1696.

Balch, W.M., Gordon, H.R., Bowler, C., Drapeau, D.T., Booth, E.S., 2005. Calcium carbonate budgets in the surface global ocean based on MODIS data. Journal of Geophysical

Research 110, C07001.

Benincá, E., Huisman, J., Heerkloss, R., Jöhnk, K.D., Branco, P., Van Nes, E.H., Scheffer, M., Ellner, S.P., 2008. Chaos in a long-term experiment with a plankton community. Nature 451, 822-825.

Benitez-Nelson, C.R., Buesseler, K.O., Karl, D., Andrews, J., 2001. A time-series study of particular matter export in the North Pacific subtropical gyre based upon ^{234}Th: ^{238}U disequilibrium. Deep-Sea Research 48 (12), 2595-2611.

Benitez-Nelson, C.R., Moore, W.S., 2006. Future applications of ^{234}Th in aquatic ecosystems. Marine Chemistry 100 (3-4), 163-165.

Béthoux, J. P., Prieur, L., 1983. Hydrologie et circulation en Méditerranée Nord-Occidentale. Pétroles et Techniques 299, 25-34.

Béthoux, J.P., Prieur, L., and Bong, J.-H., 1988. The Ligurian current off the French Riviera. Oceanologica Acta SP, 59-67.

Biermann, A., Engel, A., 2010. Effect of CO_2 on the properties and sinking velocity of aggregates of the coccolithophore *Emiliania huxleyi*. Biogeosciences 7 (3), 1017-1029.

Birkner, F.B., and J.J. Morgan, 1968. Polymer flocculation kinetics of dilute colloidal suspensions. Journal of the American Water Works 60, 175-191.

Bishop, J.K., Edmond, J.M., Ketten, D.R., Bacon, M.B., Silker, W.B., 1977. The chemistry, biology and vertical flux of particulate matter from the upper 400 m of the equatorial Atlantic Ocean. Deep-Sea Research I 24, 511-548.

Bishop, J.K.B., Ketten, D.R., Edmond, J.M., 1978. The chemistry, biology, and vertical flux of particulate matter from the upper 400 m of the Cape Basin in the southeast Atlantic Ocean. Deep-Sea Research 25, 1121-1161.

Borchard, C., Borges, A.V., Händel, N., Engel, A., 2011. Biogeochemical response of *Emiliania huxleyi* (PML B92/11) to elevated CO_2 and temperature under phosphorous limitation: a chemostat study. Journal of Experimental Marine Biology and Ecology 410, 61-71.

Borchard, C., Engel, A., 2011. Organic matter exudation by *Emiliania huxleyi* under simulated future ocean conditions. Biogeosciences Discussions 9, 1199-1236.

Borman, A.H., de Jong, E.W., Huizinga, M., Kok, D.J., Westbroek, P., Bosch, L., 1982. The role in $CaCO_3$ crystallization of an acid Ca^{2+}-binding polysaccharide associated with coccoliths of *Emiliania huxleyi*. European Journal of Biochemistry 129, 179-183.

Brew, H.S., Moran, S.B., Lomas, M.W., Burd, A.B., 2009. Plankton community composition, organic carbon and thorium-234 particle size distributions, and particle export in the Sargasso Sea. Journal of Marine Research 67, 845-868.

Bruland, K.W., Silver, M.W., 1981. Sinking rates of fecal pellets from gelatinous zooplankton (Salps, Pteropods, Doliolids). Marine Biology 63, 295-300.

Bruland, K.W., Coale, K.H., 1986. Surface Water $^{234}Th/^{238}U$ disequilibria: spatial and temporal variations of scavenging rates within the Pacific Ocean. In: Burton, J.D., Brewer, P.G., Chesselet, R. (Eds.), Dynamic Processes in the Chemistry of the Upper Ocean. Plenum Press, pp 159-172.

Buat-Ménard, P., Davies, J., Remoudaki, E., Miquel, J.-C., Bergametti, G., Lambert, C.E., Ezat, U., Quetal, C., La Rosa, J., Fowler, S.W., 1989. Non steady-state biological removal of atmospheric particles from Mediterranean surface waters. Nature 340 (6229), 131-134.

Buesseler, K.O., Cochran, J. K., Bacon, M. P., Livingston, H. D., Casso, S. A., Hirschberg, D., Hartman, M. C., Fleer, A. P., 1992. Determination of thorium isotopes in seawater by nondestructive and radiochemical procedures. Deep-Sea Research I 39, 1103-1114.

Buesseler, K.O., Andrews, J.A., Hartman, M.C., Belastock, R., Chai,, F., 1995. Regional estimates of the export flux of particulate organic carbon derived from thorium-234 during the JGOFS EqPac program. Deep-Sea Research II 42 (2-3), 777-804.

Buesseler, K.O., 1998a. The decoupling of production and particulate export in the surface ocean. Global Biogeochemical Cycles 12 (2), 297-310.

Buesseler, K., Ball, L., Andrews, J., Benitez-Nelson, C., Belastock, R., Chai, F., Chao, Y., 1998b. Upper ocean export of particulate organic carbon in the Arabian Sea derived from thorium-234. Deep-Sea Research I 45, 2461-2487.

Buesseler, K.O., Steinberg, D.K., Michaels, A.F., Johnson, R.J., Andrews, J.E., Valdes, J.R., Price, J.F., 2000. A comparison of the quantity and quality of material caught in a neutrally buoyant versus surface-tethered sediment trap. Deep-Sea Research I 47, 277-294.

Buesseler, K.O., Ball, L., Andrews, J., Cochran, J.K., Hirschberg, D.J., Bacon, M.P., Fleer, A., Brzezinski, M., 2001. Upper ocean export of particulate organic carbon and biogenic silica in the Southern Ocean along 170°W. Deep-Sea Research II 48 (4275-4297).

Buesseler, K.O., Andrews, J.E., Pike, S., Charette, M.A., Goldson, L.E., Brzezinski, M.A., Lance, V.P., 2005. Particle export during the Southern Ocean Iron Experiment (SOFeX). Limnology and Oceanography 50, 311-327.

Buesseler, K.O., Benitez-Nelson, C.R., Moran, S.B., Burd, A., Charette, M., Cochran, J.K., Coppola, L., Fisher, N.S., Fowler, S.W., Gardner, W.D., Guo, L.D., Gustafsson, O.,

Lamborg, C., Masqué, P., Miquel, J.C., Passow, U., Santschi, P.H., Savoye, N., Stewart, G., Trull, T., 2006. An assessment of particulate organic carbon to thorium-234 ratios in the ocean and their impact on the application of ^{234}Th as a POC flux proxy. Marine Chemistry 100, 213-233.

Buesseler, K.O., Lamborg, C.H., Boyd, P.W., Lam, P.J., Trull, T.W., Bidigare, R.R., Bishop, J.K.B., Casciotti, K.L., Dehairs, F., Elskens, M., Honda, M., Karl, D.M., Siegel, D.A., Silver, M.W., Steinberg, D.K., Valdes, J., Mooy, B.V., Wilson, S., 2007a. Revisiting carbon flux through the ocean's twilight zone. Science 316, 567-570.

Buesseler, K.O., Antia, A.N., Chen, M., Fowler, S.W., Gardner, W.D., Gustafsson, O., Harada, K., Michaels, A.F., Rutgers van der Loeff, M., Sarin, M., Steinberg, D.K., Trull, T., 2007b. An assessment of the use of sediment traps for estimating upper ocean particle fluxes. Journal Marine Research 65, 345-416.

Buesseler, K.O., Trull, T.W., Steinberg, D.K., Silver, M.W., Siegel, D.A., Saitoh, S.I., Lamborg, C.H., Lam, P.J., Karl, D.M., Jiao, N.Z., Honda, M.C., Elskens, M., Dehairs, F., Brown, S.L., Boyd, P.W., Bishop, J.K.B., Bidigare, R.R., 2008. VERTIGO (VERtical Transport In the Global Ocean): as study of particle source and flux attenuation in the North Pacific. Deep-Sea Research II 55 (14-15), 1522-1539.

Buessler, K.O., Boyd, .P.W., 2009. Shedding light on processes that control particle export and flux attenuation in the twilight zone of the open ocean. Limnology and Oceanography 54 (4), 1210-1232.

Burd, A.B., Moran, S.B., Jackson, G.A., 2000. A coupled adsorption-aggregation model of the POC/^{234}Th ratio of marine particles. Deep-Sea Research I 47, 103-120.

Burd, A.B., Jackson, G.A., Moran, S.B., 2007. The role of the particle size spectrum in estimating POC fluxes from ^{234}Th/^{238}U disequilibrium. Deep-Sea Research I 54, 897-918.

Burd, A.B., Jackson, G.A., 2009. Particle aggregation. Annual Reviews of Marine Science 1, 65-90.

Burd, A.B., Hansell, D.A., Steinberg, D.K., Anderson, T.R., Aristegui, J., Baltar, F., Beaupre, S.R., Buesseler, K.O., DeHairs, F., Jackson, G.A., Kadko, D.C., Koppelmann, R., Lampitt, R.S., Nagata, T., Reinthaler, T., Robinson, C., Robison, B.H., Tamburini, C., Tanaka, T., 2010. Assessing the apparent imbalance between geochemical and biochemical indicators of meso- and bathypelagic biological activity: What the @$#! is wrong with present calculations of carbon budgets? Deep-Sea Research II 57 (16), 1557-1571.

Cai, P., M. Dai, W. Chen, T. Tang, K. Zhou, 2006. On the importance of the decay of ^{234}Th in determining size-fractionated C/^{234}Th ratio on marine particles. Geophysical Research Letters 33, L23602.

Cadée, G.C., 1985. Macroaggregates of *Emiliania huxleyi* in sediment traps. Marine Ecology Progress Series 24, 193-196.

Camp, T.R., and Stein, P.C., 1943. Velocity gradients and internal work in fluid motion. Journal of Boston Society of Civil Engineers 30, 219-237.

Chase, Z., Anderson, R.F., Fleisher, M.Q., Kubik, P.W., 2002. The influence of particle composition and particle flux on scavenging of Th, Pa and Be in the ocean. Earth and Planetary Science Letters 204, 215-229.

Charette, M.A., Moran, S.B., Bishop, J.K.B., 1999. ^{234}Th as a tracer of particulate organic carbon export in the subarctic Northeast Pacific Ocean. Deep-Sea Research II 46 (11-12), 2833-2861.

Chisholm, S.W., 2000. Oceanography: Stirring times in the Southern Ocean. Nature 407, 685-687.

Claquin, P., Probert, I., Lefebvre, S., and Veron, B., 2008. Effects of temperature on photosynthetic parameters and TEP production in eight species of marine microalgae. Aquatic Microbial Ecology 51, 1-11.

Clegg, S.L., Whitfield, M., 1990. A generalised model for the scavenging of trace metals in the open ocean, I, particle cycling. Deep-Sea Research I 37, 809-832.

Coale, K.H., Bruland, K.W., 1985. ^{234}Th:^{238}U disequilibria within the California Current. Limnology and Oceanography 30 (1), 22-33.

Coale, K.H., Bruland, K.W., 1987. Oceanic stratified euphotic zone as elucidated by ^{234}Th:^{238}U disequilibria. Limnology and Oceanography 32 (1), 189-200.

Coale, K.H., 1990. Labyrinth of doom: a device to minimize the "swimmer" component in sediment trap collections. Limnology and Oceanography 35 (6), 1376-1381.

Cochran, J.K., Buesseler, K.O., Bacon, M.P., Livingston, H.D., 1993. Thorium isotopes as indicators of particle dynamics in the upper ocean: results from the JGOFS North Atlantic Bloom experiment. Deep-Sea Research I 40, 1569-1595.

Cochran, J.K., Buesseler, K.O., Bacon, M.P., Wang, H.W., Hirschberg, D.J., Ball, L., Andrews, J., Crossin, G., Fleer, A., 2000. Short-lived thorium isotopes (^{234}Th, ^{228}Th) as indicators of POC export and particle cycling in the Ross Sea, Southern Ocean. Deep-Sea Research II 47, 3451-4390.

Cochran, J.K., Masqué, P., 2003. Short-lived U/Th radionuclides in the ocean: tracers for scavenging rates, export fluxes, and particle dynamics. In: Bourdon, B., Henderson, G.M., Lundstrom, C.C., Turner, S.P. (Eds.), Uranium-Series Geochemistry, Reviews in Mineralogy and Geochemistry, vol. 52. Mineralogy Society of America, Washington, DC, pp. 461-492.

Cochran, J.K., Miquel, J-C., Armstrong, R.A., Fowler, S.W., Masqué, P., Gasser, B., Hirschberg, D.J., Szlosek, J., Rodriguez y Baena, A.M., Verdeny, E., Stewart, G.M., 2009. Time-series measurements of ^{234}Th in water column and sediment trap samples from the northwestern Mediterranean Sea. Deep-Sea Research II 56, 1487-1501.

Collier, J.L., Lovindeer, R., Xi, Y., Radway, J.C., Armstrong, R.A., 2012. Differences in growth and physiology of marine *Synechococcus* (cyanobacteria) on nitrate versus ammonium are not determined solely by nitrogen source redox state. Journal of Phycology 48 (1), 106-117.

Coppola, L., Roy-Barman, M., Wassmann, P., Mulsow, S., Jeandel, C., 2002. Calibration of sediment traps and particulate organic carbon export using ^{234}Th in the Barents Sea. Marine Chemistry 80, 11-26.

Currie, R., 1962. Pigments in zooplankton faeces. Nature 193, 956-957.

Dam, H.G., Drapeau, D.T., 1995. Coagulation efficiency, organic-matter glues and the dynamics of particles during a phytoplankton bloom in a mesocosm study. Deep-Sea Research II 42, 111-123.

De Bodt, C., Van Oostende, N., Harlay, J., Sabbe, K., Chou, L., 2010. Individual and interacting effects of pCO_2 and temperature on *Emiliania huxleyi* calcification: study of the calcite production, the coccolith morphology and the coccosphere size. Biogeosciences 7, 1401-1412.

Decho, A.W., 1990. Microbial exopolymer secretions in ocean environments: Their role(s) in food webs and marine processes. Oceanography and Marine Biology Annual Review 28, 73-153.

de Jong, E.W., Bosch, L., Westbroek, P., 1976. Isolation and characterization of Ca^{2+}-binding polysaccharide associated with coccoliths of *Emiliania huxleyi* (Lohmann) Kamptner. European Journal of Biochemistry 70, 611-621.

de Jong, E.W., van Rens, L., Westbroek, P., Bosch, L., 1979. Biocalcification by the marine alga *Emiliania huxleyi* (Lohmann) Kamptner. European Journal of Biochemistry 99, 559-567.

De La Rocha, C.L., Passow, U., 2006. Accumulation of mineral ballast on organic aggregates. Global Biogeochemical Cycles 20, GB1013.

De La Rocha, C.L., Passow, U., 2007. Factors influencing the sinking of POC and the efficiency of the biological carbon pump. Deep-Sea Research II 54, 639-658.

de Wilde, P.A.W.J., Duineveld, G.C.A., Berghuis, E.M., Lavaleye, M.S.S., Kok, A., 1998. Late-summer mass deposition of gelatinous phytodetritus along the slope of the N.W.

European Continental Margin. Progress in Oceanography 42, 165-187.

Donnelly, R.J., 1991. Taylor-Couette flow: The early days. Physics Today 44 (11), 32-39.

Drapeau, D.T., Dam, H.G., Grenier, G., 1994. An improved flocculator design for use in particle aggregation experiments. Limnology and Oceanography 39, 723-729.

Edzwald, J.K., Upchurch, J.B., O'Melia, C.R., 1974. Coagulation in estuaries. Environmental Science and Technology 8, 58-63.

Elimelech, M., Gregory, J., Jia, X., and Williams, R. (Eds.), 1995. Particle deposition and aggregation: measurement, modelling, and simulation. Elsevier, Oxford, pp. 441.

Emerson, S., Quay, P., Karl, D., Winn, C., Tupas, L., Landry, M., 1997. Experimental determination of the organic carbon flux from open-ocean surface waters. Nature 389 (6654), 951-954.

Engel, A., 2000. The role of transparent exopolymer particles (TEP) in the increase in apparent particle stickiness (α) during the decline of a diatom bloom. Journal of Plankton Research 22, 485-497.

Engel, A., Delille, B., Jacquet, S., Riebesell, U., Rochelle-Newall, E., Terbrüggen, A., Zondervan, I., 2004. Transparent exopolymer particles and dissolved organic carbon production by *Emiliania huxleyi* exposed to different CO_2 concentrations: a mesocosm experiment. Aquatic Microbial Ecology 34, 93-104.

Engel, A., Szlosek, J., Abramson, L., Liu, Z., Lee, C., 2009a. Investigating the effect of ballasting by $CaCO_3$ in *Emiliania huxleyi*, I: Formation, settling velocities and physical properties of aggregates. Deep-Sea Research II 56, 1396-1407.

Engel, A., Abramson, L., Szlosek, J., Liu, Z., Stewart, G., Hirschberg, D., Lee, C., 2009b. Investigating the effect of ballasting by $CaCO_3$ in *Emiliania huxleyi*, II: Decomposition of particulate organic matter. Deep-Sea Research II 56, 1408-1419.

Engel, A., 2009. Determination of Marine Gel Particles. In: Wurl, O. (Ed.), Practical Guidelines for the Analysis of Seawater. CRC Press, Boca Raton, FL, pp. 125-142.

Eppley, R.W., Peterson, B.J., 1979. Particulate organic matter flux and planktonic new production in the deep ocean. Nature 282, 677-680.

Fabrés, J., Calafat, A., Sanchez-Vidal, A., Canals, M., Heussner, S., 2002. Composition and spatio-temporal variability of particle fluxes in the Western Alboran Gyre, Mediterranean Sea. Journal of Marine Systems 33-34, 431-456.

Falkowski, P., Scholes, R. J., Boyle, E., Canadell, J., Canfield, D., Elser, J., Gruber, N., Hi30,

bbard, K., Hogberg, P., Linder, S., Mackenzie, F. T., Moore, B., Pedersen, T., Rosenthal,Y., Smetacek, V., Steffen, W., 2000. The global carbon cycle: A test of our knowledge of Earth as a system. Science 290, 291-296.

Fernández, E., Boyd, P., Holligan, P.M., Harbour, D.S., 1993. Production of organic and inorganic carbon within a large-scale coccolithophore bloom in the northeast Atlantic Ocean. Marine Ecology Progress Series 97, 271-285.

Fichtinger-Schepman, A.M.J., Kamerling, J.P., Vliegenthart, J.F.G., de Jong, E.W., Bosch, L., Westbroek, P., 1979. Composition of a methylated, acidic polysaccharide associated with coccoliths of *Emiliania huxleyi* (Lohmann) Kamptner. Carbohydrate Research 69, 181-189.

Flexas, M.M., Durrieu de Madron, X., Garcia, M.A., Canals, M., Arnau, P., 2002. Flow variability in the Gulf of Lions during the MATER HFF experiment (March-May 1997). Journal of Marine Systems 33-34, 197-214.

Font, J., Puig, P., Salat, J., Palanques, A., Emelianov, M., 2007. Sequence of hydrographic changes in NW Mediterranean deep water due to the exceptional winter of 2005. Scientia Marina 71 (2), 339-346.

Fowler, S.W., Knauer, G.A., 1986. Role of large particles in the transport of elements and organic compounds through the oceanic water column. Progress in Oceanography 16, 147-194.

Fowler, S.W., Buat-Ménard, P., Yokoyama, Y., Ballestra, S., Holm, E., van Nguyen, H., 1987. Rapid removal of Chernobyl fallout from Mediterranean surface waters by biological activity. Nature 329, 56-58.

Fritz, J.J., Balch, W.M., 1996. A light-limited continuous culture study of *Emiliania huxleyi*: determination of coccolith detachment and its relevance to cell sinking. Journal of Experimental Marine Biology and Ecology 207, 127-147.

Fritz, J.J., 1999. Carbon fixation and coccolith detachment in the coccolithophore *Emiliania huxleyi* in nitrate-limited cyclostats. Marine Biology 133, 509-518.

Gardner, W.D., 1980. Sediment trap dynamics and calibration: a laboratory evaluation. Journal of Marine Research 38, 17-39.

Gardner, W.D., 1980. Field assessment of sediment traps. Journal Marine Research 38, 41-52.

Gardner, W.D., 1985. The effect of tilt on sediment trap efficiency. Deep-Sea Research 32 (3), 349-361.

Gardner, W.D., 1997. The flux of particles to the deep sea: Methods, measurements, and

mechanisms. Oceanography 10 (3), 116-121.

Gardner, W.D., 2000. Sediment trap technology and surface sampling in surface waters. In: Hanson, R.B., Ducklow, H.W., Field, J.G. (Eds.), The Changing Ocean Carbon Cycle, A Midterm Synthesis of the Joint Global Ocean Flux Study. Cambridge University Press, pp. 240-281.

Gibbs, R.J., 1982. Floc stability during Coulter counter analysis. Journal of Sedimentary Petrology 52, 657-660.

Godoi, R.H.M., Aerts, K., Harlay, J., Kaegi, R., Ro, C.-U., Chou, L., Van Grieken, R., 2009. Organic surface coating on coccolithophores - *Emiliania huxleyi*: its determination and implication in the marine carbon cycle. Microchemical Journal 91 (2), 266-271.

Gõni, M.A., Yunker, M.B., Macdonald, R.W., Eglinton, T.I., 2000. Distributions and sources of organic biomarkers in arctic sediments from the Mackenzie River and Beaufort Shelf. Marine Chemistry 71 (23-51).

Goutx, M., Wakeham, S.G., Lee, C., Duflos, M., Guigue, C., Liu, Z., Moriceau, B., Sempéré, R., Tedetti, M., Xue, J., 2007. Composition and degradation of marine particles with different settling velocities in the northwest Mediterranean Sea. Limnology and Oceanography 52, 1645-1664.

Grant, H.L., Stewart, R.W., Moilliet, A., 1962. Turbulence spectra from a tidal channel. Journal of Fluid Mechanics 2, 241-268.

Guillard, R.R.L., Ryther, J.H., 1962. Studies of marine planktonic diatoms. Canadian Journal of Microbiololgy 8, 229-239.

Gust, G., Bowles, W., Giordano, S., Huettel, M., 1996. Particle accumulation in a cylindrical sediment trap under laminar and turbulent steady flow: an experimental approach. Aquatic Sciences 58, 297-326.

Gustafsson, O., Larsson, J., Andersson, P., Ingri, J., 2006. The POC/^{234}Th ratio of settling particles isolated using split flow-thin cell fractionation (SPLITT). Marine Chemistry 100 (3-4), 314-322.

Gutiérrez-Rodriguez, A., Latasa, M., Estrada, M., Vidal, M., Marrase, C., 2010. Carbon fluxes through major phytoplankton groups during the spring bloom and post-bloom in the Northwestern Mediterranean Sea. Deep-Sea Research I: Oceanographic Research Papers 57 (4), 486-500.

Hamm, C.E., 2002. Interactive aggregation and sedimentation of diatoms and clay-sized lithogenic material. Limnology and Oceanography 47 (6), 1790-1795.

Hansen, J.L.S., Timm, U., Kiørboe, T., 1995. Adaptive significance of phytoplankton

stickiness with emphasis on the diatom *Skeletonema costatum*. Marine Biology 123, 667-676.

Harlay, J., Borges, A.V., Van Der Zee, C., Delille, B., Godoi, R.H.M., Schiettecatte, L.-S., Roevros, N., Aerts, K., Lapernat, P.-E., Rebreanu, L., Groom, S., Daro, M.-H., Van Grieken, R., Chou, L., 2010. Biogeochemical study of a coccolithophore bloom in the northern Bay of Biscay (NE Atlantic Ocean) in June 2004. Progress in Oceanography 86, 317-336.

Hedges, J.I., Stern, J.H., 1984. Carbon and nitrogen determinations of carbonate-containing solids. Limnology and Oceanography 29, 657-663.

Henriksen, K., Stipp, S.L.S., 2009. Controlling biomineralzation: the effect of solution composition on coccolith polysaccharide functionality. Crystal Growth and Design 9, 2088-2097.

Hill, P.S., 1992. Reconciling aggregation theory with observed vertical fluxes following phytoplankton blooms. Journal of Geophysical Research 97, 2295-2308.

Hill, P.S., 1998. Controls on floc size in the sea. Oceanography 11 (2), 13-18.

Hoagland, K., Rosowski, J., Gretz, M., Roemaer, S., 1993. Diatom extracellular polymeric substances: function, fine structure, chemistry, and physiology. Journal of Phycology 29, 537-566.

Holligan, P.M., Viollier, M., Harbour, D.S., Camus, P., Champagne-Philippe, M., 1983. Satellite and ship studies of coccolithophore production along a continental shelf edge. Nature 304, 339-342.

Holligan, P.M., Fernández, E., Aiken, J., Balch, W.M., Boyd, P., Burkill, P.H., Finch, M., Groom, S.B., Malin, G., Muller, K., Purdie, D.A., Robinson, C., Trees, C.C., Turner, S.M., van der Wal, P., 1993. A biogeochemical study of the coccolithophore, *Emiliania huxleyi*, in the North Atlantic. Global Biogeochemical Cycles 7 (4), 879-900.

Honjo, S., 1982. Seasonality and interaction of biogenic and lithogenic particulate flux at the Panama Basin. Science 218, 883-884.

Hung, C.-C., Gong, G.-C., 2007. Export flux of POC in the main stream of the Kuroshio. Geophysical Research Letters 34, L18606.

Hung, C.-C., Moran, S.B., Cochran, J.K., J.K., Guo, L., Santschi, P.H., 2008. Comment on "How accurate are ^{234}Th measurements in seawater based on the MnO_2-impregnated cartridge technique?" by Pinghe Cai et al. . Geochemistry Geophysics Geosystems 9, Q02009.

Hung, C.-C., Gong, G.-C., 2010. POC/^{234}Th ratios in particles collected in sediment traps in

the northern South China Sea. Estuarine, Coastal and Shelf Science 88 (3), 303-310.

Hung, C.-C., Xu, C., Santschi, P.H., Zhang, S.-J., Schwehr, K.A., Quigg, A., Guo, L., Gong, G.-C., Pinckney, J.L., Long, R.A., Wei, C.-L., 2010. Comparative evaluation of sediment trap and ^{234}Th-derived POC fluxes from the upper oligotrophic waters of the Gulf of Mexico and the subtropical northwestern Pacific Ocean. Marine Chemistry 121, 132-144.

Hung, C.-C., Gong, G.-C., Santschi, P.H., 2012. ^{234}Th in different size classes of sediment trap collected particles from the Northwestern Pacific Ocean. Geochimica et Cosmochimica Acta 91, 60-74.

Ingalls, A.E., Lee, C., Wakeham, S.G., Hedges, J.I., 2003. The role of biominerals in the sinking flux and preservation of amino acids in the Southern Ocean along 170˚W. Deep-Sea Research II 50, 709-734.

Iversen, M.H., Ploug, H., 2010. Ballast minerals and the sinking of carbon flux in the ocean: carbon-specific respiration rates and sinking velocity of marine snow aggregates. Biogeosciences 7, 2613-2624.

Jackson, G.A., 1990. A model of the formation of marine algal flocs by physical coagulation processes. Deep Sea Research A. 37 (8), 1197-1211.

Jackson, G.A., Lochmann, S., 1993. Modeling coagulation of algae in marine ecosystems. In: Buffle, J. and van Leeuwen, H.P. (Eds.), Environmental Particles, vol. 2. Lewis Publisher, Ann Arbor, pp. 387-414.

Jackson, G.A., 1995. TEP and coagulation during a mesocosm experiment. Deep-Sea Research II 42, 215-222.

Jackson, G.A. (Ed.), 2005. Coagulation theory and models of oceanic plankton aggregation. CRC Press, Boca Raton, FL.

Jackson, G.A., Kiørboe, T., 2008. Maximum phytoplankton concentrations in the sea. Limnology and Oceanography 53 (1), 395-399.

Jin, X., Gruber, N., Dunne, J.P., Sarmiento, J.L., Armstrong, R.A., 2006. Diagnosing the contribution of phytoplankton functional groups to the production and export of particulate organic carbon, $CaCO_3$, and opal from global nutrient and alkalinity distributions. Global Biogeochemical Cycles 20, GB2015.

Kahl, L.A., Vardi, A., Schofield, O., 2008. Effects of phytoplankton physiology on export flux. Marine Ecology Progress Series 354, 3-19.

Karakas, G., Nowald, N., Schäfer-Neth, C., Iversen, M., Barkmann, W., Fischer, G., Marchesiello, P., Schlitzer, R., 2009. Impact of particle aggregation on vertical fluxes

of organic matter. Progress in Oceanography 83, 331-341.

Kepkay, P.E., 2000. Colloids and the ocean carbon cycle. In: Wangersky, P. (Ed.), The Handbook of Environmental Chemistry. SpringerVerlag, Berlin/Heidelberg, Heidelberg, pp. 35-56.

King, J., K., 1974. Preserved amino acids from silicified protein in fossil radiolaria. Nature 252, 690-692.

Kiørboe, T., Andersen, K.P., Dam, H.G., 1990. Coagulation efficiency and aggregate formation in marine phytoplankton. Marine Biology 107, 235-245.

Kiørboe, T., Hansen, J.L.S., 1993. Phytoplankton aggregate formation: observations of patterns and mechanisms of cell sticking and the significance of exopolymeric material. Journal of Plankton Research 15, 993-1018.

Kiørboe, T., Lundsgaard, C., Olsen, M., Hansen, J.L.S., 1994. Aggregation and sedimentation process during a spring phytoplankton bloom: a field experiment to test coagulation theory. Journal of Marine Research 52, 197-323.

Kiørboe, T., Tiselius, P., Mitchell-Innes, B., Hansen, J.L.S., Visser, A.W., Mari, X., 1998. Intensive aggregate formation with low vertical flux during an upwelling-induced diatom bloom. Limnology and Oceanography 43 (1), 104-116.

Klaas, C., Archer, D.E., 2002. Association of sinking organic matter with various types of mineral ballast in the deep sea: Implications for the rain ratio. Global Biogeochemical Cycles 16, 1116.

Koch, S., 2007. Growth and calcification of the coccolithophore *Emiliania huxleyi* under different CO_2 concentrations, Institut für Chemie und Biologie des Meeres der Carl von Ossietzky Universität, Oldenburg, Germany.

Kok, D.J., Blomen, L.J.M.J., Westbroek, P., Bijvoet, O.L.M., 1986. Polysaccharide from coccoliths ($CaCO_3$ biomineral): influence on cyrstallization of calcium oxalate monohydrate. European Journal of Biochemistry 158, 167-172.

Kranck, K., Milligan, T.G., 1988. Macroflocs from diatoms: *in situ* photography of particles in Bedford Basin, Nova Scotia. Marine Ecology Progress Series 44, 183-189.

Kriest, I., Evans, G.T., 1999. Representing phytoplankton aggregates in biogeochemical models. Deep-Sea Research II 46, 1841-1859.

Langer, G., Nehrke, G., Thoms, S., Stoll, H., 2009. Barium partitioning in coccoliths of *Emiliania huxleyi*. Geochemica et Cosmochimica Acta 73, 2899-2906.

La Violette, P.E., 1994. Overview of the major forcings and water masses of the western

Mediterranean Sea. In: Violette, P.E. (Ed.), Seasonal and interannual variability of the western Mediterranean Sea. American Geophysical Union, Washington DC, p. 373.

Lee, C., Wakeham, S.G., 1992. Organic matter in the water column – future research challenges. Marine Chemistry 39, 95-118.

Lee, C., Armstrong, R.A., Cochran, J.K., Engel, A., Fowler, S.W., Goutx, M., Masqué, P., Miquel, J.C., Peterson, M., Tamburini, C., Wakeham, S., 2009a. MedFlux: investigations of particle flux in the Twilight Zone. Deep-Sea Research II 56 (18), 1363-1368.

Lee, C., Peterson, M.L., Wakeham, S.G., Armstrong, R.A., Cochran, J.K., Miquel, J.C., Fowler, S.W., Hirschberg, D., Beck, A., Xue, J., 2009b. Particulate organic matter and ballast fluxes measured using time-series and settling velocity sediment traps in the northwestern Mediterranean Sea. Deep-Sea Research II 56 (18), 1420-1436.

Lepore, K., Moran, S.B., Burd, A.B., Jackson, G.A., Smith, J.N., Kelly, R.P., Kaberi, H. Stavrakakis, S., Assimakopoulou, G., 2009. Sediment trap and *in-situ* pump size-fractionated POC/^{234}Th ratios in the Mediterranean Sea and Northwest Atlantic: Implications for POC export. Deep-Sea Research I 56, 599-613.

Leppard, G.G., 1995. The characterization of algal and microbial mucilage and their aggregates in aquatic ecosystems. Science of the Total Environment 165, 103-131.

Li, Y.-H., 2005. Controversy over the relationship between major components of sediment-trap materials and the bulk distribution coefficients of ^{230}Th, ^{231}Pa, and ^{10}Be. Earth and Planetary Science Letters 233, 1-7.

Linschooten, C., van Bleijswijk, J.D.L., van Emberg, P.R., de Vrind, J.P.M., Kempers, E.S., Westbroek, P., de Vrind-de Jong, E.W., 1991. Role of the light-dark cycle and medium composition on the production of coccoliths by *Emiliania huxleyi* (Haptophyceae). Journal of Phycology 27, 82-86.

Liu, Z., Stewart, G., Cochran, J.K., Lee, C., Armstrong, R.A., Hirschberg, D.J., Gasser, B., Miquel, J.-C., 2005. Why do POC concentrations measured using Niskin bottle collections differ from those using *in situ* pumps? Deep-Sea Research I 52, 1324-1344.

Liu, Z., Lee, C., Wakeham, S.G. 2006. Effects of mercuric chloride and protease inhibitors on degradation of particulate organic matter from the diatom *Thalassiosira pseudonana*. Organic Geochemistry 37, 1003-1018.

Liu, Z., Mao, J., Peterson, M.L., Lee, C., Wakeham, S.G., Hatcher, P.G., 2009. Characterization of sinking particles from the northwest Mediterranean Sea using advanced solid-state NMR. Geochimica et Cosmochimica Acta 73, 1014-1026.

Livingston, H.D., Cochran, J.K., 1987. Determination of transuranic and thorium isotopes in ocean water: In solution and in filterable particles. Journal of Radioanalytical and

Nuclear Chemistry 115 (2), 299-308.

Logan, B.E., Grossart, H.-P., Simon, M., 1994. Direct observation of phytoplankton, TEP, and aggregates on polycarbonate filters using brightfield microscopy. Journal of Plankton Research 16 (12), 1811-1815.

Logan, B.E., Passow, U., Alldredge, A.L., Grossart, H.-P., Simon, M., 1995. Rapid formation and sedimentation of large aggregates is predictable from coagulation rates (half-lives) of transparent exopolymer particles (TEP). Deep-Sea Research II 42, 203-214.

Lorenzen, C.J., Welschmeyer, N.A., 1983. The *in situ* sinking rates of herbivore fecal pellets. J. Plankton Res. 5, 929-933.

Luo, S., Ku, T.-L., 2004. On the importance of opal, carbonate, and lithogenic clays in scavenging and fractionating ^{230}Th, ^{231}Pa and ^{10}Be in the ocean. Earth and Planetary Science Letters 220, 201-211.

Maiti, K., Benitez-Nelson, C.R., Buesseler, K.O., 2010. Insights into particle formation and remineralization using the short-lived radionuclide, Thorium-234. Geophysical Research Letters 37, L15608.

Mantoura, R.F.C., Llewellyn, C.A., 1983. Trace enrichment of marine algal pigments for use with HPLC-diode array spectroscopy. Journal of High-Resolution Gas Chromotography and Chromotography Communications 7, 632-635.

Mari, X., 2008. Does ocean acidification induce an upward flux of marine aggregates? Biogeosciences 5, 1023-1031.

Martin, J.H., Knauer, G.A., Karl, D.M., Broenkow, W.W., 1987. VERTEX: Carbon cycling in the northeast Pacific. Deep-Sea Research 34, 267-285.

Martín, J., Palanques, A., Puig, P., 2006. Composition and variability of downward particulate matter fluxes in the Palamós submarine canyon (NW Mediterranean). Journal of Marine Systems 60, 75-97.

Martín, J., Sanchez-Cabeza, J.A., Eriksson, M., Lévy, I., Miquel, J.C., 2009. Recent accumulation of trace metals in sediments at the DYFAMED site (Northwestern Mediterranean Sea). Marine Pollution Bulletin 59, 146-153.

Marty, J.C., Goutx, M., Guigue, C., Leblond, N., Raimbault, P., 2009. Short-term changes in particulate fluxes measured by drifting sediment traps during end summer oligotrophic regime in the NW Mediterranean Sea. Biogeosciences 6 (5), 887-899.

Marty, J.C., Chiavérini, J., 2010. Hydrological changes in the Ligurian Sea (NW Mediterranean, DYFAMED site) during 1995-2007 and biogeochemical consequences. Biogeosciences Discussions 7, 1377-1406.

McCave, I.N., 1975. Vertical flux of particles in the ocean. Deep-Sea Research 22, 491-502.

McCave, I.N., 1984. Size spectra and aggregation of suspended particles in the deep ocean. Deep-Sea Research 31 (4), 329-352.

McCave, I.N., Hall, I.R., Antia, A.N., Chou, L., Dehairs, F., Lampitt, R.S., Thomsen, L., van Weering, T.C.E., Wollast, R., 2001. Distribution, composition and flux of particulate material over the European margin at 47˚-50˚N. Deep-Sea Research II 48, 3107-3139.

McDonnell, A.M.P., Buesseler, K.O., 2010. Variability in the average sinking velocity of marine particles. Limnology and Oceanography 55 (5), 2085-2096.

Millot, C., 1999. Circulation in the Western Mediterranean Sea. Journal of Marine Systems 20, 432-442.

Miquel, J.C., Fowler, S.W., La Rosa, J., Buat-Menard, P., 1994. Dynamics of the downward flux of particles and carbon in the open northwestern Mediterranean Sea. Deep-Sea Research I 41, 243-261.

Miquel, J.-C., Martín, J., Gasser, B., Rodriguez y Baena, A., Toubal, T., Fowler, S.W., 2011. Dynamics of particle flux and carbon export in the northwestern Mediterranean Sea: A two decade time-series study at the DYFAMED site. Progress in Oceanography 91, 461-481.

Moore, W. S., 1969. Measurement of ^{228}Ra and ^{228}Th in seawater. Journal of Geophysical Research 74, 694-704.

Mopper, K., Zhou, J., Ramana, K.S., Passow, U., Dam, H.G., Drapeau, D.T., 1995. The role of surface-active carbohydrates in the flocculation of a diatom bloom in a mesocosm. Deep-Sea Research II 41, 47-73.

Moran, S.B., Charette, M.A., Pike, S.M., Wicklund, C.A., 1999. Differences in seawater particulate organic carbon concentration in samples collected using small-volume and large-volume methods: the importance of DOC adsorption to the filter blank. Marine Chemistry 67, 33-42.

Moran, S.B., Weinstein, S.E., Edmonds, H.N., Smith, J.N., Kelly, R.P., Pilson, M.E.Q., Harrison, W.G., 2003. Does ^{234}Th/^{238}U disequilibrium provide an accurate record of the export flux of particulate organic carbon from the upper ocean? Limnology and Oceanography 48, 1018-1029.

Morris, R.J., Bone, Q., Head, R., Braconnot, J.C., Nival, P., 1988. Role of salps in the flux of organic matter to the bottom of the Ligurian Sea. Marine Biology 97 (2), 237-241.

Müller, M.N., Antia, A.N., LaRoche, J., 2008. Influence of cell cycle phase on calcification in the coccolithophore *Emiliania huxleyi*. Limnology and Oceanography 53 (2), 506-512.

Murnane, R.J., Cochran, J. K., Buesseler, K.O., Bacon, M. P., 1996. Least-squares estimates of thorium, particle, and nutrient cycling rate constants from the JGOFS North Atlantic Bloom Experiment. Deep-Sea Research I 43, 239-258.

Myklestad, S.M., 1995. Release of extracellular products by phytoplankton with special emphasis on polysaccharides. Science of the Total Environment 165, 155-164.

Obernosterer, I., Herndl, G.J., 1995. Phytoplankton extracellular release and bacterial growth: dependence on the inorganic N:P ratio. Marine Ecology Progress Series 116, 247-257.

O'Melia, C.R., Tiller, C.L. (Eds.), 1993. Physicochemical aggregation and deposition in aquatic environments. Lewis Publishers, Boca Raton, FL.

Paasche, E., 1998. Roles of nitrogen and phosphorus in coccolith formation in *Emiliania huxleyi* (Prymnesiophyceae). European Journal of Phycology 33, 33-42.

Paasche, E., 2002. A review of the coccolithophorid *Emiliania huxleyi* (Prymnesiophyceae), with particular reference to growth, coccolith formation, and calcification–photosynthesis interactions. Phycologia 40, 503-529.

Panagiotopoulos, C., Sempéré, R., Lafont, R., Kerhervé, P., 2001. Sub-ambient temperature effects on separation of monosaccharides by HPAEC-PAD. Application to marine chemistry. Journal of Chromatography A 920, 13-22.

Passow, U., Alldredge, A.L., 1994. Distribution, size and bacterial colonization of transparent exopolymer particles (TEP) in the ocean. Marine Ecology Progress Series 113, 185-198.

Passow, U., Alldredge, A.L., 1995a. Aggregation of a diatom bloom in a mesocosm: The role of transparent exopolymer particles (TEP). Deep-Sea Research II 42 (1), 99-109.

Passow, U., Alldredge, A.L., 1995b. A dye-binding assay for the spectrophotometric measurement of transparent exopolymer particles (TEP). Limnology and Oceanography 40, 1326-1335.

Passow, U., 2002. Transparent exopolymer particles (TEP) in aquatic environments. Progress in Oceanography 55, 287-333.

Passow, U., 2004. Switching perspectives: do mineral fluxes determine particulate organic carbon fluxes or vice versa? Geochemistry Geophysics Geosystems 5, Q04002.

Passow, U., De La Rocha, C.L., 2006. Accumulation of mineral ballast on organic aggregates. Global Biogeochemical Cycles 20, GB1013.

Passow, U., Dunne, J., Murray, J.W., Balistrieri, L., Alldredge, A.L., 2006. Organic carbon to ^{234}Th ratios of marine organic matter. Marine Chemistry 100 (3-4), 323-336.

Penna, A., Berluti, S., Magnani, M., 1999. Influence of nutrient ratios on the *in vitro* extracellular polysaccharide production by marine diatoms from the Adriatic Sea. Journal of Plankton Research 21, 1681-1690.

Peterson, M.L., Hernes, P.J., Thoreson, D.S., Hedges, J.I., Lee, C., Wakeham, S.G., 1993. Field evaluation of a valved sediment trap. Limnology and Oceanography 38, 1741-1761.

Peterson, M.L., Wakeham, S.G., Lee, C., Askea, M., Miquel, J.C., 2005. Novel techniques for collection of sinking particles in the ocean and determining their settling rates. Limnology and Oceanography Methods 3, 520-532.

Peterson, M.L., Fabres, J., Wakeham, S.G., Lee, C., Miquel, J.C., 2009. Sampling the vertical flux in the upper water column using a large diameter free-drifting NetTrap adapted to an indented rotating sphere settling velocity sediment trap. Deep-Sea Research II 56, 1547-1557.

Pilskaln, C.H., Lehmann, C., Paduan, J.B., Silver, M.W., 1998. Spatial and temporal dynamics in marine aggregate abundance, sinking rate and flux: Monterey Bay, central California. Deep-Sea Research II 45, 1803-1837.

Pitcher, G.C., Walker, D.R., Mitchell-Innes, B.A., Moloney, C.L., 1991. Short-term variability during an Anchor station study in the southern Benguela upwelling system: phytoplankton dynamics. Progress in Oceanography 28, 39-64.

Pruppacher, H.R., Klett, J.D. (Eds.), 1980. Microphysics of Clouds and Preciptation. D. Riedel Publishing Co., Boston, pp. 734.

Quigley, M.S., Santschi, P.H., Hung, C.-C., Guo, L., Honeyman, B.D., 2002. Importance of acid polysaccharides for ^{234}Th complexation onto marine organic matter. Limnology and Oceanography 47, 367-377.

Riebesell, U., Wolf-Gladrow, D.A., 1992. The relationship between physical aggregation of phytoplankton and particle flux: a numerical model. Deep-Sea Research 39 (7/8), 1085-1102.

Riegman, R., Stolte, W., Noordeloos, A.A.M., Slezak, D., 2000. Nutrient uptake and alkaline phosphatase (ec 3:1:3:1) activity of *Emiliania huxleyi* (PRYMNESIOPHYCEAE) during growth under N and P limitation in continuous cultures. Journal of Phycology 36, 87-96.

Riemann, F., 1989. Gelatinous phytoplankton detritus aggregates on the Atlantic deep-sea bed: Structure and mode of formation. Marine Biology 100, 533-539.

Rodriguez y Baena, A.M., Fowler, S.W., and J.C. Miquel, 2007. Particulate organic carbon: natural radionuclide ratios in zooplankton and their freshly produced fecal pellets from the NW Mediterranean (MedFlux 2005). Limnology and Oceanography 52 (3), 966-974.

Roy-Barman, M., Coppola, L., Souhaut, M., 2002. Thorium isotopes in the western Mediterranean Sea: an insight into the marine particle dynamics. Earth and Planetary Science Letters 196, 161-174.

Rutgers van der Loeff, M.M., Buesseler, K.O., Bathmann, U., Hense, I., Andrews, J., 2002. Comparison of carbon and opal export rates between summer and spring bloom periods in the region of Antarctic Polar Front, SE Atlantic. Deep-Sea Research II 49 (18), 3849-3870.

Rutgers van der Loeff, M., Sarin, M.M., Baskaran, M., Benitez-Nelson, C., Buesseler, K.O., Charette, M., Dai, M., Gustafsson, O., Masqué, P., Morris, P.J., Orlandini, K., Rodriguez y Baena, A., Savoye, N., Schmidt, S., Turnewitsch, R., Vöge, I., Waples, J.T., 2006. A review of present techniques and methodological advances in analyzing ^{234}Th in aquatic systems. Marine Chemistry 100, 190-212.

Sadeghi, A., Dinter, T., Vountas, M., Taylor, B., Altenburg-Soppa, M., Bracher, A., 2012. Remote sensing of coccolithophore blooms in selected oceanic regions using the PhytoDOAS method applied to hyper-spectral satellite data. Biogeosciences 9, 2127-2143.

Santschi, P.H., Murray, J.W., Baskaran, M., Benitez-Nelson, C.R., Guo, L.D., Hung, C.-C., Lamborg, C., Moran, S.B., Passow, U., Roy-Barman, M. 2006. Thorium speciation in seawater. Marine Chemistry 100, 250-268.

Savoye, N., Benitez-Nelson, C., Burd, A.B., Cochran, J.K., Charette, M., Buesseler, K.O., Jackson, G.A., Roy-Barman, M., Schmidt, S., Elskens, M., 2006. ^{234}Th sorption and export models in the water column: A review. Marine Chemistry 100 (3-4), 234-249.

Savoye, N., Trull, T.W., Jacquet, S.H.M., Navez, J., Deharis, F., 2008. ^{234}Th-based export fluxes during a natural iron fertilization experiment in the Southern Ocean (KEOPS). Deep-Sea Research II 55, 841-855.

Schmidt, S., Andersen, V., Belviso, S., Marty, J.-C., 2002. Strong seasonality in particle dynamics of north-western Mediterranean surface waters as revealed by ^{234}Th/^{238}U. Deep-Sea Research I 49 (8), 1507-1518.

Schröder, K., Gasparini, G.P., Tangherlini, M., Astraldi, M., 2006. Deep and intermediate water in the western Mediterranean under the influence of the Eastern

Mediterranean Transient. Geophysical Research Letters 33, L21607.

Sheridan, C.C., Lee, C., Wakeham, S.G., Bishop, J.K.B., 2002. Suspended particle organic composition and cycling in surface and midwaters of the equatorial Pacific Ocean. Deep-Sea Research I 49 (11), 1983-2008.

Siegel, D.A., Deuser, W.G., 1997. Trajectories of sinking particles in the Sargasso Sea: modeling of statistical funnels above deep-ocean sediment traps. Deep-Sea Research I 44, 1519-1541.

Silver, M.W., Gowing, M.M., 1991. The particle flux and biological components. Progress in Oceanography 26, 75-113.

Smetacek, V., Pollehne, F., 1986. Nutrient cycling in pelagic systems: a reappraisal of the conceptual framework. Ophelia 26, 401-428.

Smith, J.N., Moran, S.B., Speicher, E.A., 2006. On the accuracy of upper ocean particulate organic carbon export fluxes estimated from $^{234}Th/^{238}U$ disequilibrium. Deep-Sea Research I 53 (5), 860-868.

Smith, R.O., Bryden, H.L., Stansfield, K., 2008. Observations of new western Mediterranean deep water formation using Argo floats 2004-2006. Ocean Science 4, 133-149.

Soloviev, A.V., Vershinsky, N.V., Bezverchnii, V.A., 1988. Small scale turbulence measurements in the thin surface layer of the ocean. Deep-Sea Research 35, 1859-1874.

Somasundaran, P., 2006. Encyclopedia of Surface and Colloid Science. vol. 6, CRC: Taylor & Francis Group, New York, pp. 6675.

Speicher, E.A., Moran, S.B., Burd, A.B., Delfanti, R., Kaberi, H., Kelly, R.P., Papucci, C., Smith, J.N., Stavrakakis, S., Torricelli, L., Zervakis, V., 2006. Particulate organic carbon export fluxes and size-fractionated POC/^{234}Th ratios in the Ligurian, Tyrrhenian and Aegean Seas. Deep-Sea Research I 53, 1810-1830.

Spencer, D. W., Brewer, P. G., Fleer, A., Honjo, S., Krishnaswami, S., Nozaki, Y. 1978. Chemical fluxes from a sediment trap experiment in the deep Sargasso Sea. Journal of Marine Research 36, 493-523.

Staats, N., Stal, L.J., Mur, L.R. , 2000. Exopolysaccharide production by the epipelic diatom *Cylindrotheca closterium*: effects of nutrient conditions. Journal of Experimental Marine Biology and Ecology 249, 13-27.

Steinberg, D.K., Van Mooy, B.A.S., Buesseler, K.O., Boyd, P.W., Kobari, T., Karl, D.M., 2008. Bacterial vs. zooplankton control on sinking particle flux in the ocean's twilight zone. Limnology and Oceanography. 53 (4), 1327-1338.

Stemmann, L., 1998. Particulate matter spatio-temporal analysis using a new video system, in the north-western Mediterranean Sea. Influence of biological production, terrigenous inputs and hydro-dynamical forcings. Ph.D. Thesis, Universite d'Oceanologie Biologie, Paris, France.

Stemmann, L., Gorsky, G., Marty, J.-C., Picheral, M., Miquel, J.-C., 2002. Four-year study of large-particle vertical distribution (0-1000m) in the NW Mediterranean in relation to hydrology, phytoplankton, and vertical flux. Deep-Sea Research II 49 (11), 2143-2162.

Stewart, G., Cochran, J.K., Xue, J., Lee, C., Wakeham, S.G., Armstrong, R.A., Masqué, P., Miquel, J.C, 2007a. Exploring the connection between ^{210}Po and organic matter in the northwester Mediterranean. Deep-Sea Research I 54, 415-427.

Stewart, G., Cochran, J.K., Miquel, J.C., Masqué, P., Szlosek, J., Rodriguez y Baena, A.M., Fowler, S.W., Gasser, B., Hirschberg, D.J., 2007b. Comparing POC export from ^{234}Th/^{238}U and ^{210}Po/^{210}Pb disequilibria with estimates from sediment traps in the northwest Mediterranean. Deep-Sea Research I 54, 1549-1570.

Stewart, G.M., Fisher, N.S., 2003. Bioaccumulation of polonium-210 in marine copepods. Limnology and Oceanography 48, 2011-2019.

Suess, E., 1980. Particulate organic carbon flux in the oceans–surface productivity and oxygen utilization. Nature 288, 260-263.

Swift, D.M., Wheeler, P., 1991. Evidence of an organic matrix from diatom biosilica. Journal of Phycology 28, 202-209.

Szlosek, J., Cochran, J.K., Miquel, J.C., Masqué, P., Armstrong, R.A., Fowler, S.W., Gasser, B., Hirschberg, D.J., 2009. Particulate organic carbon–^{234}Th relationships in particles separated by settling velocity in the northwest Mediterranean Sea. Deep-Sea Research II 56, 1519-1532.

Trull, T., Buesseler, K., Bray, S., Moy, C., Ebersbach, F., Lamborg, C., Pike, S., Manganini, S., 2008. *In-situ* measurement of mesopelagic particle sinking rates and the control of carbon transfer to the ocean interior during the Vertical Flux in the Global Ocean (VERTIGO) voyages in the North Pacific. Deep-Sea Research II 55 (14-15), 1684-1695.

van der Wal, P., de Jong, E.W., Westbroek, P., de Bruijn, W.C., Mulder-Stapel, A.A., 1983. Ultrastructural polysaccharide localization in calcifying and naked cells of the coccolithophorid *Emiliania huxleyi*. Protoplasma 118, 157-168.

van Duuren, F.A., 1968. Defined velocity gradient model flocculator. Journal of the Sanitary Engineering Division: Proceedings of the American Society of Civil Engineers 94,

671-682.

Verdugo, P., Alldredge, A.L., Azam, F., Kirchman, D.L., Passow, U., Santschi, P.H., 2004. The oceanic gel phase: a bridge in the DOM-POM continuum. Marine Chemistry 92, 67-85.

Verdugo, P., Santschi, P.H., 2010. Polymer dynamics of DOC networks and gel formation in seawater. Deep-Sea Research II 57, 1486-1493.

Vieira, A.A.H., Ortolano, P. I. C., Giroldo, D., Oliveira, M. J. D., Bittar, T. B., Lombardi, A. T., Sartori, A. L., Paulsen, B. S., 2008. Role of hydrophobic extracellular polysaccharide of *Aulacoseira granulata* (Bacillariophyceae) on aggregate formation in a turbulent and hypereutrophic reservoir. Limnology and Oceanography 53, 1887-1899.

Waite, A.M., Hill, P.S., 2006. Flocculation and phytoplankton cell size can alter ^{234}Th-based estimates of the vertical flux of particulate organic carbon in the sea. Marine Chemistry 100 (3-4), 366-375.

Wakeham, S.G., Lee, C., 1993. Production, transport, and alteration of particulate organic matter in the marine water column. In: Engel, M.H., Macko, S.A. (Eds.), Organic geochemistry. Plenum Press, pp. 145-169.

Wakeham, S.G., Lee, C., Peterson, M.L., Liu, Z., Szlosek, J., Putnam, I., Xue, J., 2009. Organic compound composition and fluxes in the Twilight Zone–time series and settling velocity sediment traps during MedFlux. Deep-Sea Research II 56, 1437-1453.

Waples, J.T., Benitez-Nelson, C., Savoye, N., Rutgers van der Loeff, M., Baskaran, M., Gustafsson, O., 2006. An introduction to the application and future use of ^{234}Th in aquatic systems. Marine Chemistry 100 (3-4), 166-189.

Weilenmann, U., O'Melia, C.R., Stumm, W., 1989. Particle transport in lakes: models and measurements. Limnology and Oceanography 34, 1-18.

Weiner, S., Erez, J., 1984. Organic matrix of the shell of the foraminifer, Heterostegina depressa. Journal of Foraminiferal Research 14, 206-212.

Welschmeyer, N.A., 1982. The dynamics of phytoplankton pigments: Implications for zooplankton grazing and phytoplankton growth. Ph.D. Thesis, University of Washington, Seattle, Washington, 176 p.

Welschmeyer, N.A., Lorenzen, C.J., 1984. Carbon-14 labeling in phytoplankton carbon and chlorophyll *a* carbon: Determination of specific growth rates. Limnology and Oceanography 29, 135-145.

Welschmeyer, N.A., Lorenzen, C.J., 1985. Chlorophyll budgets: Zooplankton grazing and phytoplankton growth in a temperate fjord and the Central Pacific Gyres. Limnology

and Oceanography 30, 1-21.

Wurl, O., Holmes, M., 2008. The gelatinous nature of sea-surface microlayer. Marine Chemistry 110, 89-97.

Xue, J., Armstrong, R.A., 2009. An improved "benchmark" method for estimating particle settling velocities from time-series sediment trap fluxes. Deep-Sea Research II 56, 1479-1486.

Xue, J., Lee, C., Wakeham, S.G., Armstrong, R.A., 2011. Using principal components analysis (PCA) with cluster analysis to study the organic geochemistry of sinking particles in the ocean. Organic Geochemistry 42 (4), 356-367.

Yoon, W.D., Marty, J.-C., Sylvain, D., Nival, P., 1996. Degradation of faecal pellets in *Pegea confoederata* (*Salpidae, Thaliacea*) and its implication in the vertical flux of organic matter. Journal of Experimental Marine Biology and Ecology 203, 147-177.

APPENDIX

Appendix A

Chapter 3

Hydrography at the DYFAMED site during the 2005 MedFlux expedition

Important water masses at the DYFAMED site during the MedFlux sampling include Atlantic Water (AW; 0–200 m), Levantine Intermediate Water (LIW; 400–600 m) and Western Mediterranean Deep Water (WMDW). In addition, the depth zone of 100–200 m is often characterized by Modified Atlantic Water (MAW). The MAW is relatively warm (14–15˚C), but temperatures can be variable distinguished by its characteristic eastward motion and susceptibility to physical mixing and air-sea interactions. At the Strait of Gibraltar, AW starts with a salinity of ~36.5-37.5 PSU and as it moves eastward as MAW its salinity increases (38.0–38.3 PSU; Millot, 1999; Smith et al. 2008). MAW is difficult to identify especially during the long mixing periods of the winter (Dec –May) while in the Ligurian subbasin adjacent to the westward flowing Northern Current (NC; Millot, 1999). The distinction between water masses becomes muted due to strong northwesterly winds advecting and mixing in water from the North Current (Béthoux et al. 1988, Millot, 1999). This water mass is sometimes referred to as the Western Intermediate Water (WIW; Millot, 1999). We observe that the MAW transitioned to the WIW at 60 m for all sampling dates in March (Fig. 3.A2). The underlying WIW originates around 60 m and persists to ~150 m on 9 March 2005 and to ~200 m on 13, 14 March (Fig. 3.A2a-c). In general the data show a weak density gradient and thermocline within the depth range of 200-300 m (Fig. 3.A2a-c).

Underlying the zone of convergence for the MAW and WIW is the LIW, typically between 400-600 m. The LIW has a potential temperature of ~13.2˚C and salinities 38.45-38.75 PSU. All of the water masses within the upper 600 m can be homogenized due to violent mixing resulting from wind induced density instability of the water column (Marty and Chiavérini, 2010). We see evidence of this on 13 - 14 March 2005 (Fig. 3.A2b, c). Below the salinity maximum (~38.6 PSU), presumably the LIW core, we see a strong density gradient after which temperature and salinity decrease (Fig. 3.A2). The WMDW, formed from the deep convection of the AW and LIW, lies within the western basin centered at ~2000 m (Smith et al. 2008, La Violette 1994).

Table 3.A1. Sample collection dates and depths

Year	Sample Collection Method	Date sampled	Depths sampled (m)
2005	SV1	4 March-28 April	524, 1918
	SV2	"	313, 524, 924, 1918
	TS	"	313, 924
	pump	9 March	2, 25, 60, 100, 150, 200, 300, 350, 400, 600, 800, 1200, 1500, 1800
	pump	14 March	5, 25, 50, 75, 100, 150, 200, 300, 350, 400, 500, 600, 800, 900
	pump	30 April	0, 25, 35, 50, 75, 100, 125, 150, 200, 300, 500, 750

Table 3.A1. Dates and depths sampled at DYFAMED spring 2005 by IRSC sediment trap (settling velocity and time series mode) and *in situ* pumps.

Table 3.A2. Settling Velocity sediment trap POC/^{234}Th and compound ratios

Depth (m)	Trap ID	Settling Velocity class (m d^{-1})	POC/^{234}Th† (µmol dpm^{-1})			fuco : Chl a	phytin : Chl a	(phide + pyro) : Chl a
313	SV2	0.68-5.4	1.02	±	0.04	0.00	4.09	6.2
		5.4-11	1.59	±	0.18	1.15	0.95	8.1
		11-22	2.22	±	0.23	1.17	0.89	7.2
		22-49	1.42	±	0.13	1.10	0.88	8.7
		49-98	1.64	±	0.12	0.87	0.79	7.7
		98-140	1.26	±	0.11	0.74	0.65	5.9
		140-196	1.21	±	0.10	1.13	0.87	9.0
		196-326	1.04	±	0.05	0.95	0.80	6.7
		326-490	0.93	±	0.05	1.05	1.05	8.1
		490-980	1.32	±	0.07	1.08	0.96	8.0
		>980	1.82	±	0.22	1.03	0.95	7.5
		Weighted Avg	**2.76**	**±**	**0.10**	**0.83**	**1.49**	**7.39**
524	SV1	0.68-5.4	0.92	±	0.04	0.95	0.85	3.9
		5.4-11	0.88	±	0.02	0.97	1.12	5.6
		11-22	1.09	±	0.03	1.08	0.79	7.4
		22-49	0.93	±	0.03	0.69	0.88	6.0
		49-98	1.18	±	0.05	1.46	0.79	8.9
		98-140	1.16	±	0.06	0.00	1.13	6.0
		140-196	1.12	±	0.05	0.00	0.94	6.6
		196-326	1.38	±	0.07	0.00	0.77	6.2
		326-490	1.41	±	0.08	1.18	0.93	7.1
		490-980	1.04	±	0.05	0.00	0.72	7.4
		>980	0.85	±	0.03	1.12	1.03	6.0
		Weighted Avg	**0.99**	**±**	**0.02**	**0.55**	**0.85**	**6.30**
	SV2	0.68-5.4	1.48	±	0.10	1.03	0.05	2.6
		5.4-11	1.02	±	0.03	0.00	9.12	4.8
		11-22	0.83	±	0.03	1.00	0.28	4.1
		22-49	0.84	±	0.03	1.24	0.98	8.6
		49-98	1.11	±	0.05	1.28	1.21	8.7
		98-140	1.00	±	0.05	1.09	0.79	4.4
		140-196	0.73	±	0.03	1.28	0.61	4.6
		196-326	0.80	±	0.03	1.23	0.91	5.3
		326-490	0.85	±	0.04	0.00	0.84	7.4
		490-980	1.79	±	0.09	1.48	1.08	9.4
		>980	0.85	±	0.02	1.20	1.16	6.4
		Weighted Avg	**0.93**	**±**	**0.02**	**1.04**	**0.93**	**6.11**

Continued

Depth (m)	Trap ID	Settling Velocity class (m d^{-1})	POC/^{234}Th† (µmol dpm^{-1})			fuco : Chl a	phytin : Chl a	(phide + pyro) : Chl a
1918	SV1	0.68-5.4	1.13	±	0.06	0.94	1.08	3.0
		5.4-11	0.46	±	0.01	0.80	1.04	5.9
		11-22	0.43	±	0.01	0.99	0.90	5.9
		22-49	0.40	±	0.01	1.01	1.02	7.3
		49-98	0.49	±	0.02	0.00	1.52	10.1
		98-140	0.69	±	0.03	1.47	1.01	8.7
		140-196	0.50	±	0.02	0.00	1.53	7.0
		196-326	0.51	±	0.02	0.00	1.35	10.2
		326-490	0.66	±	0.04	0.00	1.18	8.7
		490-980	0.75	±	0.04	0.00	1.51	6.9
		>980	0.44	±	0.01	0.97	1.06	7.6
		Weighted Avg	**0.50**	**±**	**0.01**	**0.29**	**1.29**	**7.50**
	SV2	0.68-5.4	1.38	±	0.15	0.00	2.52	7.21
		5.4-11	0.45	±	0.01	1.09	1.27	5.77
		11-22	0.45	±	0.01	1.16	1.15	4.96
		22-49	0.40	±	0.01	0.87	1.37	6.00
		49-98	0.35	±	0.01	0.00	1.04	6.60
		98-140	0.30	±	0.01	0.96	0.85	7.19
		140-196	0.56	±	0.02	0.00	1.68	8.10
		196-326	0.61	±	0.03	0.00	1.77	7.79
		326-490	0.58	±	0.03	0.00	1.99	7.77
		490-980	0.56	±	0.02	0.00	0.68	5.15
		>980	0.40	±	0.01	0.97	1.26	7.62
		Weighted Avg	**0.44**	**±**	**0.01**	**0.19**	**1.50**	**6.89**

Table 3.A2. Settling velocity sediment trap POC/^{234}Th and pigment compound ratios.

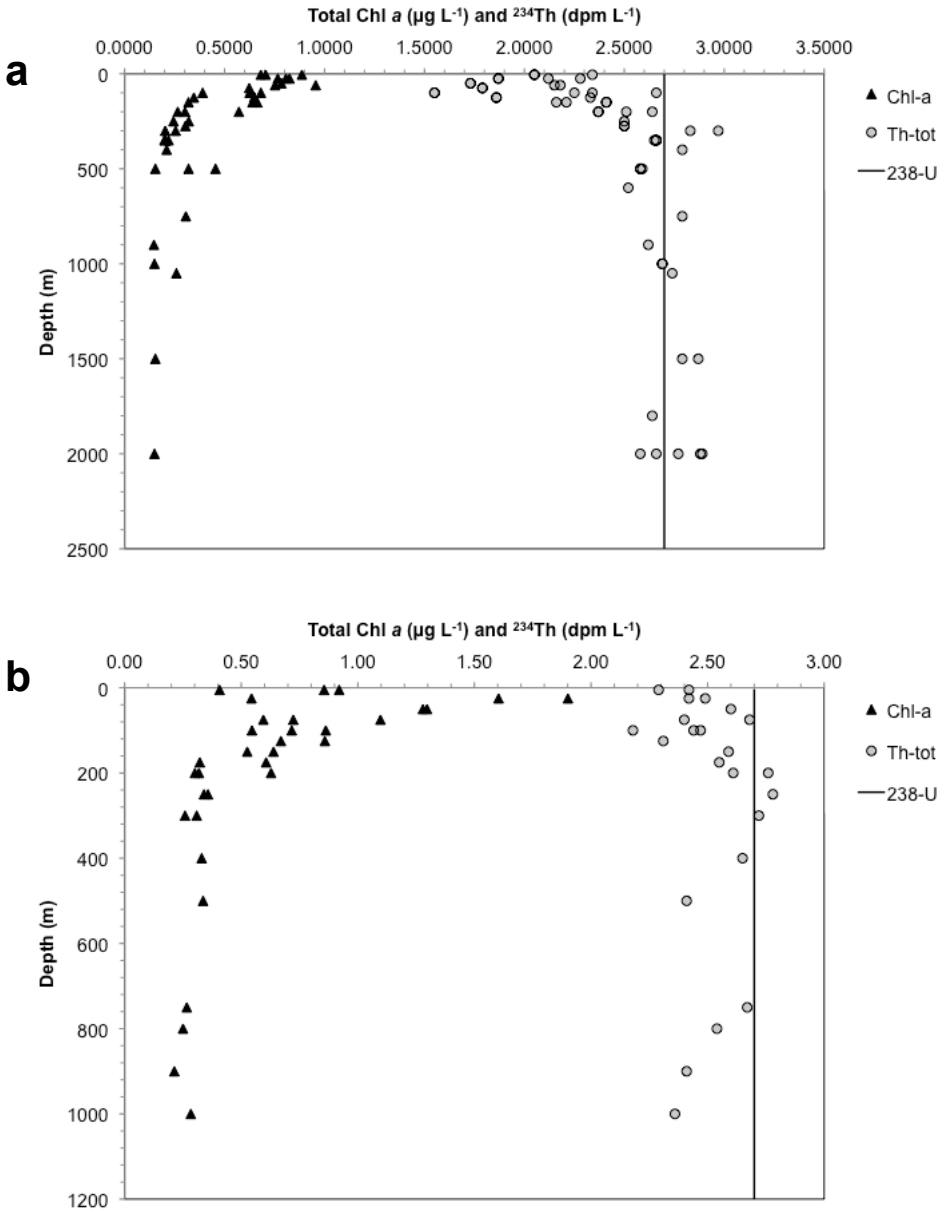

Fig. 3.A1. Depth profiles for chlorophyll-*a* (µg l^{-1}) and total ^{234}Th activity (dpm l^{-1}) plotted versus depth in (a) 9, 11 March and (b) 13, 14 March.

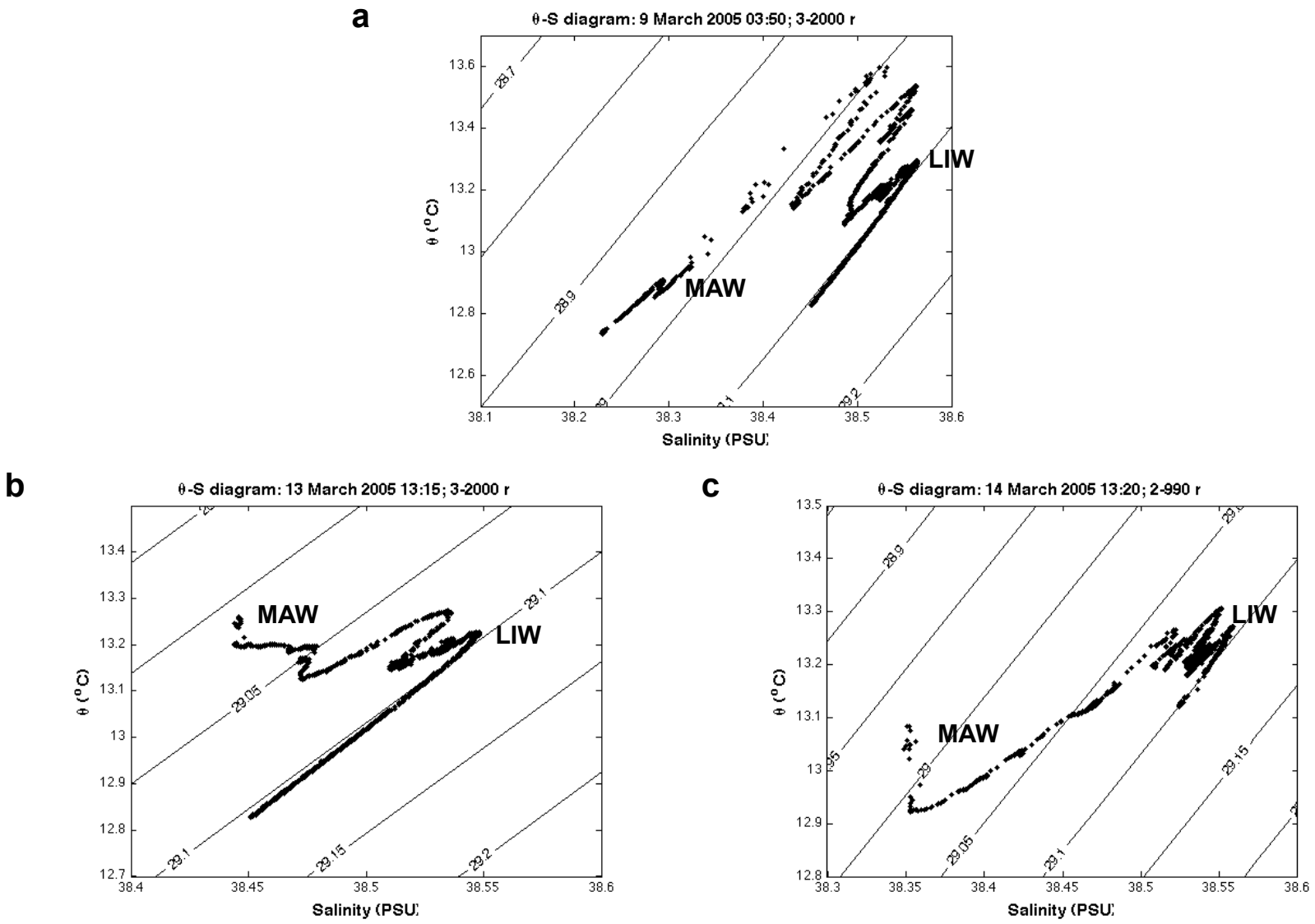
a
θ-S diagram: 9 March 2005 03:50; 3-2000 r
LIW
MAW
θ (°C)
Salinity (PSU)
b
θ-S diagram: 13 March 2005 13:15; 3-2000 r
MAW
LIW
θ (°C)
Salinity (PSU)
c
θ-S diagram: 14 March 2005 13:20; 2-990 r
LIW
MAW
θ (°C)
Salinity (PSU)

Figure 3.A2. θ-S plots based on CTD cast data for sampling days at the time of sediment trap deployment and retrieval: (a) 9 March, (b) 13 March, (c) 14 March.

References

Béthoux, J.P., Prieur, L., and Bong, J.-H., 1988. The Ligurian current off the French Riviera. Oceanologica Acta SP, 59-67.

La Violette, P.E., 1994. Overview of the major forcings and water masses of the western Mediterranean Sea. In: Violette, P.E. (Ed.), Seasonal and interannual variability of the western Mediterranean Sea. American Geophysical Union, Washington DC, p. 373.

Marty, J.C., Chiavérini, J., 2010. Hydrological changes in the Ligurian Sea (NW Mediterranean, DYFAMED site) during 1995-2007 and biogeochemical consequences. Biogeosciences Discussions 7, 1377-1406.

Millot, C., 1999. Circulation in the Western Mediterranean Sea. Journal Marine of Systems 20, 423-442.

Smith, R.O., Bryden, H.L., Stansfield, K., 2008. Observations of new western Mediterranean deep water formation using Argo floats 2004-2006. Ocean Science 4, 133-149.

APPENDIX B

Chapter 4

Coagulation theory–coagulation kernel

The equation for the rectilinear version of the laminar shear coagulation kernel for particles with *i* and *j* elemental particles having radii of r_i and r_j, respectively, is

$$\beta_{ij} = \frac{4}{3}\sqrt{\frac{\epsilon}{\gamma}}(r_i + r_j)^3 \tag{4.A1}$$

where ε is the turbulence kinetic energy dissipation rate ($m^2\ s^{-3}$) and γ is the kinematic viscosity ($m^2\ s^{-1}$). The shear rate equals $\sqrt{(\varepsilon/\gamma)}$. Rewriting Eq. 4.A1 in terms of mean shear rate, $\overline{G}$ (s^{-1}), and diameter (*d*) we have

$$\beta_{ij} = \frac{4}{3}\overline{G}(d_i/2 + d_j/2)^3 \tag{4.A2}$$

where $\overline{G}$ is the laminar flow in the annular space between Couette Chamber cylinders and is given by:

$$\overline{G} = 4\pi\omega \cdot r_2 r_1 \left(r_2^2 - r_1^2\right)^{-1} \tag{4.A3}$$

where ω is the angular velocity (s^{-1}) and r_1 and r_2 are the inner and outer radii, respectively (van Duuren, 1968).

For the case of a monodisperse system $d_i = d_j = d_1$, the diameter of the elemental particle, a cell Eq. 4.A2 reduces to

$$\overline{\beta}_{ij} = \overline{\beta}_{11} = 8 \cdot \overline{G} \cdot \frac{1}{6}\overline{d}_1^3. \tag{4.A4}$$

Using Eq. 4.A4, the coagulation rate $\overline{\beta}_{11}\overline{C}_{1,t\to 0}$ from Eq. 1 can be put in terms of the solid volume fraction, $\sum_{i=1}^{\infty}\overline{V}_{1,initial}$ or Φ (ppm) and is expressed as

$$\beta_{11}\overline{C}_1(t\to 0) = 8{\cdot}\overline{G}{\cdot}\frac{1}{6}\overline{d}_1^3{\cdot}\overline{C}_{1,initial} = \frac{8\overline{G}}{\pi}\left(\frac{1}{6}\pi\overline{d}_1^3 \cdot \overline{C}_{1,initial}\right) = \frac{8\overline{G}}{\pi}\left(\phi \cdot \overline{C}_{1,initial}\right). \tag{4.A5}$$

Estimates of detached coccoliths–comparison of methods

Coccolith detachment was estimated by 3 methods: Coulter Counter PSD, image analysis of microscope samples, and calculations based on Fritz and Balch (1996) (Table 4.A1). The number of free coccoliths in the experiment medium prior to aggregation ranges from ~1

to 17 coccoliths per cell, increasing with decreasing growth rate. The estimates vary depending on the method used, however there is good agreement between estimates for most replicate coagulation experiments (Table 4.A1). The difference in the free coccolith per cell estimates may be explained by the different sources for these samples: Coulter Counter estimates were estimated from PSD of medium used within Couette flow device at a sampling time of 1 min (sampled from the chemostat overflow) and image analysis estimates were determined from size analysis of alcian blue stained microscope samples, which used medium collected at the end of the coagulation experiment.

In addition, the assumptions used to distinguish coccoliths in each technique may have affected the accuracy of each method. The Coulter Counter method and image analysis method likely put an upper and lower limit on the detached coccolith per cell values, respectively. Particles $<x^*_{cut}$ were assumed to be coccoliths in the PSD. It is possible the Coulter Counter method for enumerating free coccoliths might have included other cellular debris. Image analysis samples were limited to tracking those particles (coccoliths, cells, aggregates, etc) that were stained by Alcian blue dye. Thus, it is likely that the dramatic difference in image analysis derived values for experiment day 14 were in part due to low amounts of stainable exopolymer material coating particle surfaces.

In this study, cells were light and nutrient limited, stressors shown to increase coccolith detachment rates (Fritz and Balch, 1996 and Fritz, 1999, respectively). Yet, calculated detached estimates were on the low range of those reported elsewhere for *Emiliania huxleyi* grown as continuous cultures at low growth rates (Fritz and Balch, 1996; Fritz, 1999). According to the Fritz (1999) study, at growth rates of 0.67 to 0.2 d^{-1}, cells experienced coccolith losses of 9 – 27 coccoliths $cell^{-1}$. Additionally, Fritz and Balch (1996) and Fritz (1999) found good agreement between calculated and measured detachment rates. However, for this study, the calculated coccolith detachment per cell values were lower than those measured by Coulter Counter (~1.25× lower) and image analysis samples (~2.5× lower) (Table 4.A1).

The predominant difference between the procedures for assessing coccolith abundance in this study versus that of Fritz and Balch (1996) and Fritz (1999) is the sampling frequency and duration. Coccolith abundances were determined using material from the over flow, not the within the chemostat vessel. Coccolith abundances estimated by Coulter Counter and image analysis were determined on the experiment day only once after the over flow collection period of 1.5 to 3 d (for 0.3 and 0.1 d^{-1} dilution rates, respectively) had ended. Whereas the study conducted by Fritz (1999) measured coccolith each day for 5-10 days at each growth rate and samples were taken from the continuous culture vessel. This may indicate a requisite for accurate coccolith detachment rates for cells of different growth rates is frequent sampling and sampling over a long durations of time, such that the sampling duration minimizes the effect of changing detachment to dilution rate ratios.

We used the Coulter Counter-derived detached coccoliths per cell to determine the relative difference between different experiment days (Table 4.4). Balch et al. (1993) reported that cells lost coccoliths in "modes" respective of the cells current nutrient level and the number of coccoliths layers covering the cell when the cell was actively dividing. It is sufficient for the means of this study to note that the measured and calculated coccolith losses per cell were similar in order of magnitude to one another (Table 4.A1) and within range of those observed in other experiments (Fritz, 1999).

Exploratory data analysis–Gauss model fitting of the PSD

In an attempt to robustly quantify the loss of monomers over the coagulation incubations while representing the characteristic shape and magnitude of the cell peak observed from the Coulter Counter PSD we chose to fit the monomer data to a Gaussian distribution using the likelihood method. Moreover, according to coagulation theory the decrement of total abundance of particles with time should be accompanied by the increase in numbers of particle larger than monomers, starting with dimers, trimers and so forth. Hence we fit double Gaussian curves to the data one centered at the ESD of the monomers (cells) and one centered at the estimated ESD of the dimer (d_i+d_i). Admittedly the time resolution of the evolution of the PSD is not fine enough to capture all dimer formation; however, if significant coagulation occurred an increase in dimers should be evident.

The maximum likelihood method is a statistical technique provides parameter estimates with associated confidence intervals (Edwards, 1992; Hilborn and Mangel, 1997). As per common practice, we employ the use of the logarithm of the likelihood, log(likelihood), which facilitates the comparison of likelihood values that are themselves very small numbers (Edwards, 1992). The maximum likelihood approach prescribes the use of a parameter referred to as the maximum likelihood estimate that reveals the value for the parameters with the most support from the data. As such, finding the maximum likelihood estimate is equivalent to minimizing the negative log(likelihood). The equation used to minimize the negative log(likelihood) is

$$n[log(\sigma) + \frac{1}{2}log(2\pi)] + \sum_{i=1}^{n} \frac{(Y_i - m)^2}{2\sigma^2} \tag{4.A5}$$

where the terms within the sigma are based on a Gaussian error distribution between the predicted values and the data. Y_i represents the error function of the combined two Gaussian peaks, that of the monomer and dimer curves, summing from the largest part of the particle size distribution to a designated cut-off value on the left shoulder of the monomer curve where it is lowest before going up again due to inclusion of cellular debris such as coccoliths (see Fig. 4.A1). The cumulative sum is discretized bin-by-bin with bin designations established by the Coulter Counter. The sum of the data points going from right to left in the PSD are represented as *m*. The number of data points is *n*, representing the number of bins used, and the standard deviation between the predicted double Gaussian peaks and the actual data is σ.

The maximum likelihood analysis was carried using a simulated annealing (SA) algorithm that was a modification of the C program written by R.A. Armstrong for Collier et al. (2012). The model was run for each time point of every experiment separately for individual x_{cut} values that varied between 2.5 and 4.5 μm (n = 8550; 17 experiments, 6 to 9 time points each, 45 different cut off values). To automate the algorithm runs, Bash and Python scripts were written by W.C. Chow and implemented by J.S. Chow. Inputs for a single experiment includes the Coulter Counter derived PSD (mean of 3 runs) for each time point. The model metropolizes on the number concentration data for the Coulter Counter designated bins one time point at a time. Pertinent input values for the SA model run are the estimated lower and upper bounds on the integral probability for the monomer Gaussian distribution and the dimer Gaussian distribution integrating from 60 μm to the

cut-off value, henceforth referred to as M_{tot} and D_{tot}. Additional input parameters include the model for the monomer Gaussian curve (mean μ_{mono}, standard deviation σ_{mono}) and the cut-off value, x_{cut}. The SA method is used to find an acceptable solution in a relatively short period of time optimizing for the parameters M_{tot}, D_{tot}, μ_{mono}, and σ_{mono}. Output for each experiment model run yields the sum of gathered statistics for each time point (optimal M_{tot}, D_{tot}, μ_{mono}, and σ_{mono}) as well as the cumulative sum of number concentration of particles for the Gaussian model results of the monomer distribution. An output value for the Gaussian cumulative sum is reported for each Coulter Counter designated bin from the largest particle class (≥60 μm) to the lowest (≤ cut-off value, x_{cut}).

To get better estimates of parameter values numerous calls were made to the random number generator and the SA model was run 10 times for each experiment. The application of the SA algorithm required ~300 hours of computing time using 38 machines for the 17 number of coagulation experiments. The seed for the random number generator was set to the current time of the system clock time for each run, thus ensuring a unique seed for each model run. An α value was calculated for each experiment where $\sum_{i=1}^{\infty} C_{i,t}$ of each time point was used to estimate *slope* was the Gaussian cumulative sum from the model output. Coagulation efficiency, α, was estimated for each of the 10 runs and then averaged. These values were not significantly different than those obtained using the Coulter Counter PSD data applying x^*_{cut} and $\alpha_{complete}$ (Eq. 6). Overall, the data analysis showed there is a very low signal to noise ratio for the experiments performed here. Yet, the consistent trend in α values with growth rate across experiment years and replicate coagulation experiments suggest this method's utility to look at broad changes in cell coagulation when cell conditions are changed.

Table 4.A1. Detached coccolith per cell estimates

Growth Rate (d^{-1})	Day	Device ID	No. of detached coccoliths per cell		
			Coulter Counter	Image Analysis	Calculated†
0.63 ± 0.03	10	C	NA	NA	NA
		D	NA	NA	NA
0.35 ± 0.00	14	C	7.4	1.2 ± 0.1	5.6
		D	7.0	1.7 ± 0.6	7.3
0.03 ± 0.00	22	C	16.8	5.3 ± 0.6	10.2
		D	17.1	6.1 ± 0.8	9.0
0.12 ± 0.08	25	C	5.9	4.4 ± 0.1	7.3
		D	7.1	7.0 ± 4.9	5.6

NA – not applicable

Table 4.A1. Detached coccoliths per cell estimates determined using Coulter Counter and Alcian blue stained microscope samples (Image Analysis). Detached coccolith volume is the % of total particle volume of $<x^*_{cut}$ particles determined using Coulter Counter data. Data for microscope samples were evaluated by first using the circularity tool and particle sizing to semi-automatically enumerate coccoliths and cells. Cells from experiment day 10 assumed to show little to no loss of coccoliths prior to coagulation experiment. †Day 14, 22, and 25 change in diameter per coccolith was calculated as 0.048 μm and cumulative coccoliths per cell was calculated as 32, except for day 22 Couette flow device C where it was 0.39 μm and 21 coccoliths.

Table 4.A2. Sugar composition

Day	Sample ID	CCHO (µmol C l^{-1})	%Fuc		%Rha		%Ara+GalN		%GlcN		%Gal		%Glc		%Man+Xyl		%Gal-URA+ Glc-URA	
2006, <0.45 µm HMW-dCCHO																		
26	chemostat	15.46	6.26	(0.23)	6.31	(0.12)	14.1	(0.4)	-		14.7	(1.0)	41.3	(1.8)	7.57	(0.55)	9.74	(3.15)
34		36.46	9.37	(0.16)	17.2	(0.1)	14.0	(0.1)	-		21.5	(0.0)	21.4	(0.3)	8.03	(0.22)	8.50	(1.64)
40		47.15	9.91	(0.13)	21.6	(0.2)	16.2	(0.1)	-		23.3	(0.4)	14.6	(0.4)	8.11	(0.27)	6.21	(1.06)
2007, tCCHO																		
10	chemostat	37.44	1.17	(0.01)	5.83	(0.14)	6.28	(0.02)	0.80	(0.03)	9.73	(0.09)	48.3	(0.4)	8.96	(0.04)	19.0	(0.2)
	C	14.38	2.61	(0.04)	38.9	(3.2)	2.37	(0.01)	-		6.37	(0.67)	11.8	(1.1)	5.04	(0.28)	32.9	(8.4)
	D	10.29	2.25	(0.06)	39.9	(3.6)	2.93	(0.34)	-		5.21	(0.44)	13.1	(0.5)	5.61	(0.16)	30.9	(8.0)
14	chemostat	44.92	0.99	(0.01)	1.75	(0.03)	5.74	(0.03)	0.35	(0.01)	4.45	(0.07)	71.3	(0.3)	3.17	(0.01)	12.2	(0.2)
	C	54.14	1.39	(0.01)	7.42	(0.01)	2.12	(0.00)	-		5.40	(0.05)	81.7	(0.8)	1.05	(0.02)	0.97	(0.44)
	D	26.91	1.10	(0.00)	0.67	(0.00)	2.19	(0.00)	-		20.3	(0.0)	73.2	(0.0)	2.49	(0.00)	0.01	(0.00)
22	chemostat	94.08	1.44	(0.01)	5.27	(0.13)	7.35	(0.09)	0.56	(0.02)	6.56	(0.03)	54.9	(0.0)	13.4	(0.1)	10.5	(0.2)
	C	36.96	3.10	(0.15)	36.9	(0.3)	3.34	(0.23)	-		6.40	(0.62)	23.9	(2.2)	1.29	(0.07)	25.1	(0.43)
	D	32.34	3.51	(0.30)	40.1	(4.1)	2.91	(0.05)	-		3.57	(0.03)	24.4	(0.1)	1.18	(0.09)	24.3	(0.91)
25	chemostat	91.99	1.35	(0.02)	4.56	(0.02)	7.87	(0.02)	0.57	(0.00)	5.86	(0.04)	54.4	(0.2)	13.9	(0.1)	11.5	(0.2)
	C	76.77	1.96	(0.01)	12.8	(0.2)	3.09	(0.06)	-		4.82	(0.19)	72.8	(1.3)	2.54	(0.14)	2.03	(0.80)
2007, <0.45 µm HMW-dCCHO																		
10	chemostat	9.97	2.66	(0.12)	5.82	(0.20)	16.1	(0.6)	1.81	(0.01)	11.3	(0.0)	23.0	(0.1)	20.0	(0.6)	19.2	(0.6)
	C	6.01	3.05	(0.41)	-		2.30	(0.34)	-		4.76	(4.34)	10.4	(8.24)	2.75	(0.00)	76.7	(6.57)
	D	4.66	2.13	(0.09)	8.62	(0.00)	1.09	(0.07)	-		0.70	(0.00)	7.77	(2.10)	2.94	(1.61)	76.7	(40.6)
14	chemostat	7.41	2.49	(0.01)	1.85	(0.05)	22.0	(0.3)	1.24	(0.01)	7.82	(0.19)	29.4	(0.5)	17.6	(0.7)	17.5	(0.6)
	C	12.23	5.79	(0.07)	6.27	(0.00)	9.22	(0.02)	-		17.8	(0.2)	41.4	(1.3)	12.6	(0.1)	6.98	(0.1)
	D	3.64	2.68	(0.00)	0.88	(0.00)	7.63	(0.00)	-		30.4	(0.0)	51.2	(0.0)	7.18	(0.00)	0.08	(0.00)
22	chemostat	26.28	2.94	(0.05)	6.37	(0.05)	19.7	(0.5)	1.10	(0.00)	8.22	(0.08)	15.3	(0.1)	24.7	(0.5)	21.7	(0.4)
	C	13.48	5.06	(0.06)	20.7	(2.0)	8.19	(0.28)	-		3.76	(0.28)	5.43	(0.04)	7.43	(0.45)	49.4	(2.3)
	D	10.71	2.91	(0.08)	34.4	(1.2)	7.14	(0.12)	-		10.2	(0.1)	6.53	(0.64)	4.92	(0.18)	33.9	(0.3)

continued

Table 4.A2. ***2007, <0.45 µm HMW-dCCHO, continued***

Day	Sample ID	CCHO (µmol C l^{-1})	%Fuc		%Rha		%Ara+GalN		%GlcN		%Gal		%Glc		%Man+Xyl		%Gal-URA+ Glc-URA	
25	chemostat	27.46	2.77	(0.07)	6.46	(0.22)	20.6	(0.1)	0.98	(0.03)	8.46	(0.10)	17.1	(0.4)	22.7	(0.2)	20.8	(1.4)
	C	11.21	7.35	(0.23)	7.83	(0.06)	15.8	(0.4)	-		15.6	(0.3)	23.7	(0.5)	19.3	(0.3)	10.5	(0.1)
	D	10.07	9.54	(0.00)	8.79	(0.00)	14.4	(0.0)	-		35.5	(0.0)	24.5	(0.0)	7.24	(0.00)	0.02	(0.00)
2007, <1000 kDa HMW-dCCHO																		
10	C	7.25	2.79	(0.22)	2.34	(0.18)	6.97	(0.14)	2.93	(0.69)	7.04	(0.21)	35.1	(0.6)	33.0	(0.6)	9.89	(2.4)
	D	15.98	-	-	4.40	(0.24)	1.36	(0.01)	0.31	(0.04)	-		2.89	(0.05)	1.79	(0.02)	89.2	(0.65)
14	C	9.24	2.33	(0.56)	2.50	(0.10)	6.76	(0.06)	-		5.20	(0.15)	66.3	(0.3)	6.67	(0.00)	10.3	(1.1)
	D	5.85	2.82	(0.00)	1.87	(0.00)	6.63	(0.00)	2.18	(0.00)	12.8	(0.0)	64.6	(0.0)	5.50	(0.00)	3.55	(0.00)
22	C	35.05	1.72	(0.12)	2.98	(0.21)	8.93	(0.13)	0.27	(0.06)	13.7	(1.2)	61.9	(4.9)	8.83	(0.93)	1.71	(0.02)
	D	21.89	1.64	(0.08)	16.7	(0.9)	2.43	(0.01)	-		2.07	(0.03)	16.3	(0.1)	1.70	(0.11)	59.2	(2.8)
25	C	13.15	5.22	(0.54)	4.81	(0.38)	14.0	(0.5)	-		15.3	(0.1)	39.6	(1.0)	21.1	(2.7)	-	
	D	10.51	5.05	(0.00)	1.97	(0.00)	11.8	(0.0)	1.11	(0.00)	17.5	(0.0)	51.2	(0.0)	8.19	(0.00)	3.17	(0.00)

Table 4.A2. Composition of sugars (mol%) for each size fraction (total: tCCHO and colloidal: <0.45-HMW-dCCHO and <1000 kDA-HMW-dCCHO) for each growth rate in 2006 and 2007. Also shown are the sum of all sugar concentrations for each sample (µmol l^{-1}). Values are mean values and standard deviations (in parentheses) of two injections of each sample. Combined carbohydrate samples include the following sugars: fucose (Fuc), rhamnose (Rha), arabinose (Ara)+galactosamine (GalN) (quantified together due to coelution), glucosamine (GlcN), galactose (Gal), glucose (Glc), mannose (Man)+xylose (Xyl) (quantified together due to co-elution), galacturonic acid (Gal-URA)+glucuronic acid (Glc-URA) (quantified together due to co-elution in coagulation experiment samples). Samples for 2006 were limited to the dissolved fraction.

Table 4.A3. 2007 correlated coefficients of chemical and physical data associated with coagulation

	Growth Rate	Total Alkalinity	Det. liths: cell	TEP:Chl-*a*	<1000kDa-HMW-dURA	<1000kDa-HMW-dCAP	<0.45µm-HMW-dCAP	<0.45µm-HMW-dURA	tCHHO	Alcian Blue stained cells
α	-0.55	-0.55	0.30	0.53	0.35	0.36	0.48	-0.36	0.64	0.31
Total Alkalinity	**1.00**	–	–	–	–	–	–	–	–	–
Det. liths : cell	**-0.93**	**-0.93**	–	–	–	–	–	–	–	–
TEP:Chl-*a*	**-0.94**	**-0.97**	**0.88**	–	–	–	–	–	–	–
<1000kDa-HMW-dCAP	***-0.79***	***-0.82***	**0.89**	**0.85**	–	–	–	–	–	–
<0.45µm-HMW-dCAP	-0.51	-0.48	0.38	0.37	***0.79***	–	–	–	–	–
tCHHO	-0.62	-0.67	0.52	***0.80***	0.02	0.75	–	–	–	–
tCAP	***-0.80***	***-0.80***	0.62	0.77	0.37	0.60	0.40	–	–	0.32
tURA	-0.69	-0.68	***0.82***	0.57	0.68	***0.82***	0.58	-0.15	–	-0.52
Alcian blue stained cells	0.02	-0.02	-0.27	0.21	-0.52	-0.08	-0.12	-0.42	0.55	–
Circular Aggregates	-0.36	-0.43	0.49	0.61	-0.28	0.69	-0.12	-0.38	0.67	0.34
Non-circular Aggregates	-0.56	-0.58	***0.81***	0.59	0.26	***0.81***	0.09	-0.13	0.33	-0.39

Not significant: <0.78
Significant (p<0.05): 0.78–0.82 (in italics).
Highly Significant (p<0.01): >0.82 (in bold)

Table 4.A3. 2007 correlated coefficients of chemical and physical data associated with coagulation. Abbreviations for variables: Det.– detached; Lith – coccoliths; <1000 kDa-HMW-d – <1000 kDa high molecular weight dissolved; CAP – colloidal acidic polysaccharides; URA – uronic acids (galacturonic acid and glucuronic acid); t – total; AB – Alcian blue.

Table 4.A4. Summary of α results

α	Source
0–0.98	Kiørboe & Hansen (1993)
0.001–0.13	Drapeau et al. (1994)
0.01–0.6	Kiørboe et al. (1994)
8×10^{-5}	Passow et al. (1994)
0.03–0.8	Dam & Drapeau (1995)
0–0.7	Hansen & Kiørboe (1997)
~0–0.4	Kiørboe et al. (1998)
<0.1–1	Engel (2000)
0.15–0.37	Vieira et al. (2008)
0.2–1.15	This study

Table 4.A4. Summary of α results from this and previous studies.

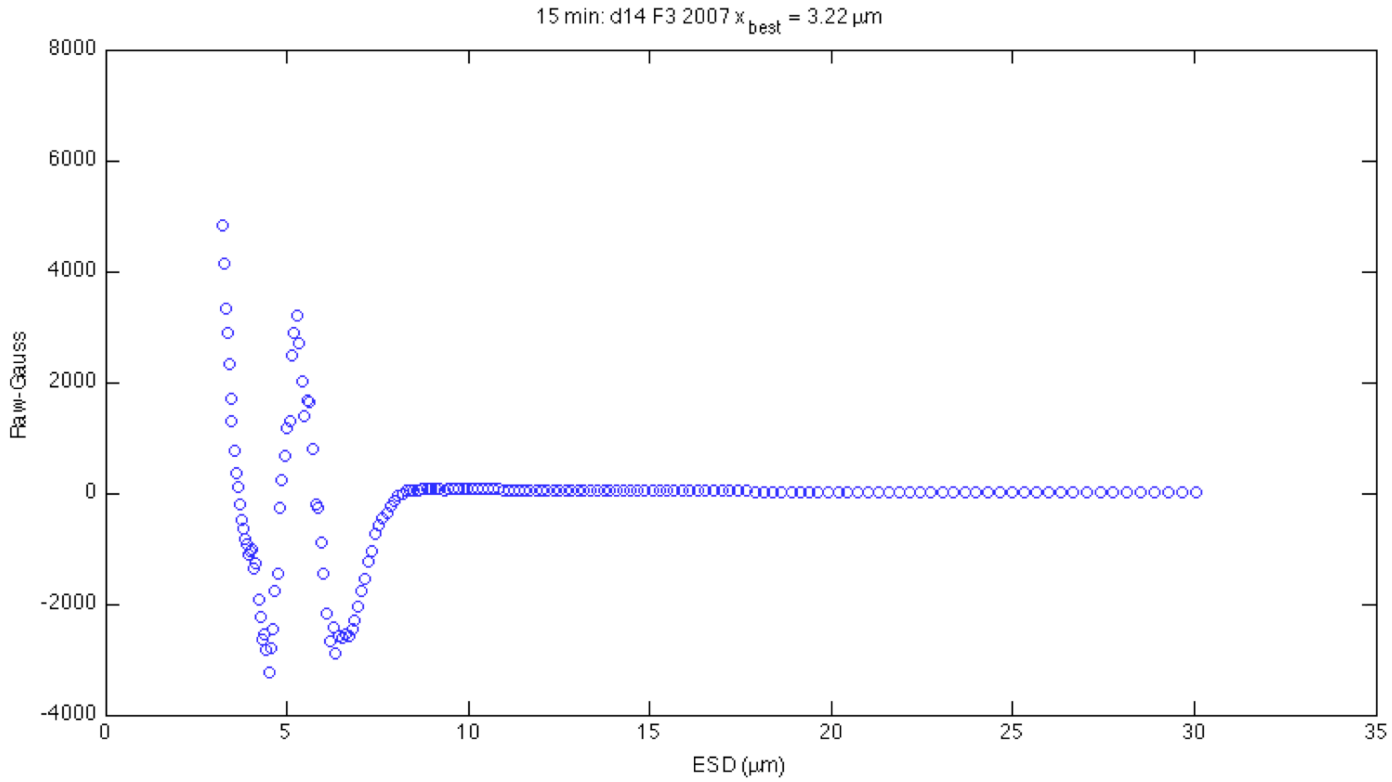

Fig. 4.A1. Example of difference in raw (Coulter Counter enumerated) and Gauss (model results) particles size distribution. For all experiments and time points we see the same trend: 1) raw PSD have higher abundances of particles left of the cell peak (~5 µm) indicating the presence of coccoliths (<3 µm); 2) steeper shoulders than the Gauss model results (Raw-Gauss is <0); 3) monomer peak is higher than predicted by Gauss model results (peak near 5 µm); and the right shoulder of the raw PSD is broader than the Gauss model results (broader dip on right of peak ~6-7 µm and slight elevation above 0 from ~8 µm to 15 µm).

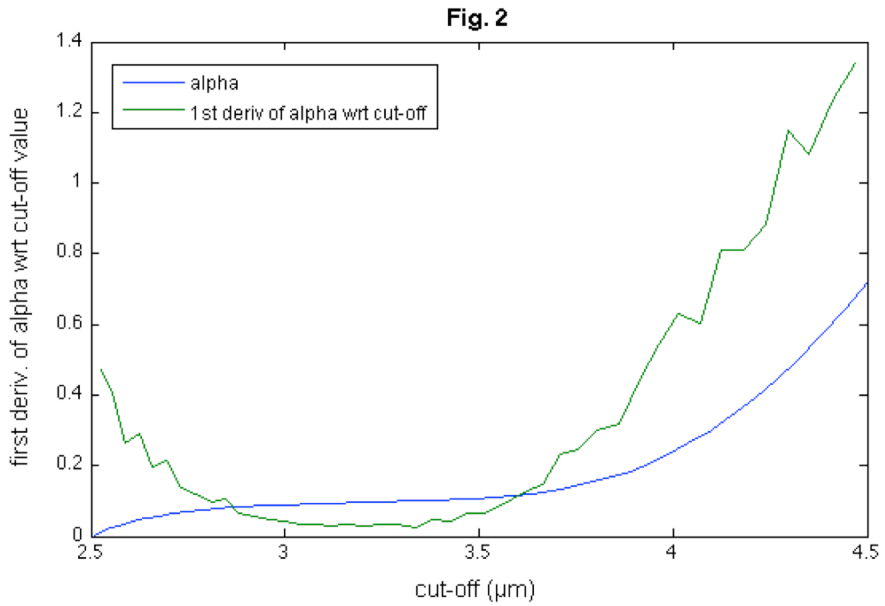

Figure 4.A2. Example of 2007 experiment α_{var} and the first derivative of α_{var} for different x_{cut} values (ranging from 2.5–4.5 µm).

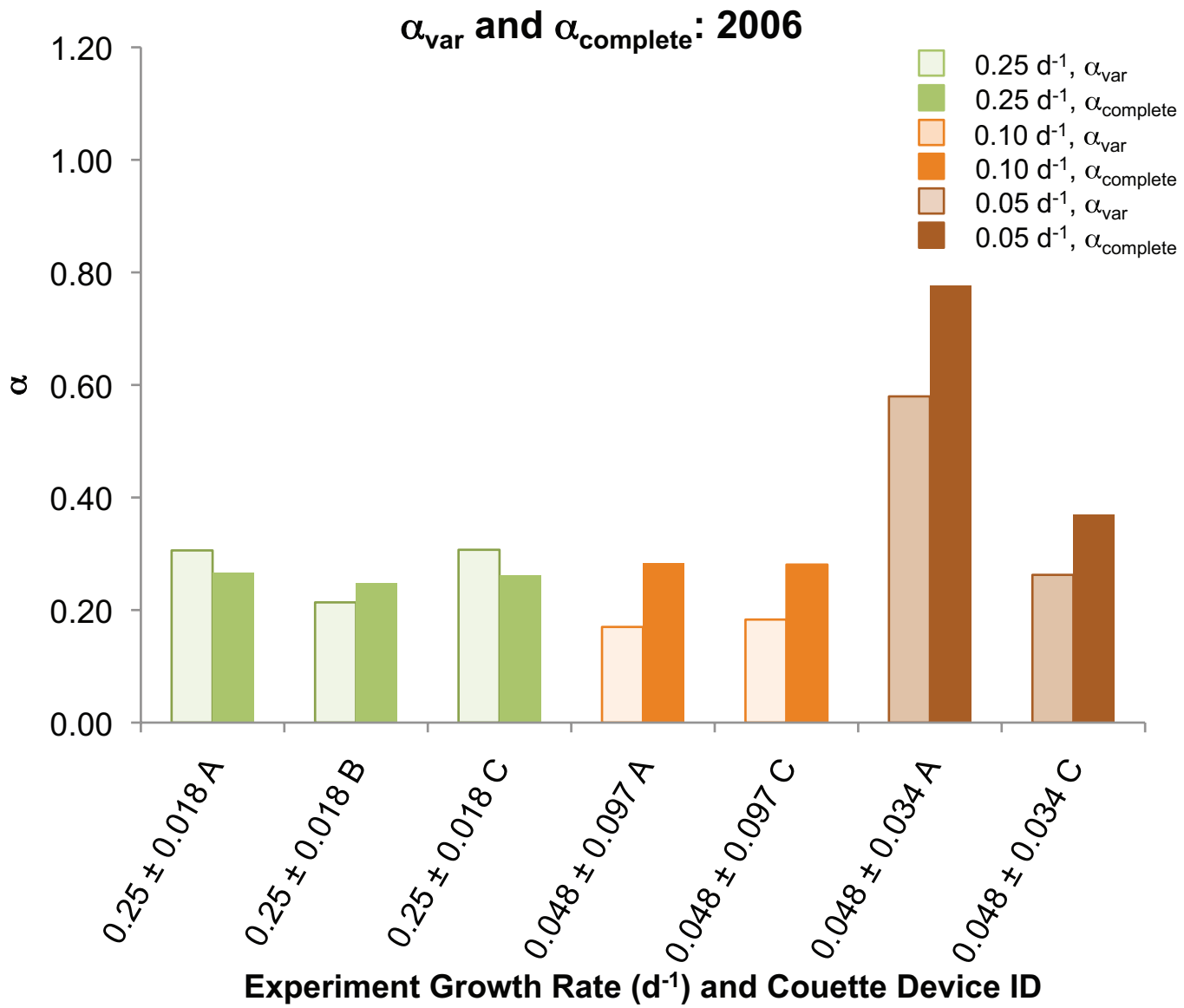
α_{var} and $\alpha_{complete}$: 2006
0.25 d^{-1}, α_{var}
0.25 d^{-1}, $\alpha_{complete}$
0.10 d^{-1}, α_{var}
0.10 d^{-1}, $\alpha_{complete}$
0.05 d^{-1}, α_{var}
0.05 d^{-1}, $\alpha_{complete}$
α
1.20
1.00
0.80
0.60
0.40
0.20
0.00
0.25 ± 0.018 A
0.25 ± 0.018 B
0.25 ± 0.018 C
0.048 ± 0.097 A
0.048 ± 0.097 C
0.048 ± 0.034 A
0.048 ± 0.034 C
Experiment Growth Rate (d^{-1}) and Couette Device ID

Figure 4.A3a. 2006 α_{var} (light shade of color) and $\alpha_{complete}$ (dark shade of color) for experiments at different growth rates.

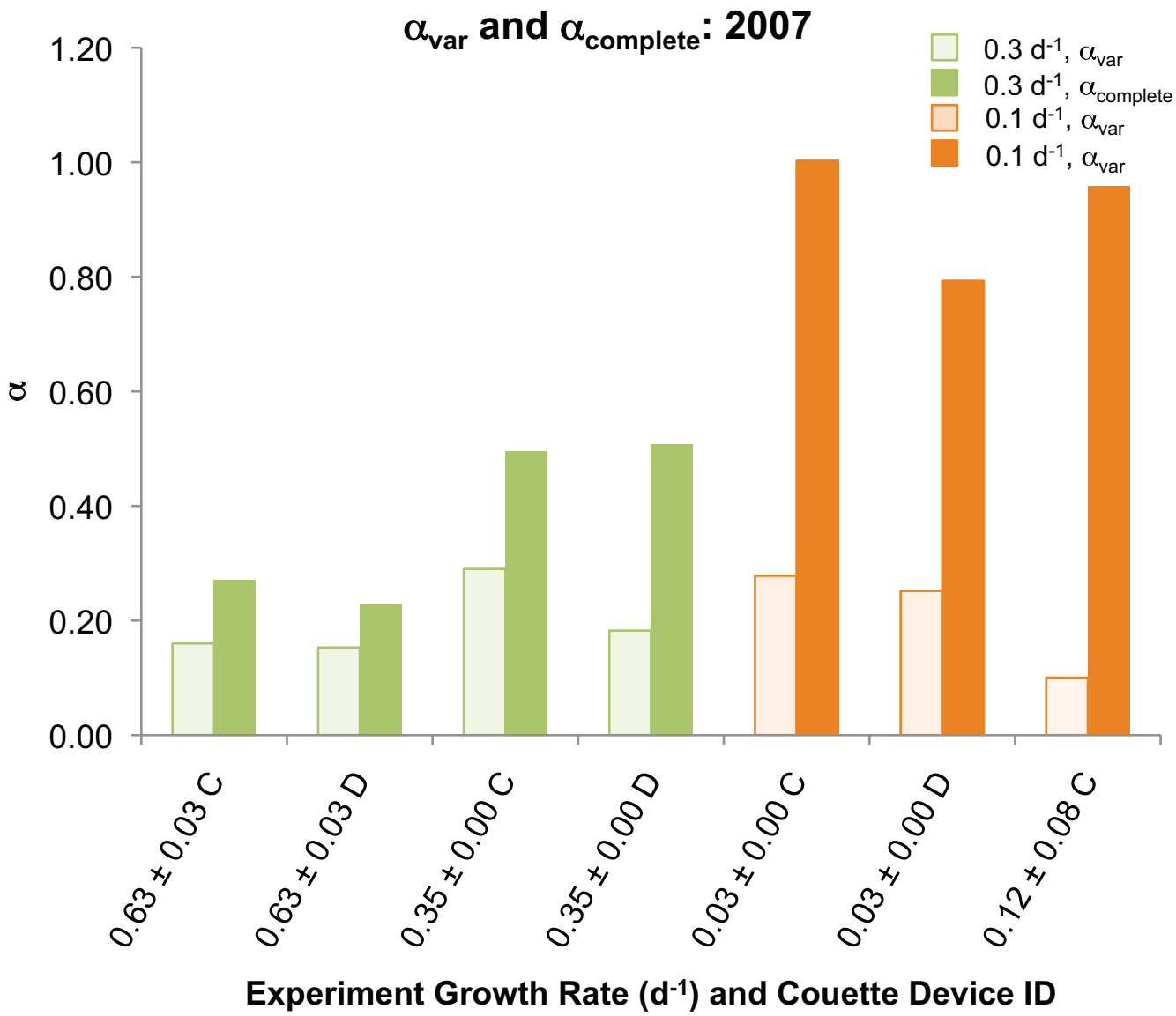
α_{var} and $\alpha_{complete}$: 2007
0.3 d^{-1}, α_{var}
0.3 d^{-1}, $\alpha_{complete}$
0.1 d^{-1}, α_{var}
0.1 d^{-1}, α_{var}
1.20
1.00
0.80
0.60
0.40
0.20
0.00
α
0.63 ± 0.03 C
0.63 ± 0.03 D
0.35 ± 0.00 C
0.35 ± 0.00 D
0.03 ± 0.00 C
0.03 ± 0.00 D
0.12 ± 0.08 C
Experiment Growth Rate (d^{-1}) and Couette Device ID

Figure 4.A3b. 2007 α_{var} (light shade of color) and $\alpha_{complete}$ (dark shade of color) for experiments at different growth rates.

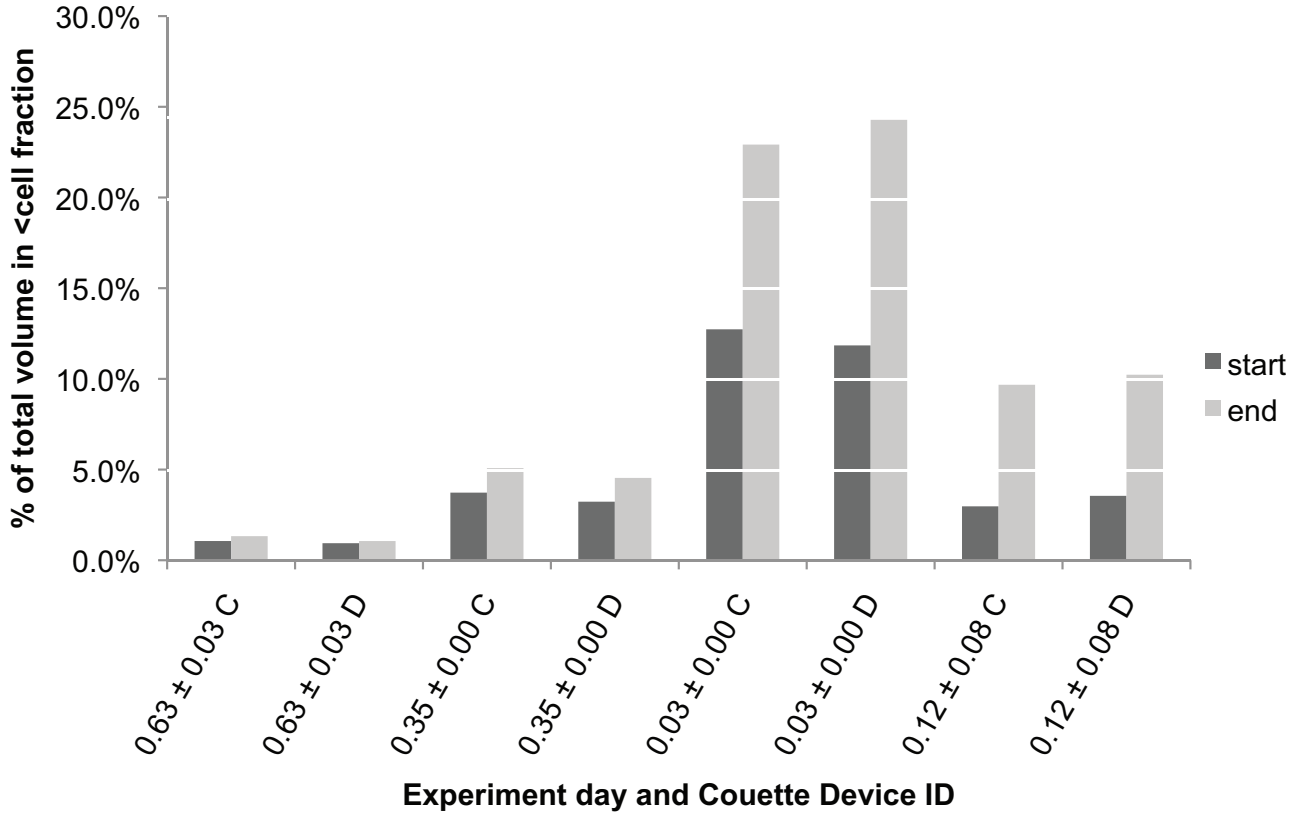

Figure 4.A4. 2007 % of total CCP volume comprised of particles smaller than monomers (coccoliths) for each coagulation experiment.

References

Balch, W.M., K.A. Kilpatrick, P.M. Holligan, and T. Cucci, 1993. Coccolith production and detachment by *Emiliania huxleyi*. Journal of Phycology 29 (5), 566-575.

Collier, J.L., Lovindeer, R., Xi, Y., Radway, J.C., Armstrong, R.A., 2012. Differences in growth and physiology of marine *Synechococcus* (cyanobacteria) on nitrate versus ammonium are not determined solely by nitrogen source redox state. Journal of Phycology 48 (1), 106-117.

Fritz, J.J., Balch, W.M., 1996. A light-limited continuous culture study of *Emiliania huxleyi*: determination of coccolith detachment and its relevance to cell sinking. Journal of Experimental Marine Biology and Ecology 207, 127-147.

Fritz, J.J., 1999. Carbon fixation and coccolith detachment in the coccolithophore *Emiliania huxleyi* in nitrate-limited cyclostats. Marine Biology 133, 509-518.

van Duuren, F.A., 1968. Defined velocity gradient model flocculator. Journal of the Sanitary Engineering Division: Proceedings of the American Society of Civil Engineers 94, 671-682.